INTERPRETATION OF H-11B4 HYDRAULIC TESTS AND THE H-11 MULTIPAD PUMPING TEST OF THE CULEBRA DOLOMITE AT THE WASTE ISOLATION PILOT PLANT (WIPP) SITE

Richard L. Beauheim
Sandia National Laboratories
Earth Sciences Division
Albuquerque, New Mexico

ABSTRACT

Drillstem tests, slug tests, a small-scale pumping test, and a large-scale pumping test of the Culebra Dolomite Member of the Rustler Formation were performed in 1988 at the H-11 hydropad at the Waste Isolation Pilot Plant (WIPP) site in southeastern New Mexico. The drillstem, slug, and small-scale pumping tests were conducted in well H-11b4 to evaluate well and aquifer properties in preparation for a tracer test. The large-scale pumping test, known as the H-11 multipad test, was performed by pumping well H-11b1 in the southern part of the WIPP site at a rate of six gpm for 63 days and monitoring drawdown and recovery responses in three other wells on the H-11 hydropad and at 11 observation wells within a three-mile radius. Responses were observed in 10 of these distant wells. The H-11 multipad pumping test complemented the H-3 and WIPP-13 multipad pumping tests conducted in the central and northern portions of the WIPP site in late 1985 and early 1987, respectively.

Individual well tests at various locations around the WIPP site have demonstrated that the Culebra is a laterally heterogeneous water-bearing unit. The responses measured at observation wells to pumping tests in heterogeneous systems cannot be rigorously interpreted using standard analytical (as opposed to numerical) techniques developed for tests in homogeneous porous media. Application of analytical techniques to data from tests of heterogeneous media results in evaluations of average hydraulic properties between pumping and observation wells that are nonunique in the sense that they are representative only of the responses

3

DISCLAIMER

DISCLAIMER

observed when a hydraulic stress is imposed at a certain location. These "apparent" hydraulic properties do, however, provide a qualitative understanding of the nature and distribution of both hydraulic properties and heterogeneities or hydraulic boundaries within the tested area.

The interpretations of the responses at the test and observation wells provided the following information: The Culebra is a fractured, double-porosity system at H-11 with a transmissivity between 27 and 43 ft^2/day and a storativity between 3.4×10^{-5} and 1.5×10^{-4}. Drawdown during the multipad test appeared to be largely concentrated to the north and south of H-11; wells to the east and west showed relatively low-magnitude responses. The rapid and high-magnitude responses observed at DOE-1, H-3b2, and H-15 during the multipad test are believed to reflect the presence of a fracture network extending to the north from H-11. Numerical simulations indicate that the fracture network also extends south of H-11, but no wells are currently situated within it.

Double-porosity hydraulic behavior was observed at DOE-1 during the multipad test, and at both DOE-1 and H-3b2 during other pumping tests performed at those locations. The fractures appear to continue past DOE-1 to the north toward H-15, although H-15 itself lies in a lower transmissivity, apparently single-porosity zone. Apparent transmissivities in the region north of H-11 range from 7.1 to 9.0 ft^2/day and apparent storativities range from 2.4×10^{-6} to 8.4×10^{-6}. Apparent transmissivities between H-11 and observation wells to the west, southwest, and southeast, where fracturing in the Culebra decreases and single-porosity hydraulic behavior is observed, range from 6.0 to 21.0 ft^2/day and apparent storativities range from 1.8×10^{-5} to 6.5×10^{-5}. Interpretation of the responses to the multipad test observed at the western and southern wells was complicated by an anomalous and widespread rise in water levels of unknown origin.

Thus, the analyses of the responses measured at observation wells to the H-11 multipad pumping test are consistent with a conceptualization of two distinct domains within a heterogeneous portion of the Culebra south of the center of the WIPP site: a fractured region having low storativity extending to the north and south from H-11, and a relatively unfractured region west, southwest, and southeast of H-11 having higher storativity. This conceptualization is being refined using numerical-modeling techniques to simulate the H-11 multipad test and other tests at the WIPP site, in an attempt to define a distribution of hydraulic properties that will reproduce the responses observed.

ACKNOWLEDGEMENTS

TABLE OF CONTENTS

FIGURES

10

TABLES

INTERPRETATION OF H-11B4 HYDRAULIC TESTS
AND THE H-11 MULTIPAD PUMPING TEST
OF THE CULEBRA DOLOMITE
AT THE WASTE ISOLATION PILOT PLANT (WIPP) SITE

1. INTRODUCTION

This report presents the results of hydraulic tests performed in well H-11b4 and of the H-11 multipad pumping test of the Culebra Dolomite Member of the Rustler Formation at the Waste Isolation Pilot Plant (WIPP) site in southeastern New Mexico (Figure 1-1). The WIPP is a U.S. Department of Energy research and development facility designed to demonstrate safe disposal of transuranic radioactive wastes resulting from the nation's defense programs. The WIPP facility lies in bedded halite in the lower Salado Formation. The hydraulic tests discussed in this report were conducted in the Culebra Dolomite Member of the Rustler Formation, which overlies the Salado Formation. The tests were performed by Sandia National Laboratories, Albuquerque, New Mexico, and/or by INTERA Technologies, Inc., under the technical direction of Sandia National Laboratories.
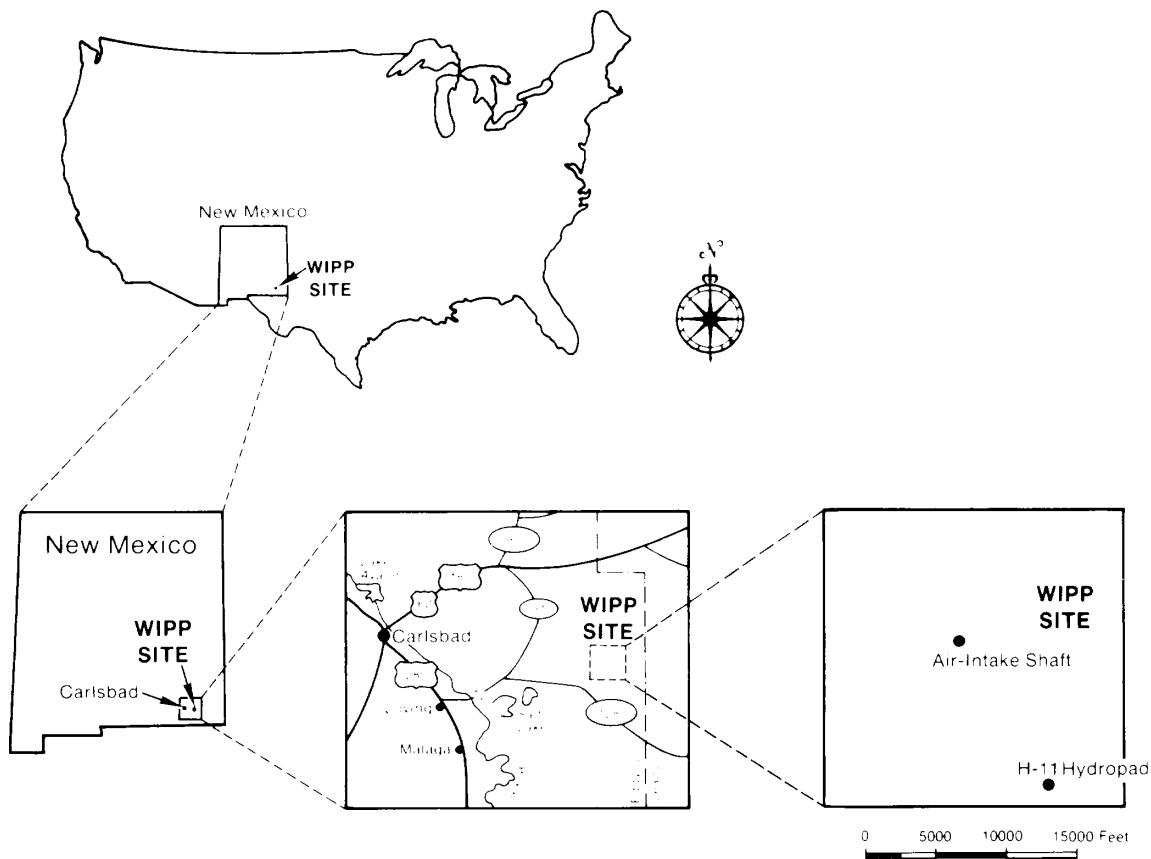
Figure 1-1. Location of the WIPP Site.

When the H-11 hydropad was constructed in 1983, three wells were completed to the Culebra dolomite: H-11b1, H-11b2, and H-11b3 (Figure 1-2). Interpretation of pumping tests performed in those three wells was the subject of a report by Saulnier (1987). The H-11 multipad pumping test was designed as a combination large-scale pumping test and convergent-flow tracer test. To provide an additional tracer-injection well on the H-11 hydropad, well H-11b4 was drilled in February and March 1988. Drillstem tests (DSTs), slug tests, and a 50-hr pumping test were then performed in H-11b4 to evaluate aquifer and well properties at that location to aid in design and interpretation of the planned tracer test.

The pumping well for the H-11 multipad/tracer test was H-11b1, which is located approximately 10,380 ft southeast of the center of the WIPP site (Figure 1-3). H-11b1 was pumped at a rate of about six gallons per minute (gpm) for 63 days from May 5 to July 7, 1988

(calendar days 126 to 189) to provide a converging flow field for a test using conservative (i.e., non-sorbing) tracers, and to create a hydraulic stress which could be measured over the southern part of the WIPP site. The test is termed a "multipad" test because hydraulic responses were observed in wells completed on a number of drilling pads. The test was intended to complement the H-3 and WIPP-13 multipad tests conducted in late 1985 and early 1987, respectively (Beauheim, 1987a,b). Together, the three multipad tests provided measurable and spatially overlapping hydraulic responses over most of the 16-square-mile WIPP site. Data from the test are to be used to improve the calibration of the groundwater-flow model first developed by Haug et al. (1987), and later expanded and updated by LaVenue et al. (1988). In particular, the test was intended to provide additional information on the location and properties of an area of relatively high transmissivity which the model indicates exists near H-11 and extends to the south.
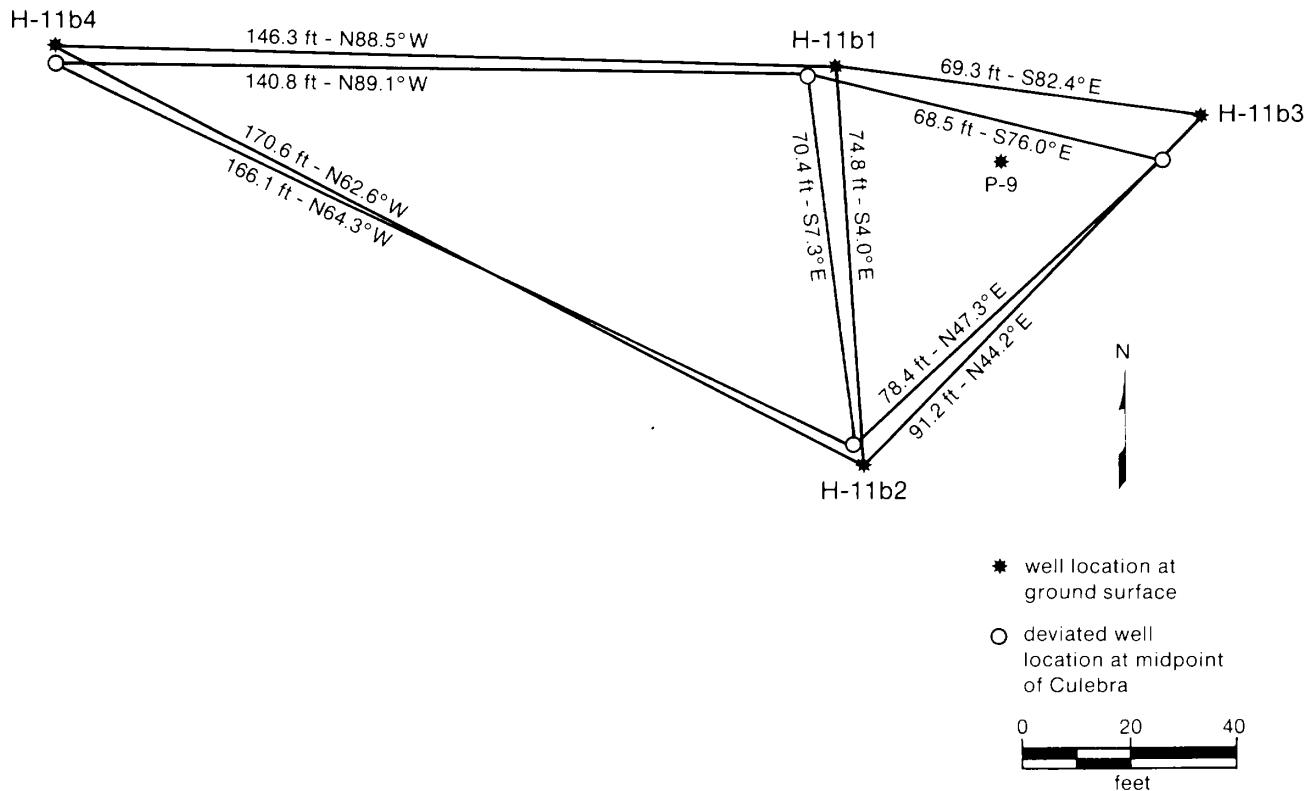
Figure 1-2. Well Locations on the H-11 Hydropad.

14

During the H-11 multipad test, fluid pressures were measured in the pumping well and the other three wells on the H-11 hydropad, and water levels were measured on a regular basis in 11 observation wells completed in the Culebra dolomite at distances ranging from 3970 to 15,530 ft from H-11b1 (Figure 1-3). Except to the northwest, responses to the pumping were observed at all wells within a 2-mile radius of H-11b1. The northwestern extent of observable responses was constrained by the on-going construction of the Air-Intake Shaft for the WIPP (Figure 1-1), which produced a pressure transient within the Culebra at nearby wells of greater magnitude than might have resulted from the pumping test.

This report presents interpretations of the hydraulic tests performed in H-11b4 and of the fluid-pressure and water-level responses resulting from the H-11 multipad test. Interpretation of the results of the H-11 tracer test will be contained in a later report.
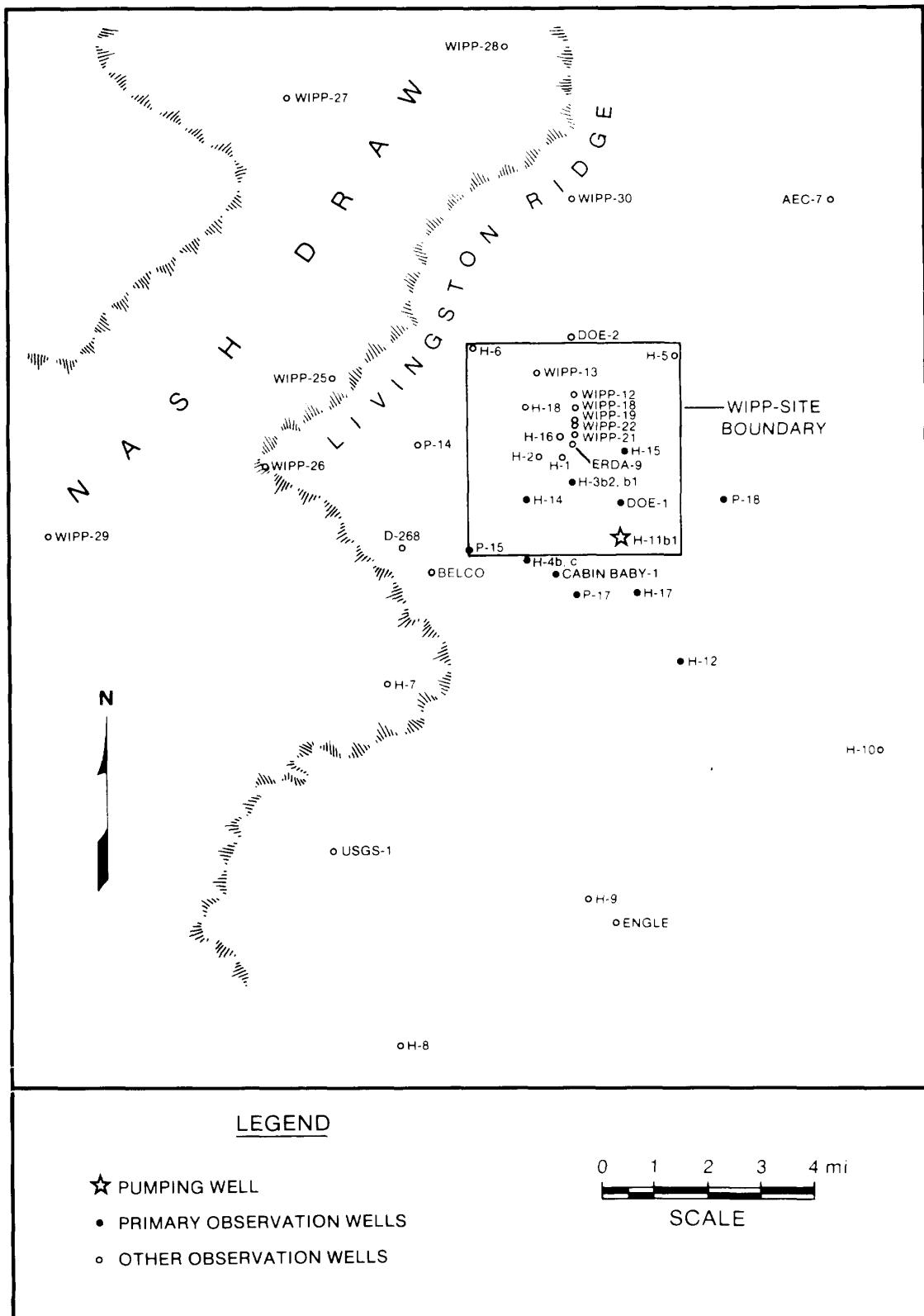
Figure 1-3. Locations of Wells in the Vicinity of the WIPP Site.

2. SITE HYDROGEOLOGY

The WIPP site is located in the northern part of the Delaware Basin in southeastern New Mexico. WIPP-site geologic investigations have concentrated on the upper seven formations typically found in that part of the Delaware Basin. These are, in ascending order, the Bell Canyon Formation, the Castile Formation, the Salado Formation, the Rustler Formation, the Dewey Lake Red Beds, the Dockum Group, and the Gatuña Formation (Figure 2-1). All of these formations are of Permian age, except for the Dockum Group, which is of Triassic age, and the Gatuña, which is a Quaternary deposit. Of these formations, only the Bell Canyon and the Rustler contain regionally continuous saturated intervals with sufficient permeability to allow well testing by standard hydrogeological techniques.

The Rustler Formation dips about 2.4° to the east at the H-11 hydropad. The top of the Rustler lies 2857 ft above mean sea level (amsl) (553 ft deep) at H-11b4, and 2848 ft amsl (560 ft deep) 215 ft to the east at H-11b3 (Mercer, in preparation, a). Potash-exploration hole P-9, drilled in 1976 and subsequently plugged with cement from its total depth to the surface, is the only hole on what is now the H-11 hydropad to penetrate the bottom of the Rustler (Figure 1-2). In P-9, the Rustler was found from 562 to 881 ft below ground surface (Jones, 1978). At the H-11 hydropad, the Rustler consists of five members (in ascending order): an unnamed lower member, the Culebra Dolomite Member, the Tamarisk Member, the Magenta Dolomite Member, and the Forty-niner Member. The Culebra, which ranges from 723 to 746 ft deep at H-11b4 to 735 to 760 ft deep at H-11b3, is a fractured, moderate yellowish-brown, finely crystalline, vuggy, silty dolomite (Mercer, in preparation, a). The Culebra is the principal water-bearing member of the Rustler, and is considered to be the most important potential groundwater-transport pathway for radionuclides that may escape from the WIPP facility to reach the accessible environment. The vast majority of hydrologic tests performed at the WIPP site have examined the hydraulic properties of the Culebra. Saulnier (1987) determined an average transmissivity of 25 ft^2/day for the Culebra at the H-11 hydropad from four pumping tests performed in 1984 and 1985.

The Culebra is confined by the underlying unnamed member, which is composed of a layered sequence of mudstone, siltstone, anhydrite, and halite, and by the overlying Tamarisk Member, which is composed of anhydrite and gypsum with a single mudstone/claystone interbed. The Culebra water levels in early 1987 at H-11b1 were about 442 ft below ground surface (Stensrud et al., 1988a), or about 288 ft above the top of the Culebra. The Culebra fluid at H-11 has a total dissolved solids concentration of about 117,000 mg/l, primarily due to sodium and chloride, and a specific gravity of about 1.08 at 23°C (Randall et al., 1988).

SYSTEM	SERIES	GROUP	FORMATION	MEMBER
RECENT	RECENT		SURFICIAL DEPOSITS	
QUATER-NARY	PLEISTO-CENE		MESCALERO CALICHE	
			GATUÑA	
TRIASSIC		DOCKUM	UNDIVIDED	
PERMIAN	OCHOAN		DEWEY LAKE RED BEDS	
			RUSTLER	Forty-niner
				Magenta Dolomite
				Tamarisk
				Culebra Dolomite
				unnamed
			SALADO	
			CASTILE	
	GUADALUPIAN	DELAWARE MOUNTAIN	BELL CANYON	
			CHERRY CANYON	
			BRUSHY CANYON	

Figure 2-1. WIPP-Area Stratigraphic Column.

3. TEST AND OBSERVATION WELLS

A number of different wells were involved in the different episodes of testing performed at the H-11 hydropad in 1988. The only well involved in the H-11b4 DSTs and slug tests was H-11b4 itself. Both H-11b4 and H-11b1 were monitored during the H-11b4 pumping test. All four H-11 wells, as well as 11 other wells completed to the Culebra dolomite, were monitored during the H-11 multipad pumping test. In addition, water levels in two wells completed to the Magenta dolomite were also monitored during the H-11 multipad test. The locations and configurations of all of these wells are discussed below.

All four wells on the H-11 hydropad were completed in a similar fashion, although the sequence of well-construction events was slightly different for H-11b4 than for H-11b1, H-11b2, and H-11b3 (Mercer, in preparation, a). H-11b1, H-11b2, and H-11b3 were drilled, cored, and reamed to a diameter of 4.75 inches from the surface to their total depths in the upper part of the unnamed lower member of the Rustler. The holes were then reamed to a 7.875-inch diameter down to the lower Tamarisk or upper Culebra, and 5.5-inch casing was cemented from there to the surface, leaving the Culebra and lower part of the hole open. At H-11b4, a 7.875-inch hole was drilled and reamed to a depth of 715 ft, about eight ft above the top of the Culebra, and 5.5-inch casing was set and cemented from 714 ft to the surface. The hole was then cored and reamed through the Culebra to a depth of 765.3 ft to a diameter of 4.75 inches. The final as-built configurations of the H-11 wells are shown in Figure 3-1. The relative locations of the H-11 wells, both at the surface and as they have deviated at the midpoint of the Culebra (Saulnier et al., 1987; Stensrud et al., 1988b), are shown in Figure 1-2.
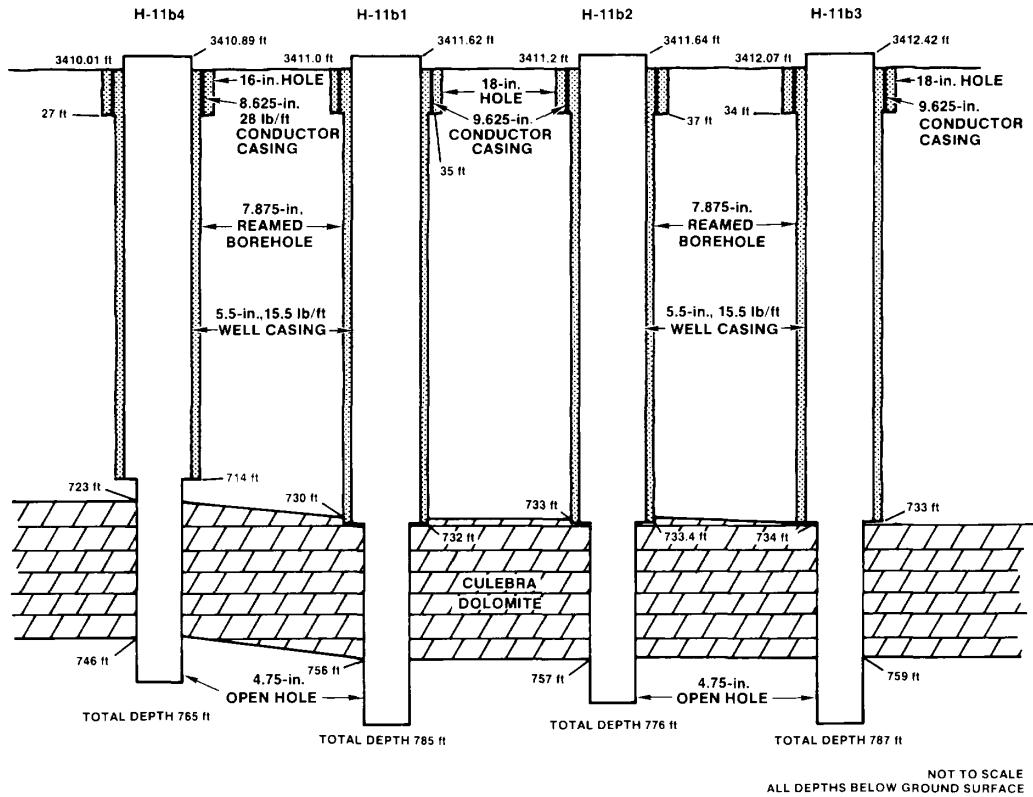
Figure 3-1. As-Built Configurations of the H-11 Wells.

Water levels were measured regularly in 11 key distant Culebra wells during the H-11 multipad pumping test. These include DOE-1, H-3b2, H-4b, H-12, H-14, H-15, H-17, P-15, P-17, P-18, and Cabin Baby-1 (Figure 1-3). Of these, all but P-18 and perhaps P-15 showed apparent responses to the test. Other wells in the vicinity of the WIPP site were monitored biweekly to monthly during the H-11 multipad test as part of the ongoing regional water-level monitoring (Stensrud et al., in preparation). Except for other wells on the H-3 and H-4 hydropads, none of the other Culebra wells responded observably to the pumping at H-11b1. Distances and directions from H-11b1 to the key observation wells are listed in Table 3-1.

The key distant observation wells are completed in a variety of fashions. H-3b2 (Figure 3-2), H-4b (Figure 3-3), H-14 (Figure 3-4), and H-15 (Figure 3-5) are cased from the surface to the lower Tamarisk, and are open through the Culebra to their total depths in the upper part of the unnamed lower member (INTERA, 1986; Mercer et al., 1981; Mercer, in preparation, b). H-12 (Figure 3-6) and H-17 (Figure 3-7) are cased from the surface to the lower Tamarisk, and are open through the Culebra to cement plugs in the unnamed lower member (Mercer, in preparation, c; d). DOE-1 (Figure 3-8) and Cabin Baby-1 (Figure 3-9) are completed with casing cemented from the surface to the upper Salado, perforations across the Culebra intervals, and bridge plugs lower in the casing isolating open intervals of the wells (HydroGeoChem, 1985; Stensrud et al., 1987). P-15 (Figure 3-10), P-17 (Figure 3-11), and P-18 (Figure 3-12) are cased to their total depths in the upper Salado, perforated across the Rustler-Salado contact zone and the Culebra, and have bridge plugs set between the Rustler-Salado and Culebra perforations (Stensrud et al., 1988a; 1987; 1988b). P-18 also has a production-injection packer (PIP) set on 2.375-inch tubing above the Culebra to minimize wellbore storage (Stensrud et al., 1988b). Thus, access for water-level measurements is through the open casing in H-3b2, H-4b, H-12, H-14, H-15, H-17, DOE-1, P-15, P-17, and Cabin Baby-1, and through tubing attached to a PIP in P-18.

TABLE 3-1

POSITIONS OF OBSERVATION WELLS RELATIVE TO PUMPING WELL H-11b1

Observation Well	Distance From H-11b1 (ft)	Direction From H-11b1
H-11b2	70.4*	S 7.3° E
H-11b3	68.5*	S 76.0° E
H-11b4	140.8*	N 89.1° W
DOE-1	3970	N 6.4° W
H-3b2	7940	N 42.5° W
H-4b	9960	S 78.0° W
H-12	13250	S 24.2° E
H-14	10640	N 67.5° W
H-15	8960	N 0.3° W
H-17	5440	S 12.6° E
P-15	15530	S 86.3° W
P-17	7180	S 40.8° W
P-18	10690	N 68.4° E
Cabin Baby-1	7910	S 63.7° W

*deviated hole locations at midpoint of Culebra

Water levels in two wells completed in the Magenta dolomite were also monitored on a regular basis during the H-11 multipad pumping test: H-3b1 and H-4c (Figure 1-3). H-3b1 is cased from the surface to a depth of 897 ft in the upper Salado. The casing is perforated across the Rustler-Salado contact, the Culebra, and the Magenta (Mercer and Orr, 1979). Two bridge plugs isolate the three sets of perforations (Figure 3-13). Magenta water levels are measured in the well casing above the upper bridge plug (Saulnier et al., 1987). H-4c is cased from the surface to a depth of 609.5 ft in the unnamed lower member of the Rustler. The hole is open from that depth to a total depth of 661 ft in the upper Salado (Mercer et al., 1981). The casing is perforated across the Culebra and Magenta. Bridge plugs separate the Culebra perforations from the lower open portion of the hole and from the Magenta perforations (Figure 3-14; Saulnier et al., 1987). No responses to the pumping at H-11b1 were detected in the Magenta at either H-3b1 or H-4c.
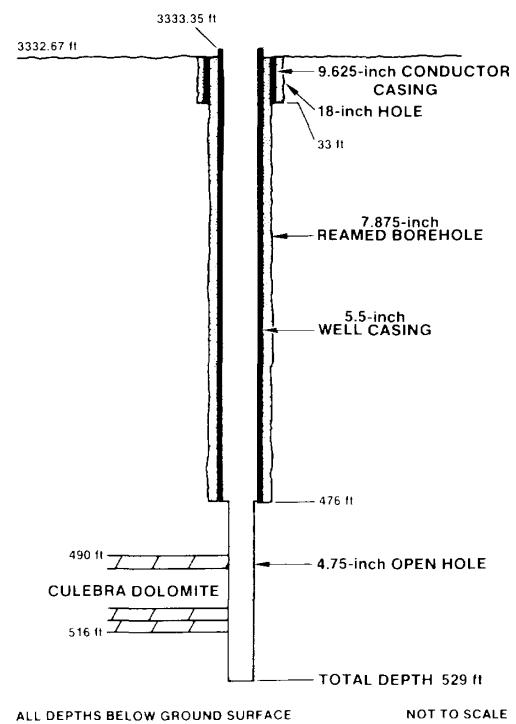
Figure 3-3. Configuration of Observation Well H-4b.
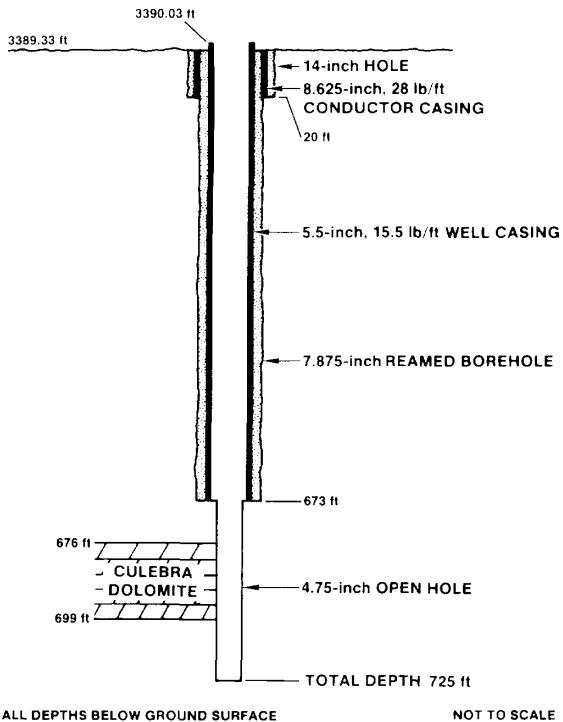
Figure 3-2. Configuration of Observation Well H-3b2.
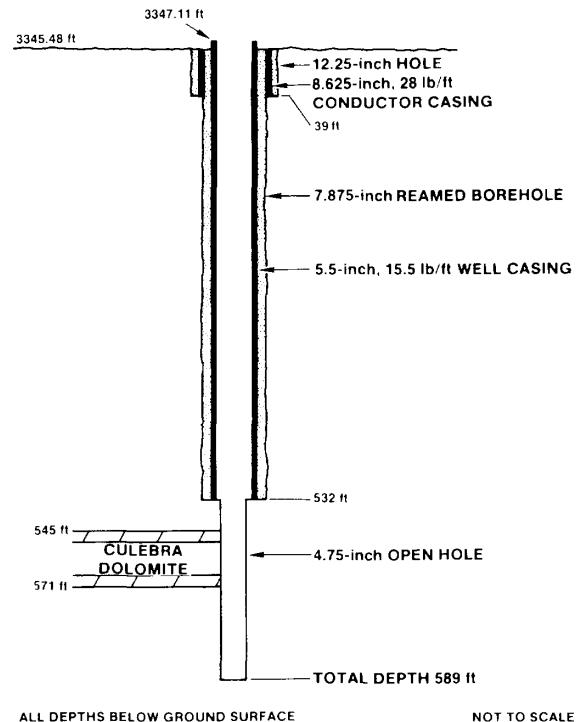
Figure 3-4. Configuration of Observation Well H-14.

20
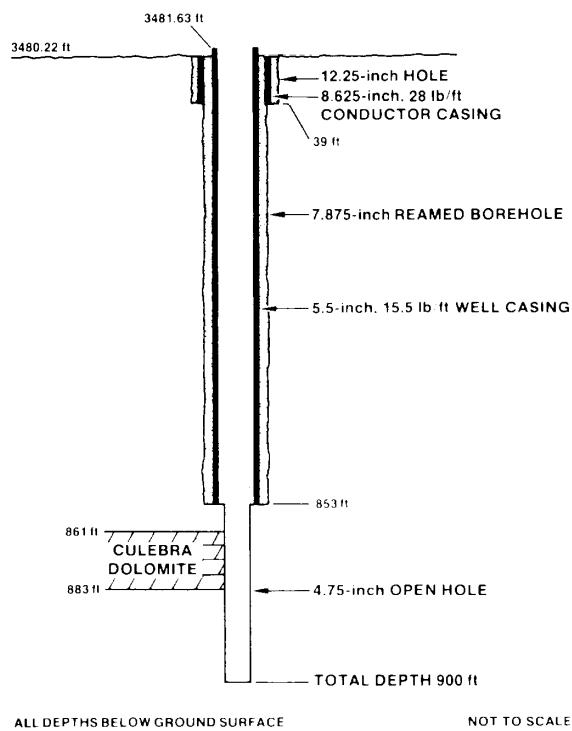
Figure 3-5. Configuration of Observation Well H-15.

Labels (left to right, top to bottom):
3481.63 ft
3480.22 ft
12.25-inch HOLE
8.625-inch, 28 lb/ft CONDUCTOR CASING
39 ft
7.875-inch REAMED BOREHOLE
5.5-inch, 15.5 lb ft WELL CASING
853 ft
861 ft
CULEBRA DOLOMITE
883 ft
4.75-inch OPEN HOLE
TOTAL DEPTH 900 ft
ALL DEPTHS BELOW GROUND SURFACE   NOT TO SCALE
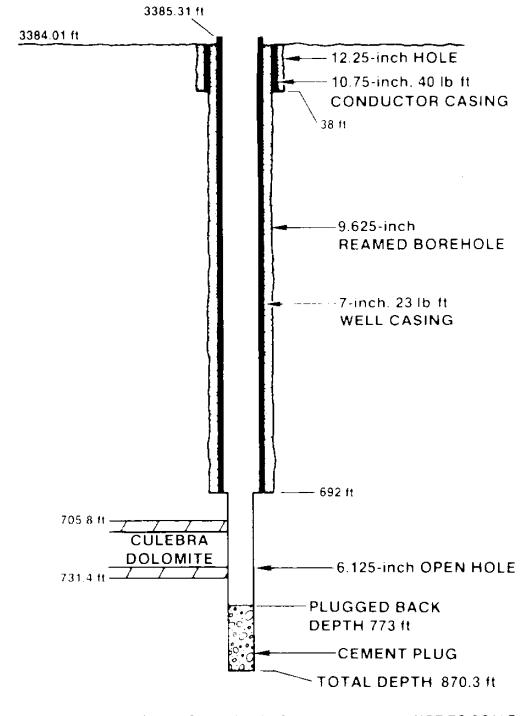
Figure 3-7. Configuration of Observation Well H-17.

Labels:
3385.31 ft
3384.01 ft
12.25-inch HOLE
10.75-inch, 40 lb ft CONDUCTOR CASING
38 ft
9.625-inch REAMED BOREHOLE
7-inch, 23 lb ft WELL CASING
692 ft
705.8 ft
CULEBRA DOLOMITE
731.4 ft
6.125-inch OPEN HOLE
PLUGGED BACK DEPTH 773 ft
CEMENT PLUG
TOTAL DEPTH 870.3 ft
ALL DEPTHS BELOW GROUND SURFACE   NOT TO SCALE
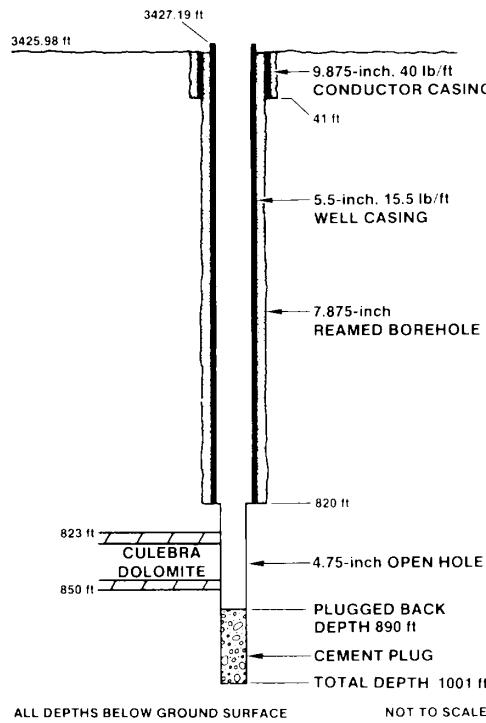
Figure 3-6. Configuration of Observation Well H-12.

Labels:
3427.19 ft
3425.98 ft
9.875-inch, 40 lb/ft CONDUCTOR CASING
41 ft
5.5-inch, 15.5 lb/ft WELL CASING
7.875-inch REAMED BOREHOLE
820 ft
823 ft
CULEBRA DOLOMITE
850 ft
4.75-inch OPEN HOLE
PLUGGED BACK DEPTH 890 ft
CEMENT PLUG
TOTAL DEPTH 1001 ft
ALL DEPTHS BELOW GROUND SURFACE   NOT TO SCALE
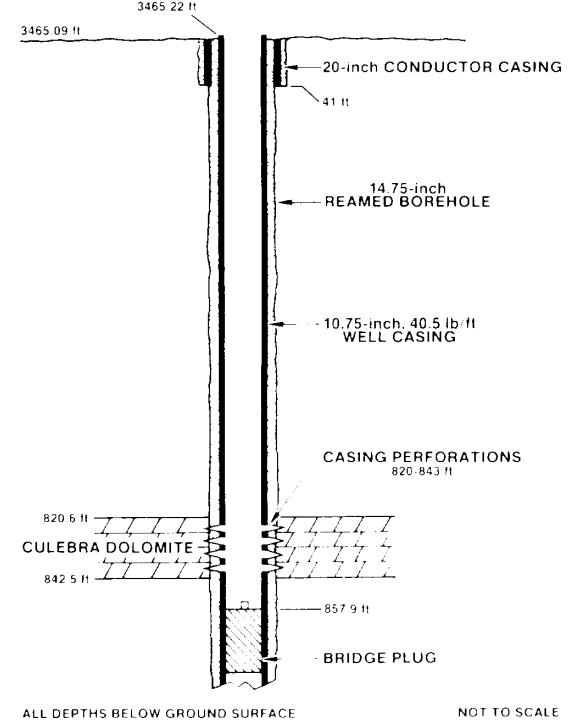
Figure 3-8. Configuration of Observation Well DOE-1.

Labels:
3465.22 ft
3465.09 ft
20-inch CONDUCTOR CASING
41 ft
14.75-inch REAMED BOREHOLE
10.75-inch, 40.5 lb/ft WELL CASING
CASING PERFORATIONS 820-843 ft
820.6 ft
CULEBRA DOLOMITE
842.5 ft
857.9 ft
BRIDGE PLUG
ALL DEPTHS BELOW GROUND SURFACE   NOT TO SCALE

21
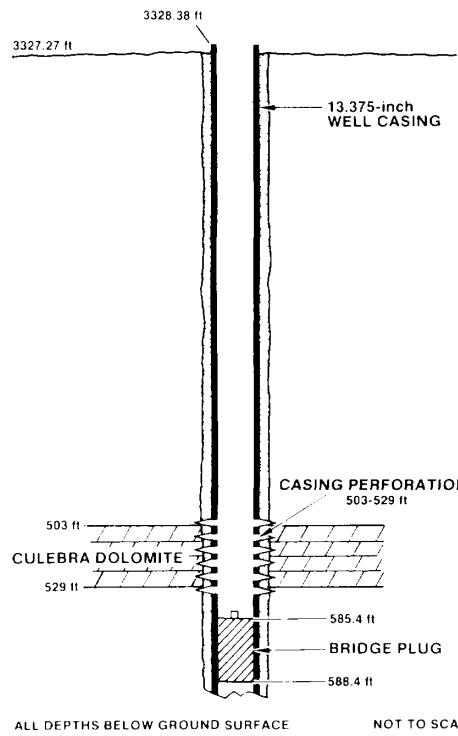
Figure 3-9.   Configuration of Observation Well Cabin Baby-1.
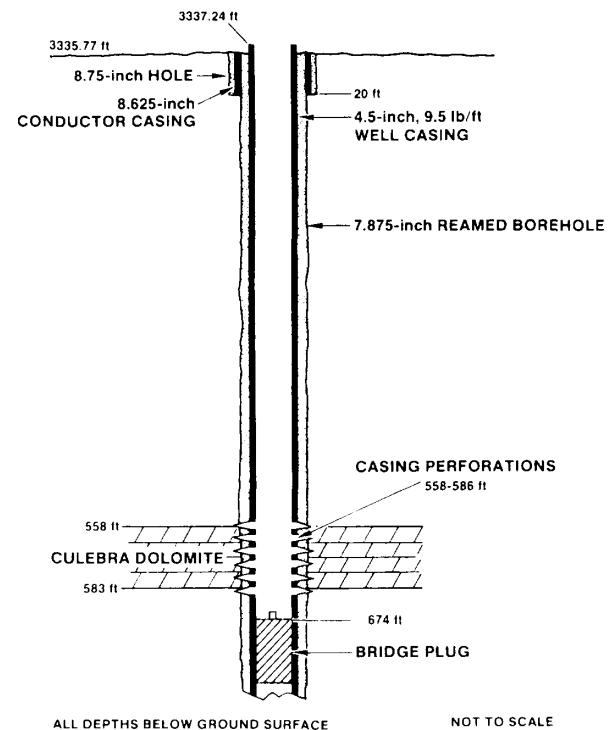
Figure 3-11. Configuration of Observation Well P-17.
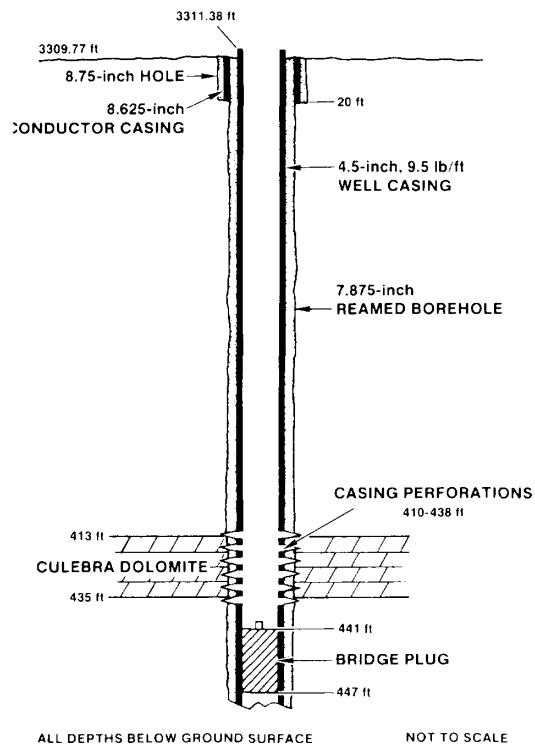
Figure 3-10. Configuration of Observation Well P-15.
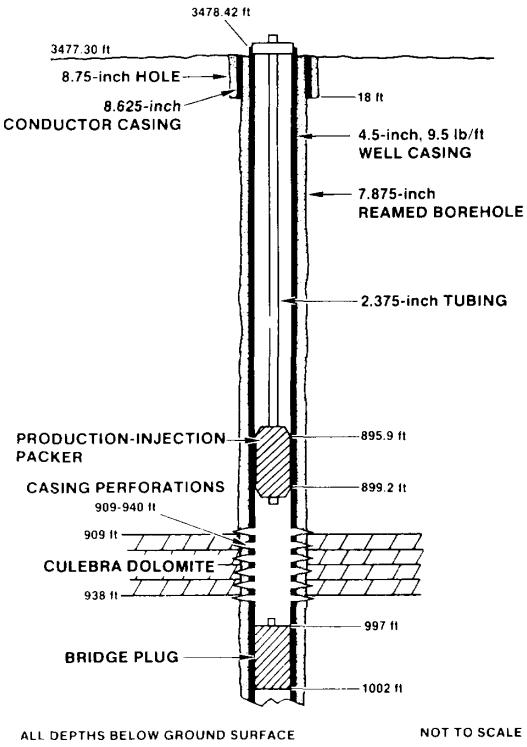
Figure 3-12. Configuration of Observation Well P-18.

22
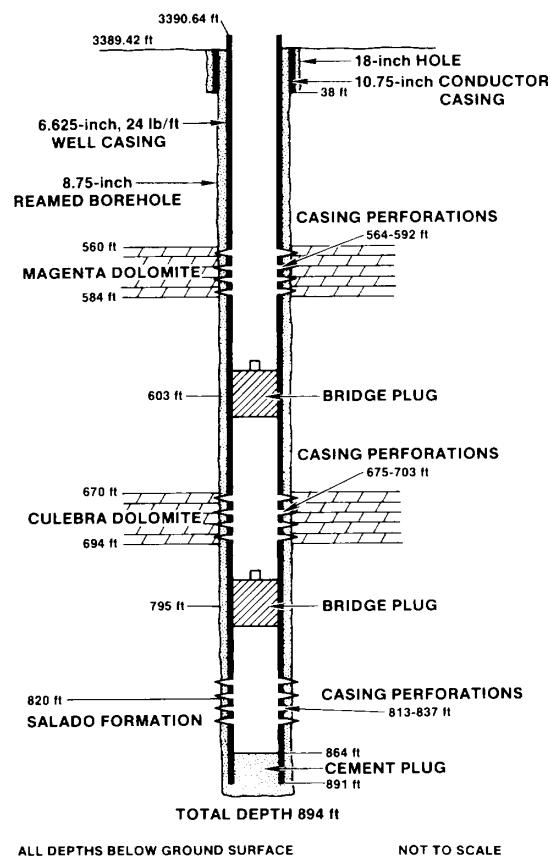
Figure 3-13. **Configuration of Magenta Observation Well H-3b1.**
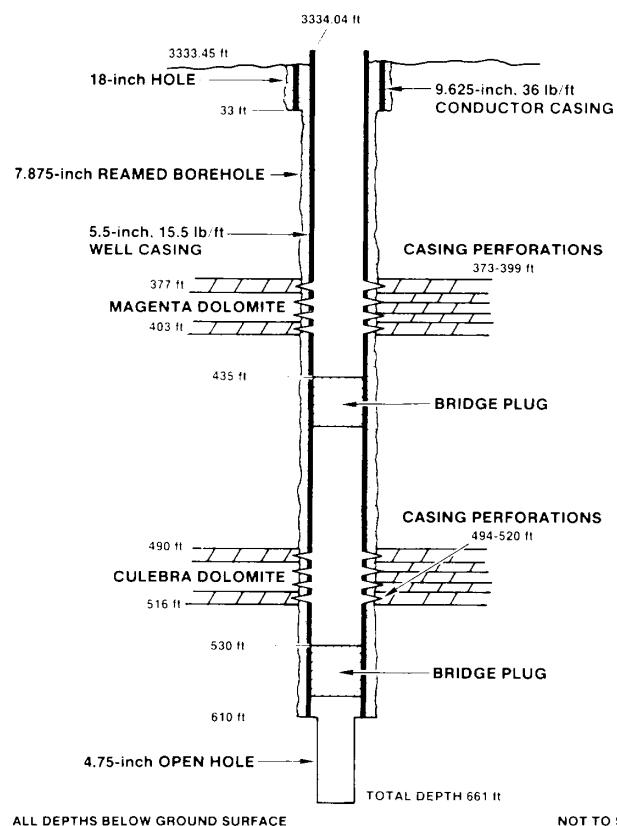
Figure 3-14. **Configuration of Magenta Observation Well H-4c.**

4. TEST INSTRUMENTATION

The instrumentation and procedures used for the H-11 testing are described in detail in Stensrud et al. (1988b and in preparation). Brief discussions of the equipment used for the H-11b4 DSTs and slug tests, the H-11b4 pumping test, and the H-11 multipad pumping test are also presented below. Additional information on hydraulic-test procedures can be found in Beauheim (1987c).

NOTE: The use of brand names in this report is for identification only, and does not imply endorsement of specific products by Sandia National Laboratories.

4.1 H-11b4 DSTs and Slug Tests

The downhole equipment used for the H-11b4 DSTs and slug tests was a single-packer Hydrological Test Tool supplied by Baker Service Tools (BST) of Houston, Texas. The single-packer Hydrological Test Tool consists of a water-inflatable packer, a circulating valve, a shut-in tool, a J-slot tool used for packer inflation and deflation, various crossovers, and a sensor carrier containing three quartz-crystal temperature-compensated pressure transducers (Figure 4-1). Two of the transducers are ported through the tool to the hole below the packer and the third transducer is ported out to the hole above the packer. A seamless, stainless-steel, two-conductor wireline connects the transducers to the data-acquisition system (DAS) at the surface. The Hydrological Test Tool was lowered to the desired test depth on 2.375-inch tubing. The configuration of the tool in H-11b4 during the testing is shown in Figure 4-2.

The DAS at the surface for the H-11b4 DSTs and slug tests consisted of a Hewlett Packard (HP)-9000 Model 310 desktop computer for system control, a BST SC-2 interface unit which linked the downhole transducers with the rest of the system, an HP-5316A universal counter which measured the frequencies of the current pulses sent by the transducers, an HP-9133L disk drive for data storage, an Epson FX-85 printer for real-time data listing, and an HP-9872S plotter for real-time data plotting (Figure 4-3). The HP-5316A universal counter is calibrated by the Sandia Standards Laboratory every six months, and the transducers were calibrated in a

Baker Service Tools laboratory before being sent to the field. The data-acquisition software was written and is maintained by G-Tech Corporation of Houston. Additional information on this data-acquisition system can be found in Stensrud et al. (1988b).

4.2 H-11b4 Pumping Test

Both downhole and uphole equipment was used during the H-11b4 pumping test to provide flow control and fluid-pressure measurements. The downhole equipment in the pumping well, H-11b4, consisted of a 3-horsepower (hp) Red Jacket 32BC pump suspended below a Baski air-inflatable packer on 2.375-inch tubing, with Druck PDCR-830 and PDCR-10/D strain-gauge pressure transducers strapped to the pipe above the packer (Figure 4-4). The PDCR-830 transducer was connected to the test interval below the packer via a feed-through line through the packer. The PDCR-10/D transducer measured the fluid pressure in the well annulus above the packer. The uphole equipment consisted of a backpressure ball valve, a Precision totalizing flow meter, a Dole orifice valve, and a calibrated standpipe to provide a backup means of estimating the pumping rate (Figure 4-5).

The downhole equipment in H-11b1 consisted of a Baski air-inflatable packer set in the well casing on 1.5-inch galvanized line pipe and a Druck PDCR-10/D transducer which accessed the test interval via a feed-through line through the packer (Figure 4-4).

The DAS at the surface for the H-11b4 pumping test consisted of an HP-9000 Model 310 desktop computer for system control, Tektronix PS-503A dual power supplies to provide power to the transducers, an HP-3495A signal scanner for channel switching, an HP-3455A digital voltmeter (DVM) to measure the transducer output, an HP-9133L disk drive for data storage, an Epson FX-85 printer for real-time data listing, and an HP-9872S plotter for real-time data plotting (Figure 4-6). The HP-3455A DVM is calibrated by the Sandia Standards Laboratory every six months, and the transducers were calibrated in the field using a Heise pressure gauge before installation in the wells. The data-acquisition software was written and is
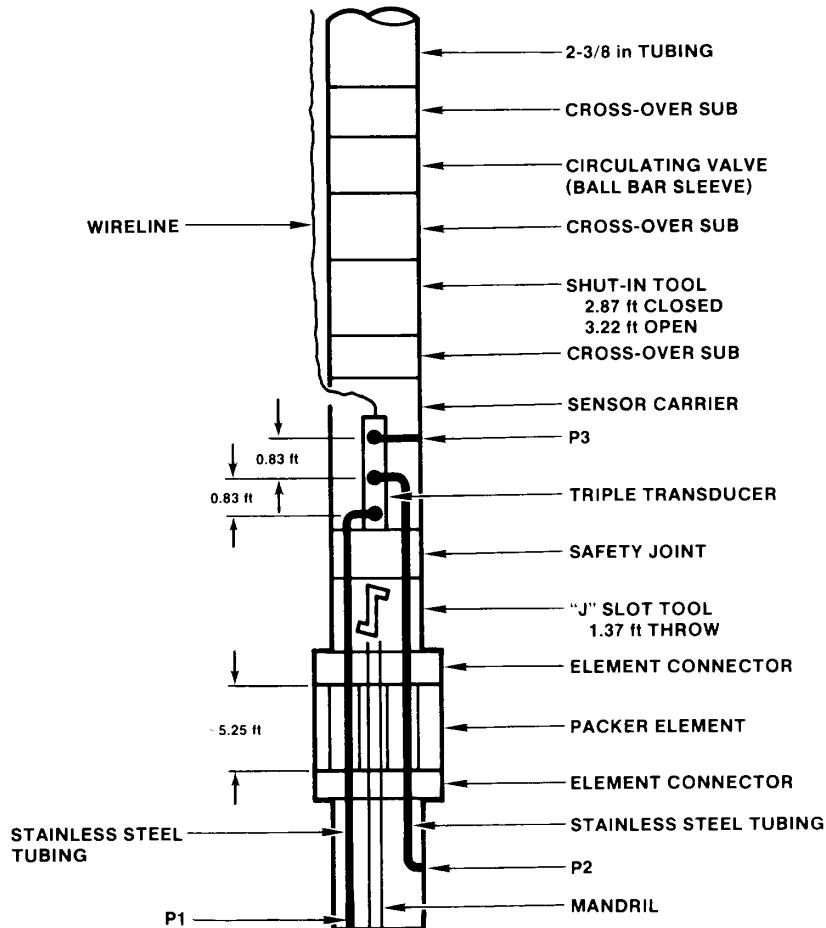
Figure 4-1. Baker Service Tools Hydrological Test Tool.

maintained by G-Tech Corporation of Houston. Additional information on this data-acquisition system can be found in Stensrud et al. (1988b).

4.3 H-11 Multipad Pumping Test

The flow-control and fluid-pressure-measurement equipment used in the pumping well, H-11b1, was very similar to that used for the H-11b4 pumping test (Section 4.2). The only differences were that the discharge line from the pump to the surface was 1.5-inch-galvanized line pipe instead of 2.375-inch tubing, and

an additional Druck PDCR-10/D strain-gauge pressure transducer was strapped to the pipe above the packer and connected to the test interval via a feed-through line through the packer as a backup to the primary test-interval transducer (Figure 4-7). The uphole equipment was identical to that used for the H-11b4 pumping test (Figure 4-5).

The three observation/tracer-injection wells on the H-11 hydropad were equipped with packers, pressure transducers, and tracer-injection assemblies (Figure 4-7). Each tracer-injection assembly was

H-11b4

TO DAS
(SEE FIG. 4-3)
3410.01 ft
3410.89 ft

27 ft

16-in. HOLE
8.625-in.,28 lb/ft
CONDUCTOR CASING

2.375-in. TUBING

7.875-in.
REAMED BOREHOLE

WIRELINE

5.5-in.,15.5 lb/ft
WELL CASING

692.6 ft

BST
HYDROLOGICAL
TEST TOOL
(SEE FIG. 4-1)

714 ft
723 ft

SENSOR CARRIER
P3:702.42 ft
P2:703.25 ft
P1:704.07 ft

PACKER 716.9-721.1 ft

725.5 ft

CULEBRA
DOLOMITE

746 ft

4.75-in.
OPEN HOLE
TOTAL DEPTH 765 ft

NOT TO SCALE
ALL DEPTHS BELOW GROUND SURFACE

Figure 4-2.   Configuration of H-11b4 During DSTs and Slug Tests.

placed in the open Culebra interval of a well beneath a 4.5-inch Baski air-inflatable packer set near the bottom of the well casing on 2.375-inch tubing. A 1.5-inch Baski air-inflatable packer was set inside the mandril of the larger packer, and controlled access to the tracer-injection assembly below. Two Druck strain-gauge transducers were strapped to the tubing above each larger packer. One transducer was connected to the Culebra interval via a feed-through line through the packer, and the other transducer measured fluid pressure in the well annulus above the packer. All of these transducers were Druck PDCR-10/D's except for the test-interval transducer in H-11b4, which was a Druck PDCR-830.

The DAS at the surface at the H-11 hydropad consisted of an HP-9000 Model 310 desktop computer for system control, Tektronix PS-503A dual power supplies to provide power to the transducers, an HP-3495A signal scanner for channel switching, an

HP-3456A DVM to measure the transducer output, an HP-9133L disk drive for data storage, a Weathertronics Model 7105-A analog-output barometer, an Epson FX-85 printer for real-time data listing, and an HP-7475A plotter for real-time data plotting (Figure 4-8). The HP-3456A DVM is calibrated by the Sandia Standards Laboratory every six months, and the transducers were calibrated in the field using a Heise pressure gauge before installation in the wells. The barometer is sent back to the factory for calibration approximately every six months. The data-acquisition software was written and is maintained by G-Tech Corporation of Houston. Additional information on this data-acquisition system can be found in Stensrud et al. (in preparation).

Water levels in distant observation wells were measured using a total of seven Solinst water-level meters (Stensrud et al., in preparation) during the H-11 multipad pumping test. Dedicated Solinst water-level meters were mounted in boxes on the DOE-1, H-3b2, H-15, H-17, P-17, and P-18 wellheads for the duration of the test. The probes were kept in the wells a few feet above the water surfaces between readings. Another Solinst meter was used to measure water levels in the other key observation wells, and also to make the less-frequent regional water-level measurements in some of the more-distant wells. In this manner, a single instrument was used consistently at each well throughout the test.
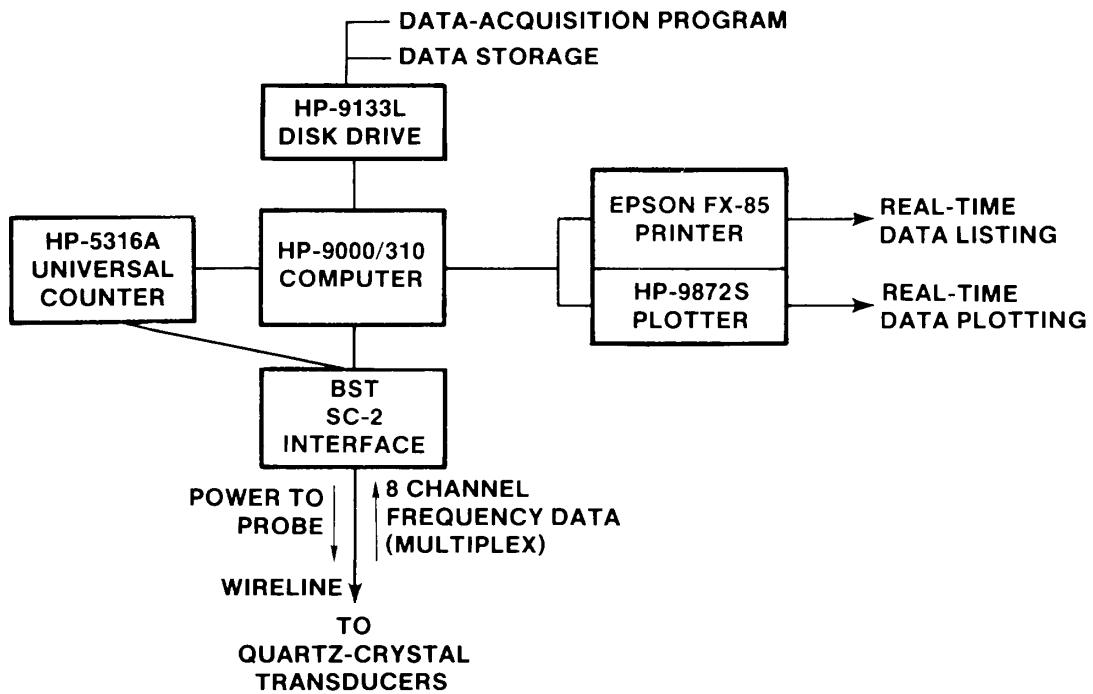
Figure 4-3. Data-Acquisition System for H-11b4 DSTS and Slug Tests.
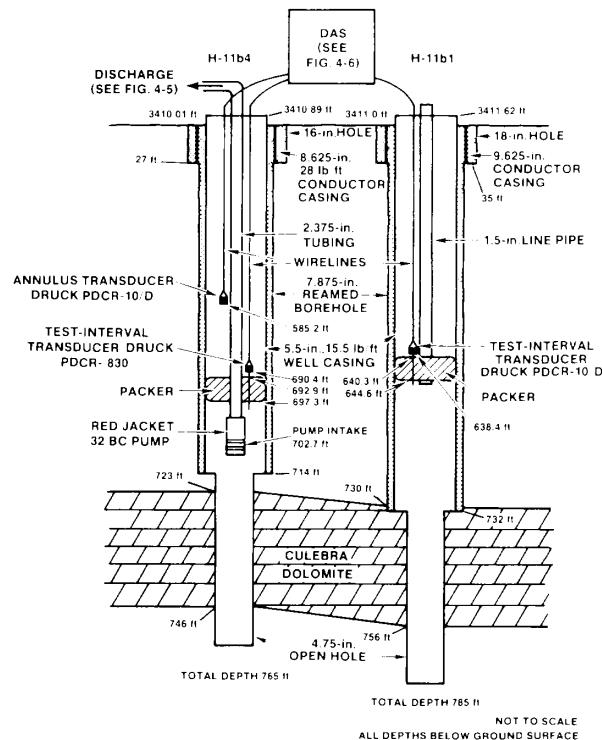
Figure 4-4. Configurations of H-11b1 and H-11b4 During the H-11b4 Pumping Test.

27

DISCHARGE-MEASUREMENT AND FLOW-REGULATION SYSTEM
FOR H-11 PUMPING TESTS
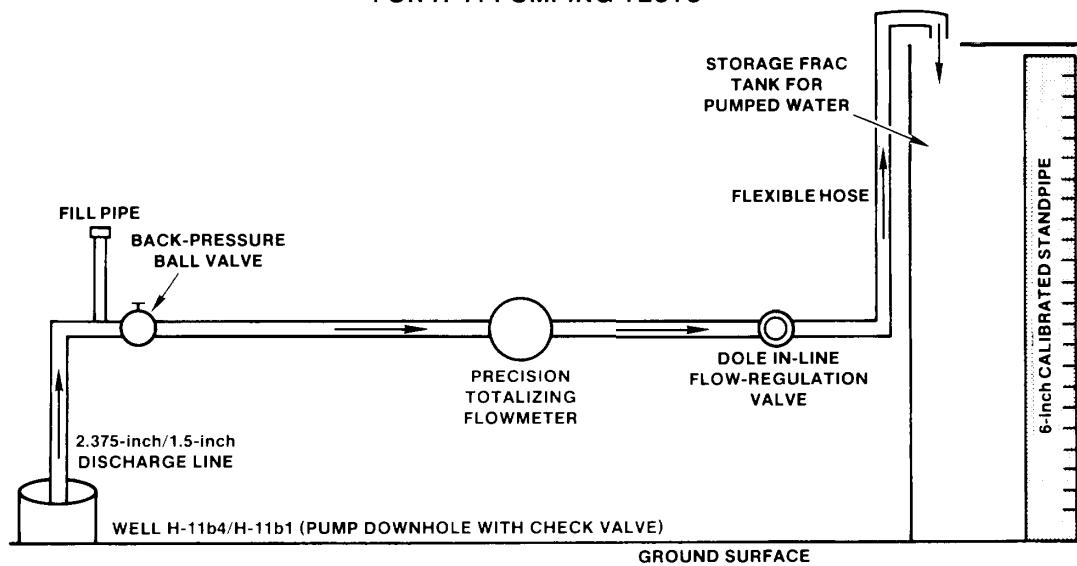
NOT TO SCALE

Modified from Stensrud et al. (1988b)

Figure 4-5. Discharge-Measurement and Flow-Regulation System for H-11 Pumping Tests.
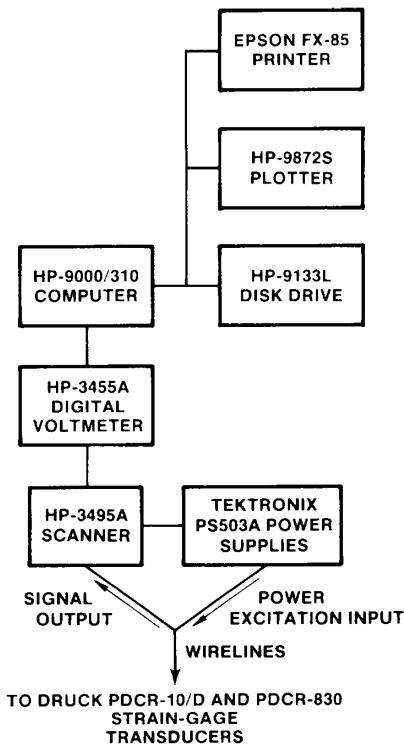
Figure 4-6. Data-Acquisition System for the H-11b4 Pumping Test.
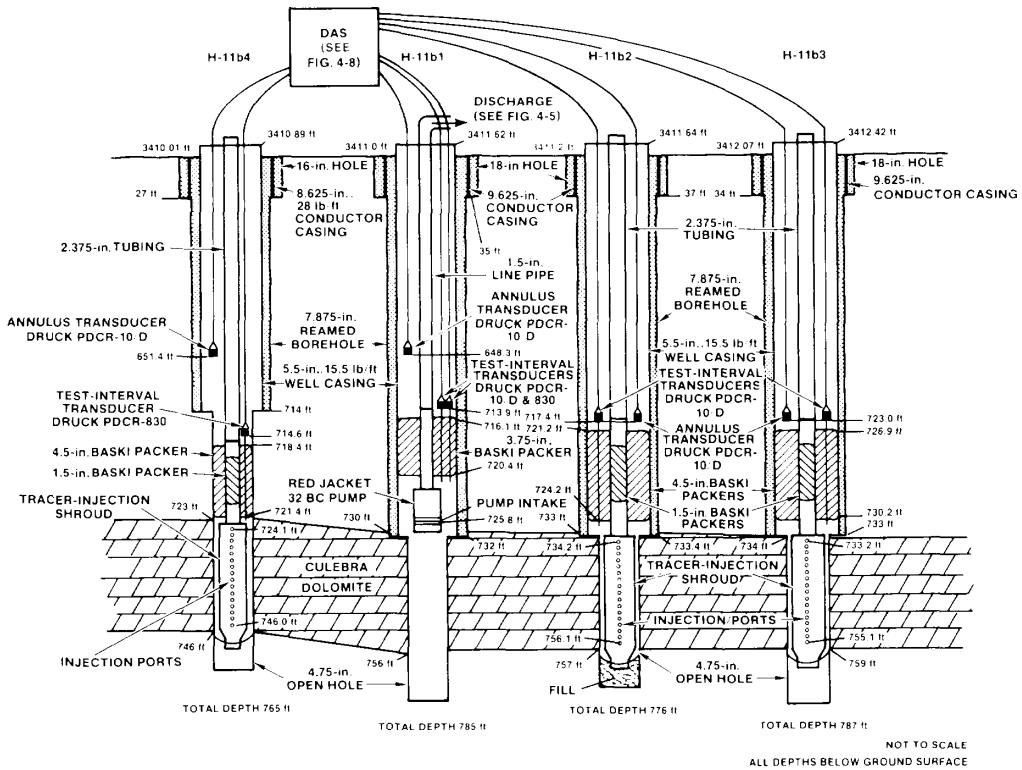
Figure 4-7. Configurations of H-11 Wells During the H-11 Multipad Pumping Test.
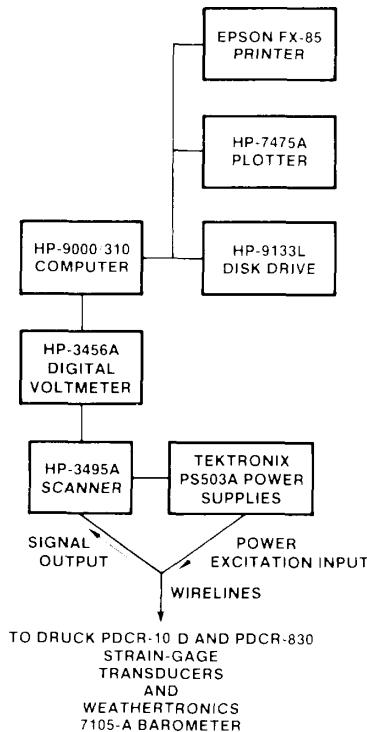
Figure 4-8. Data-Acquisition System for the H-11 Multipad Pumping Test.

29

5. TEST DATA

Extensive fluid-pressure, water-level, pumping-rate, and/or barometric-pressure data were collected during the H-11 testing. For the wells monitored by the DAS, more fluid-pressure data were collected than needed or were practically useful for analysis. Hence, abridged data sets were created by manually selecting data points to give an adequate logarithmic distribution of data through time for analysis. No other criteria were involved in the data abridgment.

During the pumping tests, some wells apparently responded not only to the pumping associated with the tests, but also to earlier hydraulic tests at different locations, barometric-pressure fluctuations, drainage into the WIPP shafts, and other factors. The factors influencing the responses observed at each well are discussed below, along with any compensations made to the data. Additionally, because the analysis techniques employed to interpret the pumping-test data require the use of pressures rather than water levels, water-level data were converted to pressure data. These conversions are also discussed below.

5.1 H-11b4 DSTs and Slug Tests

The fluid-pressure data collected during the DSTs and slug tests performed at H-11b4 on March 22, 1988 (calendar day 82) are shown in Figure 5-1. DSTs did not prove to be a suitable technique for evaluating the hydraulic properties of the Culebra at H-11b4. When the test interval was shut-in following each of the DST flow periods, 94- to 95-percent pressure recovery occurred by the first data scan six seconds later. Thus, adequate data for analysis could not be collected. The slug-withdrawal tests provided more useful data sets. No corrections or compensations of any kind were made to the slug-test data before analysis.
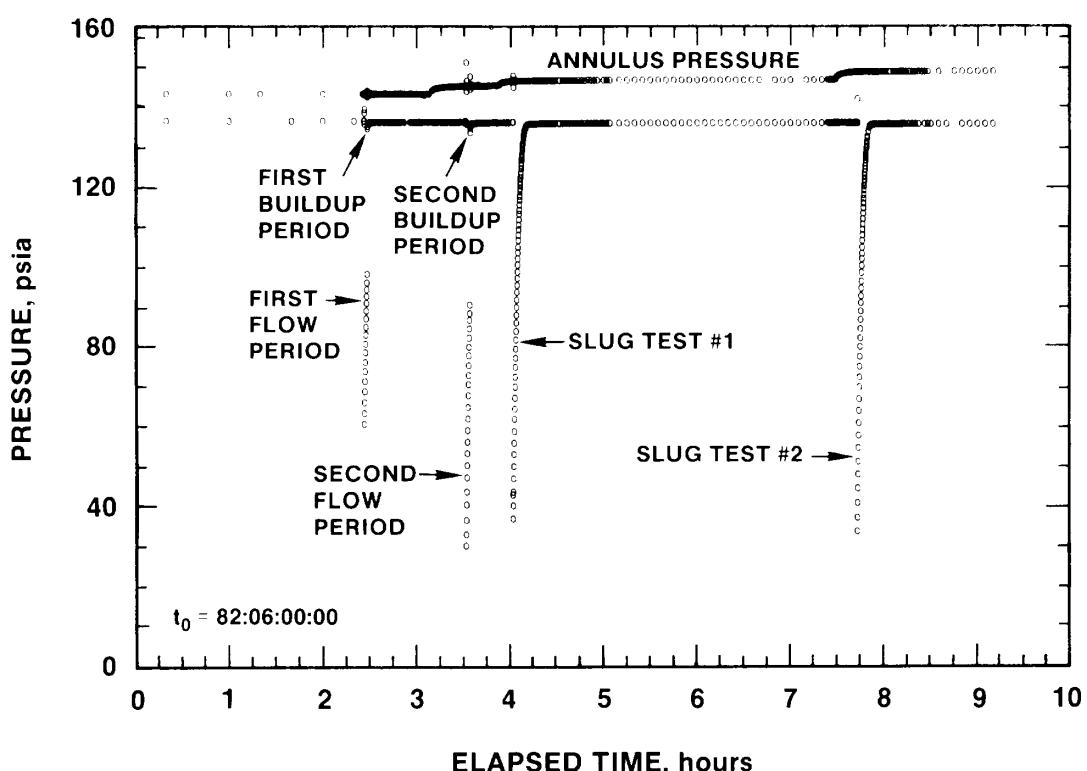
Figure 5-1.   H-11b4 DSTs and Slug Tests Pressure Record.

The pressure in the annulus between the tubing and casing above the packer in H-11b4 increased whenever the tubing was swabbed, as some of the swabbed fluid drained into the casing (Figure 5-1). The annulus pressure was stable, however, during the different phases of testing, indicating no leakage of fluid around the packer. A complete tabulation of the data from the H-11b4 DSTs and slug tests is presented in Stensrud et al. (1988b).

5.2 H-11b4 Pumping Test

H-11b4 was pumped for 50 hr from April 4 to 6, 1988 (calendar days 95 to 97). The fluid-pressure data collected from wells H-11b4 and H-11b1 during the pumping test are shown in Figure 5-2. One modification of the data from H-11b4 was required for analysis. When a pump is turned on, particularly in a packer-isolated interval, an initial instantaneous pressure drop may occur. This pressure drop is related to turbulence in the wellbore caused by the pump or to the

discontinuity at the rock/well interface or both rather than to the aquifer response (Nind, 1965). This pressure drop may be maintained for the duration of pumping, and an instantaneous recovery may be observed when the pump is turned off. Analyses using pressure-change data must ignore these turbulence-related pressure surges, and examine only the aquifer response. When the pump was turned on in H-11b4, the pressure dropped 5.44 psi between the time the pump was turned on and the next data scan 10 seconds later (Figure 5-2). Logarithmic extrapolation backwards in time from the next several data points indicates that only about 1.0 psi of the initial pressure drop was aquifer response. When the pump was turned off, the pressure recovered 5.95 psi within the first 10 seconds. Logarithmic extrapolation backwards from the next several recovery points indicates that only about 0.7 psi of the observed pressure rise was aquifer response. These extrapolations were used to define the starting pressures for calculation of test-related drawdowns and recoveries.
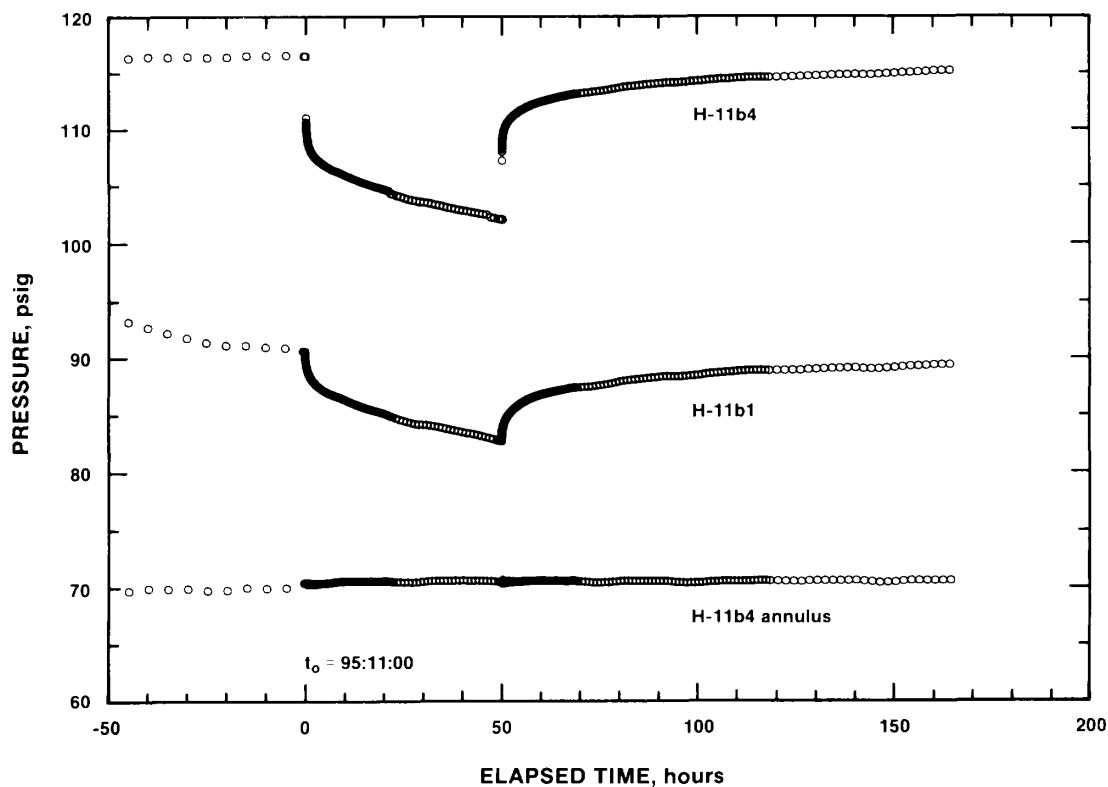
Figure 5-2. H-11b4 Pumping Test Pressure Record.

Pressures measured by all three transducers used for the test showed minor congruent diurnal fluctuations. Whether these fluctuations were related to daily temperature extremes affecting the DAS or to barometric-pressure variations is unknown; no barometric-pressure data were collected during this test. No corrections were made for these fluctuations. Their effects on the test analysis are discussed in Section 6.2. Apart from the fluctuations discussed above, the annulus pressure in H-11b4 was stable throughout the test, indicating no leakage of fluid around the packer. A complete tabulation of the data from the H-11b4 pumping test is presented in Stensrud et al. (1988b).

A total of 18,162 gallons of water were pumped from H-11b4 during the pumping test, at an average rate of 6.05 gpm. The pumping rate was constant within five percent throughout the test, ranging only from 6.00 to 6.30 gpm. The pumping-rate data from the test are tabulated in Stensrud et al. (1988b).

5.3 H-11 Multipad Pumping Test

The H-11 multipad pumping test began on May 5, 1988 (calendar day 126). The pump was turned off exactly 63 days later on July 7, 1988 (calendar day 189). Recovery monitoring continued on the H-11 hydropad until November 1, 1988 (calendar day 306), and at more distant locations through December 1988. Three qualitatively different types of data related to the hydraulic aspects of the H-11 multipad/tracer test were collected: fluid-pressure and water-level data; pumping-rate data; and barometric-pressure data. These data sets are discussed below. Data pertaining to the tracer aspects of the test will be presented and discussed in a later report.

5.3.1 Fluid-Pressure and Water-Level Data. Extensive fluid-pressure or water-level data or both were collected from the pumping well and key observation wells before the H-11 multipad pumping test began, during the 63-day (1512-hr) pumping period, and for up to 170 days (4062 hr) of recovery. In many instances, the observed data were affected not only by the pumping test, but also by barometric-pressure changes and by residual hydraulic stresses from earlier hydraulic tests at other locations, well completions, shaft drainage, and/or other factors. Compensations could be made for the barometric

effects, using the data provided by the barometer wired to the DAS (Section 5.3.3). No quantitative compensations could be made, however, for the residual hydraulic stresses affecting the observed responses because of inadequate data on the timing, location, and magnitude of the stresses. The stresses were considered qualitatively, however, in evaluating the reliability and meaningfulness of the data interpretations presented below. Additionally, because the analysis techniques employed to interpret the data require the use of pressures rather than water levels, water-level data were converted to pressure data. The observed data and modifications made to the data to aid analysis are discussed below.

The data sets used for analysis of the H-11 multipad test, both as measured and as modified, are tabulated in Appendix A. More extensive tabulations of the measured data are contained in Stensrud et al. (in preparation).

5.3.1.1 H-11b1. The pressure in the Culebra test interval in the pumping well, H-11b1, was monitored during the test by two pressure transducers so that data would not be lost if a single transducer failed. Both transducers remained operational for the duration of the test, and consistently registered within one psi of each other. Because the data from the two transducers were redundant, the data from the Druck PDCR-830 transducer labelled S1 by the DAS (see Appendix A, Table A-1) were arbitrarily selected for analysis, and no use was made of the data from the other transducer (S2). The DAS collected more data than were necessary for analysis. Hence, an abridged data set was created by manually selecting points to give an adequate logarithmic distribution of data through time for analysis (Appendix A, Table A-1). No other criteria were involved in the data abridgment.

When the pump was turned on in H-11b1, an instantaneous pressure drop occurred (Figure 5-3) similar to that which occurred at the start of the H-11b4 pumping test (Section 5.2, Figure 5-2). The pressure drop at H-11b1, however, was about 31.2 psi, much larger than the 5.4-psi drop observed at H-11b4 even though the same pump was used at both wells and the flow rates were almost equal. At the beginning of the recovery period, the pressure in H-11b1 rose from 69.3 to 106.1 psig between the time the pump went off and
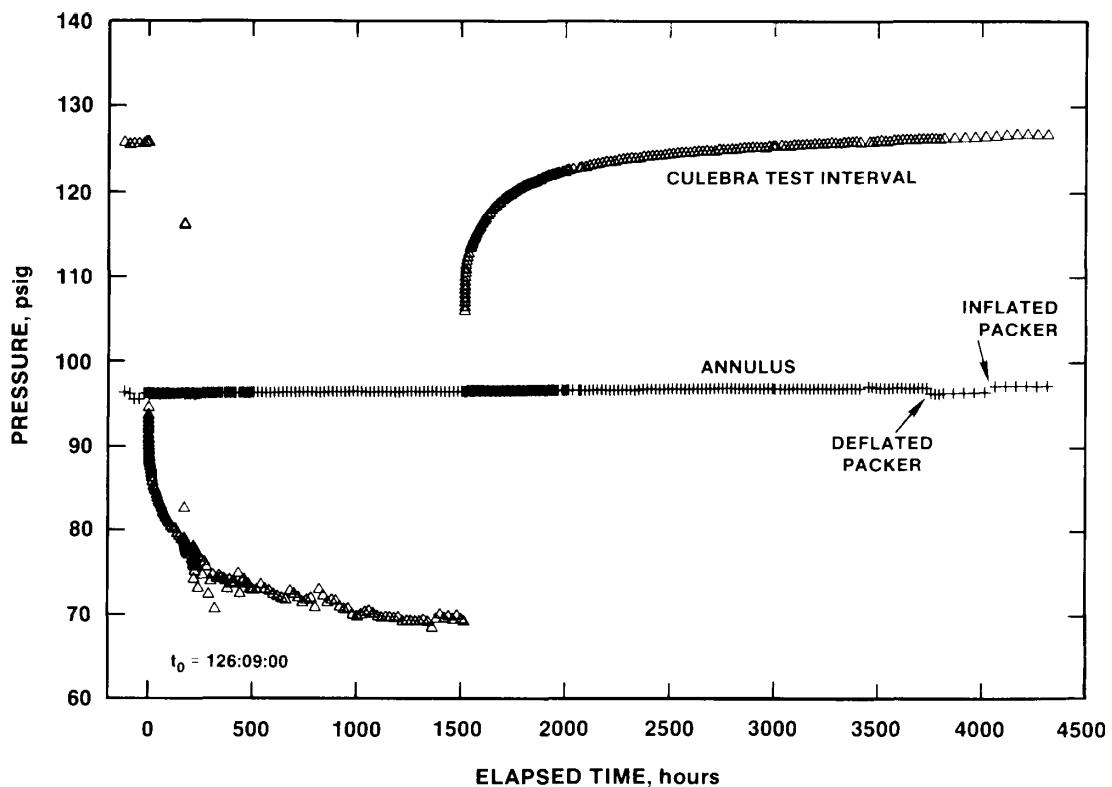
Figure 5-3. H-11b1 Pressure Record During the H-11 Multipad Pumping Test.

the first data scan 11 seconds later, an increase of 36.8 psi. These large pressure changes may indicate that more turbulence is created when water enters the H-11b1 wellbore than when water enters the H-11b4 wellbore. Logarithmic extrapolation backwards from the first several data points from the recovery period indicates that only about 0.5 psi of the pressure rise observed was an aquifer response; the remainder appears to be related to well inefficiency. Accordingly, a value of 105.6 psig was used as the starting point for pressure-change calculations for the H-11b1 recovery.

The packer in H-11b1 was deflated temporarily during the recovery period from 3749 to 4057 total elapsed test hours. This deflation had little effect on the pressure observed in the test interval (Figure 5-3) because the Culebra pressure and the pressure from the column of water above the packer were very nearly equal at this time.

Figure 5-3 also shows the pressure measured in the annulus between the casing and pipe above the packer in H-11b1 during the H-11 multipad test. This transducer, located 65.55 ft higher in the well than the test-interval transducer (Figure 4-7), showed a gradual increase in pressure totalling less than one psi during the test. This apparent rise may have been caused by transducer "drift"; i.e., a nonconstant relationship between pressure-induced strain and transducer output. No evidence was seen of communication between the annulus and the test interval during the test.

5.3.1.2 H-11b2. The fluid-pressure data collected from well H-11b2 during the H-11 multipad test are shown in Figure 5-4. The test-interval transducer appeared to begin malfunctioning 500 to 700 hr after pumping began, as it failed to show a consistent drawdown trend for the rest of the pumping period.

33
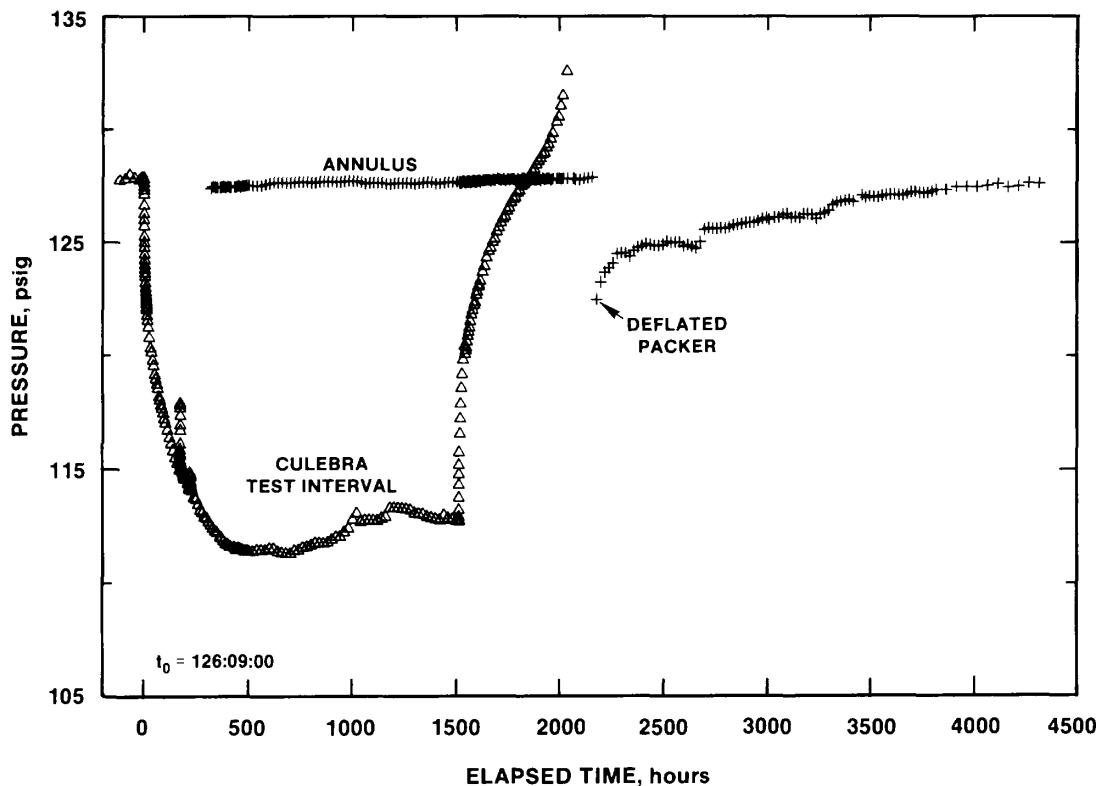
Figure 5-4. H-11b2 Pressure Record During the H-11 Multipad Pumping Test.

The transducer appeared to be functioning properly for about the first 27 hr of recovery, but then began behaving erratically, first showing a slight pressure decrease, then showing a rapid pressure rise to unrealistic values. After 581 hr of recovery, the transducer failed entirely.

The transducer measuring the fluid pressure in the annulus between the casing and tubing above the packer in H-11b2 provided meaningless data for the first 320 hr of the pumping test because of a short-circuit in a cable. The cable was repaired on May 18, 1988 (320 test hr). From that date until August 3, 1988 (2164 test hr), the apparent annulus pressure increased by about 0.5 psi in an erratic fashion (Figure 5-4). No decrease in annulus pressure during the pumping period, which would have been evidence of communication between the annulus and the test interval, was observed. On August 3, 1988 (2164 hr since the test had begun), the packer in H-11b2 was deflated so that the annulus

transducer could measure the Culebra pressure in place of the failed test-interval transducer. The annulus transducer was located at the same depth in the well as the test-interval transducer (Figure 4-7), so the two transducers should have registered similar pressures with the packer deflated. The final pressure measured by the annulus transducer at the end of the recovery period was 127.7 psig, very similar to the 127.8 psig measured by the test-interval transducer at the start of the test (Appendix A, Table A-1).

5.3.1.3 H-11b3. The fluid-pressure data collected from well H-11b3 during the H-11 multipad test are shown in Figure 5-5. The test-interval transducer appears to have functioned properly throughout the test. During the recovery period, however, the test-interval pressure reached higher values than were observed before the test began: the pressure when pumping began was 136.8 psig, and on October 7, 1988 (3717 test hr) the pressure was 140.6 psig
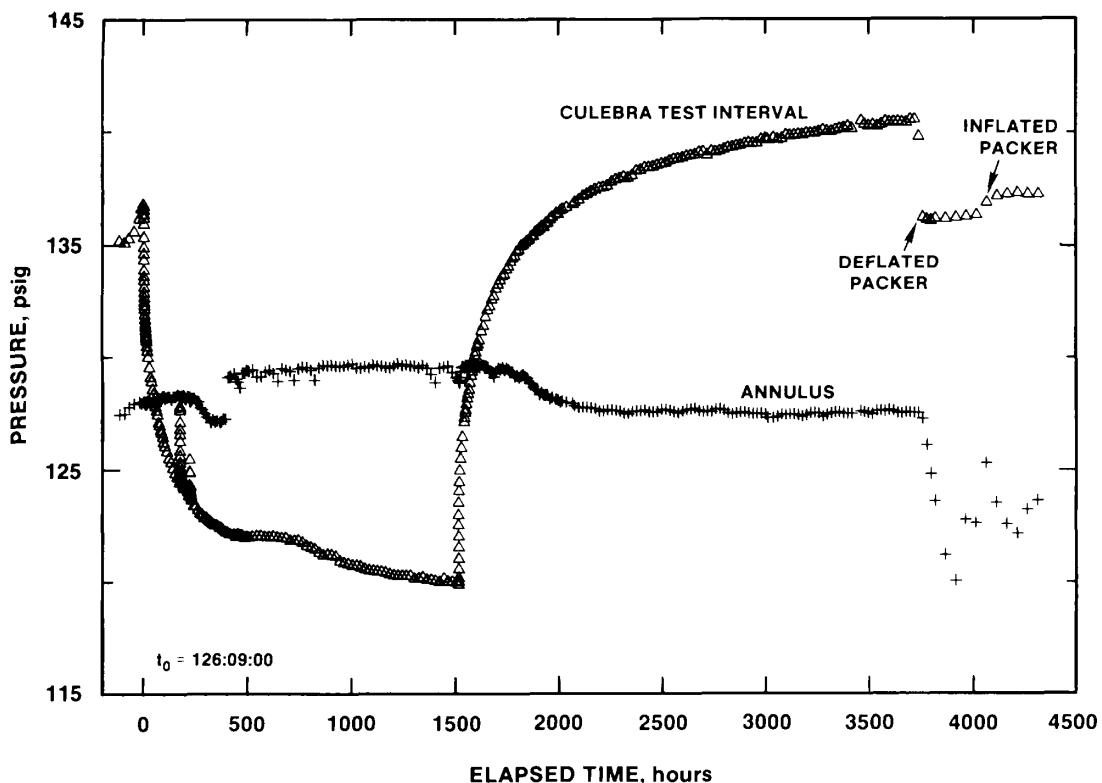
Figure 5-5. H-11b3 Pressure Record During the H-11 Multipad Pumping Test.

(Appendix A, Table A-1). Water produced from H-11b3 had been notably effervescent during pumping for the WIPP Water Quality Sampling Program (WQSP; Randall et al., 1988), raising the possibility that the observed "overpressurization" in H-11b3 might be related to an accumulation of free gas. Gas pressure in the wellbore could be greater than the water pressure in the surrounding Culebra because gas cannot displace water in a saturated porous medium until the threshold displacement pressure is reached. That is, gas pressure must overcome not only the water pressure in the rock, but also the surface tension of the water in the rock pores (Ibrahim et al., 1971). The packer in H-11b3 was therefore deflated on October 8, 1988 (3749 hr after testing began) to release any potentially trapped gas. The test-interval pressure then decreased and oscillated slightly as the Culebra and annulus pressures equilibrated, stabilizing at about 136.2 psig. The pressure increased slightly over the next 13 days to about 136.4 psig, still below the

starting pressure of 136.8 psig. The packer was reinflated on October 21 (4057 test hr), and the pressure again exceeded its starting value by rising to about 137.3 psig over the next 11 days. Although not conclusive, these observations are consistent with the accumulation and pressurization of free gas whenever the Culebra interval is isolated by a packer. Whether this hypothesized gas is a natural component of Culebra waters, or is generated in or around the well through degradation of drilling-fluid additives or tracers is not known.

The data from the annulus transducer in H-11b3 do not appear to be reliable. At the start of the test, the annulus transducer indicated a pressure over eight psi lower than that indicated by the test-interval transducer (Figure 5-5), even though both transducers were located at the same depth in the well (Figure 4-7). During the test, the annulus transducer showed a number of unexplained pressure fluctuations, particu-

larly late in the recovery period after the packer was deflated.

5.3.1.4 H-11b4. The fluid-pressure data collected from well H-11b4 during the H-11 multipad test are shown in Figure 5-6. The test-interval transducer appeared to function properly during the pumping period, but failed approximately 900 hr after recovery began. Before the transducer failed, however, it indicated a pressure of about 134 psig, higher than the 130.26 psig measured before pumping began. Accumulation of gas beneath the packer, as discussed in Section 5.3.1.3 for well H-11b3, is a possible explanation for this apparent "over-recovery".

The H-11b4 annulus transducer appears to have functioned properly throughout the test. The indicated pressure was constant within 0.5 psi until the packer was deflated on August 30, 1988 (2811 test hr). The

packer was deflated so that the Culebra pressure could be monitored by the annulus transducer after the test-interval transducer had failed. The annulus transducer showed a gradual increase in Culebra pressure until the packer was reinflated on October 21, 1988 (4057 test hr). Just before the packer was reinflated, the Culebra pressure was 99.0 psig. This value is only slightly higher than the 98.2 psig measured in the annulus shortly after the packer was originally inflated before pumping began (Appendix A, Table A-1), when the annulus and Culebra pressures should have been nearly in equilibrium (the annulus transducer was located 63.2 ft higher in the well than the test-interval transducer; Figure 4-7). The fact that little over-recovery of Culebra pressure was noted when the packer was deflated tends to confirm the supposition that the over-recovery was related to gas accumulation.
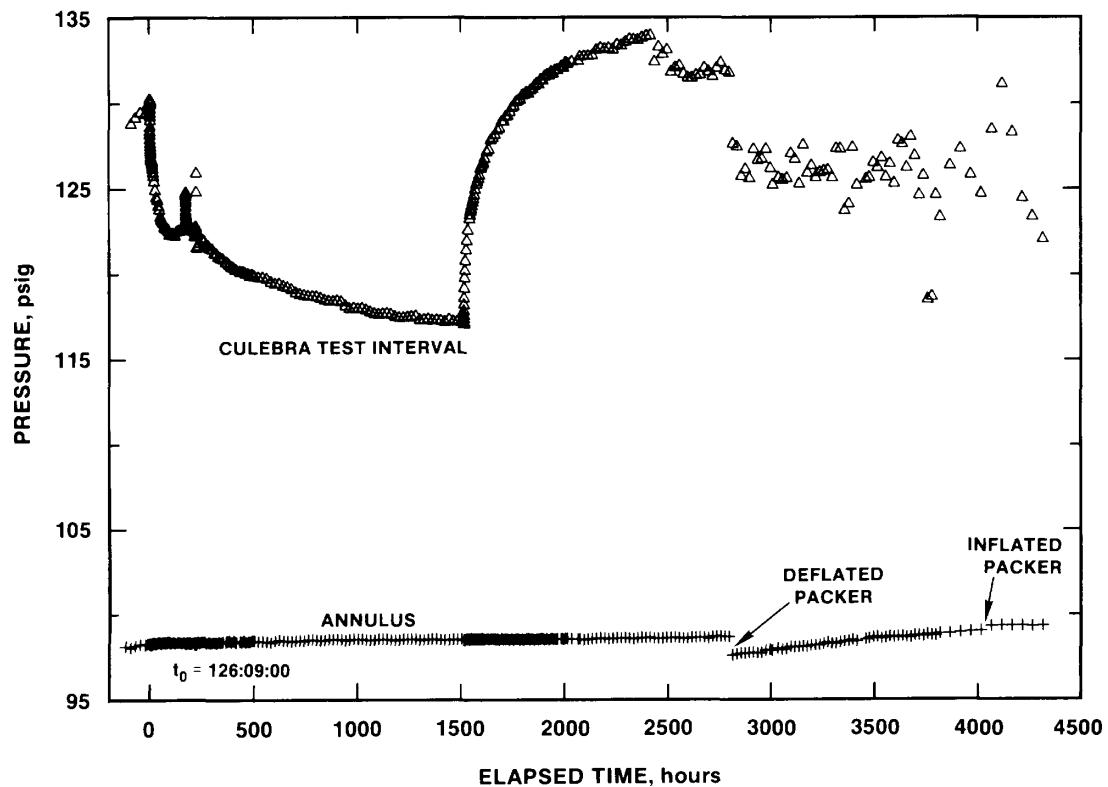
Figure 5-6. H-11b4 Pressure Record During the H-11 Multipad Pumping Test.

5.3.1.5 DOE-1. The water-level response at DOE-1 during the H-11 multipad pumping tests was a complex superposition of responses to numerous hydraulic stresses imposed over the preceding several years at the WIPP site. Figure 5-7 shows the water-level history at DOE-1 since mid-1986. Also shown on the figure are periods when the Culebra was being pumped at DOE-1 itself or at nearby wells as part of the WIPP WQSP or for well development. The figure shows that water levels in DOE-1 respond strongly to pumping at the H-3 and H-11 hydropads. The flow rate during WQSP pumping at H-15 is typically over an order of magnitude lower than at H-3 and H-11 (Randall et al., 1988), and consequently the H-15 pumping has little effect on DOE-1 water levels. Only pumping periods of two days or greater duration are noted on Figure 5-7; over 78 hr of intermittent pumping

also occurred at H-11b1, H-11b2, and H-11b4 on 18 days between January 12 and April 30, 1988 (1986 calendar days 742 to 851).

Because of the many recent hydraulic stresses on the Culebra, the water level in DOE-1 was not stabilized before the H-11 multipad pumping test began (Figure 5-8). As a result, the response to the H-11 multipad test is superimposed on a general recovery from the combination of events listed on Figure 5-7. This superposition of responses results in apparently less drawdown and more recovery being observed than would have been observed had the water level been stable before the test, as the apparent drawdown is subtracted from a rising trend, while the apparent recovery is added to the rising trend.
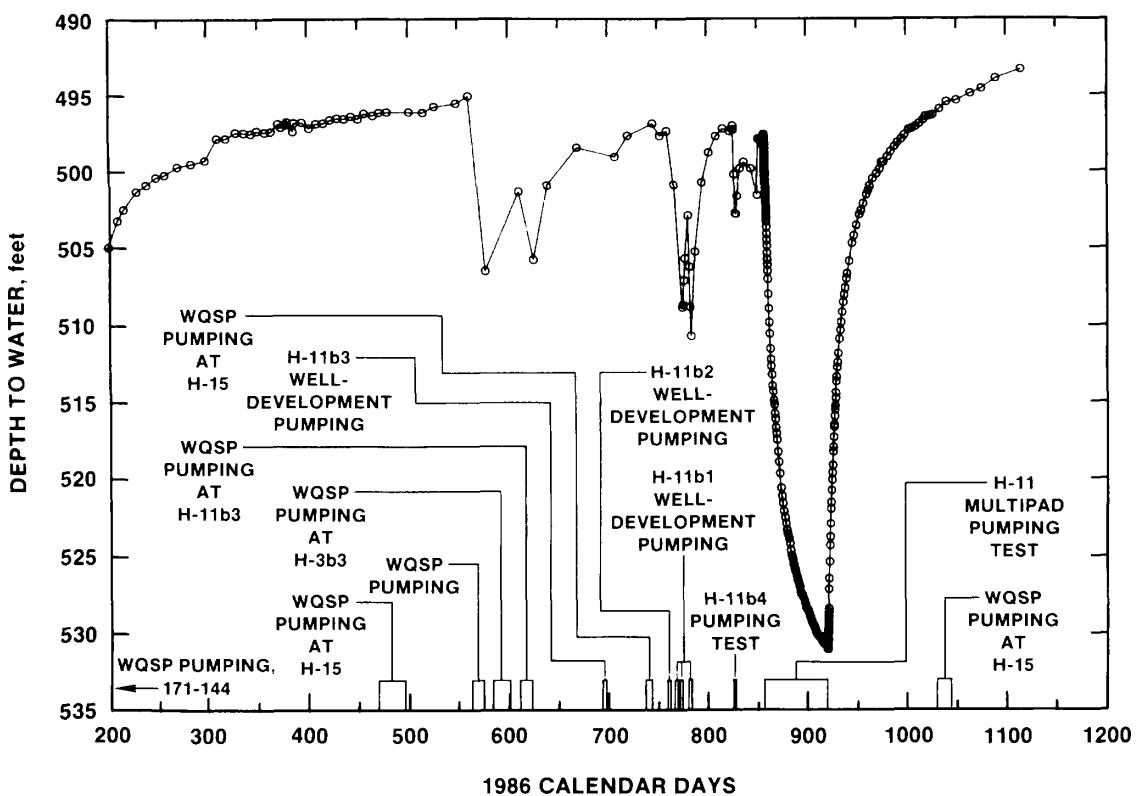
Figure 5-7. DOE-1 Water-Level History.
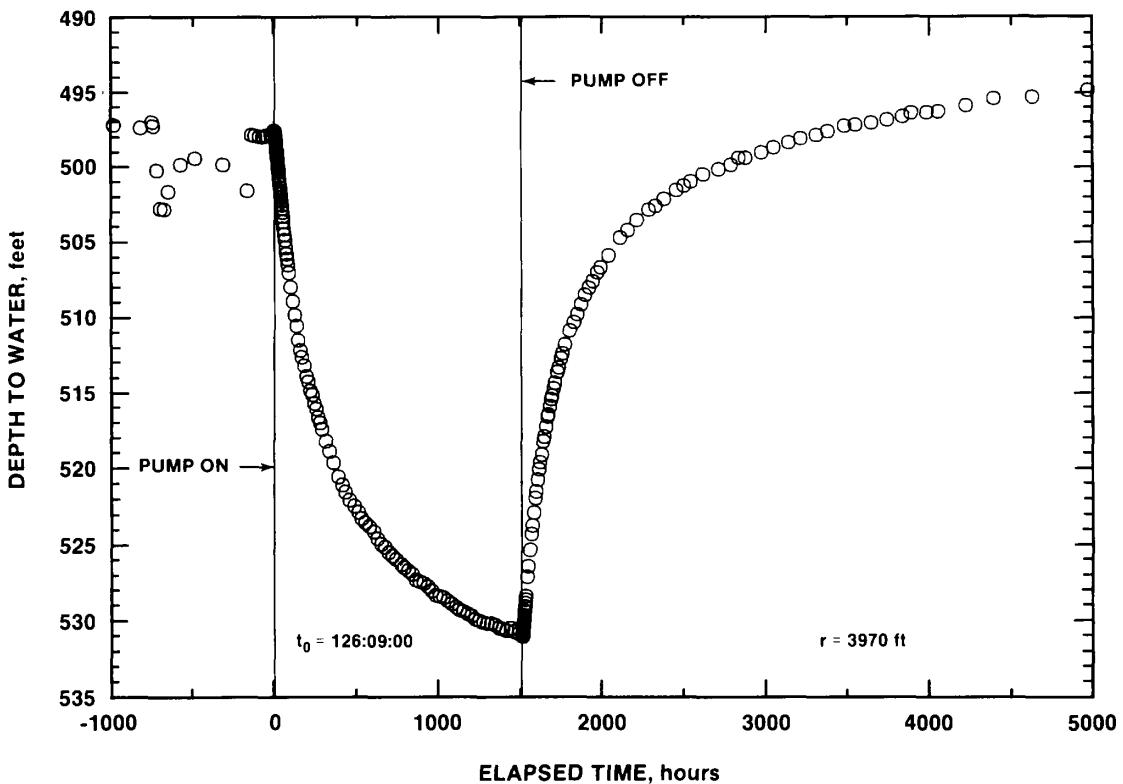
Figure 5-8. DOE-1 Water-Level Record During the H-11 Multipad Pumping Test.

Ordinarily, when a pre-existing water-level trend affects the responses observed during a pumping test, the trend is extrapolated over the duration of the test and the data derived as the deviation from that trend are used for analysis (Kruseman and DeRidder, 1979). Because the DOE-1 water level was responding to numerous stresses which had occurred at different times and locations and which had different magnitudes, however, no basis exists for defining a specific recovery trend. Thus, no compensation for the recovery trend was made before the data were analyzed; the potential effects of the recovery trend on the hydraulic properties interpreted from the analysis are discussed in Section 6.3.4.

For analysis purposes, the DOE-1 water-level data collected during the H-11 multipad test were converted to pressures by subtracting the depths to water from a datum of 831.7 ft (the depth to the middle of the Culebra from the water-level-measurement reference datum), and multiplying the remainders by 0.4625 psi/ft (the pressure/depth gradient measured in the well on August 23, 1988; Crawley, personal communication). The observed water-level data and calculated pressure data are tabulated in Appendix A, Table A-2. A plot of the pressure data is included with the final analytical simulation of the DOE-1 response to the multipad test in Section 6.3.4.

5.3.1.6 H-3b2. The water-level response at well H-3b2 during the H-11 multipad pumping test was also a superposition of responses to a number of different hydraulic stresses, although not as complex as that at DOE-1. Figure 5-9 shows the water-level history at H-3b2 since mid-1987. The times of pumping activities at nearby wells that may have contributed to the observed water-level fluctuations are also indicated on the figure. The periods when the Culebra was draining freely into the Air-Intake Shaft pilot hole and later into the full-size Air-Intake Shaft are also shown. The
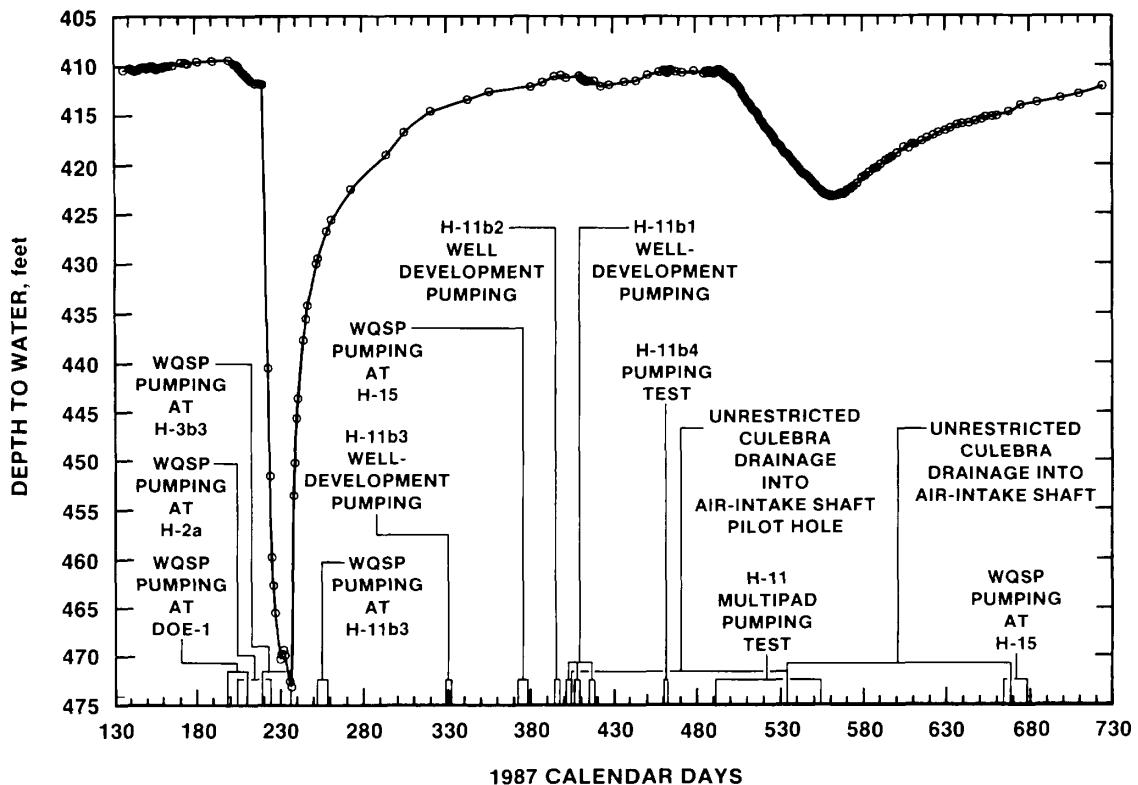
Figure 5-9. H-3b2 Water-Level History.

H-3b2 water level appears to be most strongly affected by pumping at H-3b3, DOE-1, and H-11. The WQSP pumping at H-2a and H-15 had little observable effect at H-3b2. In general, the water-level fluctuations at H-3b2 in the 1000 hr preceding the H-11 multipad test (Figure 5-10) were much smaller in magnitude than those observed at DOE-1 (Figure 5-8).

Stevens and Beyeler (1985) reported approximately 35 ft of drawdown at H-1 and approximately seven ft of drawdown at well H-3b1 in response to Culebra drainage into the Exploratory (now Construction and Salt-Handling) Shaft at the WIPP during a 70-day period in 1981. A 130-day period of free drainage into the Air-Intake Shaft pilot hole in 1987 caused approximately 20 ft of drawdown at H-1, and the subsequent 134-day period of free drainage into the open shaft caused an additional 18 ft of drawdown (Avis and Saulnier, 1989). Whatever effect the drainage at the Air-Intake Shaft location had on H-3b2 water levels is masked by the effects of different episodes of pumping at H-11. Thus, the drawdown observed at H-3b2 during the H-11 multipad test is probably not all attributable to the pumping at H-11b1, and the recovery observed after

the pump was turned off is probably an underrepresentation of the actual recovery from the test as drawdown related to Air-Intake Shaft drainage continued. After the Culebra interval in the Air-Intake Shaft was lined on October 29, 1988 (1987 calendar day 668), the rate of recovery at H-3b2 appeared to accelerate slightly (Figure 5-9).

Because of the complexity of the non-test-related stresses affecting the water levels at H-3b2 during the H-11 multipad test, no specific compensation for these stresses could be defined. Analysis was performed of the data as observed, with only qualitative consideration given to the potential effects of the extraneous stresses on the hydraulic properties interpreted (see Section 6.3.5).

The H-3b2 water-level data were converted to pressures for analysis by subtracting the depths to water from 688.2 ft (the depth to the middle of the Culebra from the water-level-measurement reference datum), and multiplying the remainders by 0.4497 psi/ft (the pressure/depth gradient measured in the well on February 24, 1987; Crawley, 1988). The
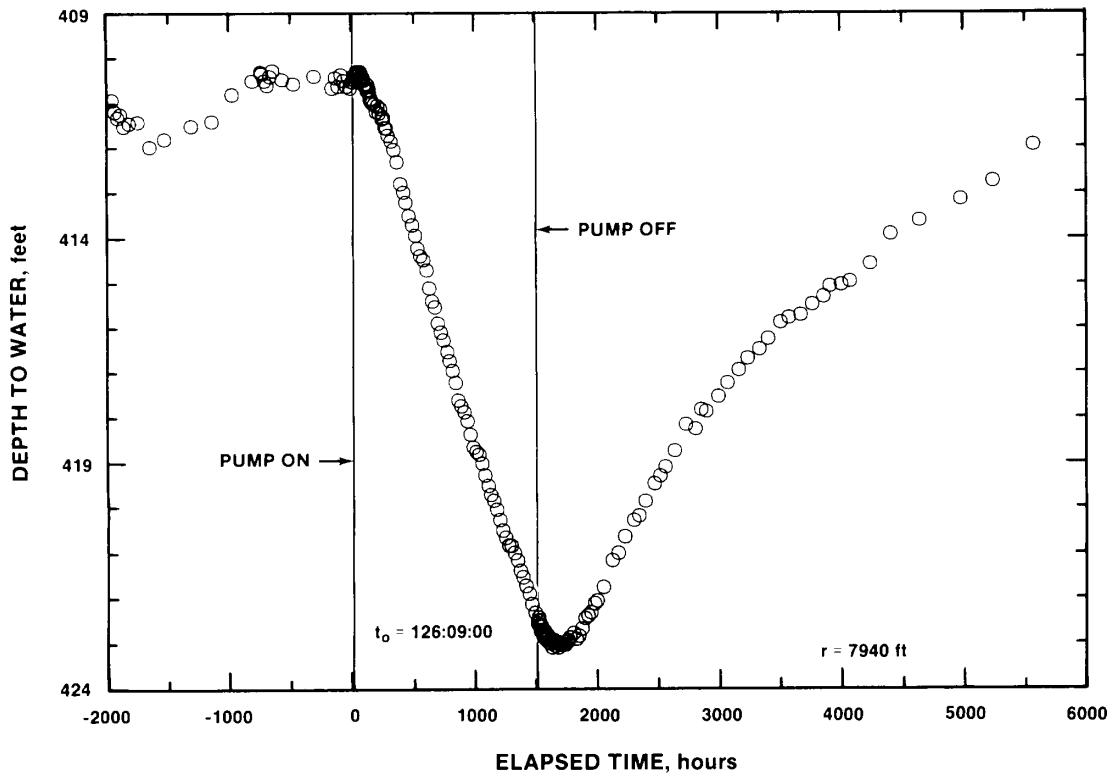
Figure 5-10. H-3b2 Water-Level Record During the H-11 Multipad Pumping Test.

observed water-level data and calculated pressure data are tabulated in Appendix A, Table A-3. A plot of the pressure data is included with the final analytical simulation of the H-3b2 response to the multipad test in Section 6.3.5.

5.3.1.7 H-4b. In contrast to DOE-1 and H-3b2, water levels at H-4b were relatively stable during the months before the H-11 multipad test (Stensrud et al., 1988b). Figure 5-11 shows H-4b water levels measured before and during the test. The most notable feature of the figure is the rapid water-level recovery beginning about 300 hr after the pump was turned off at H-11b1. The water level rose more rapidly than it drew down, reaching a level by mid-December 1988 about two ft higher than the stabilized level existing when the test began. The water-level rise has continued to the present day (May 1989), with the current water level being about four ft higher than the highest water level ever before measured in the well (Richey, 1987; Stensrud et al., in preparation). The reason for the sudden rise in water levels is unknown. No

activities are known to have occurred in the vicinity of H-4 that could have caused a rise in water levels.

Some of the fluctuations in water level shown in Figure 5-11 were caused by changes in barometric pressure. The barometric efficiency of the well was therefore evaluated so that a compensation could be made for the barometrically induced water-level fluctuations. The H-4b water-level data were first converted to pressures by subtracting the depths to water from 503.7 ft (the depth to the middle of the Culebra from the water-level-measurement reference datum), and multiplying the remainders by 0.4414 psi/ft (the pressure/depth gradient measured in the well on February 17, 1987; Crawley, 1988). The barometric-pressure data recorded by the H-11 DAS (Appendix A, Table A-1) were then converted to changes in barometric pressure by subtracting 13.06 psia, the barometric pressure at the beginning of the multipad test. The measured or interpolated barometric-pressure changes at the precise times of the H-4b water-level measurements were then
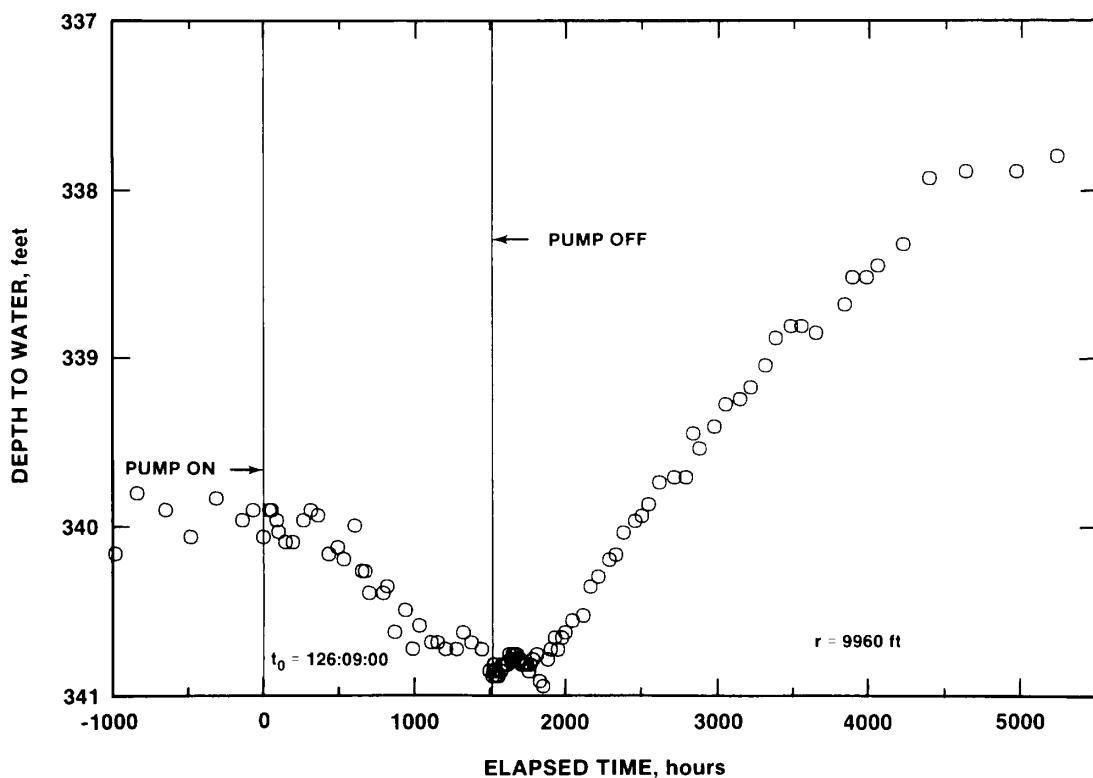
Figure 5-11. H-4b Water-Level Record During the H-11 Multipad Pumping Test.

multiplied by several decimal fractions, such as 0.5, 0.6, and 0.7, and added to the pressure data already calculated from the water-level data. The added fractional barometric-pressure change that produced the smoothest pressure curve was judged to represent the best estimate of the barometric efficiency of the well. The barometric efficiency of H-4b appears to be about 0.6. The barometric correction could only be applied to the data collected while the DAS on the H-11 hydropad was operational, from 23 hr before until 4319 hr after the beginning of pumping.

The observed water-level data, calculated pressure data, and final pressure data compensated for barometric-pressure effects are tabulated in Appendix A, Table A-4. A plot of the compensated pressure data is included with the final analytical simulation of the H-4b response to the multipad test in Section 6.3.6.

5.3.1.8 H-12. Water levels in well H-12 were stable within 0.1 ft in the months preceding the H-11 multipad test (Stensrud et al., 1988b). Figure 5-12 shows water levels measured from about 840 hr before the test began until about 2950 hr after the pump was turned off. The recovery trend seen at H-12 shows some similarities to that seen at H-4b (Figure 5-11). The H-12 recovery was rapid relative to the drawdown, and appeared to accelerate with time. The final measurements were rising sharply above the stabilized water level existing when the test began. Recovery monitoring was terminated by WQSP pumping at H-12 in mid-November 1988, at which time the water level was about 0.5 ft above its pretest level. By May 1989, the H-12 water level had recovered completely from the WQSP pumping, surpassing its prepumping level by about two ft.
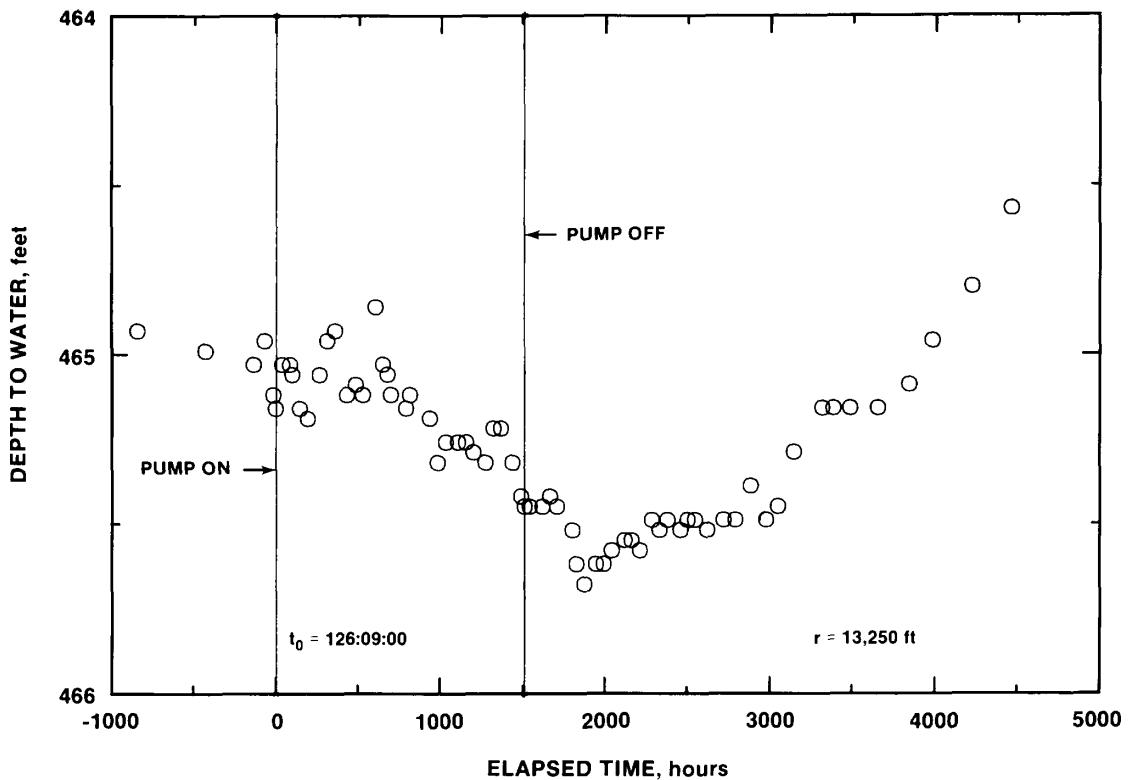
Figure 5-12. H-12 Water-Level Record During the H-11 Multipad Pumping Test.

For analysis purposes, the water-level data were converted to pressures by subtracting the depths to water from 837.7 ft (the depth to the midpoint of the Culebra from the water-level-measurement reference datum), and multiplying the remainders by 0.4687 psi/ft (the pressure/depth gradient measured in the well on September 24, 1987; Crawley, 1988). The pressure data were then compensated for barometric-pressure fluctuations using the procedure outlined in Section 5.3.1.7 and a barometric efficiency of 0.6. The observed water-level data, calculated pressure data, and final pressure data compensated for barometric-pressure effects are tabulated in Appendix A, Table A-5. A plot of the compensated pressure data is included with the final analytical simulation of the H-12 response to the multipad test in Section 6.3.7.

5.3.1.9 H-14. At the time the H-11 multipad test began, the water level in well H-14 was nearing complete recovery from WQSP pumping performed in January 1988 (Stensrud et al., 1988b). The water-level data depicted in Figure 5-13 show a drawdown trend beginning about midway through the H-11b1 pumping period and flattening at the end of the data record, with no clear recovery indicated at all.

For analysis purposes, the H-14 water-level data were converted to pressures by subtracting the depths to water from 559.8 ft (the depth to the middle of the Culebra from the water-level-measurement reference datum), and multiplying the remainders by 0.4337 psi/ft (the pressure/depth gradient measured in the well on September 22, 1987; Crawley, 1988). No other modifications were made to the H-14 data for analysis. The observed water-level data and calculated pressure data are tabulated in Appendix A, Table A-6. A plot of the pressure data is included with the final analytical simulation of the H-14 response to the multipad test in Section 6.3.8.

5.3.1.10 H-15. Water levels at H-15 responded to multiple hydraulic stresses during the year preceding the H-11 multipad test. Figure 5-14 lists a number of different pumping episodes that occurred at the WIPP site after mid-1987 that influenced water levels observed at H-15. When the H-11 multipad pumping test began, the water level in H-15 was still recovering from these earlier stresses (Figure 5-15). As was the case at DOE-1 (Section 5.3.1.5), the superposition at H-15 of the multipad-test response on the continuing recovery response(s) probably resulted in apparently
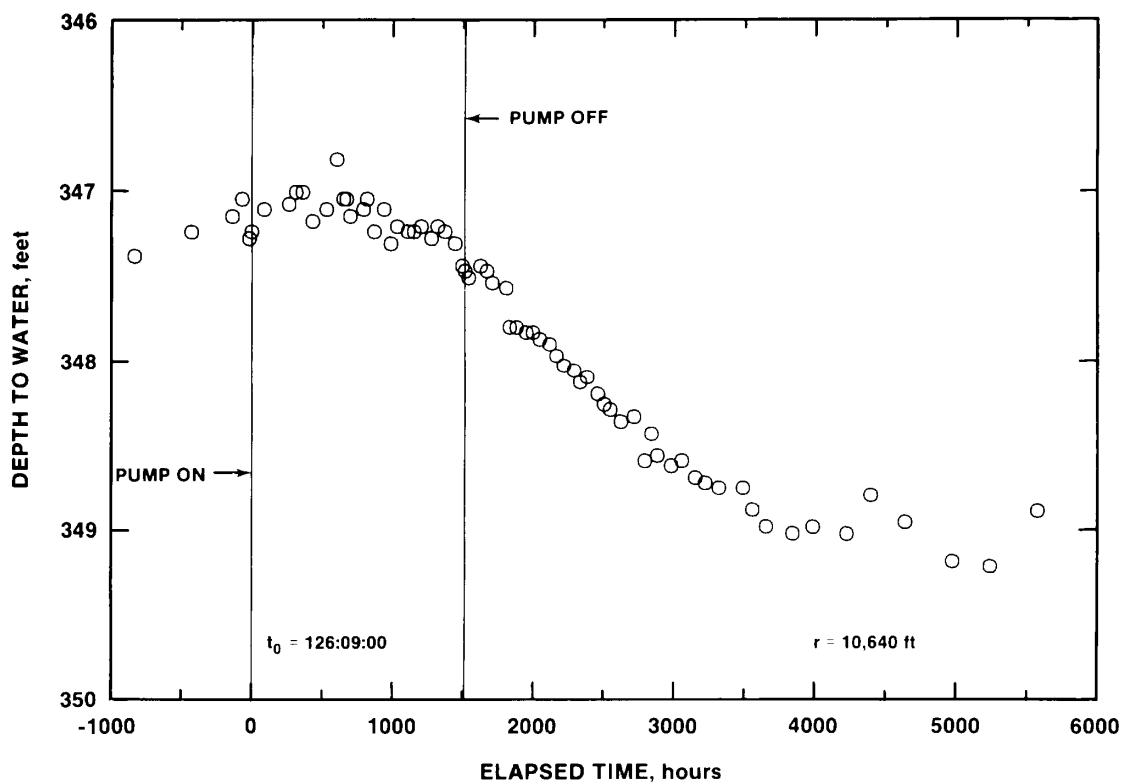
Figure 5-13.   H-14 Water-Level Record During the H-11 Multipad Pumping Test.
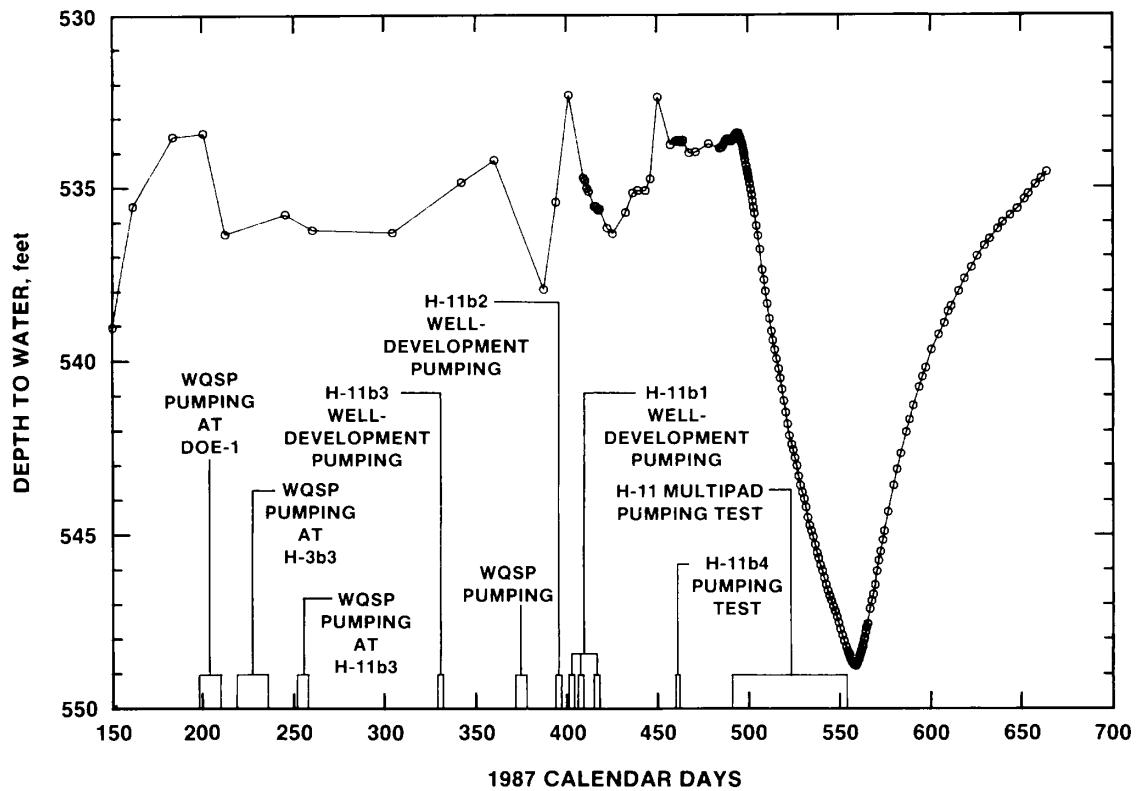
Figure 5-14.   H-15 Water-Level History.
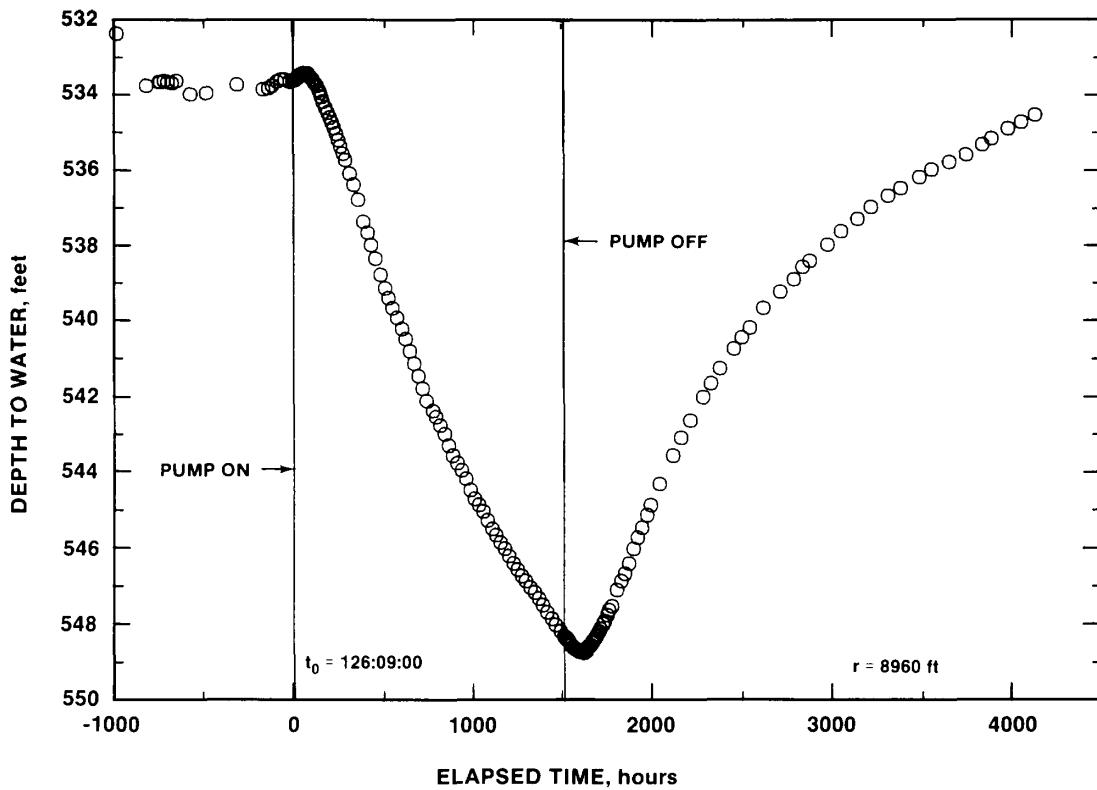
Figure 5-15. H-15 Water-Level Record During the H-11 Multipad Pumping Test.

less drawdown and more recovery being observed than would have been observed had the water level been stable before the test. No compensation for the recovery trend was made, however, because the number of superimposed components comprising the trend prevented definition of a single recovery function. H-15 recovery monitoring was terminated in late October 1988 by WQSP pumping at that location, at which time the water level was about one ft below its pretest level.

For analysis purposes, the H-15 water-level data were converted to pressures by subtracting the depths to water from 873.4 ft (the depth to the middle of the Culebra from the water-level-measurement reference datum), and multiplying the remainders by 0.4955 psi/ft (the pressure/depth gradient measured in the well on August 24, 1988; Crawley, personal communication). No other modifications were made to the H-15 data for analysis. The observed water-level data and calculated pressure data are tabulated in Appendix A, Table A-7. A plot of the pressure data is included with the final analytical simulation of the H-15 response to the multipad test in Section 6.3.9.

5.3.1.11 H-17. Water levels in H-17 were relatively stable in 1988 before the start of the H-11 multipad test (Stensrud et al., 1988b). Minor oscillations of less than one ft were observed in response to well-development pumping on the H-11 hydropad. Water levels measured in H-17 from about 980 hr before to 4970 hr after the beginning of the H-11 multipad test are shown in Figure 5-16. A notable feature on the figure is the rapid recovery that continued three ft past the stabilized water level existing at the start of the test. This over-recovery is similar to that observed at H-4b (Figure 5-11) and H-12 (Figure 5-12), and its cause is unknown. By May 1989, the H-17 water level was an additional three ft higher (Stensrud et al., in preparation).

44
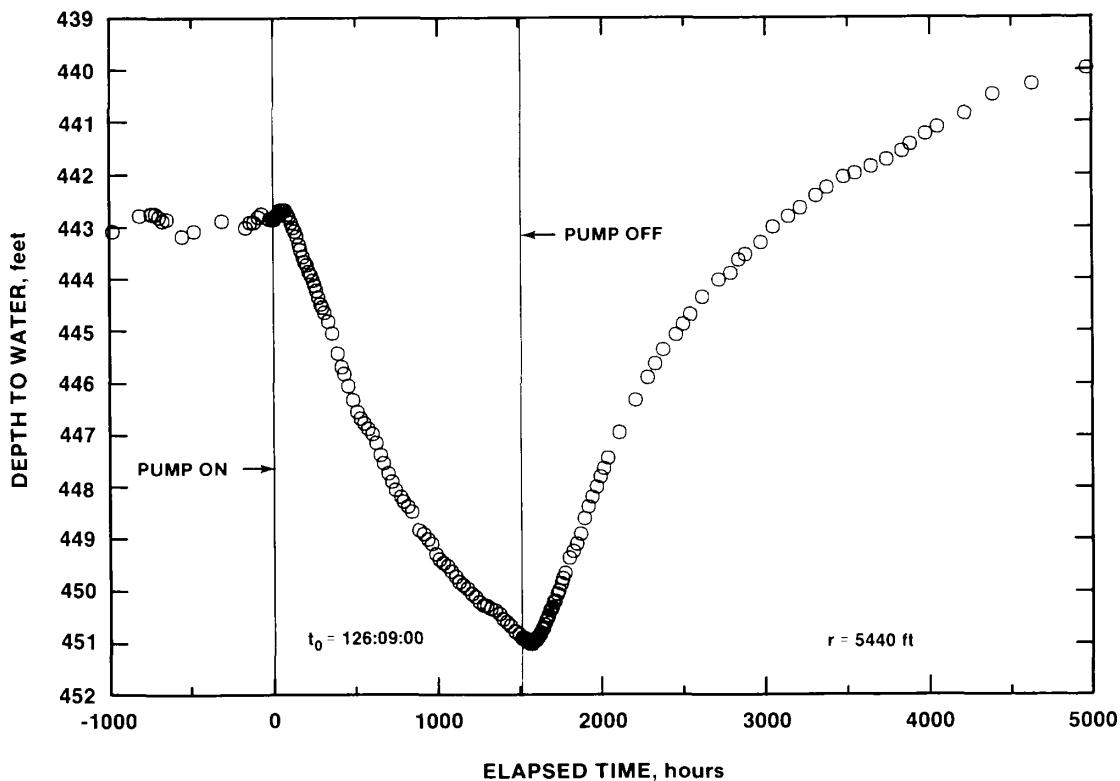
Figure 5-16. H-17 Water-Level Record During the H-11 Multipad Pumping Test.

For analysis purposes, the H-17 water-level data were converted to pressures by subtracting the depths to water from 719.9 ft (the depth to the middle of the Culebra from the water-level-measurement reference datum), and multiplying the remainders by 0.5046 psi/ft (the pressure/depth gradient measured in the well on August 3, 1988; Crawley, personal communication). No other modifications were made to the H-17 data for analysis. The observed water-level data and calculated pressure data are tabulated in Appendix A, Table A-8. A plot of the pressure data is included with the final analytical simulation of the H-17 response to the multipad test in Section 6.3.10.

5.3.1.12 P-15. Water levels in P-15 were stable within 0.5 ft in 1988 before the start of the H-11 multipad test (Stensrud et al., 1988b). Figure 5-17 shows the water-level data collected from about 830 hr before to about 4970 hr after the start of the test. Small drawdown and recovery trends are evident, with

a total data range of about one ft. A barometric compensation was attempted on the data, following the procedure outlined in Section 5.3.1.7, to try to clarify the trends. The water-level data were converted to pressures by subtracting the depths to water from 425.6 ft (the depth to the midpoint of the Culebra from the water-level-measurement reference datum), and multiplying the remainders by 0.4474 psi/ft (the pressure/depth gradient measured in the well on February 26, 1987; Crawley, 1988). A barometric efficiency of 0.6 was then used to compensate the data collected between 23 hr before and 4319 hr after the start of pumping.

A plot of the calculated pressure data compensated for barometric fluctuations is shown in Figure 5-18. Barometric-pressure data were not available to allow barometric correction of the first four and last three data points on Figure 5-18, complicating the definition of trends. Nevertheless, the drawdown and recovery
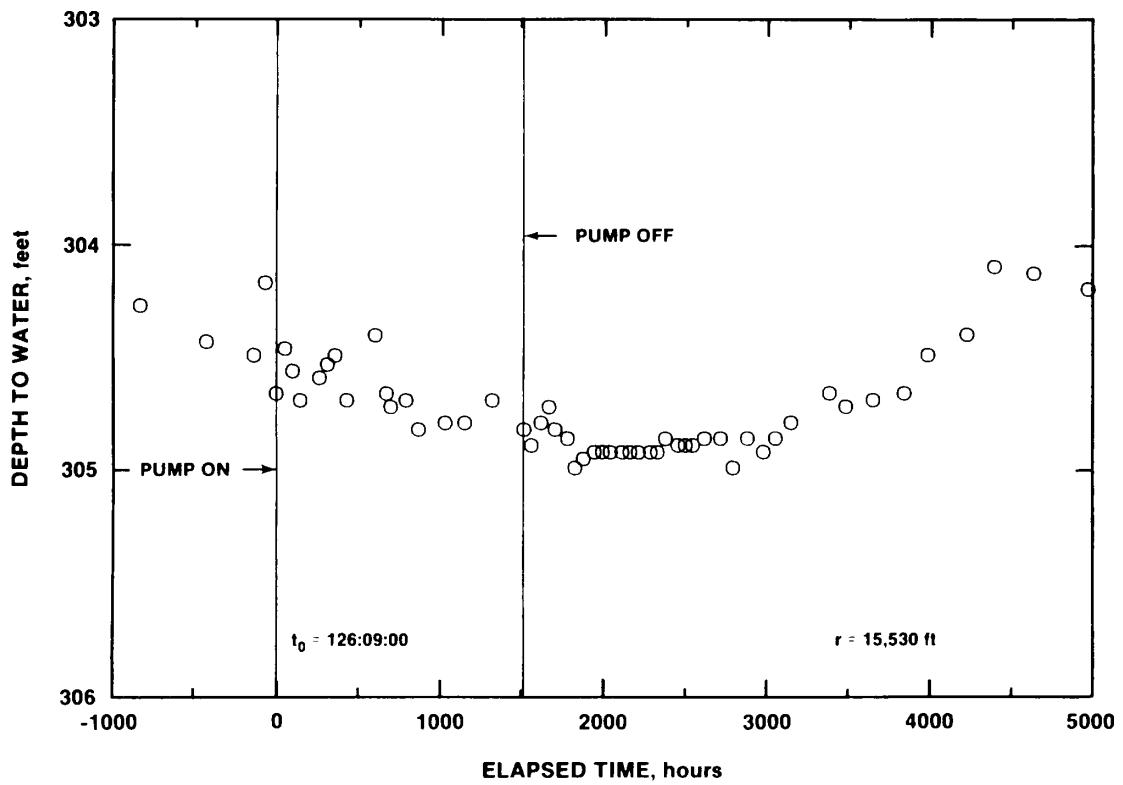
Figure 5-17. P-15 Water-Level Record During the H-11 Multipad Pumping Test.
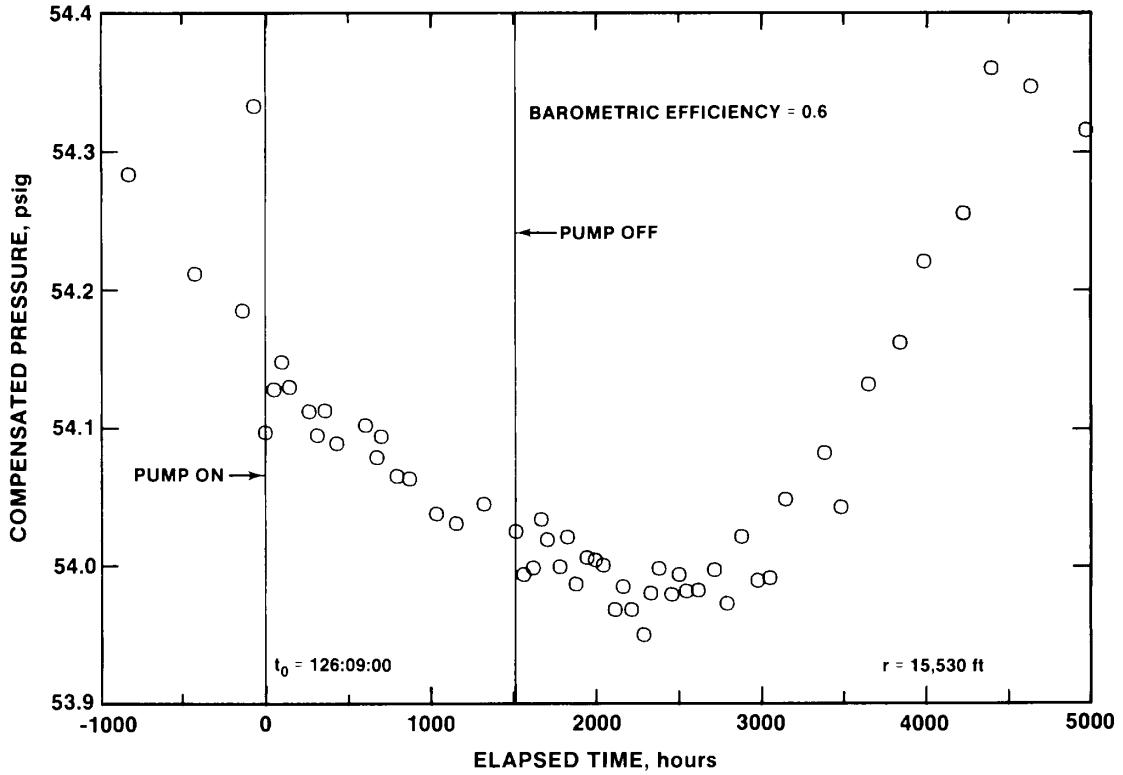
Figure 5-18. P-15 Pressure Record During the H-11 Multipad Pumping Test with Barometric Compensation.

trends are better defined than on the water-level plot (Figure 5-17). The recovery trend indicates an over-recovery similar to those seen at H-4b (Figure 5-11), H-12 (Figure 5-12), and H-17 (Figure 5-16). Again, the reason for this occurrence is unknown. The observed water-level data, calculated pressure data, and final pressure data compensated for barometric-pressure effects are tabulated in Appendix A, Table A-9.

5.3.1.13 P-17. Water levels in P-17 showed little fluctuation in 1988 before the H-11 multipad test (Stensrud et al., 1988b). Water-level data collected before and during the test are shown in Figure 5-19. An over-recovery of unknown origin is seen on the figure similar to those observed at H-4b (Figure 5-11) and H-17 (Figure 5-16). By May 1989, the P-17 water level was about four ft higher than its pre-multipad-test level (Stensrud et al., in preparation).

For analysis, the water-level data were converted to pressures by subtracting the depths to water from 572.0 ft (the depth to the midpoint of the Culebra from the water-level-measurement reference datum), and multiplying the remainders by 0.4519 psi/ft (the pressure/depth gradient measured in the well on August 12, 1987; Crawley, 1988). The pressure data were then compensated for barometric-pressure fluctuations using the procedure outlined in Section 5.3.1.7 and a barometric efficiency of 0.6. The observed water-level data, calculated pressure data, and final pressure data compensated for barometric-pressure effects are tabulated in Appendix A, Table A-10. A plot of the compensated pressure data is included with the final analytical simulation of the P-17 response to the multipad test in Section 6.3.12.
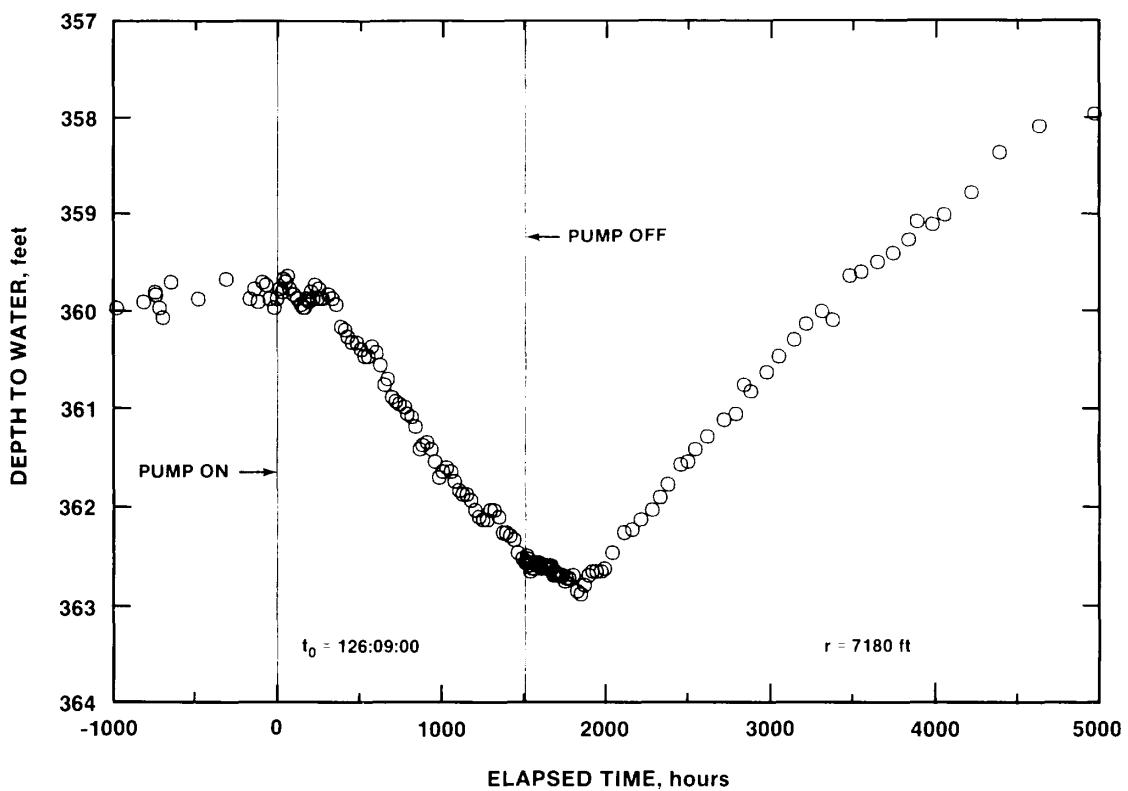
Figure 5-19. P-17 Water-Level Record During the H-11 Multipad Pumping Test.

5.3.1.14 P-18. In 12 years of water-level monitoring at P-18 (1977-1989), the water level from the Culebra has never stabilized, but has risen steadily (LaVenue et al., 1988; Stensrud et al., 1988b and in preparation). The entire record of water-level measurements made in P-18 in 1988 and January 1989 is shown in Figure 5-20. A number of changes in the rate of water-level rise were observed during this time, but none could be unequivocally ascribed to the H-11 multipad test or to any other known discrete hydraulic stress. Thus, no analysis of water-level data from P-18 was performed. The observed water-level data are tabulated in Appendix A, Table A-11.

5.3.1.15 Cabin Baby-1. Water levels in Cabin Baby-1 showed a total fluctuation of less than one ft in 1988 before the start of the H-11 multipad test (Stensrud et al., 1988b). Water-level data collected before and during the test are shown in Figure 5-21. The same type of anomalous over-recovery observed at H-4b (Figure 5-11), H-17 (Figure 5-16), and P-17 (Figure 5-19) was also observed at Cabin Baby-1. By

May 1989, the water level in Cabin Baby-1 was about 3.5 ft above its pre-multipad-test level (Stensrud et al., in preparation).

For analysis purposes, the water-level data were converted to pressures by subtracting the depths to water from 517.1 ft (the depth to the midpoint of the Culebra from the water-level-measurement reference datum), and multiplying the remainders by 0.4462 psi/ft (the pressure/depth gradient measured in the well on July 27, 1988; Crawley, personal communication). The pressure data were then compensated for barometric-pressure fluctuations using the procedure outlined in Section 5.3.1.7 and a barometric efficiency of 0.4. The observed water-level data, calculated pressure data, and final pressure data compensated for barometric-pressure effects are tabulated in Appendix A, Table A-12. A plot of the compensated pressure data is included with the final analytical simulation of the Cabin Baby-1 response to the multipad test in Section 6.3.13.
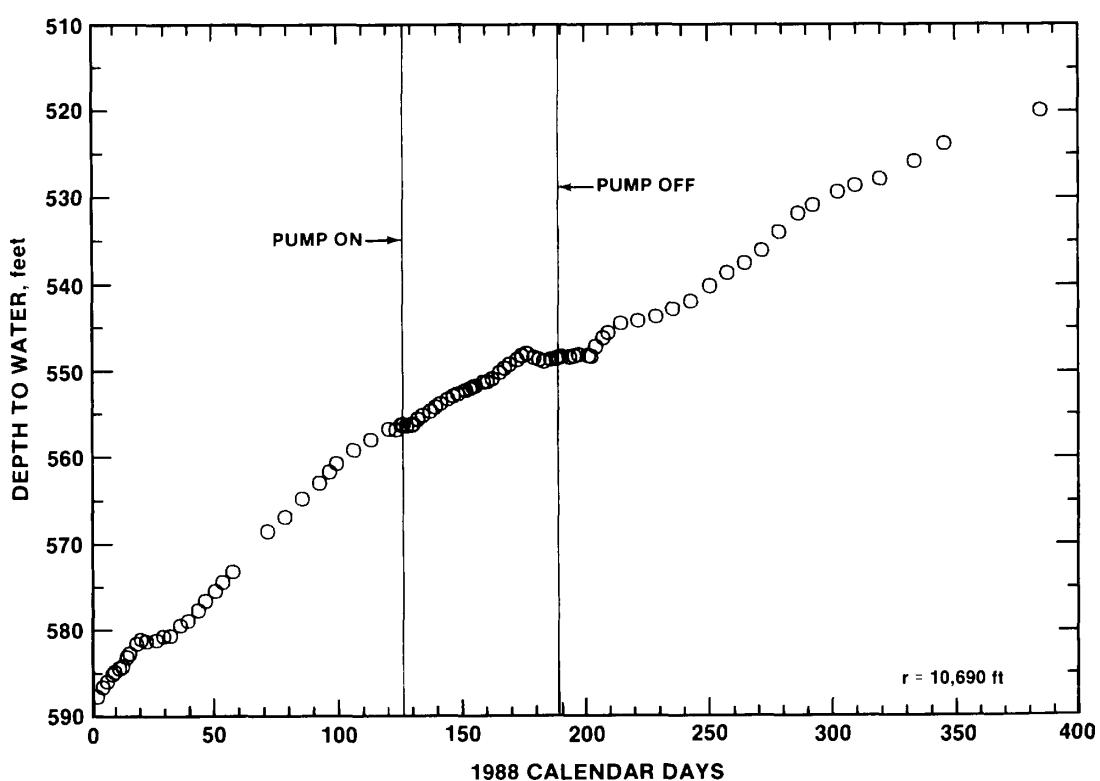
Figure 5-20. P-18 Water-Level Record.
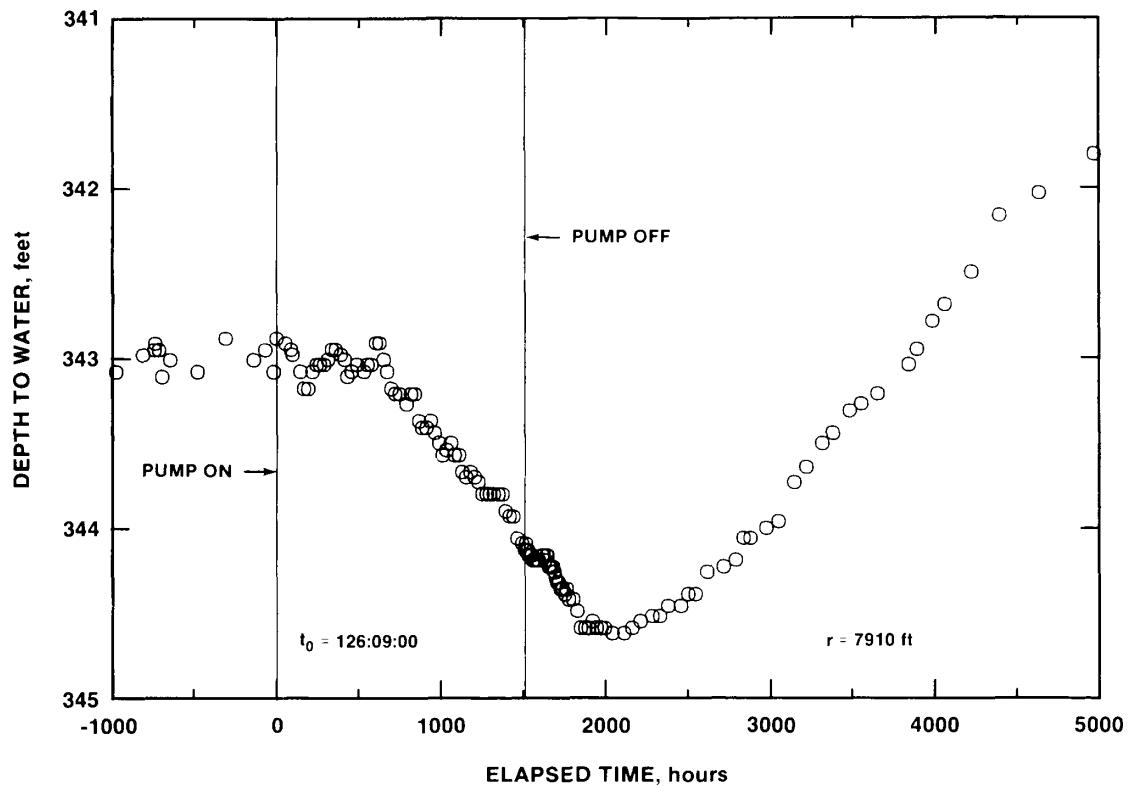
Figure 5-21. Cabin Baby-1 Water-Level Record During the H-11 Multipad Pumping Test.

5.3.1.16 H-3b1 Magenta. The nearest well to H-11b1 at which water levels from the Magenta dolomite were monitored during the H-11 multipad test was H-3b1. In early 1988, the Magenta water level in H-3b1 was still recovering from WQSP pumping performed in the well in mid-1987 (calendar days 238-245; Randall et al., 1988). The stabilized water level before the WQSP pumping was about 250 ft below the top of the well casing (Stensrud et al., 1988a). The water level in H-3b1 appeared to be stabilizing between 249 and 250 ft below the top of the well casing during the H-11 multipad test (Figure 5-22), showing no response to the test while approximately 13 ft of drawdown were observed in the Culebra 100 ft away at H-3b2 over the same period (Figure 5-10). The Magenta water level in H-3b1 had also showed no response to 62 days of pumping from the Culebra at H-3b2 in 1985 (the H-3 multipad pumping test; Beauheim, 1987a).

Later in 1988, beginning between calendar days 270 and 280 approximately, a sharp decline was observed in the H-3b1 water level. This decline is probably related to drainage from the Magenta into the Air-Intake

Shaft, 4390 ft from H-3b1. Magenta drainage into the Air-Intake Shaft pilot hole began on February 7, 1988 (calendar day 38), and into the 20-ft-diameter shaft on June 21, 1988 (calendar day 172). The Magenta water-level data from H-3b1 are tabulated in Appendix A, Table A-13.

5.3.1.17 H-4c Magenta. Water levels from the Magenta dolomite measured at well H-4c also show no response to the H-11 multipad test (Figure 5-23). In early 1988, the Magenta water level was nearing stabilization following WQSP pumping performed in September and October 1987 (calendar days 266 to 278; Randall et al., 1988). No response was observed during the pumping at H-11b1, while the Culebra water level in H-4b dropped approximately one ft over the same period (Figure 5-11). WQSP pumping performed in H-4c in July 1988 (calendar days 194 to 201; Lyon, 1989) led to a recovery response which lasted for the remainder of 1988 (Figure 5-23). The Magenta water-level data from H-4c are listed in Appendix A, Table A-14.

49
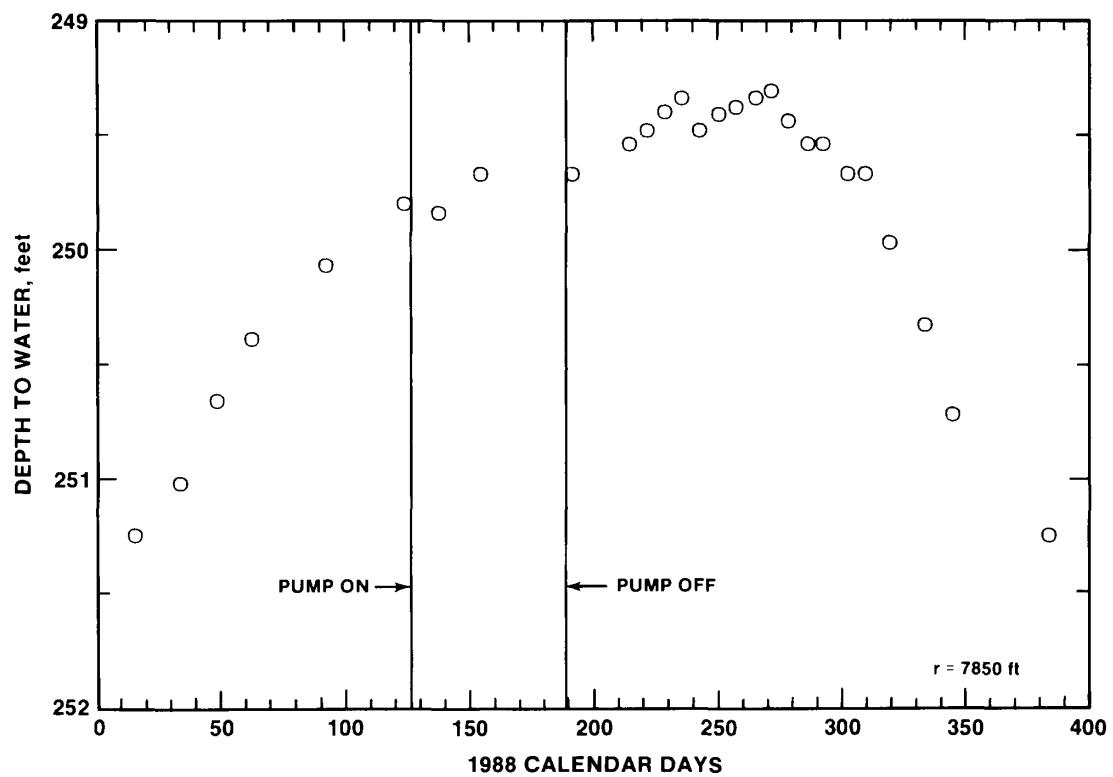
Figure 5-22. H-3b1 Magenta 1988 Water-Level Record.
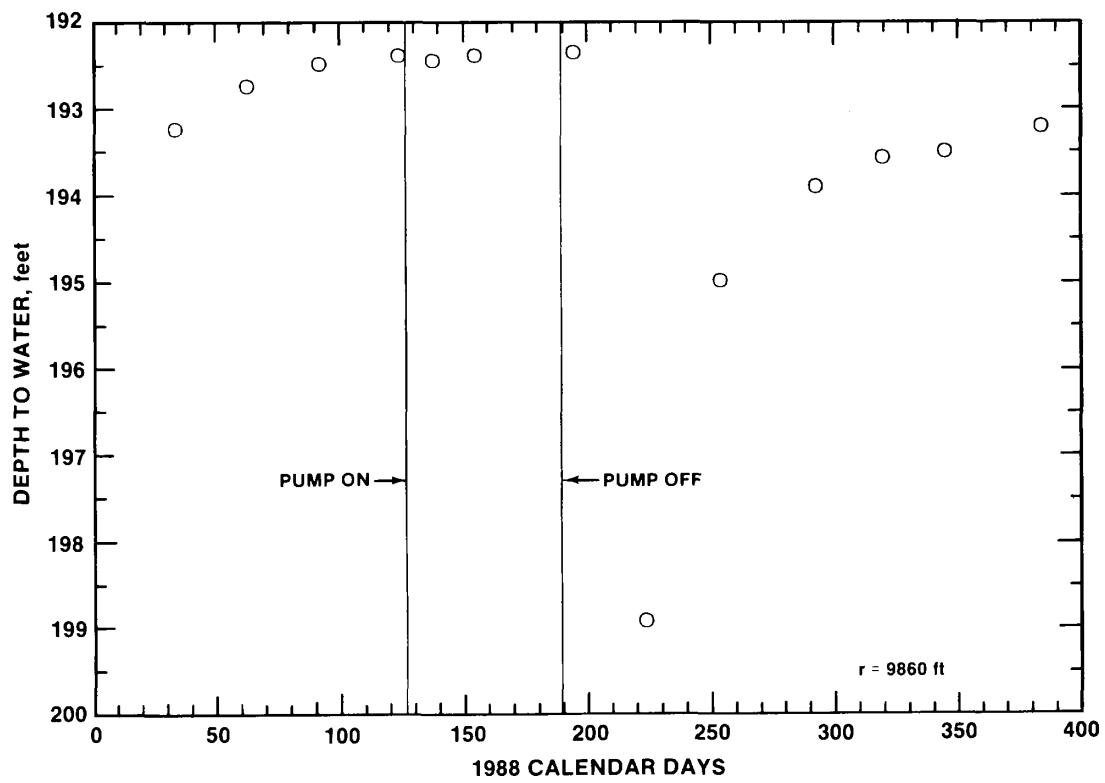
Figure 5-23. H-4c Magenta 1988 Water-Level Record.

5.3.1.18 Discussion and Summary. Water levels were measured in 11 wells completed to the Culebra dolomite and in two wells completed to the Magenta dolomite during the H-11 multipad pumping test. Apparent responses to the test were observed in all of the Culebra wells except for P-18. No responses to the test were observed in either of the Magenta wells. For each of the wells at which water-level responses to the H-11 multipad test were observed, the times at which drawdown responses were first observed, the maximum drawdowns observed, and the times at which the maximum drawdowns were observed are summarized in Table 5-1. Two qualifications must be noted with regard to the information in this table. First, because of random fluctuations in the data, a degree of subjectivity is involved in defining both response times and maximum and minimum water levels for the various wells. Second, no compensations have been made for either water-level trends existing when the

H-11 multipad test began or for trends that may have started during the test. Ignoring pre-existing rising trends at DOE-1, H-3b2, and H-15 has probably resulted in underestimation of the total drawdowns at those locations. Conversely, ignoring possible effects of drainage into the Air-Intake Shaft on water levels at H-3b2 may have resulted in an overestimation of the test-related drawdown at that location. The estimated values presented in Table 5-1 also implicitly assume that whatever hydraulic stress caused the over-recovery of water levels at H-4b, H-12, H-17, P-15, P-17, and Cabin Baby-1 did not begin until after recovery from the H-11 multipad test had begun. If this assumption is invalid, the maximum drawdowns and times of maximum drawdown presented in Table 5-1 are underestimated. Thus, the times and drawdowns presented in this table enable only qualitative comparisons and should be considered as approximations only.

TABLE 5-1

RESPONSE TIMES AND MAXIMUM DRAWDOWNS AT OBSERVATION WELLS

Observation Well	Distance from H-11b1 (ft)	Time After Pump On Until First Drawdown Observed (days)	Maximum Drawdown Observed (ft)	Time After Pump Off Until Maximum Drawdown Observed (days)
DOE-1	3970	2 hr	33.4	1 hr
H-17	5440	2	8.3	2
P-17	7180	10	2.9	10
Cabin Baby-1	7910	27	1.6	25
H-3b2	7940	3	12.6	8
H-15	8960	3	15.3	4
H-4b	9960	18	0.9	2
H-14	10,640	36	2.0	155?
P-18	10,690	no apparent response		
H-12	13,250	33	0.5	25
P-15	15,530	33	0.4	32

The above-mentioned considerations notwithstanding, several conclusions can be drawn from the data presented in Table 5-1. First, on the whole, no relationship is evident between the distance of an observation well from H-11b1 and the amount or timing of drawdown observed, indicating that the Culebra is not an isotropic, homogeneous medium on the scale of the test. Nevertheless, drawdown should occur later and be of a lower magnitude at increasing distances from H-11b1 in any particular direction. This type of distance-drawdown relationship is seen to the north of H-11b1 at DOE-1 and H-15, to the northwest at H-3b2 and H-14, to the southeast at H-17 and H-12, and in part to the southwest at P-17 and Cabin Baby-1. The responses at H-4b and P-15, however, do not fit the pattern of the other southwestern wells. Both H-4b and P-15 apparently responded sooner to pumping at H-11b1 than would have been expected from the responses observed at P-17 and Cabin Baby-1, and

H-4b apparently began to recover much more rapidly than expected. As discussed in Sections 5.3.1.7 and 5.3.1.12, factors other than the H-11 multipad test may have affected the water levels observed in H-4b and P-15 during the period of the test. This possibility is considered further in Sections 6.3.6 and 6.3.11 below.

A second conclusion that can be drawn from Table 5-1 is that the most rapid responses and highest magnitude drawdowns appear to be concentrated to the north, and to a lesser degree to the south, of the H-11 hydropad. Figure 5-24 shows a contour plot of the drawdowns measured at the end of the multipad-test pumping period. The contours are elongated to the north and south relative to their east-west positions, indicating a preferred north-south flow direction. Additional discussion of the asymmetry in observed drawdown responses is presented in Section 6.3.14.
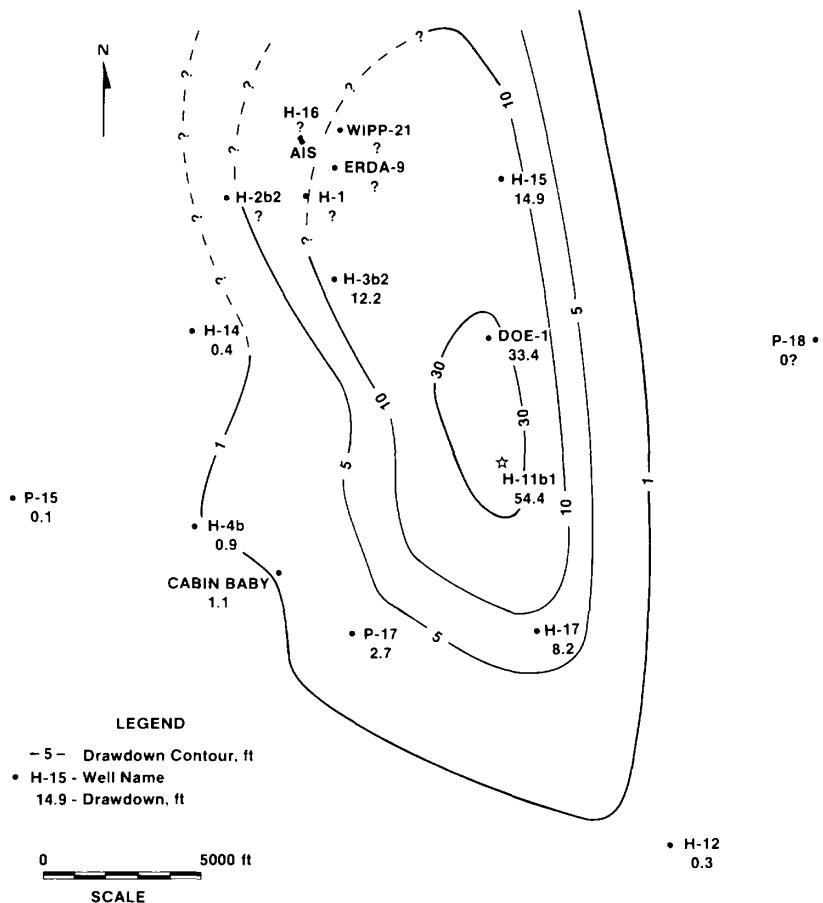
Figure 5-24. Drawdown Contours at the End of the H-11 Multipad Test Pumping Period.

The northwestern extent of observable responses to the H-11 multipad pumping test in the Culebra was constrained by free drainage of Culebra water into first the pilot hole for the Air-Intake Shaft for the WIPP (1988 calendar days 39 to 169), and later into the shaft itself (1988 calendar days 169 to 303; Stensrud et al., 1988b and in preparation). This drainage produced a pressure transient within the Culebra at nearby wells of greater magnitude than might have resulted from the pumping test. In the absence of this drainage, responses to the H-11 multipad test would probably have been evident at H-1 and ERDA-9, and possibly at H-2, H-16, and WIPP-21 (Figure 5-24).

5.3.2 Pumping-Rate Data. The pump in H-11b1 ran continuously from 0900 on May 5, 1988 (calendar day 126) until 0900 on July 7, 1988 (calendar day 189) except for two brief shutdowns. The pump stopped at about 1249 on May 12 (calendar day 133) and was restarted at 1401 that same day. The pump shut off again at about 1651 on July 3 (calendar day 185) and was restarted at 1840 that same day. A total of 548,200 gallons of water were pumped from H-11b1 during the test.

The pumping rate during the test was relatively constant; after an initial 15-minute period of adjustment, during which the pumping rate varied from 5.85 to 6.55 gpm, the pumping rate ranged only from 5.90 to 6.30 gpm for the balance of the test. The average pumping rate over the entire 1512-hr pumping period was 6.04 gpm. A slight decline in pumping rate

was observed, however, as the test proceeded. From May 5 until the shutdown on May 12, the pumping rate averaged 6.11 gpm. From May 12 until the next shutdown on July 3, the pumping rate averaged 6.05 gpm. From July 3 until the final shutdown on July 7, the average pumping rate was 6.02 gpm. The pumping-rate data are tabulated in Stensrud et al. (in preparation).

At the distant observation wells, the two brief stoppages in pumping produced no observable responses. Analyses of data from these wells were performed assuming a single pumping period lasting 1512 hr with a flow rate of 6.04 gpm. The wells on the H-11 hydropad, however, recovered appreciably each time the pump went off. Analyses of the data from the H-11 wells incorporated three pumping periods having the rates and durations listed above separated by short recovery periods.

5.3.3 Barometric-Pressure Data. The barometric pressure was measured and recorded by the DAS from 1001 on May 4 (calendar day 125) until 0800 on November 1, 1988 (calendar day 306). During this time, the barometric pressure ranged from 12.82 to 13.18 psia. Figure 5-25 shows a graph of barometric-pressure readings at approximately 10-hr intervals over the duration of the period of record. An abridged tabulation of the barometric-pressure data is included in Appendix A, Table A-1. A more complete tabulation of the data is presented in Stensrud et al. (in preparation).
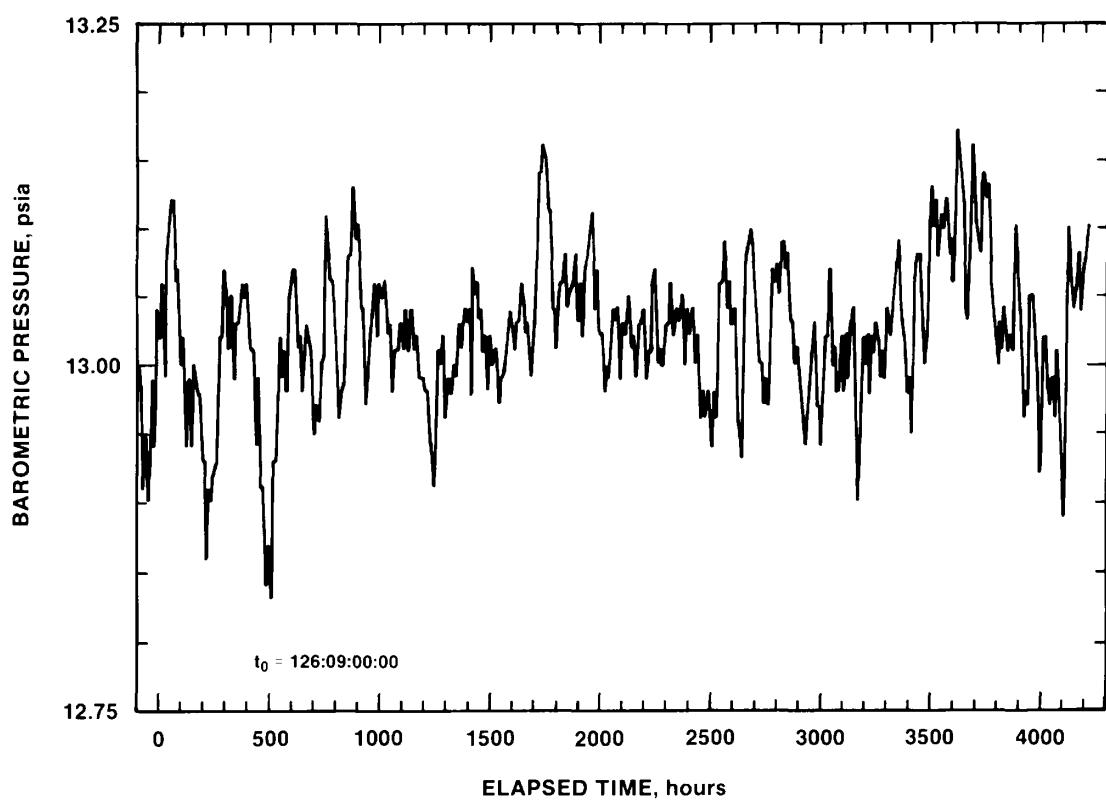
Figure 5-25. Barometric-Pressure Record During the H-11 Multipad Pumping Test.

6. ANALYTICAL INTERPRETATIONS

The data from the H-11b4 tests and from the H-11 multipad pumping test were interpreted using techniques based on analytical solutions derived for different test conditions. These analytical solutions, and the nomenclature and symbols used in the following text and figures, are discussed in Appendix B. All pumping-test analyses were performed with the INTERPRET well-test interpretation code developed by A.C. Gringarten and Scientific Software-Intercomp, which is described briefly in Appendix B. Familiarity on the part of the reader with the material in Appendix B is assumed in the following discussion.

6.1 H-11b4 Slug Tests

As discussed in Section 5.1, the fluid-pressure recovery in H-11b4 following each of the two DST flow periods was too rapid to provide useful data for analysis. The data from the slug-withdrawal tests are, however, adequate for analysis. Figure 6-1 shows a semilog plot of the data from the first slug-withdrawal test at H-11b4. Also shown is a match to a type curve that fits the early-time data (1.0 to 0.7 on the vertical axis) reasonably well. At later time, the data deviate below the type curve, indicating faster recovery than predicted by the type curve. The type curve was generated using the approach of Cooper et al. (1967), which is applicable to slug tests in a single-porosity medium.

MATCH PARAMETERS

p^* = 136.23 psia
p_i = 36.93 psia
α = 10^{-20}
β = 1.0
t = 0.0041 hr
r_c = 0.0831 ft

t_0 = 82:10:02:11

EARLY-TIME SINGLE-POROSITY FIT

□ DATA
— SINGLE-POROSITY TYPE CURVE

LATE-TIME DOUBLE-POROSITY DEVIATION FROM SINGLE-POROSITY TYPE CURVE

ELAPSED TIME, hours
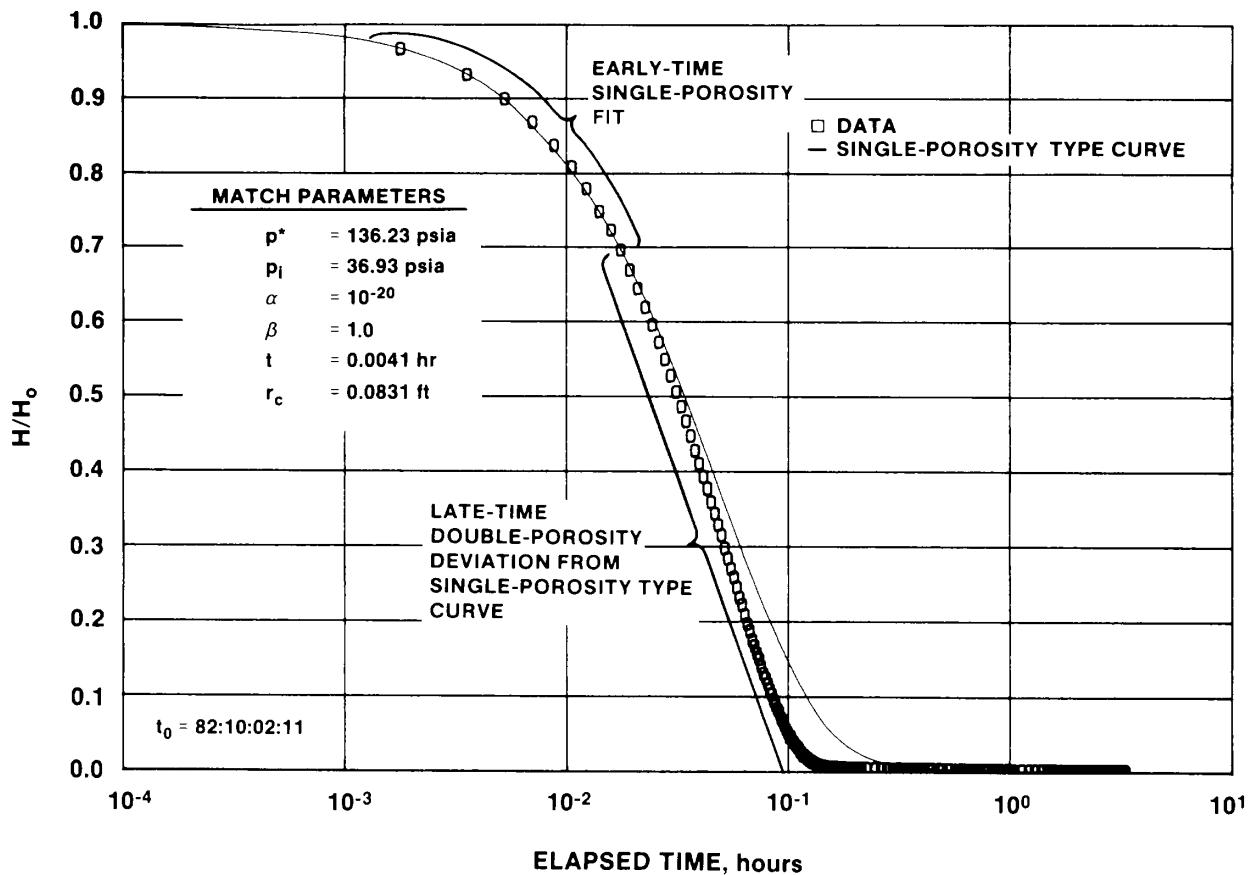
Figure 6-1. H-11b4 Slug-Test #1 Plot.

Grader and Ramey (1988) found the type of deviation from single-porosity type curves shown in Figure 6-1 to be characteristic of double-porosity media. Double-porosity media have two porosity sets that differ in terms of storage volume and permeability. Typically, the two porosity sets are a fracture network with higher permeability and lower storage, and the primary porosity of the rock matrix with lower permeability and higher storage. Two hydraulically interconnected layers with contrasting hydraulic properties can also produce a "double-porosity" response during testing. At H-11b4, the Culebra is described as a "fractured and broken, vuggy dolomite" (Mercer, in preparation, a). Grader and Ramey (1988) found that early-time data from a slug test in a double-porosity medium match a single-porosity type curve because they are representative of flow from only the fractures. When the porous matrix begins contributing fluid, recovery accelerates and deviates from the single-porosity type curve. Grader and Ramey (1988) note that the early-time fit to the single-porosity type curve provides a valid estimate of fracture transmissivity. The type-curve match shown in Figure 6-1 provides a transmissivity estimate of 40 ft^2/day (Table 6-1).

Results of the second slug-withdrawal test at H-11b4 were very similar to those of the first test. Figure 6-2 shows a semilog plot of the data from the second slug test, along with an early-time fit to a single-porosity type curve. This fit provides a transmissivity estimate of 43 ft^2/day, slightly higher than that obtained from the first test.

6.2 H-11b4 Pumping Test

For both H-11b4 and H-11b1, drawdown and recovery data were analyzed independently to define the models that best fit the different data sets. Once the analyses were completed, the consistency of the models was assessed both between drawdown and recovery at each well and between wells.

6.2.1 H-11b4. The pressure response observed at H-11b4 during the pumping test appears to be that of a well completed in a heterogeneous, double-porosity medium. Figure 6-3 shows a log-log plot of the H-11b4 drawdown data along with the best-fit simulation of those data generated with the INTERPRET well-test-analysis code (see Appendix B). The high-amplitude

oscillations seen in the pressure-derivative data in Figure 6-3 were caused by the diurnal pressure fluctuations discussed in Section 5.2, and are not considered representative of the aquifer response. The simulation shown uses a formulation for a double-porosity system with spherical matrix blocks, unrestricted interporosity flow, and a transmissivity of 42 ft^2/day (Table 6-1), and includes the effects of two no-flow boundaries at dimensionless distances of 12,000 and 30,000. In a homogeneous system, these dimensionless distances would translate to actual distances to image discharge wells of about 1900 and 3000 ft, or about half those distances to linear boundaries (see Section 6.3 and Appendix B for discussions of the relationship between dimensionless distances and actual distances to boundaries). The no-flow boundaries probably represent the effects of decreases in Culebra transmissivity away from the H-11 hydropad. Assuming a total-system compressibility of 1×10^{-5} psi^{-1} and a matrix porosity of 16%, the wellbore-skin factor (see Appendix B) for the simulation shown in Figure 6-3 is -6.0 (Table 6-1). Gringarten (1984) considers this skin factor to be representative of a stimulated well in a double-porosity medium. The storativity ratio (ω), representing the ratio of fracture storativity to total-system storativity (Appendix B), is 0.025. Figure 6-4 shows a linear-linear plot of the drawdown data and simulation.

Figure 6-5 shows a log-log plot of the H-11b4 recovery data along with the best-fit simulation generated with INTERPRET. The model used to generate this simulation differs from that used to generate the drawdown simulation in Figure 6-3 only in that it uses a skin factor of -6.4 (Table 6-1). The double-porosity formulation, transmissivity, and boundaries used by the two models are the same. The static formation pressure (p*) indicated by the recovery simulation is 116.1 psig, slightly lower than the 116.4 psig measured just before the test began (Stensrud et al., 1988b). The high-amplitude oscillations seen in the pressure-derivative data at late time in Figure 6-5 were caused by the diurnal pressure fluctuations discussed in Section 5.2, and are not considered representative of the aquifer response. A linear-linear plot of the recovery data and simulation is shown in Figure 6-6.

6.2.2 H-11b1. Figure 6-7 shows a log-log plot of the drawdown data observed at H-11b1 during the H-11b4

TABLE 6-1

SUMMARY OF WELL—RESPONSE INTERPRETATIONS

Well	Test	Barometric Efficiency	Apparent Transmissivity (ft^2/day)	Apparent Storativity	Storativity Ratio	Wellbore Skin	Distances to Image Wells Discharge (ft)	Recharge (ft)
H-11b4	slug #1	N.A.	40	N.A.	N.A.	N.A.	none	none
H-11b4	slug #2	N.A.	43	N.A.	N.A.	N.A.	none	none
H-11b4	pumping							
	drawdown (dd)	N.A.	42	N.A.	0.025	-6.0	1900;3000	none
	recovery (rc)	N.A.	42	N.A.	0.025	-6.4	1900;3000	none
H-11b1	H-11b4 pumping							
	drawdown	N.A.	41	3.4×10^{-5}	0.08	N.A.	1800;2000	none
	recovery	N.A.	41	3.4×10^{-5}	0.08	N.A.	1800;2000	none
H-11b1	multipad/rc	N.A.	27	N.A.	0.025	-6.8	2900;3300	none
H-11b3	multipad/rc	N.A.	27	1.5×10^{-4}	0.028	N.A.	1100;1200	none
H-11b4	multipad/rc	N.A.	29	8.2×10^{-5}	0.015	N.A.	1000;1900	none
DOE-1	multipad							
	drawdown	N.A.	9.0	2.4×10^{-6}	0.025	N.A.	none	28000
	recovery	N.A.	8.2	2.2×10^{-6}	0.025	N.A.	none	none
H-3b2	multipad/dd	N.A.	7.3-11	8.4×10^{-6}-1.3×10^{-5}	N.A.	N.A.	none	33000
H-14	multipad/dd	N.A.	6.0	3.7×10^{-5}	N.A.	N.A.	none	none
H-15	multipad/dd	N.A.	7.1	4.7×10^{-6}	N.A.	N.A.	none	28000
H-17	multipad/dd	N.A.	13	1.8×10^{-5}	N.A.	N.A.	none	13000
P-17	multipad/dd	0.6	21	4.7×10^{-5}	N.A.	N.A.	none	none
Cabin Baby-1	multipad/dd	0.4	13	6.5×10^{-5}	N.A.	N.A.	none	none

MATCH PARAMETERS

p^*	= 136.07 psia
p_i	= 33.88 psia
α	= 10^{-20}
β	= 1.0
t	= 0.0039 hr
r_c	= 0.0831 ft

□ DATA
— SINGLE-POROSITY TYPE CURVE

t_0 = 82:13:43:06

ELAPSED TIME, hours
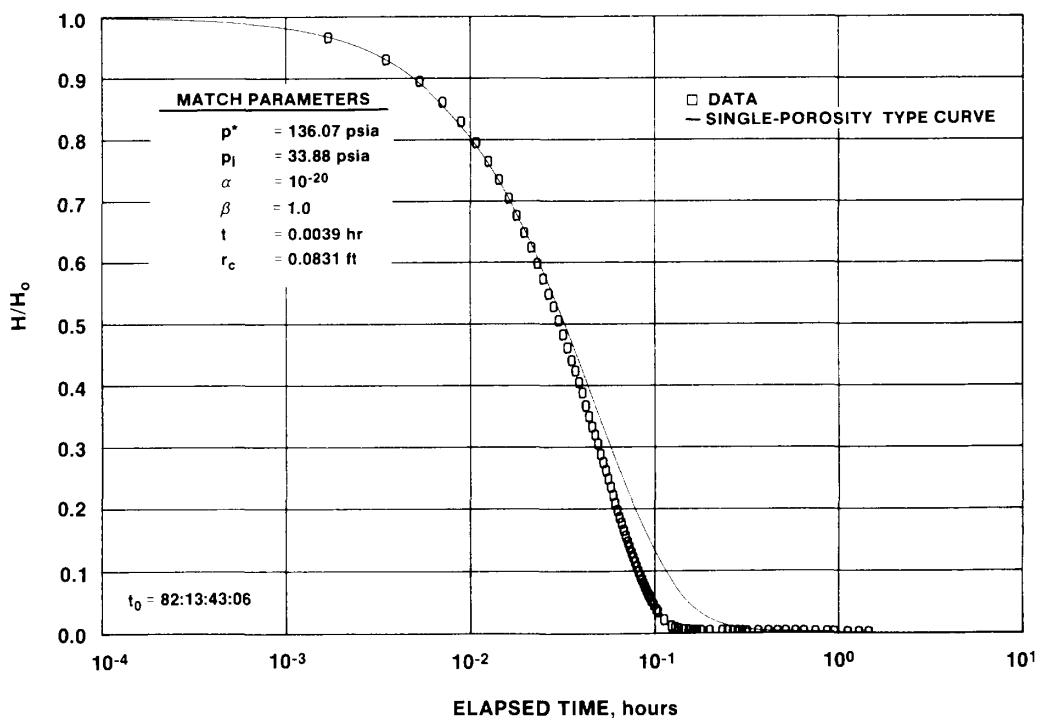
Figure 6-2. H-11b4 Slug-Test #2 Plot.

MATCH PARAMETERS

Δp	= 1.0 psi
t	= 1.0 hr
p_D	= 0.49
t_D/C_D	= 330
$(C_D e^{2s})_f$	= 2.0
$(C_D e^{2s})_{f+m}$	= 0.05
λe^{-2s}	= 0.08
p_i	= 111.92 psig

BOUNDARIES

NO-FLOW AT D_D = 12,000
                        30,000

□ PRESSURE DATA
× PRESSURE-DERIVATIVE DATA
— SIMULATIONS

DIMENSIONLESS TIME GROUP, t_D/C_D
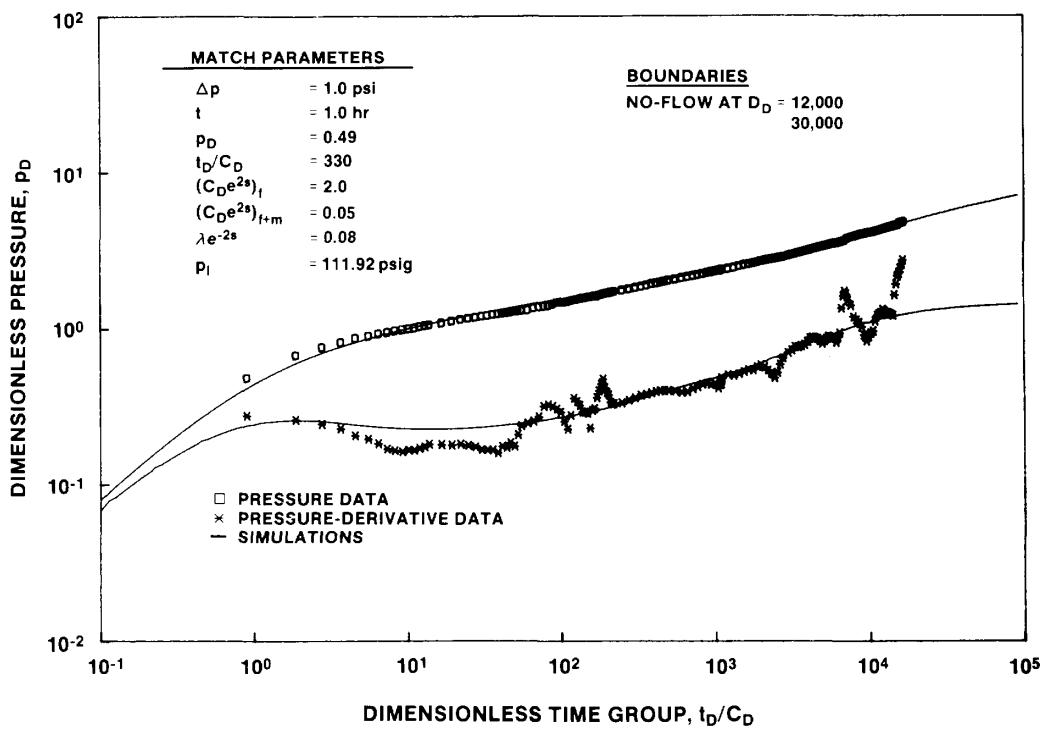
Figure 6-3.   Log-Log Plot of H-11b4 Drawdown During the H-11b4 Pumping Test.

58

MATCH PARAMETERS

Δp	= 1.0 psi
t	= 1.0 hr
p_D	= 0.49
t_D/C_D	= 330
$(C_D e^{2s})_f$	= 2.0
$(C_D e^{2s})_{f+m}$	= 0.05
λe^{-2s}	= 0.08
p_I	= 111.92 psig

BOUNDARIES
NO-FLOW AT D_D = 12,000
30,000

+ DATA
— SIMULATION

t_0 = 95:11:00
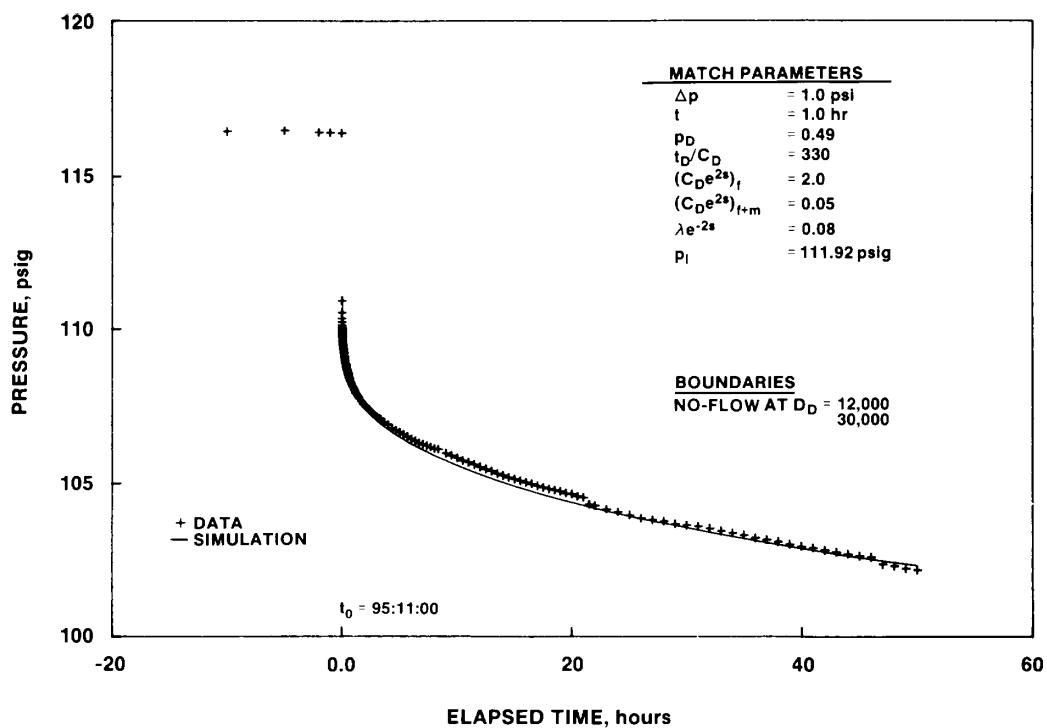
Figure 6-4. Linear-Linear Plot of H-11b4 Drawdown During the H-11b4 Pumping Test.

MATCH PARAMETERS

Δp	= 1.0 psi
t	= 1.0 hr
p_D	= 0.49
t_D/C_D	= 330
$(C_D e^{2s})_f$	= 0.8
$(C_D e^{2s})_{f+m}$	= 0.02
λe^{-2s}	= 0.2
p_I	= 107.4 psig

BOUNDARIES
NO-FLOW AT D_D = 12,000
30,000

□ PRESSURE DATA
× PRESSURE-DERIVATIVE DATA
— SIMULATIONS
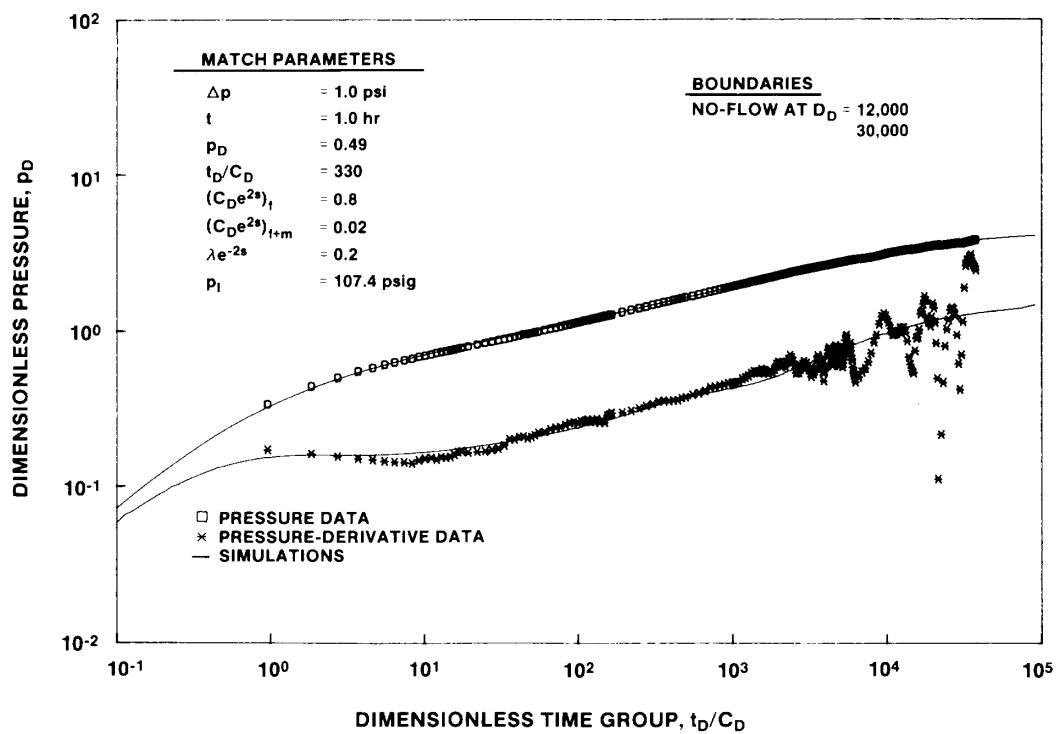
Figure 6-5. Log-Log Plot of H-11b4 Recovery During the H-11b4 Pumping Test.

59
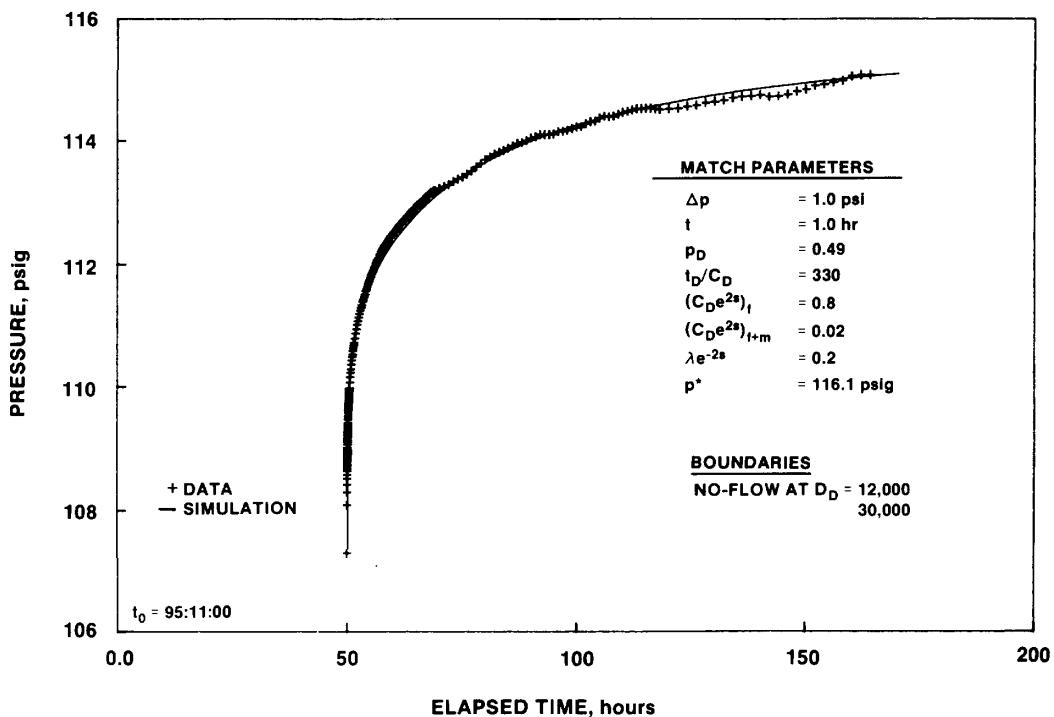
Figure 6-6. Linear-Linear Plot of H-11b4 Recovery During the H-11b4 Pumping Test.
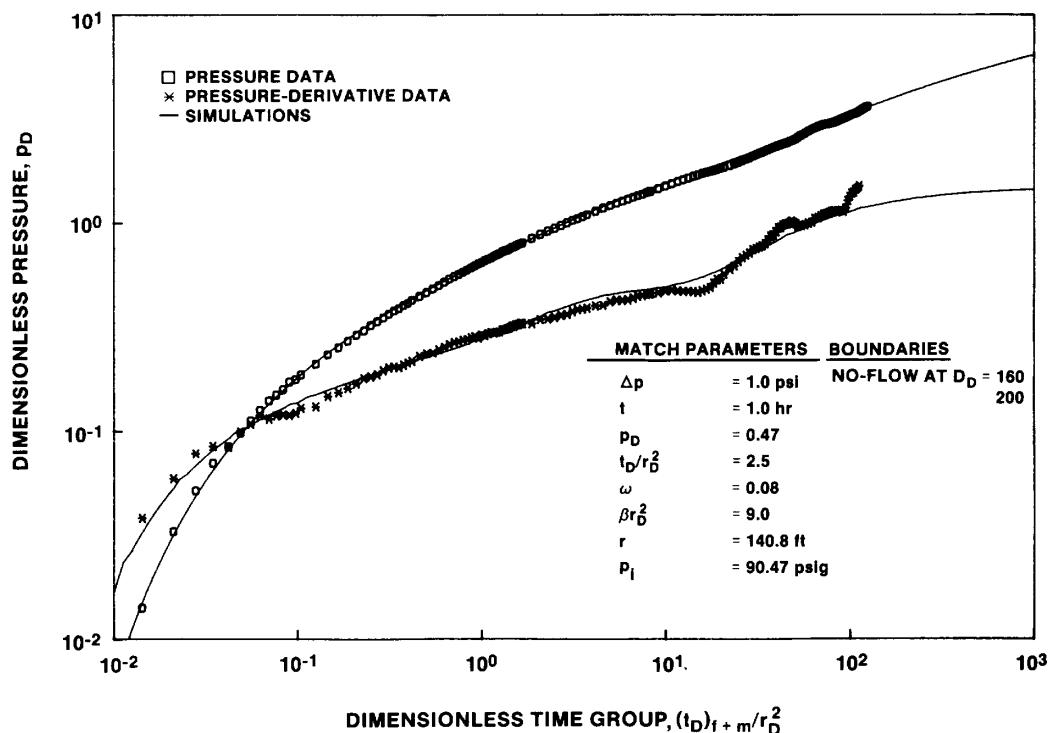
Figure 6-7. Log-Log Plot of H-11b1 Drawdown During the H-11b4 Pumping Test.

60

pumping test. As was the case with H-11b4 (Figure 6-3), the more abrupt oscillations in the pressure-derivative data were caused by the diurnal pressure fluctuations discussed in Section 5.2. A simulation of the drawdown data generated using INTER-PRET is also shown in Figure 6-7. The simulation is of a line-source well in a double-porosity medium with spherical matrix blocks and unrestricted interporosity flow. The medium has a transmissivity of 41 ft²/day, a total-system storativity of 3.4 × 10⁻⁵, and a storativity ratio (ω) of 0.08 (Table 6-1). The simulation also includes the effects of two no-flow boundaries at dimensionless distances of 160 and 200, corresponding to distances to image discharge wells of about 1800 and 2000 ft in a homogeneous system (see Section 6.3 and Appendix B).

Figure 6-8 shows a log-log plot of the H-11b1 recovery data, along with a simulation generated by INTER-PRET using exactly the same model as was used for the drawdown simulation. The simulation fits the data as well as can be expected given the oscillations caused by diurnal pressure fluctuations. Figure 6-9 shows a linear-linear plot of both the drawdown and recovery data from H-11b1, as well as the simulation. The data and the simulation are in close agreement over the entire test.

6.3 H-11 Multipad Pumping Test

The H-11 multipad pumping test data, both from the pumping well and from the observation wells, were interpreted using analytical techniques developed for tests in homogeneous, porous media. These techniques readily and rigorously accomodate such factors as double-porosity, anisotropy, and discrete boundaries. Large-scale heterogeneities, however, such as gradational changes in transmissivity and storativity with distance and direction, are not treated rigorously using these analytical techniques. In a heterogeneous system, the most information that can be obtained is a qualitative understanding of the nature of the heterogeneities and nonunique quantitative evaluations of average hydraulic properties over the distances of the observations.

For example, in a homogeneous, isotropic aquifer, water is contributed to the pumping well equally from all directions. In a heterogeneous aquifer, less perme-

able regions will contribute less water and more permeable regions will contribute more water. In a heterogeneous aquifer with smoothly and monotonically varying properties, this will cause more drawdown in the more permeable regions than would result from pumping at the same rate in a homogeneous system, and less drawdown in the less permeable regions. As a result, estimates of the transmissivity between the pumping well and an observation well in a more permeable region will be too low, and estimates of the transmissivity between the pumping well and an observation well in a less permeable region will be too high. In a more complex heterogeneous aquifer with an irregular distribution of properties, responses are more difficult to predict and could result in estimated hydraulic properties which are either too high or too low. Thus, the solution obtained from a single test in a heterogeneous aquifer is in no sense a unique description of the average hydraulic properties between any two points.

Numerical rather than analytical modeling is required to define the distribution of hydraulic properties that will best simulate the responses observed when a number of wells in a heterogeneous system are pumped concurrently or in succession. Numerical modeling of the responses to the H-11 multipad test and other tests will be performed as an extension of the modeling reported by Haug et al. (1987) and LaVenue et al. (1988). In this report, the transmissivity and storativity values derived using an analytical approach are termed the "apparent" values.

A final cautionary note is appropriate with regard to the hydraulic boundaries (image wells) used in the simulations presented below. The INTERPRET code uses image wells at specific distances from the pumping and observation wells to simulate the effects of hydraulic boundaries. In defining the distances to the boundaries, an assumption is made that the aquifer is homogeneous. If these boundaries were in fact discrete hydrogeologic features such as faults or rivers intersecting the aquifer, and if the aquifer were homogeneous, the uncertainty in the distances presented would be, at best, about ±10 percent. In the case of the Culebra, the boundaries are believed to represent a heterogeneous distribution of transmissivity, and the significance of the distances provided by the simulations is unclear. Consequently,

Figure 6-8

DIMENSIONLESS PRESSURE, p_D

□ PRESSURE DATA
✱ PRESSURE-DERIVATIVE DATA
— SIMULATIONS

10^1
10^0
10^{-1}
10^{-2}
10^{-3}

10^{-3} 10^{-2} 10^{-1} 10^0 10^1 10^2 10^3 10^4

DIMENSIONLESS TIME GROUP, $(t_D)_{t+m}/r_D^2$

MATCH PARAMETERS	
Δp	= 1.0 psi
t	= 1.0 hr
p_D	= 0.47
t_D/r_D^2	= 2.5
ω	= 0.08
βr_D^2	= 9.0
r	= 140.8 ft
p_i	= 82.75 psig

BOUNDARIES
NO-FLOW AT D_D = 160
200
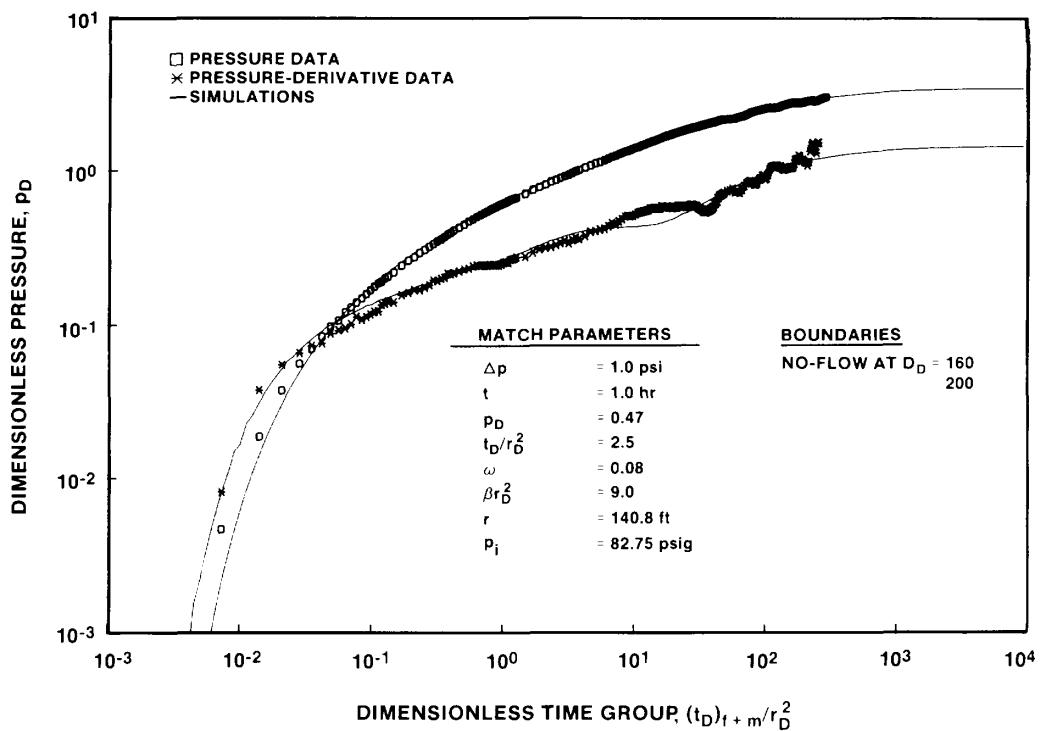
Figure 6-8. Log-Log Plot of H-11b1 Recovery During the H-11b4 Pumping Test.

Figure 6-9

PRESSURE, psig

92
90
88
86
84
82
80

+ DATA
— SIMULATION

t_0 = 95:11:00

-50 0.0 50 100 150 200

ELAPSED TIME, hours

MATCH PARAMETERS	
Δp	= 1.0 psi
t	= 1.0 hr
p_D	= 0.47
t_D/r_D^2	= 2.5
ω	= 0.08
βr_D^2	= 9.0
r	= 140.8 ft
p^*	= 90.47 psig

BOUNDARIES
NO-FLOW AT D_D = 160
200
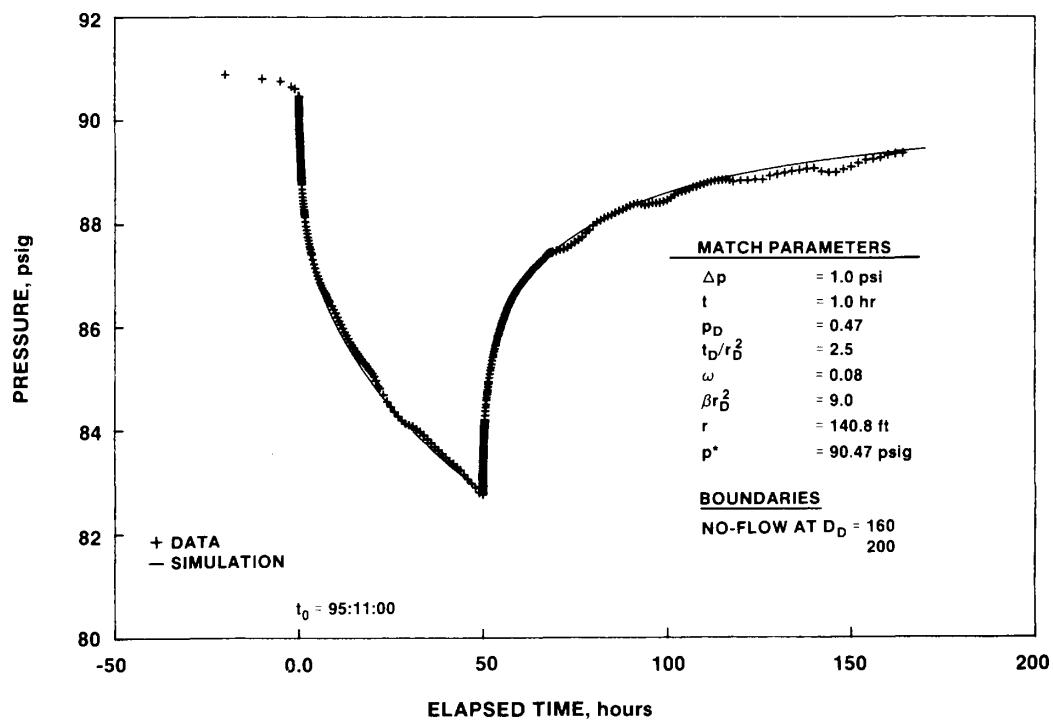
Figure 6-9. Linear-Linear Plot of H-11b1 Response During the H-11b4 Pumping Test.

the boundaries used in the simulations should not be viewed quantitatively, but should be regarded as indicators of the types of transmissivity changes occurring in different regions.

Subject to these limitations, the analytical interpretations of the H-11 multipad test data had the following objectives:

- Determine the most appropriate conceptualization of the nature of the Culebra flow system in the vicinity of the H-11 hydropad

- Quantify the hydraulic properties of the Culebra dolomite in the vicinity of the H-11 hydropad

- Determine the nature and distribution of heterogeneities in the Culebra dolomite within the area influenced by the test

- Determine apparent hydraulic properties of the Culebra dolomite between H-11b1 and observation wells

No interpretations of the drawdown data from the H-11 wells were performed because pump stoppages, pumping-rate fluctuations, and pressure fluctuations caused by tracer injection in H-11b2, H-11b3, and H-11b4 all affected the observed responses in such a way as to add uncertainty to any interpretations that might be performed. The recovery data were considered higher quality data sets amenable to less ambiguous interpretation, and formed the basis for the analyses presented below.

When possible, the drawdown and recovery data observed at the distant observation wells were interpreted separately, and then combined for additional interpretation. In most cases, the recovery data could not be interpreted in isolation from the drawdown data because of the anomalous water-level rises discussed in Section 5.3. In these cases, no separate recovery interpretations were made and the drawdown data were interpreted in conjunction with interpretation of the total test data. In the cases of H-4b, H-12, H-14, and P-15, the drawdown data were insufficient for separate interpretation, and the drawdown and recovery data were interpreted together.

6.3.1 H-11b1. Figure 6-10 shows a log-log plot of the recovery data from H-11b1 along with the best-fit simulation of those data generated by INTERPRET. The simulation shown uses a formulation for a double-porosity system with spherical matrix blocks, unrestricted interporosity flow, and a transmissivity of 27 ft^2/day (Table 6-1), and includes the effects of two no-flow boundaries at dimensionless distances of 15,000 and 20,000. Assuming a total-system compressibility of 1×10^{-5} psi^{-1} and a matrix porosity of 16%, the wellbore-skin factor for the simulation shown in Figure 6-10 is -6.8. The storativity ratio (ω) is 0.025, and the interporosity flow coefficient (λ) is 2.0×10^{-7}. Assuming a homogeneous system with the hydraulic properties listed above, the no-flow boundaries correspond to image discharge wells at distances of 2900 and 3300 ft from H-11b1. The sharp rise in the pressure-derivative data in Figure 6-10 at very late time indicates an acceleration of recovery. The reason for this acceleration is unknown, but may be related to whatever factor was responsible for the anomalous water-level rise seen at wells such as H-4b (Section 5.3.1.7).

Figure 6-11 shows a dimensionless Horner plot of the H-11b1 recovery data along with a simulation generated using the model discussed above. The simulation and data are in excellent agreement throughout the recovery period. Extrapolation of the data to infinite recovery time at the plot origin indicates a static formation pressure of 129.0 psig, whereas the actual pressure measured just before the pumping period began was only 125.9 psig (Appendix A, Table A-1). Both test-interval transducers in H-11b1 indicated pressures of 126.7 psig or greater late in the recovery period when the packer in the well was temporarily deflated. Thus, the over-recovery at H-11b1 was at least partially "real" in the sense that it represented an actual change in water level, and was not simply an accumulation of gas as discussed in Section 5.3.1.3 in relation to H-11b3.

Figure 6-12 shows a linear-linear plot and simulation of the H-11b1 recovery data. Again, the fit between the data and a simulation that assumes a static formation pressure of 129.0 psig is excellent.

6.3.2 H-11b3. A log-log plot of the recovery data from H-11b3 is shown in Figure 6-13. The plot also
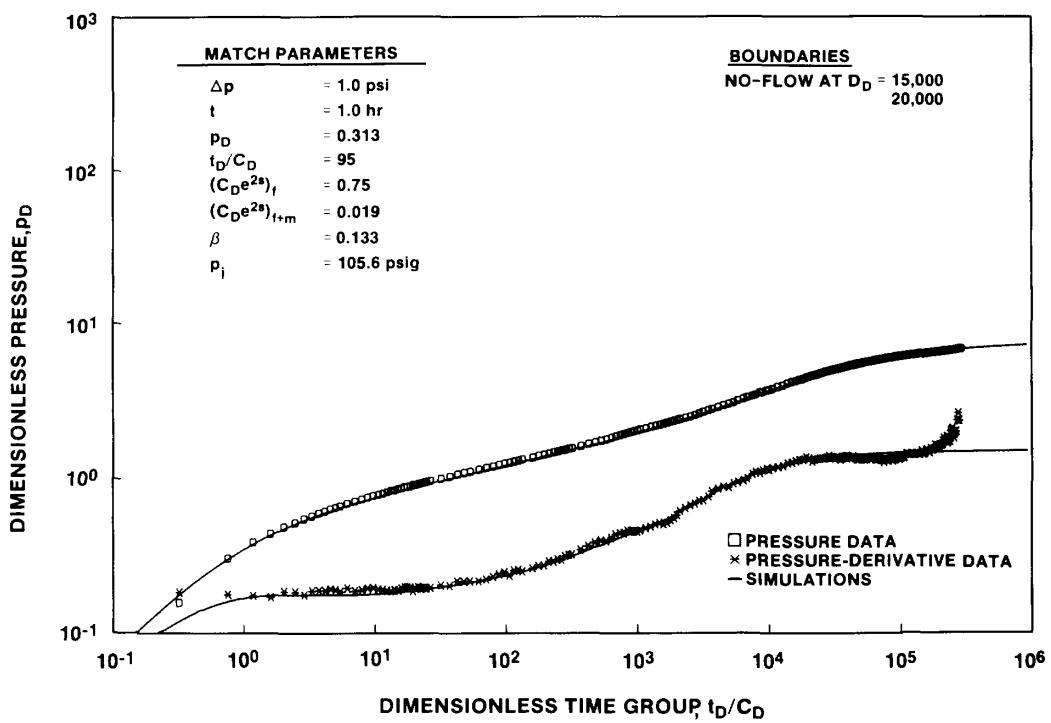
Figure 6-10. Log-Log Plot of H-11b1 Recovery During the H-11 Multipad Pumping Test.
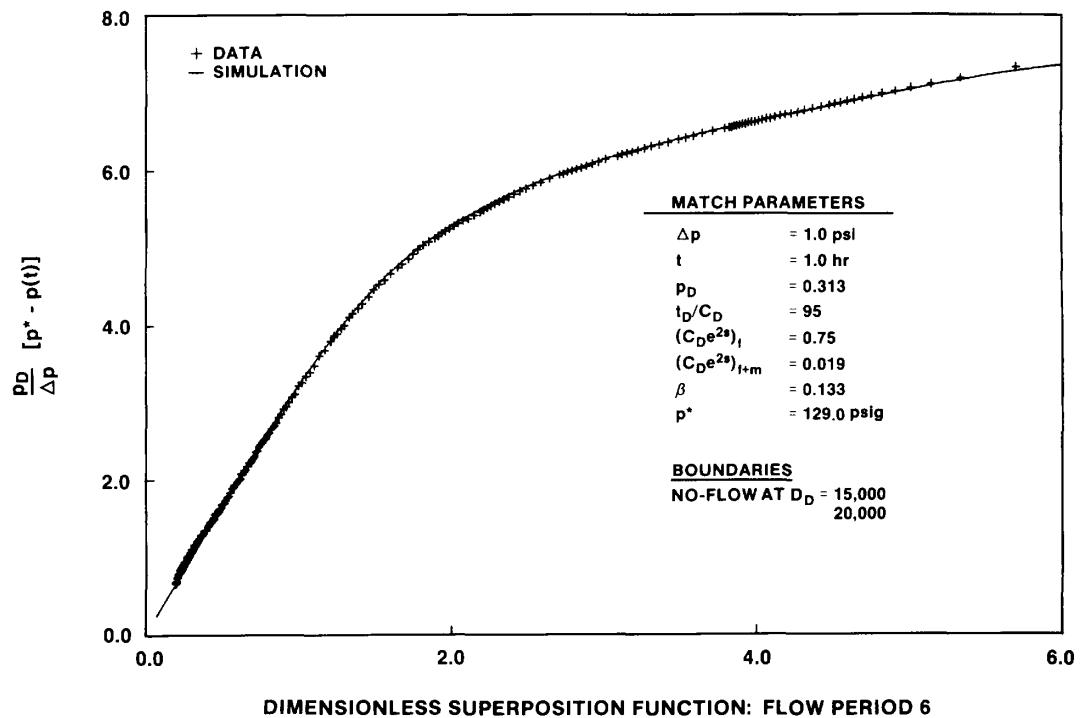
Figure 6-11. Dimensionless Horner Plot of H-11b1 Recovery During the H-11 Multipad Pumping Test.
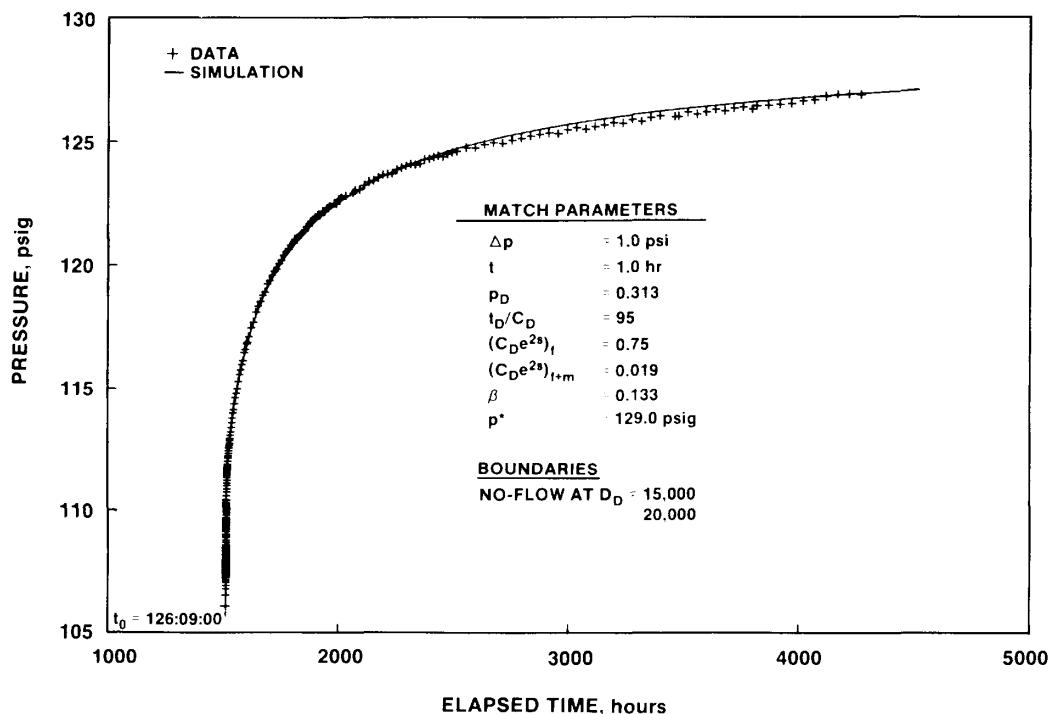
Figure 6-12. Linear-Linear Plot of H-11b1 Recovery During the H-11 Multipad Pumping Test.
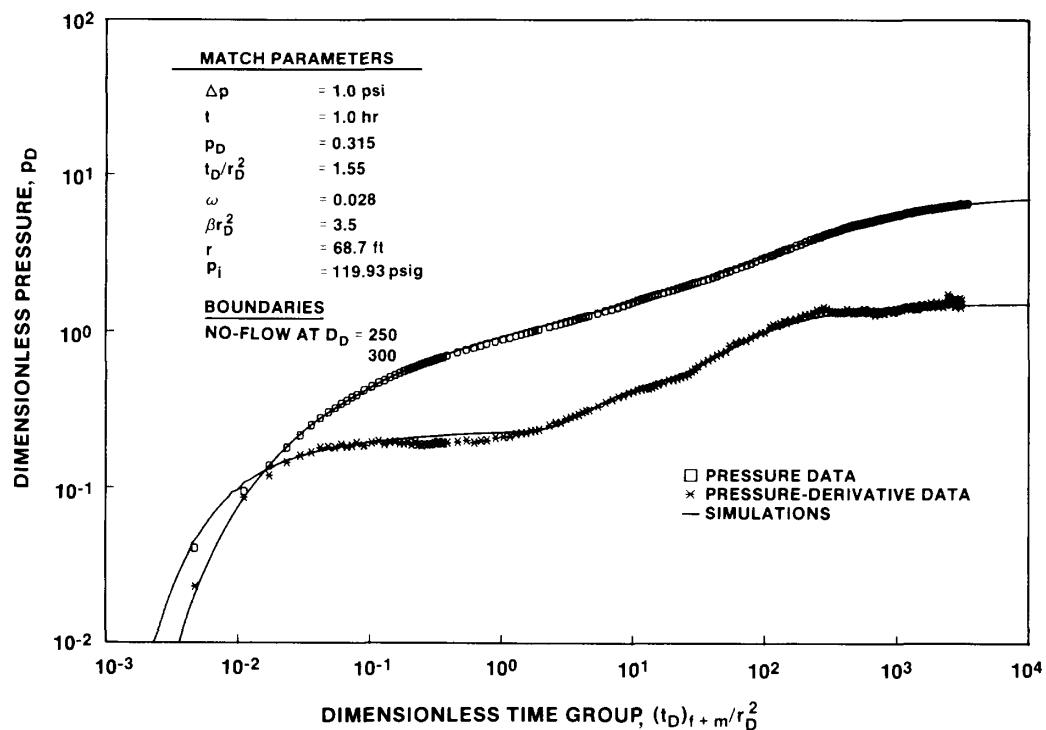
Figure 6-13. Log-Log Plot of H-11b3 Recovery During the H-11 Multipad Pumping Test.

includes the best-fit simulation of the data generated using INTERPRET. The simulation is of a line-source well in a double-porosity medium with spherical matrix blocks and unrestricted interporosity flow. The medium has a transmissivity of 27 ft^2/day, a total-system storativity of 1.5×10^{-4}, and a storativity ratio of 0.028 (Table 6-1). The simulation also includes the effects of two no-flow boundaries at dimensionless distances of 250 and 300, corresponding to image discharge wells at distances of about 1100 and 1200 ft from H-11b3.

Figure 6-14 shows a dimensionless Horner plot of the H-11b3 recovery data, along with a simulation generated using the model discussed above. The simulation extrapolation to infinite recovery time indicates the static formation pressure is 143.0 psig. The pressure at the beginning of the pumping period, however, was only 137.3 psig (Appendix A, Table A-1). The disparity between the static formation pressure indicated by the recovery data and the actual pressure at the start of the multipad test is shown on Figure 6-15. This figure shows a linear-linear plot of the H-11b3 drawdown and recovery data up to the time when the packer was deflated in H-11b3 (Section 5.3.1.3). The simulation fits the recovery data very well, but indicates a higher pressure at the start of the pumping period and more drawdown during the pumping period than were actually observed.

As discussed in Section 5.3.1.3, the apparent over-recovery of pressure at H-11b3 may have been related to gas accumulation underneath the packer in the well where the transducer accesses the test interval because the "excess" pressure vanished when the packer was deflated (Figure 5-5). If the Culebra water at the H-11 hydropad contains dissolved gas, any decrease in pressure, such as that caused by pumping, may cause gas to come out of solution and migrate to the highest elevation available. During the H-11 multipad pumping test, the highest elevation available was immediately beneath the packer in the wellbore, which is also where the transducer feedthrough accesses the test interval. The continued accumulation of free gas as drawdown continued during the pumping test might have reduced the amount of drawdown shown by the pressure transducer. When pumping ceased and recovery began, the gas would not go back into solution at as rapid a rate as it had come out, and changes in

gas pressure might simply reflect the changes in water pressure occurring in the Culebra during recovery. In this case, no analysis could be made of the drawdown data, because they would represent a superposition of a pumping-induced pressure decrease and a gas-induced pressure increase, but the recovery data could be interpreted if the gas-pressure changes closely mirrored the water-pressure changes in the Culebra.

This hypothesis is consistent with the observed pressure behavior at H-11b3 during the H-11 multipad test. The rate of drawdown observed at H-11b3 was erratic (Figure 6-15), and the total amount of drawdown observed was only 16.9 psi (Appendix A, Table A-1). The observed recovery at H-11b3 totalled 20.7 psi, and the simulation derived from the recovery data indicated a total drawdown of 23.1 psi. Considering that a total drawdown of about 15.4 psi was observed at well DOE-1 (Appendix A, Table A-2), 3900 ft farther from H-11b1 than is H-11b3, the amount of simulated drawdown at H-11b3 appears more realistic than that observed.

Without knowing more about the cause of the over-recovery of pressure while the packer was inflated in H-11b3, no definitive statement can be made about the reliability of the analysis of the recovery data. However, the analysis produced a double-porosity conceptual model for the Culebra that is both qualitatively and quantitatively consistent with interpretations of other pumping tests at the H-11 hydropad presented by Saulnier (1987), as well as with interpretations of the H-11b4 pumping test (Section 6.2) and of the H-11b1 (Section 6.3.1) and H-11b4 (Section 6.3.3) responses to the H-11 multipad test. Thus, the analysis appears to provide a realistic representation of the hydraulic properties of the Culebra dolomite between H-11b1 and H-11b3.

6.3.3 H-11b4. Figure 6-16 shows a log-log plot of the recovery data from H-11b4 along with the best-fit simulation obtained. The simulation is of a line-source well in a double-porosity medium with spherical matrix blocks and unrestricted interporosity flow. The medium has a transmissivity of 29 ft^2/day, a total-system storativity of 8.2×10^{-5}, and a storativity ratio of 0.015 (Table 6-1). The simulation also includes two no-flow boundaries at dimensionless distances of 50
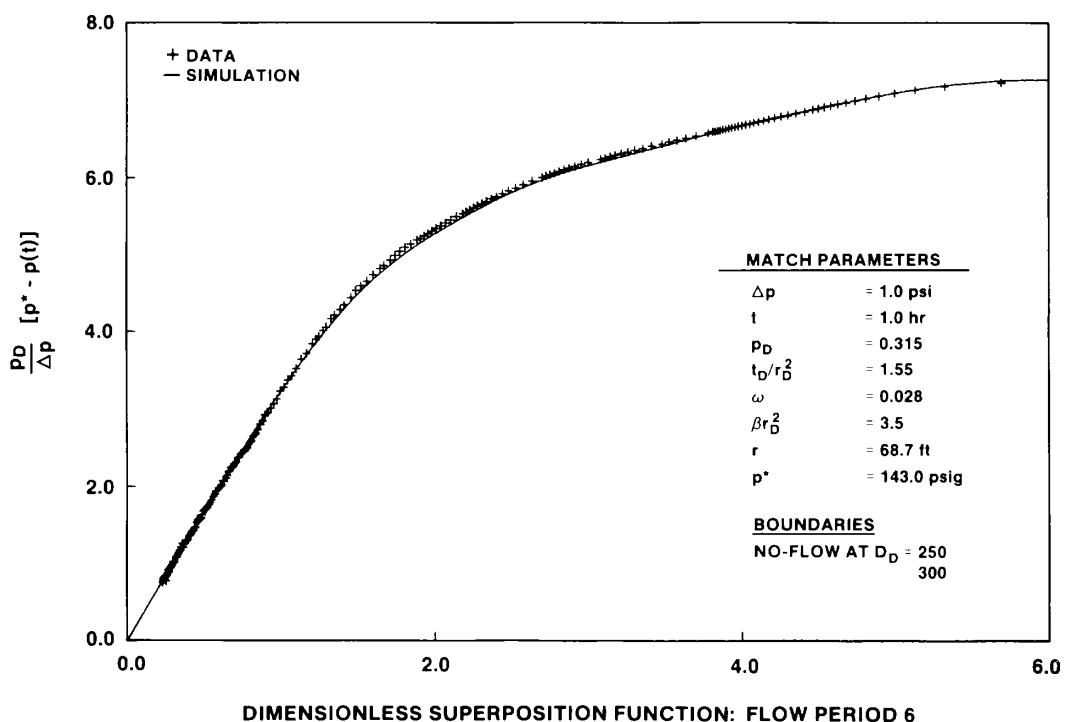
Figure 6-14. Dimensionless Horner Plot of H-11b3 Recovery During the H-11 Multipad Pumping Test.
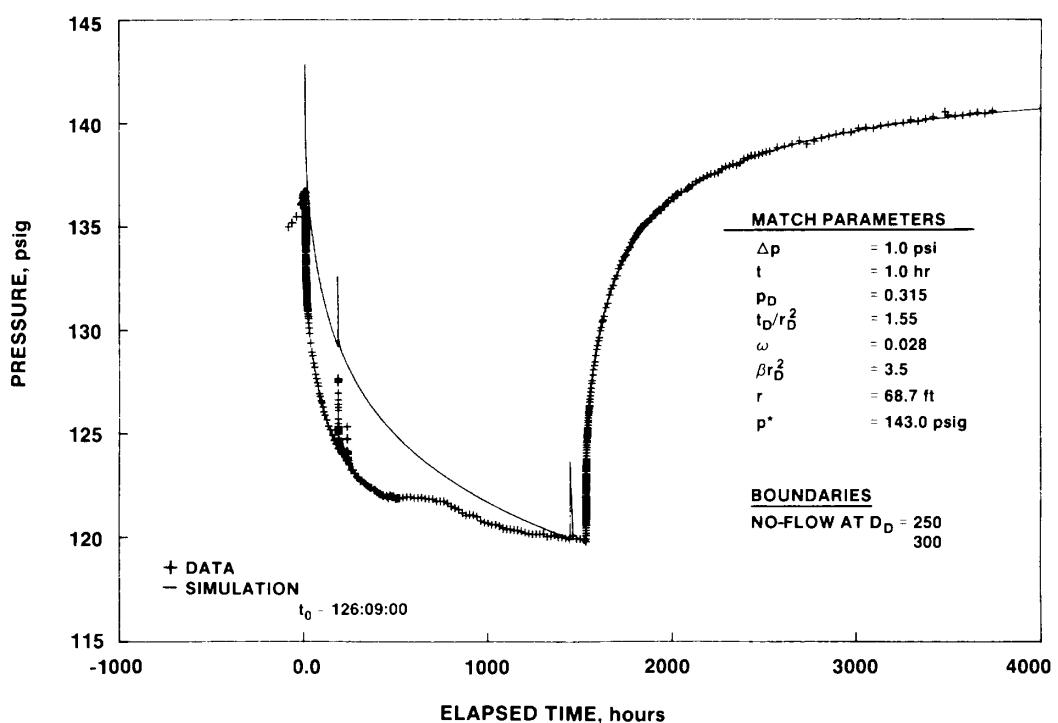
Figure 6-15.   Linear-Linear Plot of H-11b3 Response During the H-11 Multipad Pumping Test.

10^2

MATCH PARAMETERS

Δp	$= 1.0$ psi
t	$= 1.0$ hr
P_D	$= 0.341$
t_D/r_D^2	$= 0.75$
ω	$= 0.015$
βr_D^2	$= 40$
r	$= 141.3$ ft
P_i	$= 117.11$ psig

BOUNDARIES
NO-FLOW AT $D_D = 50$
                    180

□ PRESSURE DATA
✗ PRESSURE-DERIVATIVE DATA
— SIMULATIONS

10^1

10^0

10^{-1}

10^{-2}

DIMENSIONLESS PRESSURE, P_D

10^{-3} 10^{-2} 10^{-1} 10^0 10^1 10^2 10^3

DIMENSIONLESS TIME GROUP, $(t_D)_{f+m}/r_D^2$
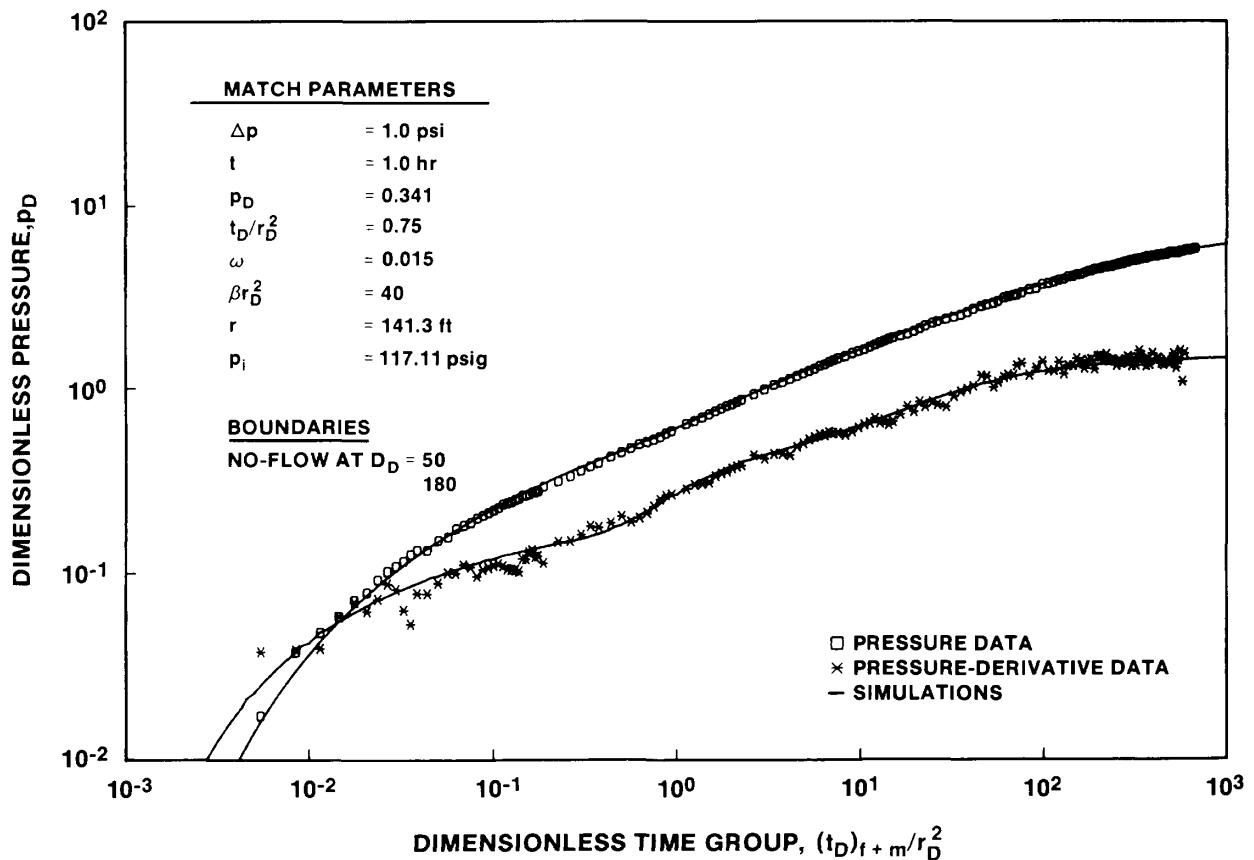
Figure 6-16. Log-Log Plot of H-11b4 Recovery During the H-11 Multipad Pumping Test.

and 180. These boundaries correspond to image discharge wells at distances of 1000 and 1900 ft from H-11b4 (see Appendix B).

A dimensionless Horner plot of the H-11b4 recovery data and simulation is shown in Figure 6-17. The simulation fits the data well assuming a static formation pressure of 138.3 psig. The pressure at the beginning of the pumping period, however, was only 130.3 psig (Appendix A, Table A-1). The 8-psi disparity between the observed pressure at the start of the test and the static formation pressure indicated by the H-11b4 recovery simulation is shown on Figure 6-18. This figure shows a linear-linear plot of the H-11b4 drawdown and recovery data along with the simulation derived from the recovery analysis. The simulation is in close agreement with the recovery data, but indicates more drawdown and a higher starting pressure than were observed.

As discussed in Section 6.3.2 with respect to H-11b3, the low amount of drawdown at H-11b4, the erratic rate of drawdown, and the apparent over-recovery may be related to some type of gas buildup underneath the packer in the well. No over-recovery was observed when the packer was deflated to allow the annulus transducer to measure the Culebra pressure after the test-interval transducer had failed (Figure 5-6). Except for the 8-psi offset discussed above, however, the recovery data appear to provide a reliable representation of the Culebra response following the H-11b1 pumping period. The simulation of the recovery is both qualitatively and quantitatively in agreement with those derived from the H-11b1 and H-11b3 recovery data, as well as with the interpretations of earlier tests at the H-11 hydropad presented by Saulnier (1987). Furthermore, the total amount of drawdown observed at H-11b4 was about 13.1 psi, whereas the simulation indicates the total

MATCH PARAMETERS

Δp	= 1.0 psi
t	= 1.0 hr
p_D	= 0.341
t_D/r_D^2	= 0.75
ω	= 0.015
βr_D^2	= 40
r	= 141.3 ft
p^*	= 138.3 psig

BOUNDARIES

NO-FLOW AT D_D = 50
180

+ DATA
— SIMULATION

DIMENSIONLESS SUPERPOSITION FUNCTION: FLOW PERIOD 6
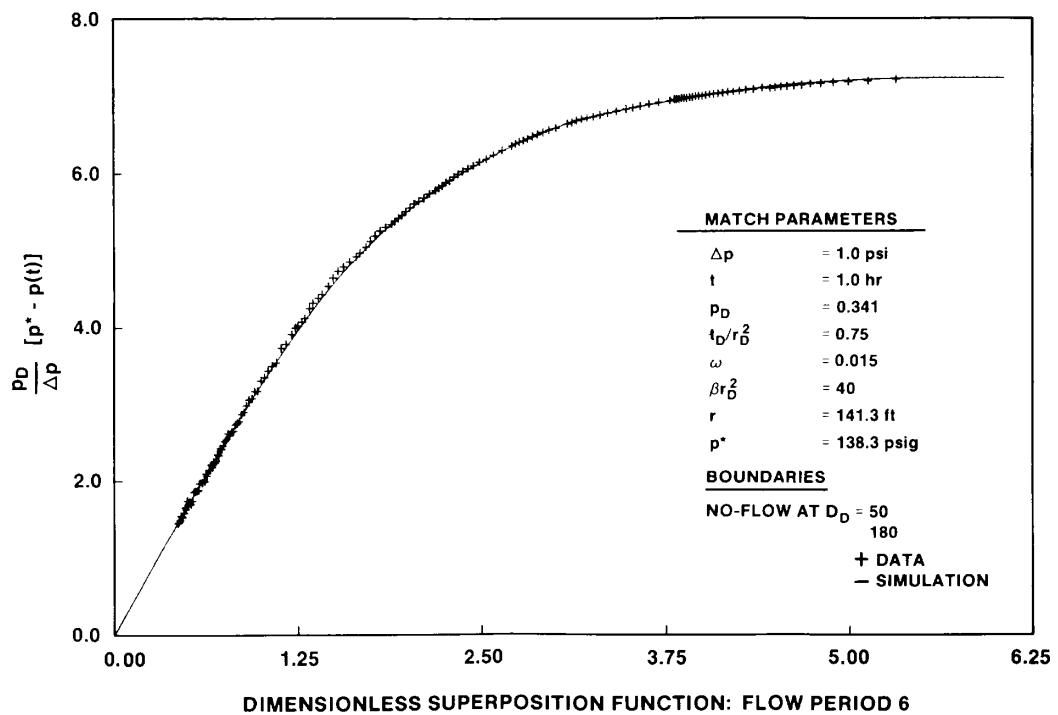
Figure 6-17. Dimensionless Horner Plot of H-11b4 Recovery During the H-11 Multipad Pumping Test.

+ DATA
— SIMULATION

t_0 = 126:09:00

MATCH PARAMETERS

Δp	= 1.0 psi
t	= 1.0 hr
p_D	= 0.341
t_D/r_D^2	= 0.75
ω	= 0.015
βr_D^2	= 40
r	= 140.8 ft
p^*	= 138.3 psig

BOUNDARIES

NO-FLOW AT D_D = 50
180

ELAPSED TIME, hours
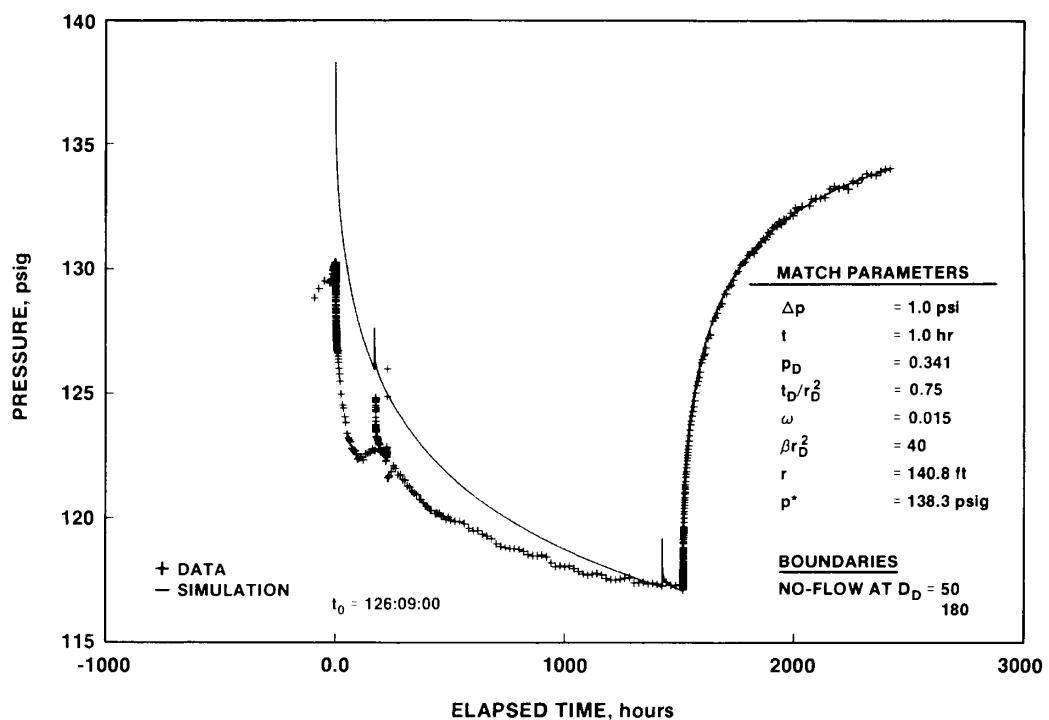
Figure 6-18. Linear-Linear Plot of H-11b4 Response During the H-11 Multipad Pumping Test.

drawdown to be about 21.2 psi. Considering that about 15.4 psi of drawdown was observed at well DOE-1 (Appendix A, Table A-2), 3830 ft farther from H-11b1 than is H-11b4, the simulated H-11b4 drawdown appears more realistic than that observed. For these reasons, the interpretation of the H-11b4 recovery data is considered to provide representative values of Culebra hydraulic properties between H-11b1 and H-11b4, despite the apparent over-recovery of pressure.

6.3.4 DOE-1.

DOE-1 is the closest of the distant observation wells to the H-11 hydropad, and was the first of the distant wells to respond to the pumping at H-11b1, showing a drawdown response only two hours after pumping began (Table 5-1). Figure 6-19 shows a log-log plot of the DOE-1 drawdown data, along with the best-fit simulation generated using INTERPRET. The simulation is of a double-porosity medium with spherical matrix blocks and unrestricted interporosity flow. The medium has an apparent transmissivity of 9.0 ft^2/day, an apparent total-system storativity of 2.4 $\times$ 10^{-6}, and a storativity ratio of 0.025 (Table 6-1). The simulation also includes the effects of a constant-pressure boundary at a dimensionless distance of 50, which causes the pressure-derivative data to decline at late time. This constant-pressure boundary corresponds to an image recharge well about 28,000 ft from DOE-1.

The effects of the apparent constant-pressure boundary are also seen in the dimensionless Horner plot of the drawdown data (Figure 6-20), in which the slope of the data trend decreases at late time. Figure 6-21 shows a linear-linear plot of both the drawdown and recovery data from DOE-1, along with the simulation generated for the drawdown analysis. The simulation fits the drawdown data well, but predicts less recovery than was observed. Both the need for the constant-pressure boundary in the drawdown simulations and the observed recovery greater than that predicted are probably caused by the water level at DOE-1 being on a general recovery trend when the H-11 multipad test began, as discussed in Section 5.3.1.5. During the pumping period, ongoing recovery from earlier hydraulic stresses would have partially counteracted the drawdown occurring in response to H-11b1 pumping, producing the same effect as a constant-pressure boundary. During the recovery period, the recovery

from earlier stresses would have been added to the recovery from the H-11b1 pumping, causing an apparent over-recovery.

Figure 6-22 shows a log-log plot of the DOE-1 recovery data, along with a simulation generated using INTERPRET. The simulation uses the same model presented above for the drawdown data, except that it uses slightly lower values of apparent transmissivity and total-system storativity of 8.2 ft^2/day and 2.2 $\times$ 10^{-6}, respectively, and includes no boundaries. The lower transmissivity results from having to fit more recovery than drawdown, and the storativity is lower because storativity is proportional to transmissivity.

Figure 6-23 shows a dimensionless Horner plot of the DOE-1 recovery data. Extrapolation of the data to infinite recovery time at the plot origin indicates a static formation pressure of 157.6 psig, whereas the actual water level measured just before the pumping period began corresponded to a pressure of only 154.5 psig (Appendix A, Table A-2). The extrapolated pressure of 157.6 psig corresponds to a depth to water in DOE-1 of about 491 ft. This value appears reasonable as a stabilized water level for DOE-1, judging from the long-term trends seen in Figure 5-7. Figure 6-24 shows a linear-linear plot of the DOE-1 drawdown and recovery data, along with the simulation generated by the recovery model. With no constant-pressure boundary, the model overpredicts the amount of drawdown, but fits the recovery data very well assuming a static formation pressure of 157.6 psig.

Because the water level in DOE-1 was rising when the H-11 multipad test began, neither the drawdown nor recovery analyses presented above, which assume a stable formation pressure at the start of the test, can be considered to be entirely correct. The apparent transmissivity and storativity values provided by the drawdown interpretation should be the most reliable, because they were derived from the early- to intermediate-time drawdown data when the magnitude of the test response was much greater than the magnitude of the recovery response to earlier stresses. The constant-head boundary indicated by the late-time drawdown data is probably not real, but instead reflects a growing equivalence between the magnitude of the drawdown response and that of the pre-existing recovery response. As discussed above, the apparent
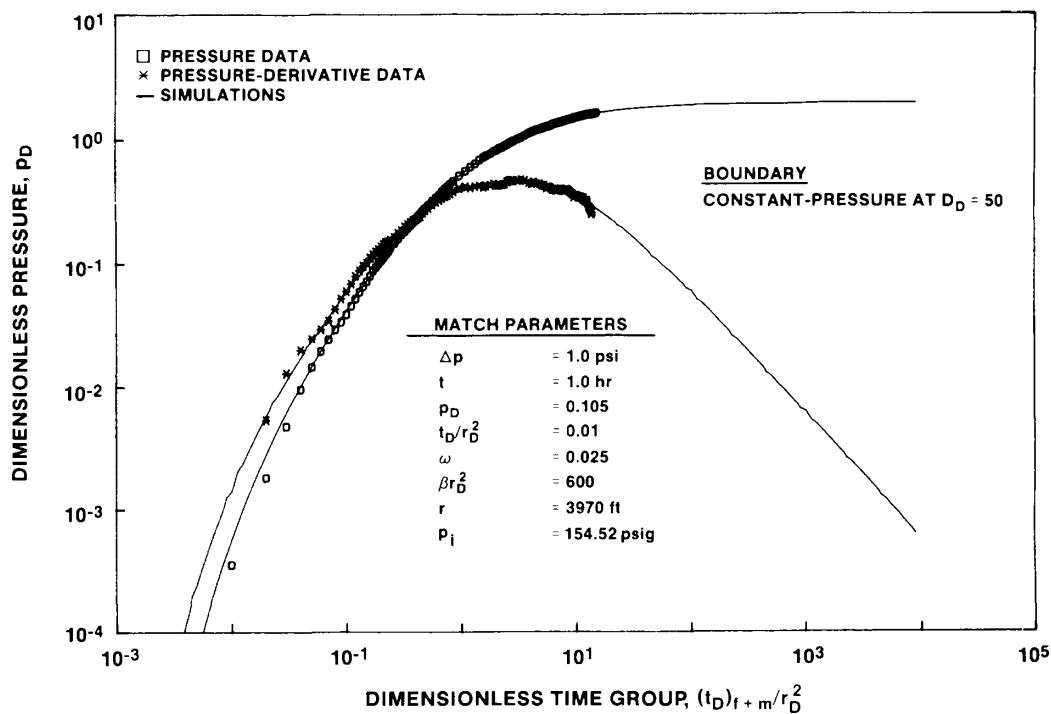
Figure 6-19. Log-Log Plot of DOE-1 Drawdown During the H-11 Multipad Pumping Test.
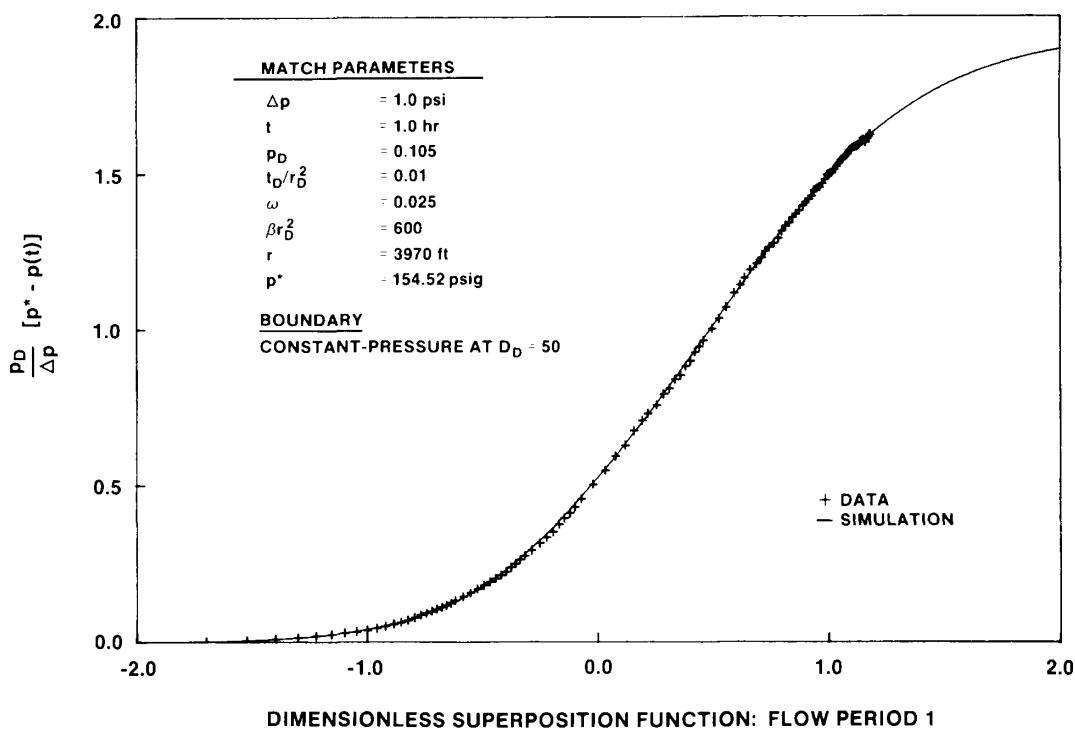
Figure 6-20. Dimensionless Horner Plot of DOE-1 Drawdown During the H-11 Multipad Pumping Test.
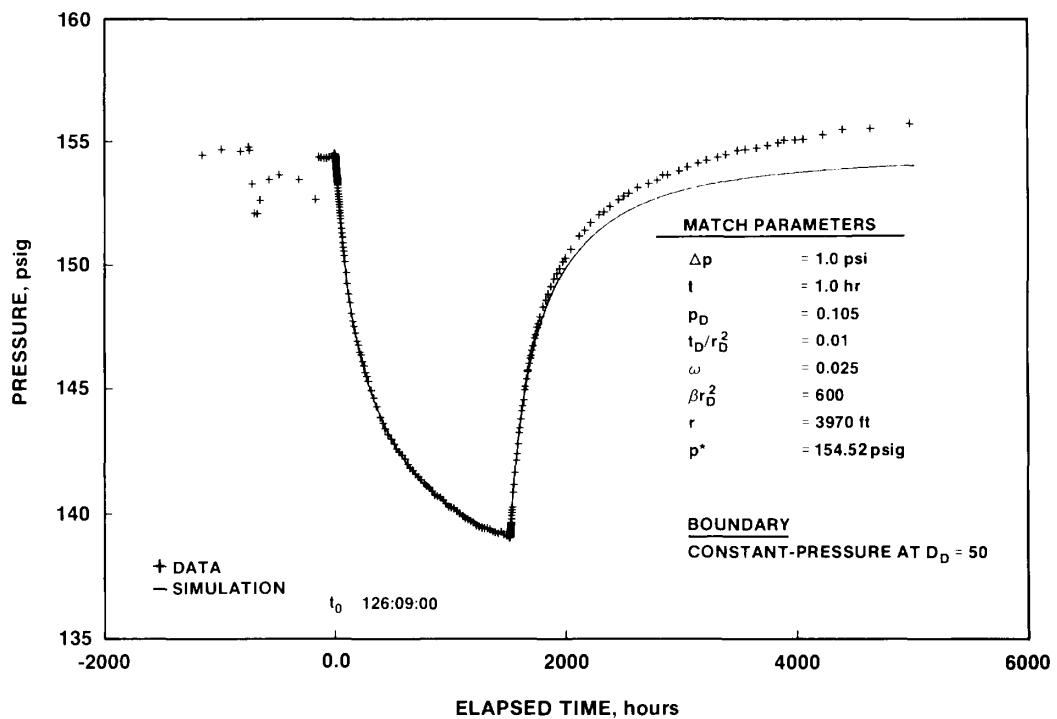
Figure 6-21. Linear-Linear Plot of DOE-1 Response During the H-11 Multipad Pumping Test with Simulation Derived from Drawdown Analysis.
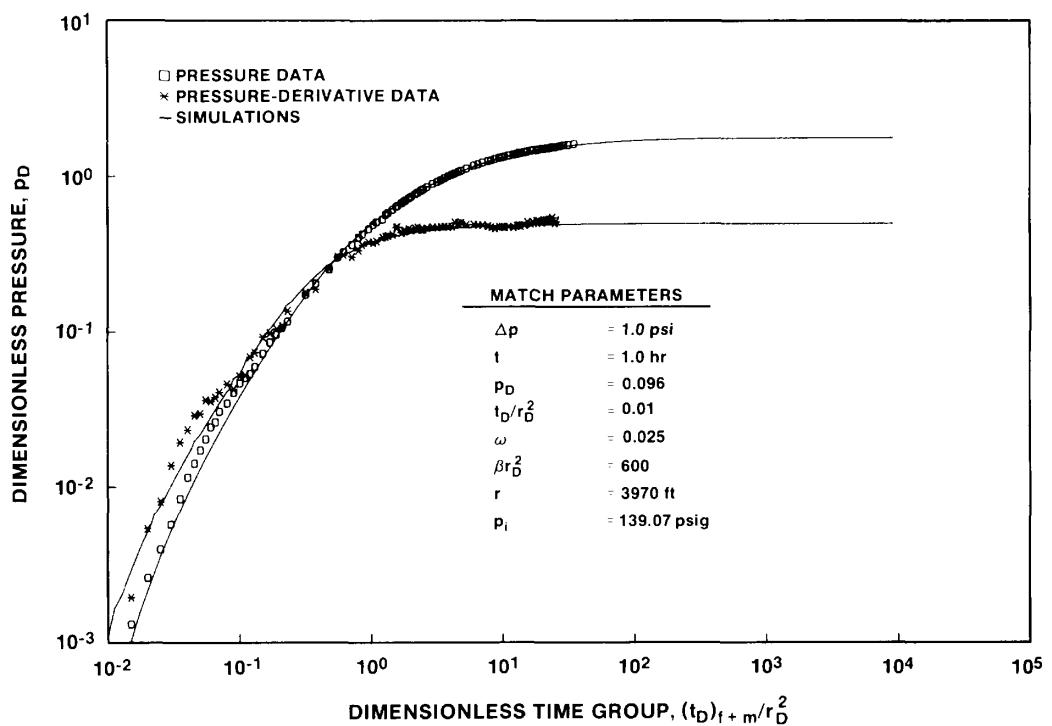
Figure 6-22. Log-Log Plot of DOE-1 Recovery During the H-11 Multipad Pumping Test.
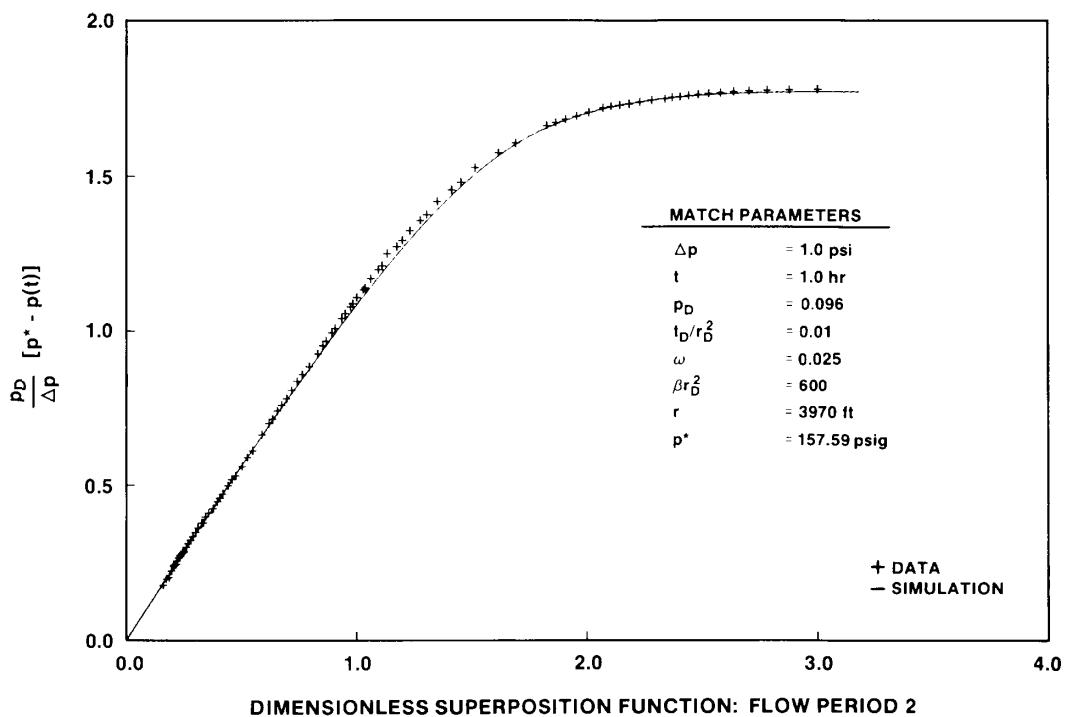
Figure 6-23. Dimensionless Horner Plot of DOE-1 Recovery During the H-11 Multipad Pumping Test.
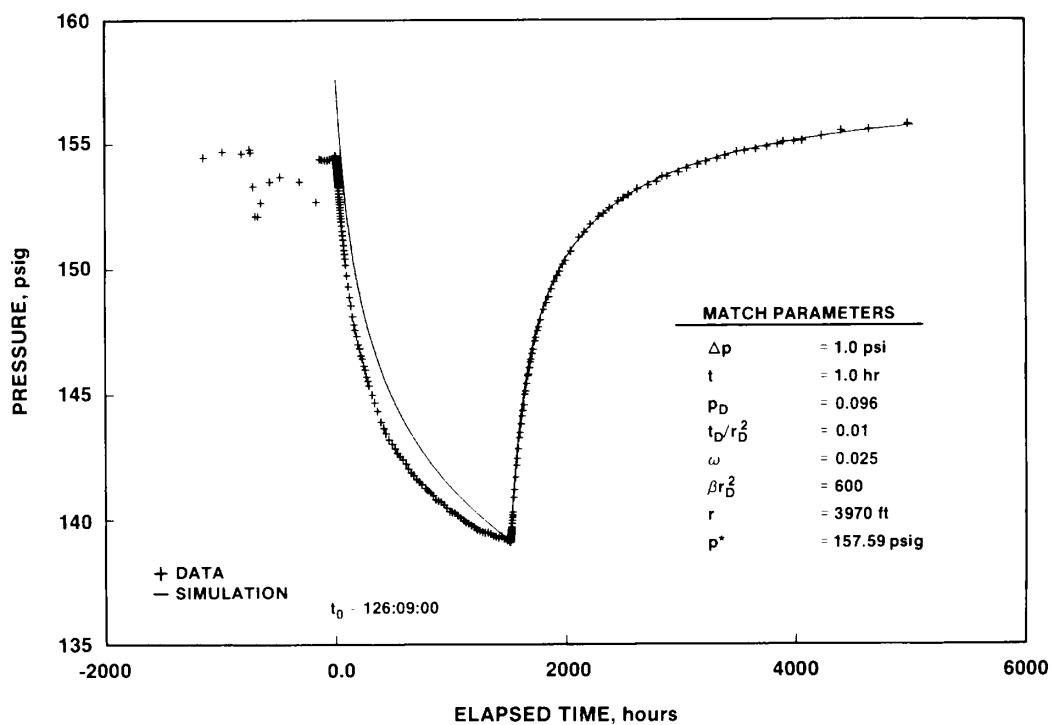
Figure 6-24. Linear-Linear Plot of DOE-1 Response During the H-11 Multipad Pumping Test with Simulation Derived from Recovery Analysis.

transmissivity and storativity values provided by the re-covery interpretation are probably too low because they account for too much recovery. The static forma-tion pressure indicated by the recovery interpretation, however, appears to be reasonable judging from pre-existing water-level trends. The fact that the same double-porosity model could be used for both the drawdown and recovery interpretations indicates that the model provides a reliable conceptualization of the hydraulic nature of the Culebra between H-11 and DOE-1.

Beauheim (1987c) reported that the Culebra at DOE-1 behaved hydraulically as a double-porosity medium with a transmissivity of 11 ft^2/day during a pumping test performed at that location in 1983. From the re-sponse observed at DOE-1 during the H-3 multipad test, Beauheim (1987a) reported apparent single-porosity behavior, an apparent transmissivity of 5.5 ft^2/day, and an apparent storativity of 1.0 × 10^{-5}. Re-examination of the data from DOE-1 during the H-3 multipad test (Appendix C) indicates that a double-porosity model with spherical matrix blocks, unrestricted interporosity flow, an apparent transmis-sivity of 5.8 ft^2/day, an apparent total-system storativity of 1.1 × 10^{-5}, a storativity ratio of 0.05, and a no-flow boundary at a dimensionless distance of eight fits the data better than the single-porosity model presented by Beauheim (1987a). As discussed in Section 6.3, the large-scale averaging of heteroge-neous hydraulic properties involved in interpreting responses at distant observation wells precludes exact quantitative agreement between results obtained from different tests with different pumping-well locations. In qualitative terms, however, both the type of model (i.e., double-porosity) and specific hydraulic parameters interpreted from the response at DOE-1 to the H-11 multipad test are in good agreement with the interpretations of DOE-1 responses to other tests.

6.3.5 H-3b2. Figure 6-25 shows a log-log plot of the drawdown data from H-3b2 during the H-11 multipad test, along with a simulation including no boundaries and a simulation including a constant-pressure bound-ary at a dimensionless distance of 17. The simulations are of a single-porosity medium with an apparent transmissivity of 7.3 ft^2/day and an apparent storativity of 8.4 × 10^{-6} (Table 6-1). The simulations are identical throughout the drawdown period, showing that the

boundary, which corresponds to an image recharge well at a distance of about 33,000 ft from H-3b2, had no effect on the response observed at H-3b2 during the H-11 multipad test pumping period. Figure 6-26 shows a dimensionless Horner plot of the drawdown data from H-3b2, along with both of the simulations discussed above. Again, the simulations are identical during the drawdown period, and fit the data well.

Figure 6-27 shows a linear-linear plot of the H-3b2 drawdown and recovery data with the two simulations discussed above. During the recovery period, the two simulations diverge with the upper curve on the figure, representing the simulation with the constant-pressure boundary, fitting the data better than the lower curve, which represents the simulation with no boundaries. After approximately 4225 hr of total test time, however, the data show a more rapid recovery than is predicted by even the simulation with the constant-pressure boundary. The beginning of this rapid recovery coincides with the lining of the Culebra interval in the Air-Intake Shaft, which reduced the leakage rate from the Culebra into the shaft.

As discussed in Section 5.3.1.6, drainage from the Culebra into the Air-Intake Shaft pilot hole and later into the open shaft itself is likely to have caused drawdown at H-3b2 during the period of the H-11 multipad test. Thus, the transmissivity and storativity values presented above may be too low as they are based on an assumption that all of the drawdown observed at H-3b2 was caused by the H-11 multipad test. Considering that a total of 12.6 ft of drawdown was observed at H-3b2 during the multipad test pumping period, and that 8.4 ft of recovery was observed before the Culebra was lined in the Air-Intake Shaft, less than one-third of the total drawdown observed is attributable to drainage into the Air-Intake Shaft. Inasmuch as transmissivity and storativity are inversely proportional to drawdown, the apparent transmissivity and storativity indicated by the response at H-3b2 to the H-11 multipad test could be as high as 11 ft^2/day and 1.3 × 10^{-5}, respectively (Table 6-1).

The response observed at H-3b2 during the H-11 multipad test appears to be that of a single-porosity medium, whereas Beauheim (1987a) reported double-porosity behavior of the Culebra at H-3 from interpreta-tion of a 1984 pumping test and the H-3 multipad
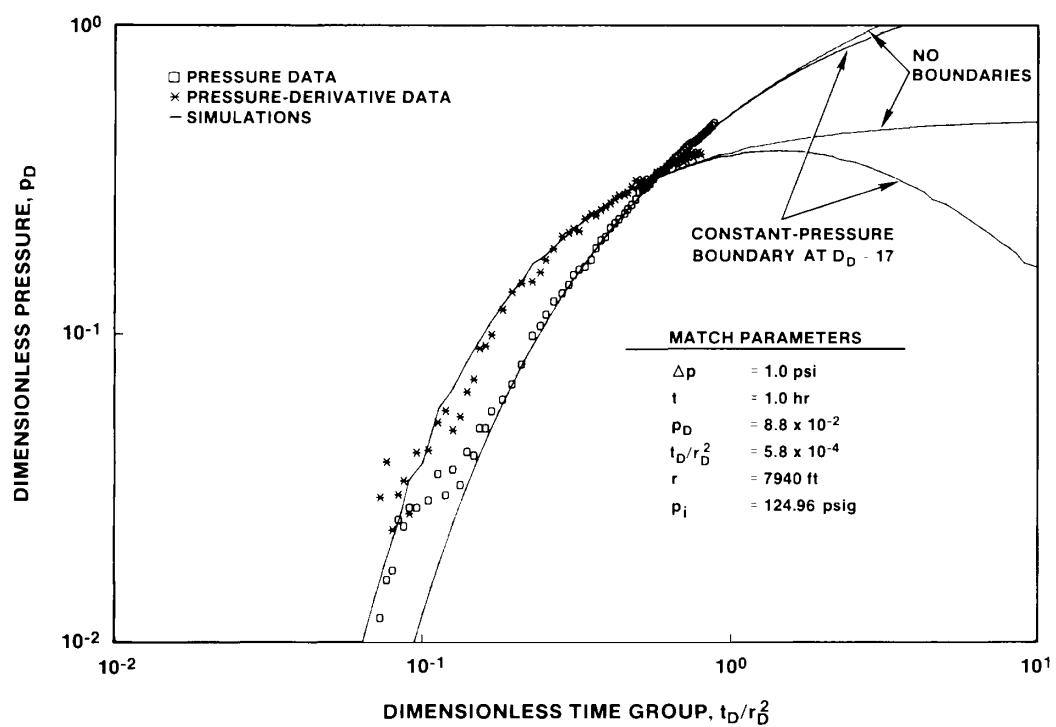
Figure 6-25. Log-Log Plot of H-3b2 Drawdown During the H-11 Multipad Pumping Test.
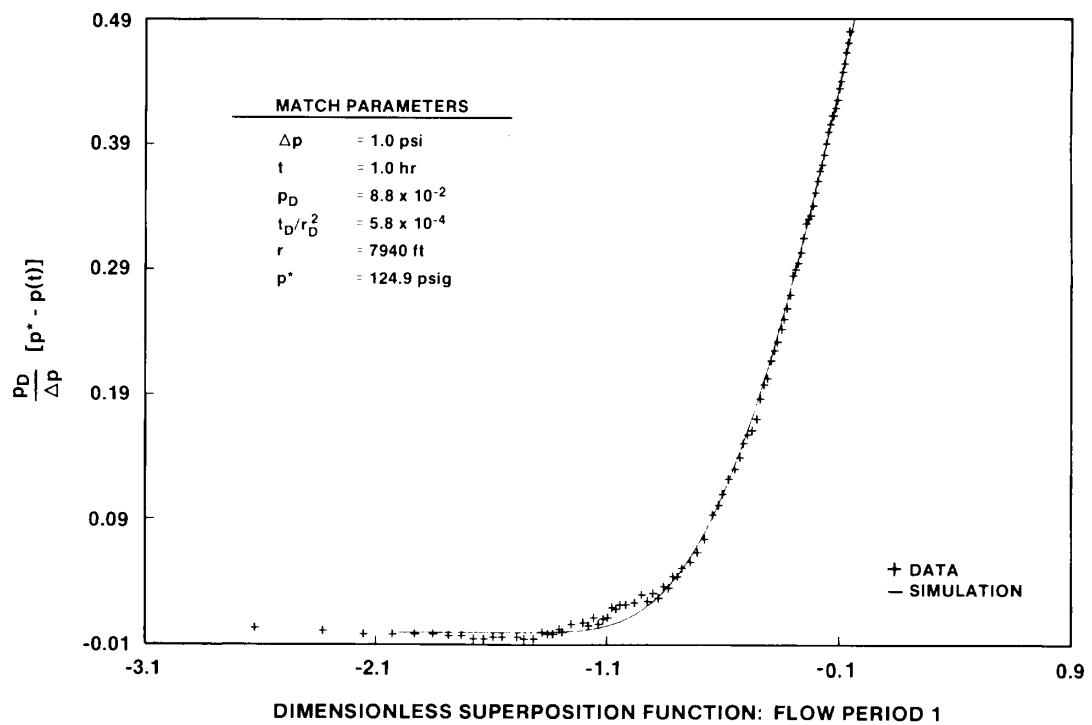

**Figure 6-26. Dimensionless Horner Plot of H-3b2 Drawdown During the H-11 Multipad Pumping Test.**
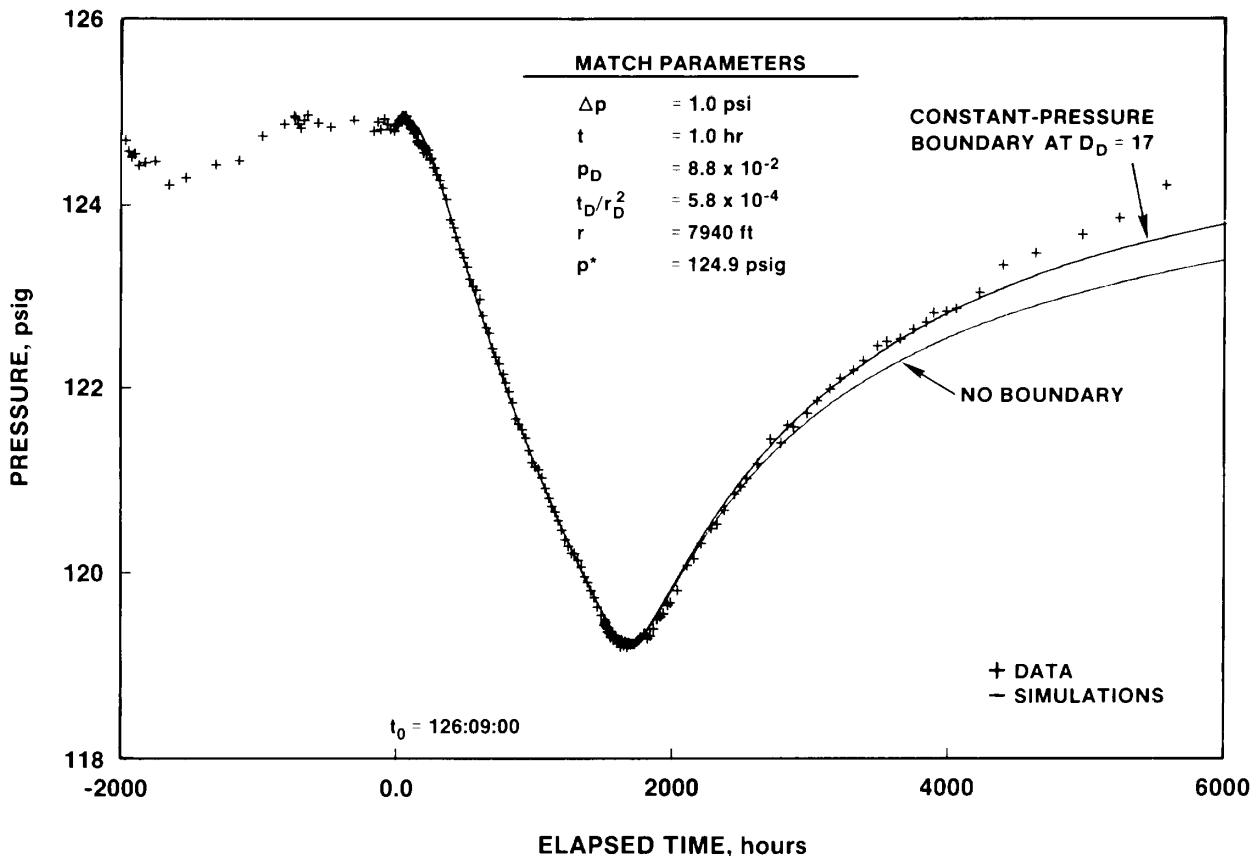
Figure 6-27. Linear-Linear Plot of H-3b2 Response During the H-11 Multipad Pumping Test.

test. As noted first by Kazemi et al. (1969) and later by Deruyck et al. (1982) and Chen et al. (1984), distinguishable double-porosity effects decrease with increasing distance from a pumping well. Transition between fracture-only and total-system behavior occurs earlier as the interporosity flow coefficient, which is proportional to the distance from the pumping well, increases (see Appendix B). Thus, if the time required for the pressure to change to an observable degree at a given location is greater than the time by which transition is complete, only a total-system response will be observed. An interporosity-flow coefficient (βr_D^2; see Appendix B) of about 7700 can be calculated for H-3b2 using the λ value of 2.0×10^{-7} and storativity ratio (ω) of 0.025 derived from the analysis of the H-11b1 response (Section 6.3.1). Using these parameters and the pressure match derived from the single-porosity analysis of the H-3b2 response, transition from fracture-only to total-system behavior should have been complete at H-3b2 after a total pressure

change of less than 0.1 psi (see Figure B-6). Therefore, no double-porosity behavior should have been observable at H-3b2.

Beauheim (1987a) reported the transmissivity of the Culebra at the H-3 hydropad to be 1.7 to 2.9 ft^2/day. The apparent transmissivity values of 7.3 to 11 ft^2/day derived above from the H-3b2 response to the H-11 multipad test are intermediate between Beauheim's (1987a) local value at H-3 and the 27 ft^2/day reported for H-11b1 in Section 6.3.1.

6.3.6 H-4b. As discussed in Section 5.3.1.7, water levels in well H-4b appeared to be responding to an unknown hydraulic stress during the H-11 multipad test. Five months after the end of the multipad-test pumping period, the water level in H-4b was about two ft higher than its pretest level, and still rising (Figure 5-11). The sudden rise in H-4b water levels raises a question as to what portion of the observed

data represents a response to the H-11 multipad test and what portion is a response to something else. Specifically, when did whatever caused the water-level rise begin? Until the cause of the water-level rise is determined, any analysis of the H-4b data must be regarded as uncertain.

Figure 6-28 shows a linear-linear plot of the water-level data from H-4b converted to pressures and compensated for barometric fluctuations (see Section 5.3.1.7), along with two simulations. Both simulations are of single-porosity media with no boundaries. The simulation with higher pressure values during most of the drawdown period and lower pressure values during the recovery period represents an attempt to match as well as possible the data collected during the H-11b1 pumping period. This simulation uses an apparent transmissivity of 37 ft²/day and an apparent storativity of 6.2×10^{-5}. The other simulation, with lower pressure values during most of the drawdown period and higher pressure values during the recovery period, represents an attempt to match the magnitude of the total drawdown observed and to match the time at which recovery apparently began. This simulation uses an apparent transmissivity of 130 ft²/day and an apparent storativity of 7.3×10^{-5}. Neither of these simulations does a good job of matching the entire data record from H-4b, particularly during recovery. Both apparent transmissivity values are also higher than expected, considering that the Culebra transmissivity at H-4c is 0.65 ft²/day (Beauheim, 1987c) and at H-11b1 is 27 ft²/day (Section 6.3.1).

Figure 6-29 presents a pair of alternative simulations of the H-4b data. The upper curve represents a single-porosity medium with an apparent transmissivity of 12 ft²/day, an apparent storativity of 3.0×10^{-5}, and three constant-pressure boundaries at a dimensionless distance of 2.2 from H-4b, while the lower curve represents the same medium with no boundaries. The upper simulation is not intended to be realistic, but does provide insight into the possible nature of the unknown hydraulic stress affecting H-4b water levels. Having more constant-pressure boundaries than the number of pumping wells implies that actual recharge is occurring. The upper simulation shown in Figure 6-29 can be conceptualized as representing the effects at H-4b of pumping at H-11b1 while another well about 16,000 ft from H-4b (assuming a homoge-

neous distribution of aquifer properties) was injecting water into the Culebra at a rate of 18 gpm (three times the H-11b1 pumping rate) during exactly the same period when H-11b1 was being pumped. No injection at any rate is known to have occurred during the H-11 multipad test, nor would any actual injection have been likely to have followed the same schedule as the H-11b1 pumping. Nevertheless, the simulation shows that the response observed at H-4b is a plausible result of a combination of the H-11 multipad test and some discrete recharge event. The hypothesized recharge event is termed "discrete" because it appears to have started suddenly. Natural (i.e., climate-related) recharge to the Culebra would be expected to cause gradual changes in water levels over long periods of time.

The lower simulation in Figure 6-29 shows the response that might have been expected in the absence of the hypothesized recharge event. This simulation shows that the recharge event may have affected H-4b water levels during the multipad-test pumping period. Without recharge, approximately three times as much drawdown might have been observed, and recovery might not have begun until approximately 800 hr after the pump was turned off at H-11b1. Considering that drawdown was not observed at H-4b until about 430 hr after the pump was turned on at H-11b1 (Table 5-1), a delay of 800 hr before the beginning of recovery would appear to be more realistic than the two days observed if the H-11 multipad test represented the only hydraulic stress on the system.

In conclusion, no defendable interpretation can be made of the data collected at H-4b during the H-11 multipad test. Simulations that include the H-11b1 pumping as the sole hydraulic stress fail to match the observed data. The data can be better fit by a simulation including injection to the Culebra, but no independent evidence is available that this injection actually occurred. The anomalously high water levels at H-4b (and other wells) are real, however, and must have an explanation. Until that explanation is found, no quantitative interpretation can be made of the data collected at H-4b during the H-11 multipad test.

6.3.7 H-12. Interpretation of the data collected at well H-12 during the H-11 multipad test presented problems similar to those encountered during the
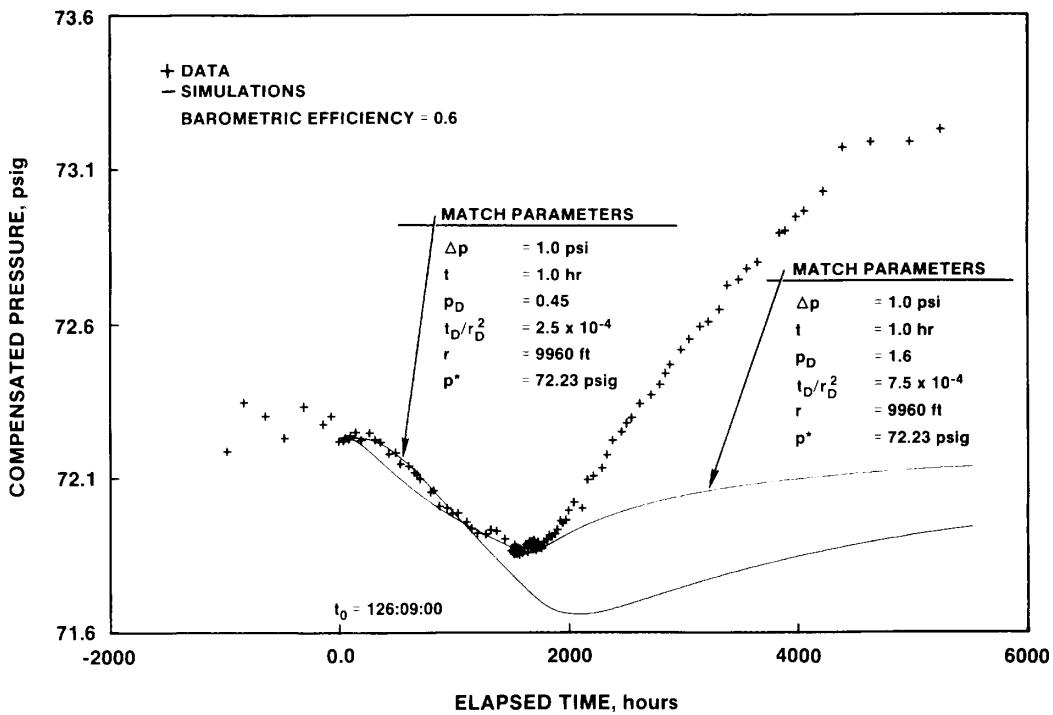
Figure 6-28. Linear-Linear Plot of H-4b Response During the H-11 Multipad Pumping Test with Simulations Matching Early Drawdown and Total Drawdown.
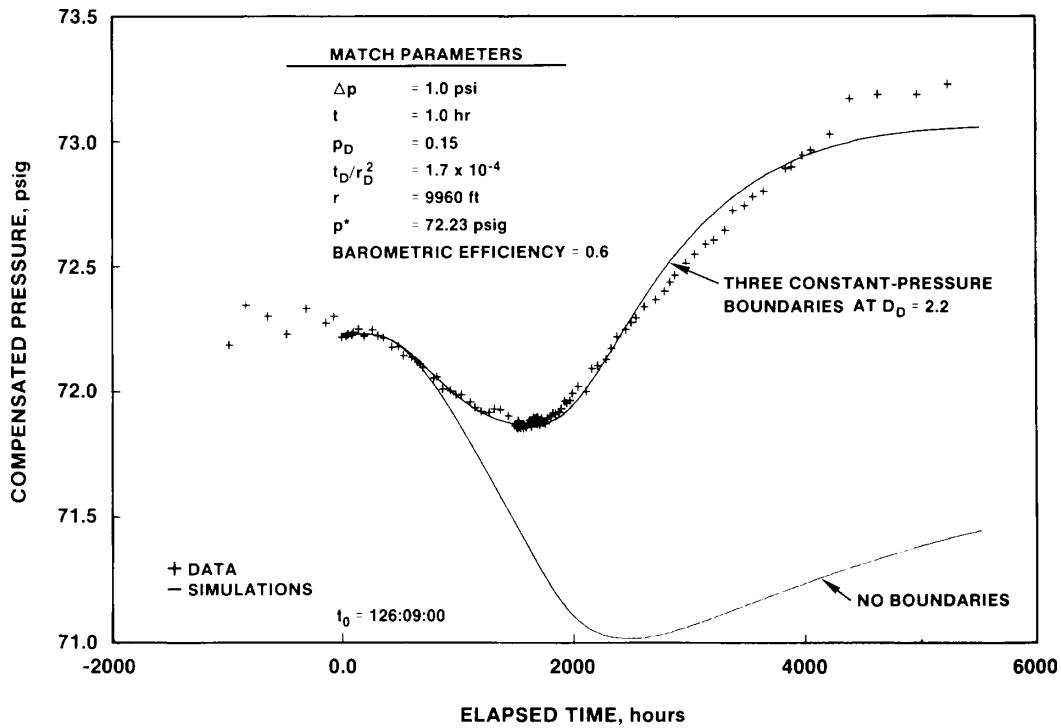
Figure 6-29. Linear-Linear Plot of H-4b Response During the H-11 Multipad Pumping Test with Simulations Including Constant-Pressure Boundaries to Match Recovery and Lacking Constant-Pressure Boundaries.

interpretation of the data from H-4b (Section 6.3.6). Figure 6-30 shows a linear-linear plot of the drawdown and recovery data from H-12 with two simulations matching different features of the data. Both simulations are of single-porosity media with no boundaries. The simulation with higher pressure values during the drawdown period and lower pressure values during recovery represents an attempt to best match the drawdown data alone. This simulation uses an apparent transmissivity of 30 ft^2/day and an apparent storativity of 6.6×10^{-5}. The second simulation represents an attempt to match the magnitude of the total drawdown observed and to match the time at which apparent recovery began. This simulation uses an apparent transmissivity of 100 ft^2/day and an apparent storativity of 9.5×10^{-5}. Neither simulation fits the entire data record well, and both produce apparent transmissivity estimates higher than the local values of Culebra transmissivity determined for both H-11b1 (27 ft^2/day; Section 6.3.1) and H-12 (0.18 ft^2/day; Beauheim, 1987c).

Figure 6-31 presents two different simulations of the H-12 data. The upper curve represents a single-porosity medium with an apparent transmissivity of 22 ft^2/day, an apparent storativity of 5.1×10^{-5}, and four constant-pressure boundaries at a dimensionless distance of 2.5 from H-12. The lower curve represents the same medium with no boundaries. The four constant-pressure boundaries in the upper simulation on Figure 6-31 are equivalent to a well about 21,000 ft from H-12 injecting water into the Culebra at a rate of about 24 gpm during the exact period when H-11b1 was being pumped. Again, no injection is known to have occurred during the H-11 multipad test. The simulation shown in Figure 6-31 is merely intended to demonstrate the nature of the hydraulic stress that, in combination with the H-11 multipad test, could have produced the response observed at H-12.

The simulation shown in Figure 6-31 with no boundaries shows the nature of the response that might have been observed in the absence of the hypothesized recharge event. Approximately twice as much drawdown might have been observed, and recovery might not have begun until 70 to 80 days after the pump was turned off at H-11b1. Considering that H-12 did not respond to H-11b1 pumping for 33 days (Table 5-1), a delay of 70 to 80 days before the onset

of recovery would be more realistic than the 25 days observed if the H-11 multipad test represented the only hydraulic stress on the system.

In conclusion, no defendable interpretation can be made of the data collected at H-12 during the H-11 multipad test. No simulation can be made to fit the observed data without invoking a recharge event of unknown origin.

6.3.8 H-14. In contrast to the data from H-4b and H-12, the data collected at H-14 during the H-11 multipad test were amenable to straightforward interpretation. Figure 6-32 presents a linear-linear plot of the water-level data from H-14 converted to pressures (see Section 5.3.1.9), along with a simulation of the data. The simulation is representative of a single-porosity medium with an apparent transmissivity of 6.0 ft^2/day, an apparent storativity of 3.7×10^{-5}, and no boundaries (Table 6-1). This apparent transmissivity value is intermediate between the transmissivity of 27 ft^2/day determined for H-11b1 (Section 6.3.1) and the transmissivity of 0.30 ft^2/day determined from drillstem and slug tests at H-14 (Beauheim, 1987c).

No clear recovery was evident at H-14 by the time monitoring after the H-11 multipad test was terminated to allow WQSP sampling of the well. This lack of recovery makes conclusions about the presence or absence of hydraulic boundaries uncertain, but has little effect on the reliability of the apparent transmissivity and storativity values.

6.3.9 H-15. Figure 6-33 shows a log-log plot of the drawdown data from H-15 during the H-11 multipad test, along with the best-fit simulation obtained. The simulation is representative of a single-porosity medium with an apparent transmissivity of 7.1 ft^2/day, an apparent storativity of 4.7×10^{-6}, and a constant-pressure boundary at a dimensionless distance of 10 (Table 6-1). This boundary corresponds to an image recharge well at a distance of about 28,000 ft from H-15 (see Appendix B). The apparent transmissivity value given above is intermediate between the transmissivity of 27 ft^2/day determined for H-11b1 (Section 6.3.1) and the transmissivity of 0.10 to 0.15 ft^2/day determined from single-well testing at H-15 (Beauheim, 1987c). Figure 6-34 shows a
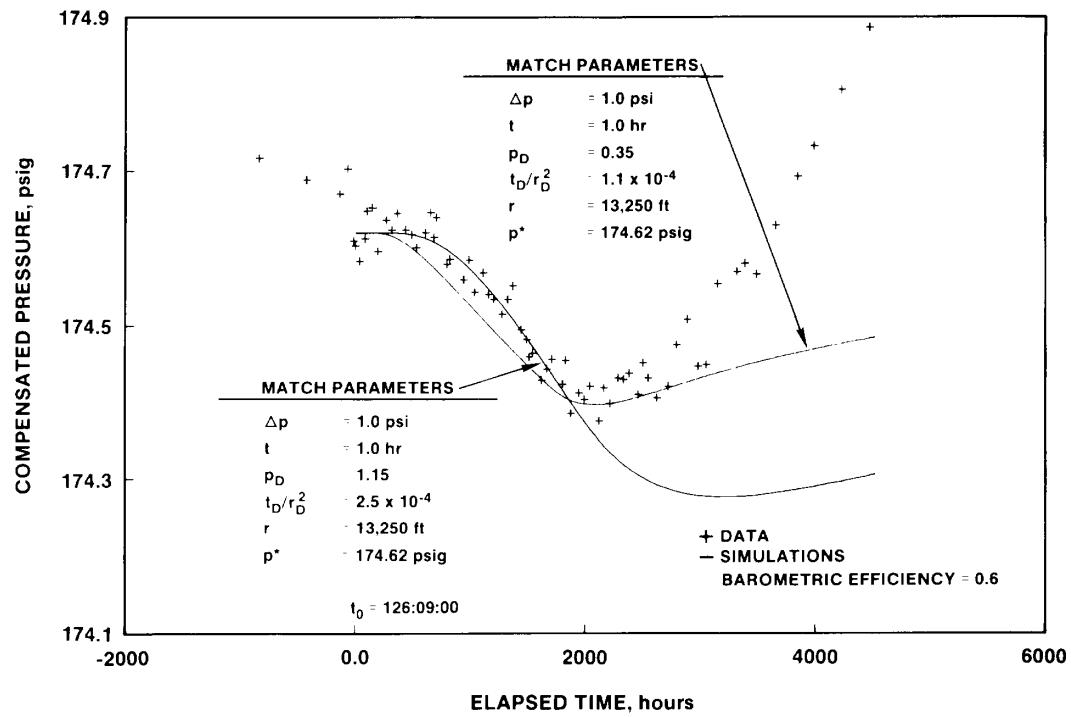
Figure 6-30. Linear-Linear Plot of H-12 Response During the H-11 Multipad Pumping Test with Simulations Matching Early Drawdown and Total Drawdown.
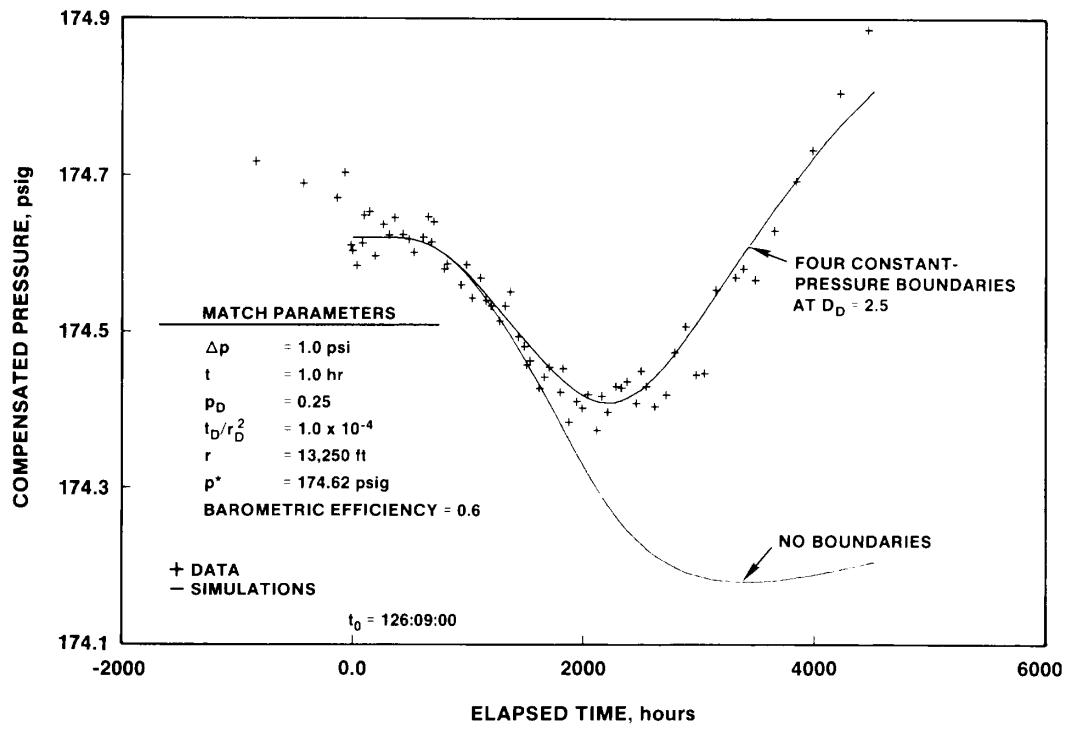
Figure 6-31. Linear-Linear Plot of H-12 Response During the H-11 Multipad Pumping Test with Simulations Including Constant-Pressure Boundaries to Match Recovery and Lacking Constant-Pressure Boundaries.
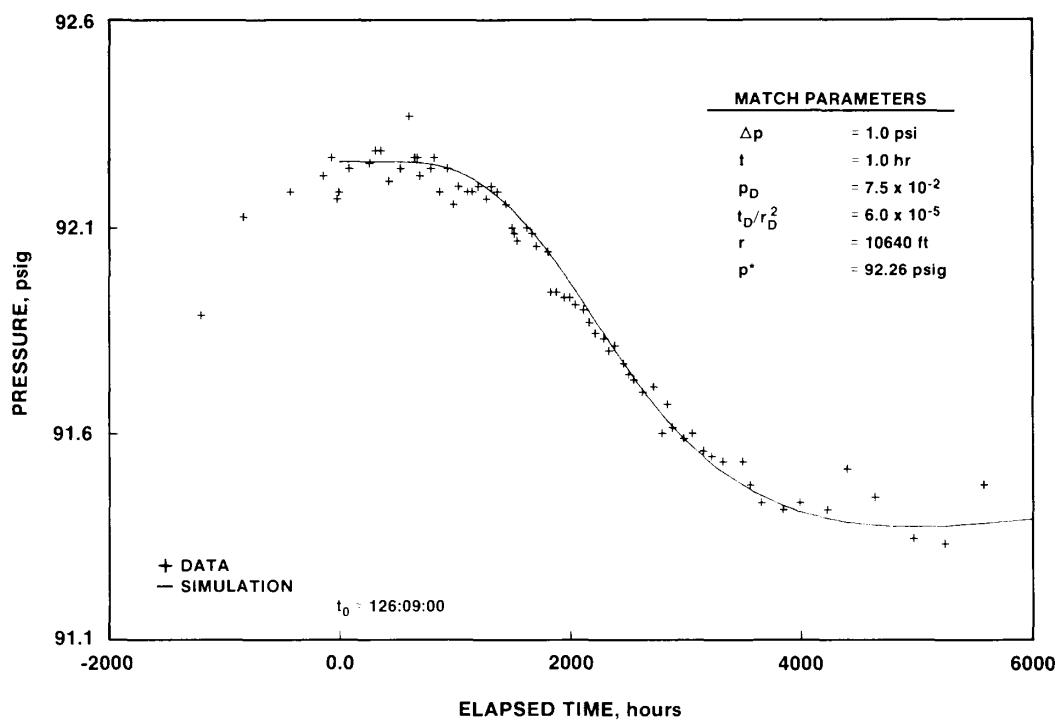
Figure 6-32. Linear-Linear Plot of H-14 Response During the H-11 Multipad Pumping Test.
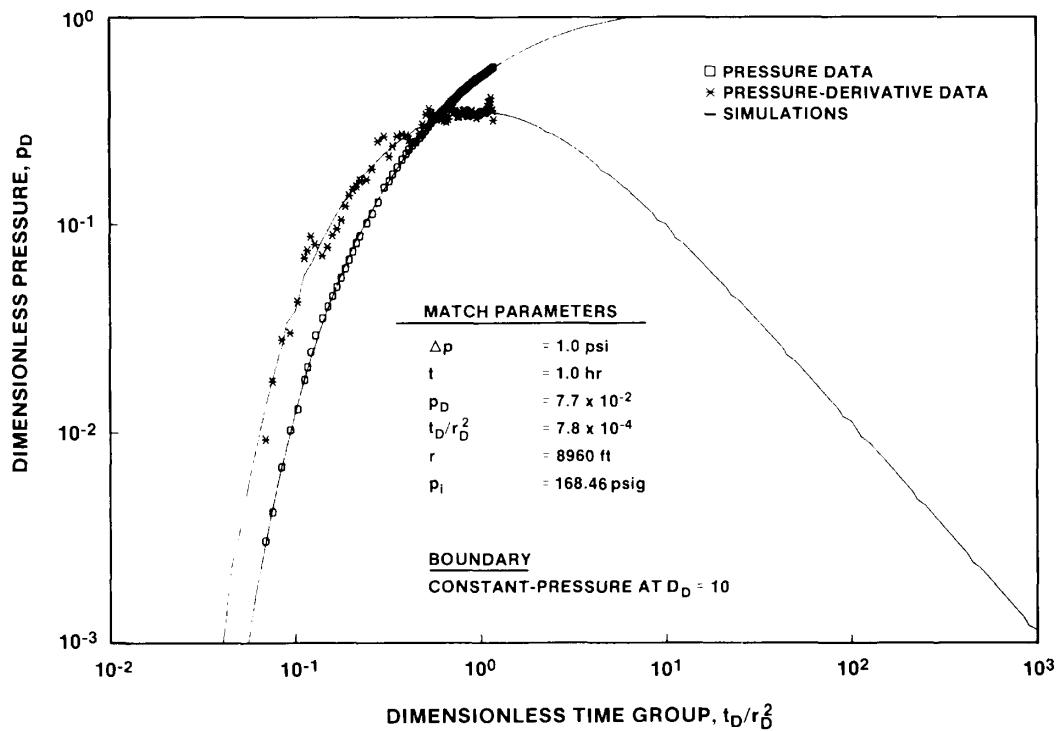
Figure 6-33. Log-Log Plot of H-15 Drawdown During the H-11 Multipad Pumping Test.

MATCH PARAMETERS

Δp	$= 1.0$ psi
t	$= 1.0$ hr
p_D	$= 7.7 \times 10^{-2}$
t_D/r_D^2	$= 7.8 \times 10^{-4}$
r	$= 8960$ ft
p^*	$= 168.46$ psig

BOUNDARY
CONSTANT-PRESSURE AT $D_D = 10$

+ DATA
— SIMULATION

DIMENSIONLESS SUPERPOSITION FUNCTION: FLOW PERIOD 1
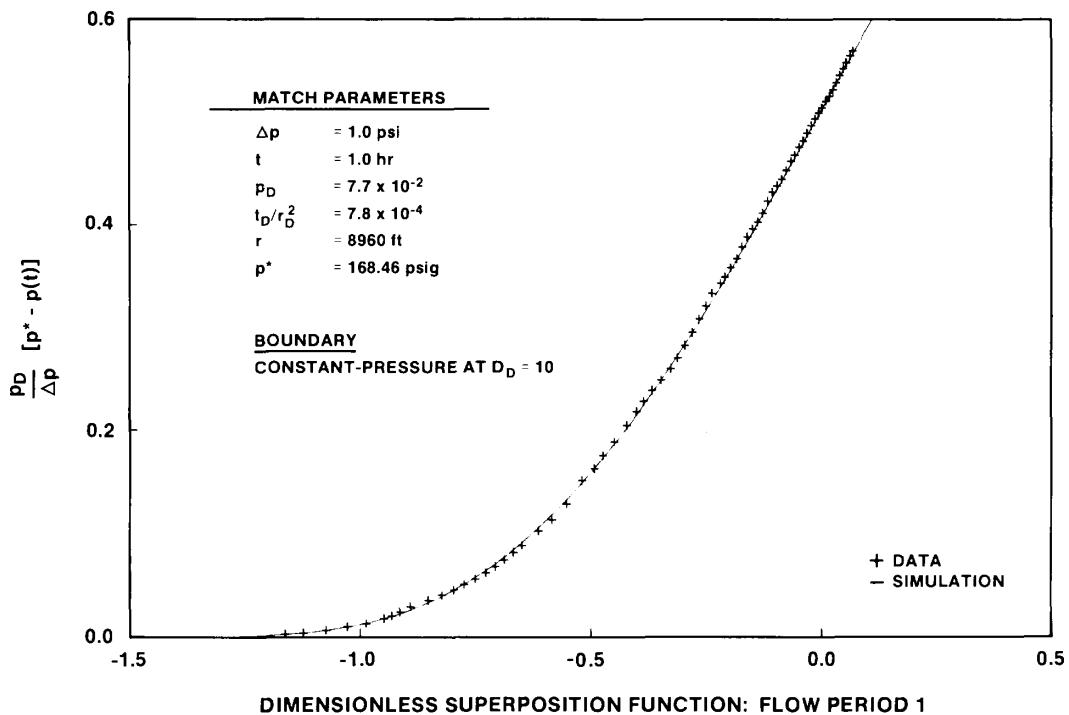
Figure 6-34. Dimensionless Horner Plot of H-15 Drawdown During the H-11 Multipad Pumping Test.

dimensionless Horner plot of the H-15 drawdown data with the same best-fit simulation.

Figure 6-35 shows a linear-linear plot of the complete drawdown and recovery data from H-15, along with the simulation derived from the drawdown analysis. The simulation shows increasingly less recovery than was observed throughout the recovery period. Figure 6-36 shows that the fit to the recovery data can be improved by making the constant-pressure boundary closer (dimensionless distance = 5) and decreasing the apparent transmissivity and storativity slightly to 5.7 ft²/day and 4.2 × 10⁻⁶, respectively, but the late-time recovery data remain above the simulation and the fit to the drawdown data degrades.

The relatively steep rise of the recovery data at late time probably reflects a superposition of recovery responses from all the hydraulic stresses that affected water levels at H-15 in 1987 and 1988 (Figure 5-14). This superposition of recovery responses may also have caused the need for the constant-pressure boundary in the simulations discussed above.

6.3.10 H-17. The hydraulic behavior observed at H-17 during the H-11 multipad test was similar to that observed at H-15. Figure 6-37 shows a log-log plot of the drawdown data from well H-17 during the H-11 multipad test, along with the best-fit simulation obtained. The simulation is representative of a single-porosity medium with an apparent transmissivity of 13 ft²/day, an apparent storativity of 1.8 × 10⁻⁵, and a constant-pressure boundary at a dimensionless distance of six (Table 6-1). This boundary corresponds to an image recharge well at a distance of about 13,000 ft from H-17 (see Appendix B). The apparent transmissivity value given above is intermediate between the transmissivity of 27 ft²/day determined for H-11b1 (Section 6.3.1) and the transmissivity of 0.22 ft²/day determined from single-well testing at H-17 (Beauheim, 1987c). Figure 6-38 shows a dimensionless Horner plot of the H-17 drawdown data with the same best-fit simulation.

The linear-linear plot of the H-17 drawdown and recovery data (Figure 6-39) shows that the simulation derived from the drawdown analysis underestimates

MATCH PARAMETERS

Δp	= 1.0 psi
t	= 1.0 hr
p_D	= 7.7 x 10^{-2}
t_D/r_D^2	= 7.8 x 10^{-4}
r	= 8960 ft
p*	= 168.46 psig

BOUNDARY
CONSTANT-PRESSURE AT D_D = 10

+ DATA
− SIMULATION

t_0 126:09:00

ELAPSED TIME, hours
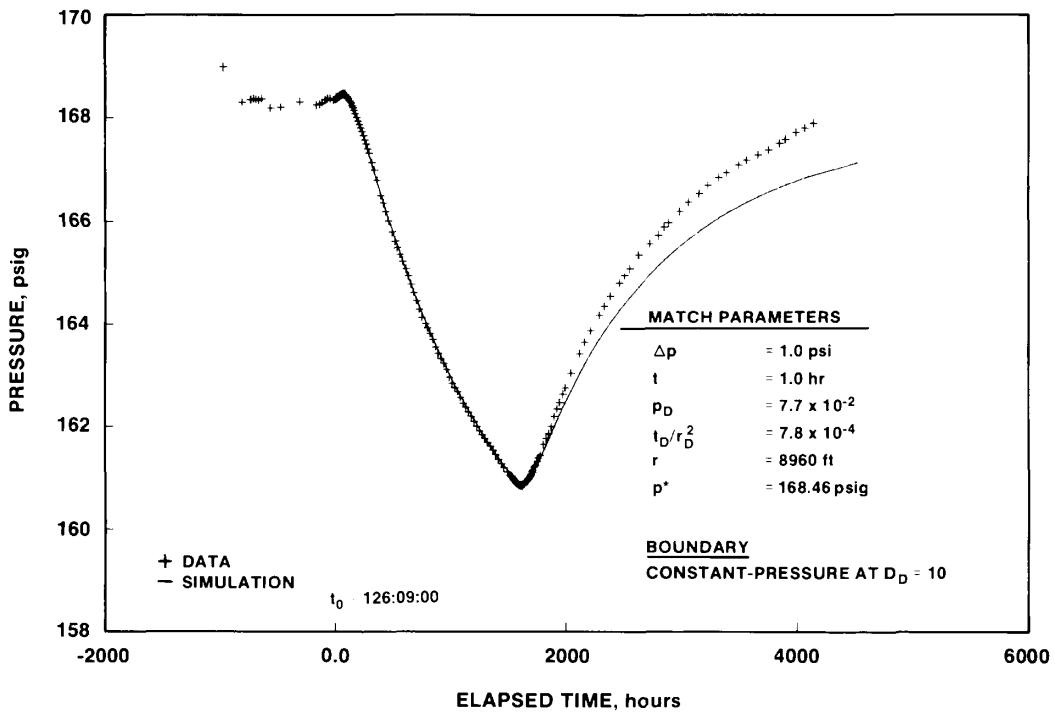
Figure 6-35.   Linear-Linear Plot of H-15 Response During the H-11 Multipad Pumping Test.

MATCH PARAMETERS

Δp	= 1.0 psi
t	= 1.0 hr
p_D	= 6.2 x 10^{-2}
t_D/r_D^2	= 7.0 x 10^{-4}
r	= 8960 ft
p*	= 168.5 psig

BOUNDARY
CONSTANT-PRESSURE AT D_D = 5

+ DATA
− SIMULATION

t_0 126:09:00

ELAPSED TIME, hours
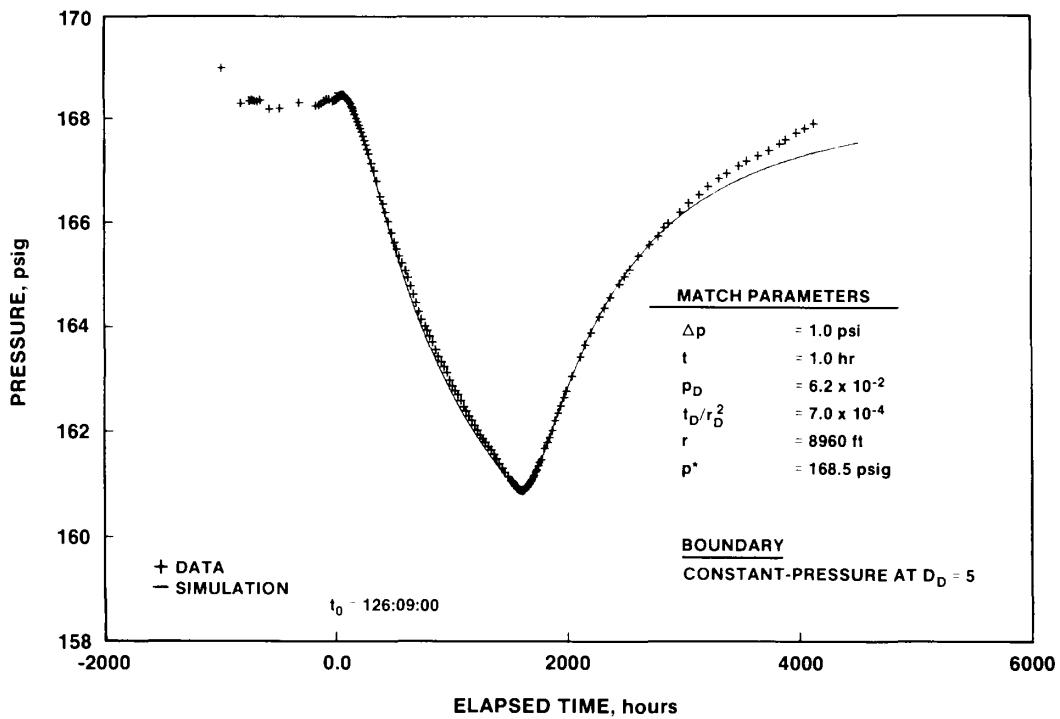
Figure 6-36.   Linear-Linear Plot of H-15 Response During the H-11 Multipad Pumping Test with Simulation Having a Closer Constant-Pressure Boundary.
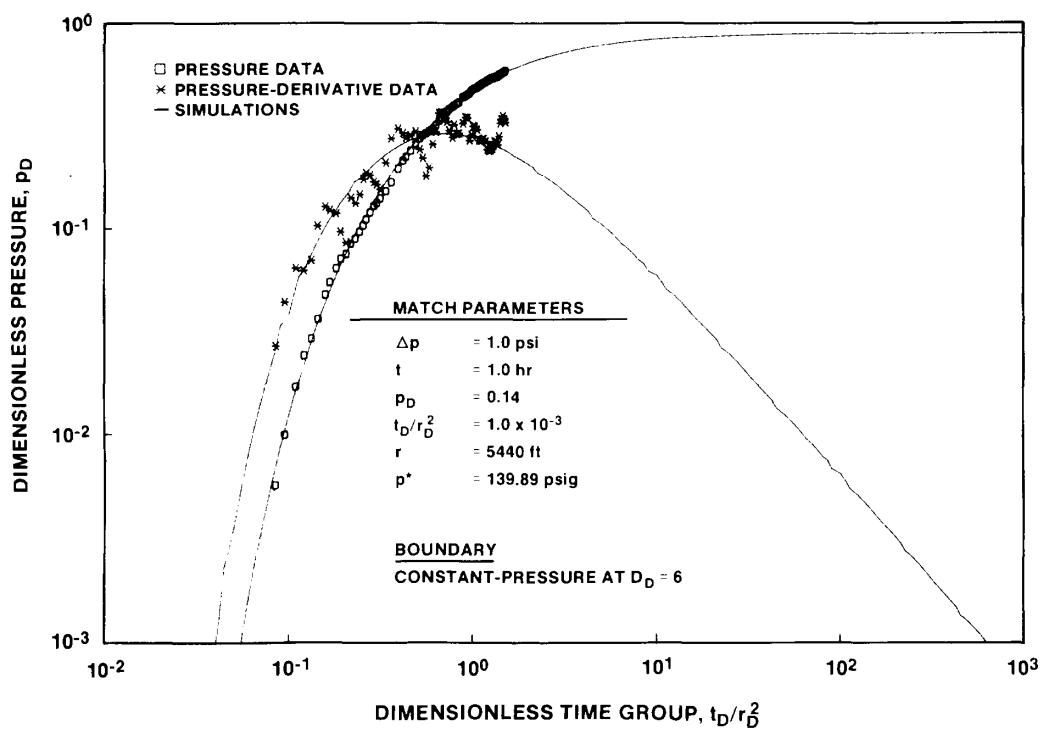
Figure 6-37. Log-Log Plot of H-17 Drawdown During the H-11 Multipad Pumping Test.
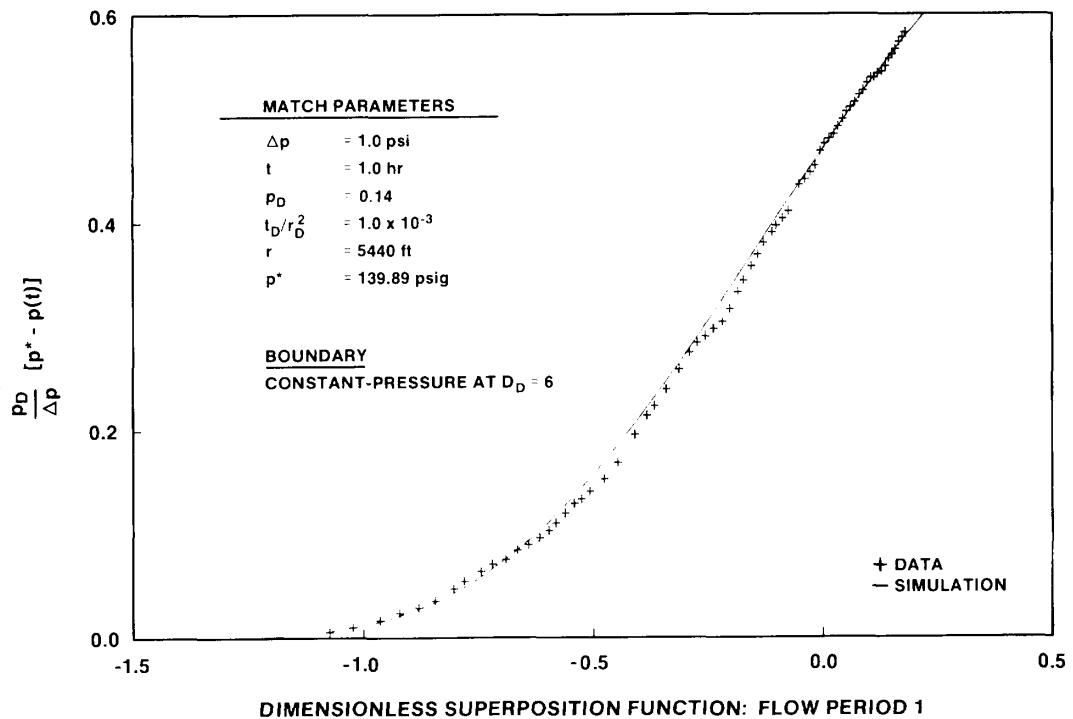
Figure 6-38. Dimensionless Horner Plot of H-17 Drawdown During the H-11 Multipad Pumping Test.

142

140

PRESSURE, psig

138

136

134

MATCH PARAMETERS

Δp — 1.0 psi

t — 1.0 hr

p_D = 0.14

t_D/r_D^2 — 1.0×10^{-3}

r = 5440 ft

p* — 139.89 psig

BOUNDARY
CONSTANT-PRESSURE AT D_D = 6

+ DATA
— SIMULATION

t_0 — 126:09:00

-2000   0.0   2000   4000   6000

ELAPSED TIME, hours
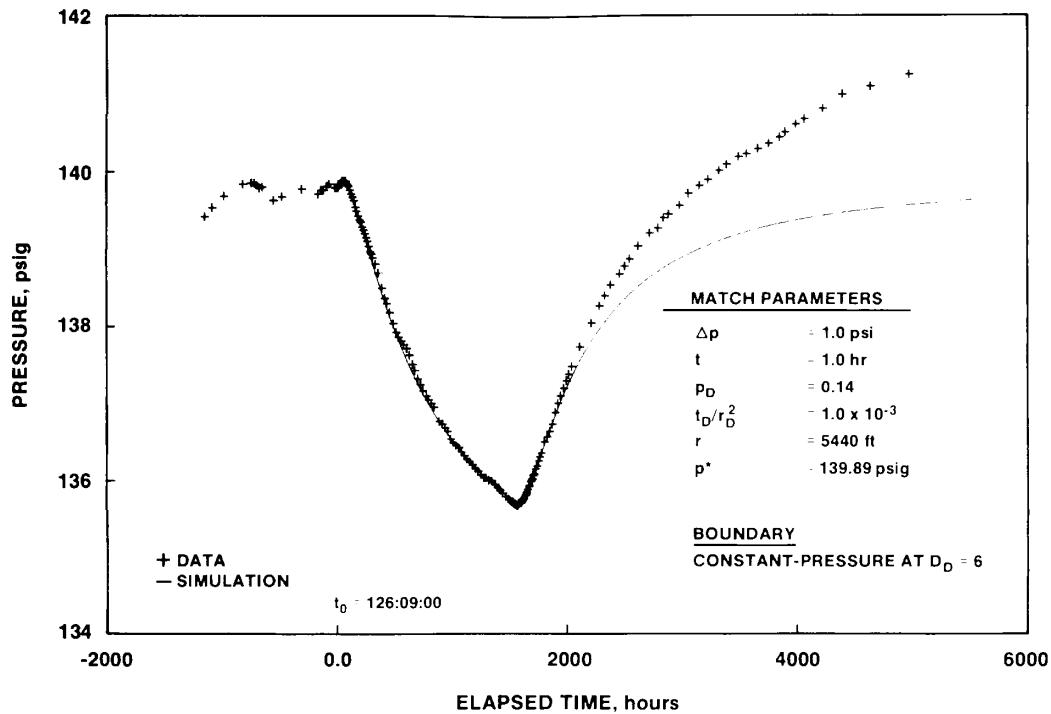
Figure 6-39. Linear-Linear Plot of H-17 Response During the H-11 Multipad Pumping Test.

recovery. Because the fluid pressure during recovery exceeded that measured at the start of the multipad test, the only way to match the observed recovery behavior would be to include some type of recharge to the Culebra, as was done for simulations of the H-4b (Figure 6-29) and H-12 (Figure 6-31) data. The constant-pressure boundary already included in the simulation may represent the first effects of this hypothetical recharge. The good fit between the simulation and the data during the drawdown period before the effects of the constant-pressure boundary are evident indicates that the apparent transmissivity and storativity values presented above are valid regardless of uncertainties in the nature and number of boundaries.

6.3.11 P-15. The data collected from well P-15 during the H-11 multipad test presented difficulties in interpretation similar to those presented by the data from H-4b (Section 6.3.6) and H-12 (Section 6.3.7). Figure 6-40 shows a linear-linear plot of the P-15 drawdown and recovery data with two different simulations. The simulation having generally lower pressure values

represents an attempt to match the magnitude of the total drawdown observed and to match the time at which apparent recovery began. This simulation is of a single-porosity medium with an apparent transmissivity of 120 ft²/day, an apparent storativity of 1.1×10^{-4}, and no boundaries. The simulation fits the drawdown data reasonably well, but fails to match the recovery data. In addition, the apparent transmissivity of 120 ft²/day is much higher than both the Culebra transmissivity of 27 ft²/day determined for H-11b1 (Section 6.3.1) and the transmissivity of 0.09 ft²/day determined from slug tests at P-15 (Beauheim, 1987c).

The second simulation shown in Figure 6-40, having generally higher pressure values, represents an attempt to match the observed data by including the effects of a hypothetical injection well. The simulation is of a single-porosity medium with an apparent transmissivity of 18 ft²/day, an apparent storativity of 3.7×10^{-5}, and three constant-pressure boundaries at a dimensionless distance of two from P-15. The three constant-pressure boundaries are equivalent to an injection well about 22,000 ft from P-15 injecting water

85

MATCH PARAMETERS

Δp	$= 1.0$ psi
t	$= 1.0$ hr
p_D	$= 0.22$
t_D/r_D^2	$= 8.5 \times 10^{-5}$
r	$= 15,530$ ft
p^*	$= 54.11$ psig

THREE CONSTANT-PRESSURE BOUNDARIES AT $D_D = 2$

MATCH PARAMETERS

Δp	$= 1.0$ psi
t	$= 1.0$ hr
p_D	$= 1.5$
t_D/r_D^2	$= 2.0 \times 10^{-4}$
r	$= 15,530$ ft
p^*	$= 54.11$ psig

NO BOUNDARIES

$t_0 = 126:09:00$

+ DATA
— SIMULATIONS

BAROMETRIC EFFICIENCY $= 0.6$

COMPENSATED PRESSURE, psig

ELAPSED TIME, hours
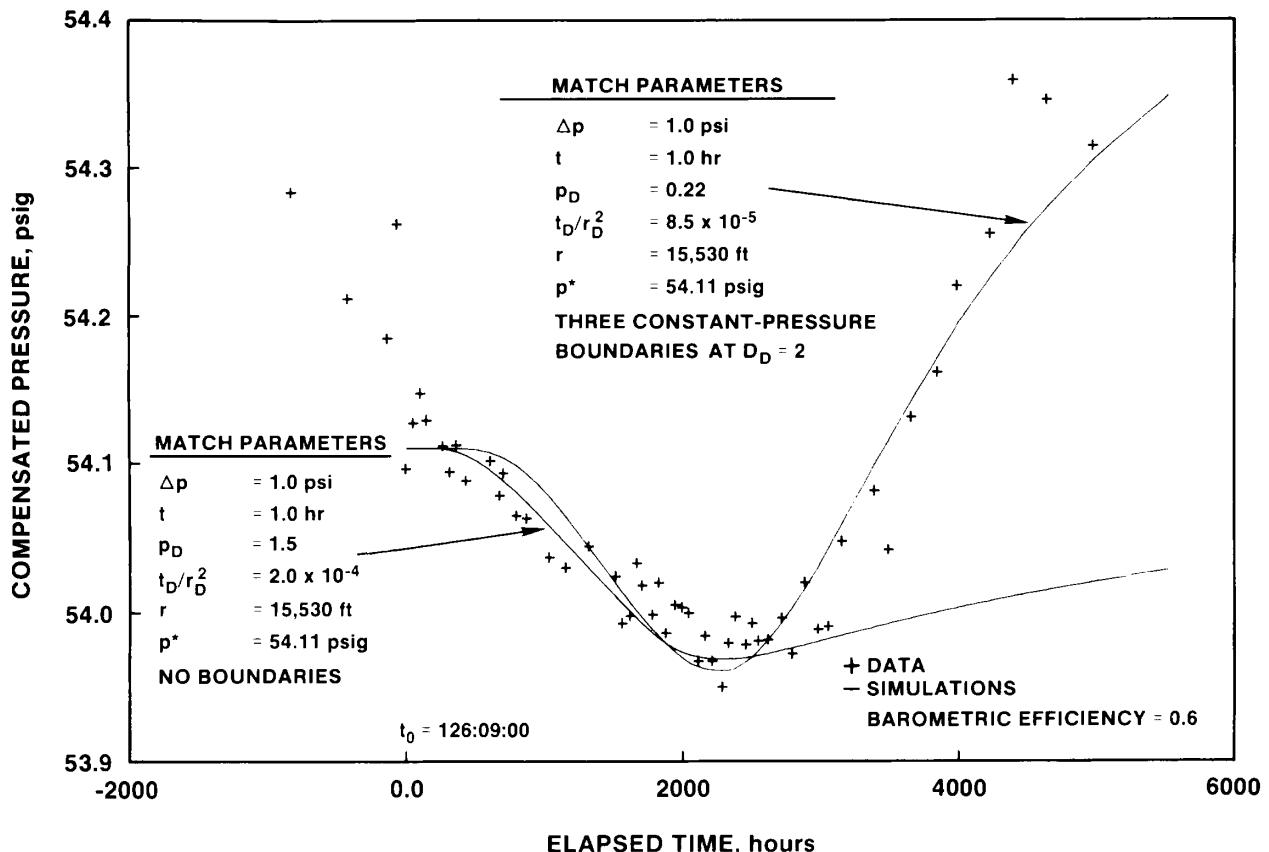
Figure 6-40. Linear-Linear Plot of P-15 Response During the H-11 Multipad Pumping Test.

into the Culebra at a rate of about 18 gpm during the exact period when H-11b1 was being pumped. The presentation of this simulation is not meant to imply that a specific injection having the parameters listed above actually occurred. Rather, the simulation is intended to show that the changes in water levels observed at P-15 are consistent with some recharge event acting in conjunction with the H-11 multipad test. Without more knowledge of the nature of this hypothesized recharge event, no defendable quantitative interpretation can be made of the data collected at P-15 during the H-11 multipad test.

6.3.12 P-17. The hydraulic behavior observed at well P-17 during the H-11 multipad test was similar to that observed at H-17. Figure 6-41 shows a log-log plot of the P-17 drawdown data, along with the best-fit simulation obtained. The simulation is of a single-porosity medium with an apparent transmissivity of 21 ft²/day, an apparent storativity of 4.7×10^{-5}, and no

boundaries (Table 6-1). This apparent transmissivity is intermediate between the Culebra transmissivity of 27 ft²/day determined for H-11b1 (Section 6.3.1) and the transmissivity of 1.0 ft²/day determined from slug tests at P-17 (Beauheim, 1987c). Figure 6-42 shows a dimensionless Horner plot of the P-17 drawdown data with the same simulation. Again, the simulation and data are in close agreement.

Figure 6-43 shows a linear-linear plot of the P-17 drawdown and recovery data, along with two simulations. The lower of the two simulation curves uses exactly the same model as was derived from the drawdown analysis. This simulation predicts that drawdown would continue longer after the end of the 1512-hr pumping period at H-11b1 than was observed, and that recovery would not be as rapid as was observed. The upper simulation curve uses the same drawdown model with the addition of ten constant-pressure boundaries at a dimensionless distance of
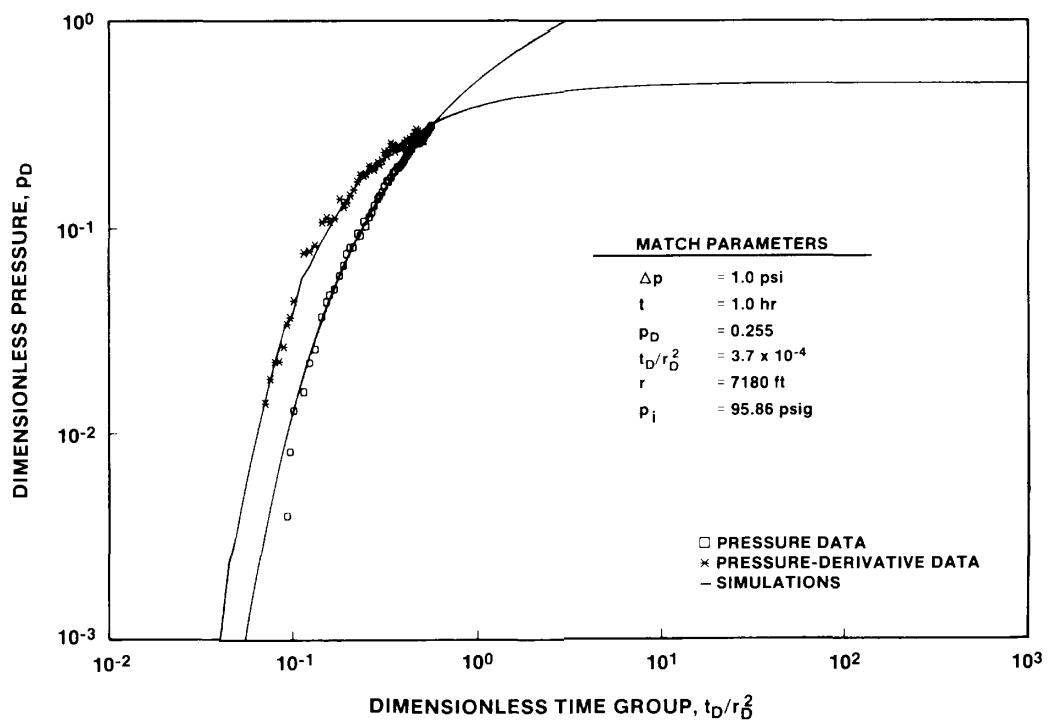
Figure 6-41. Log-Log Plot of P-17 Drawdown During the H-11 Multipad Pumping Test.
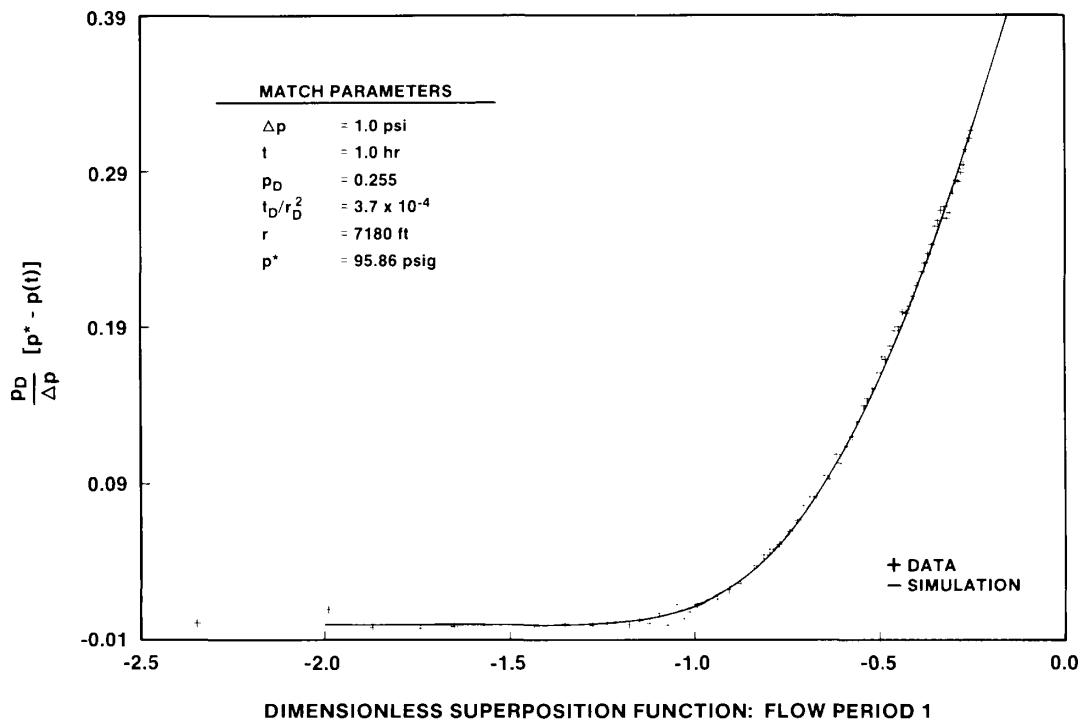

Figure 6-42. Dimensionless Horner Plot of P-17 Drawdown During the H-11 Multipad Pumping Test.
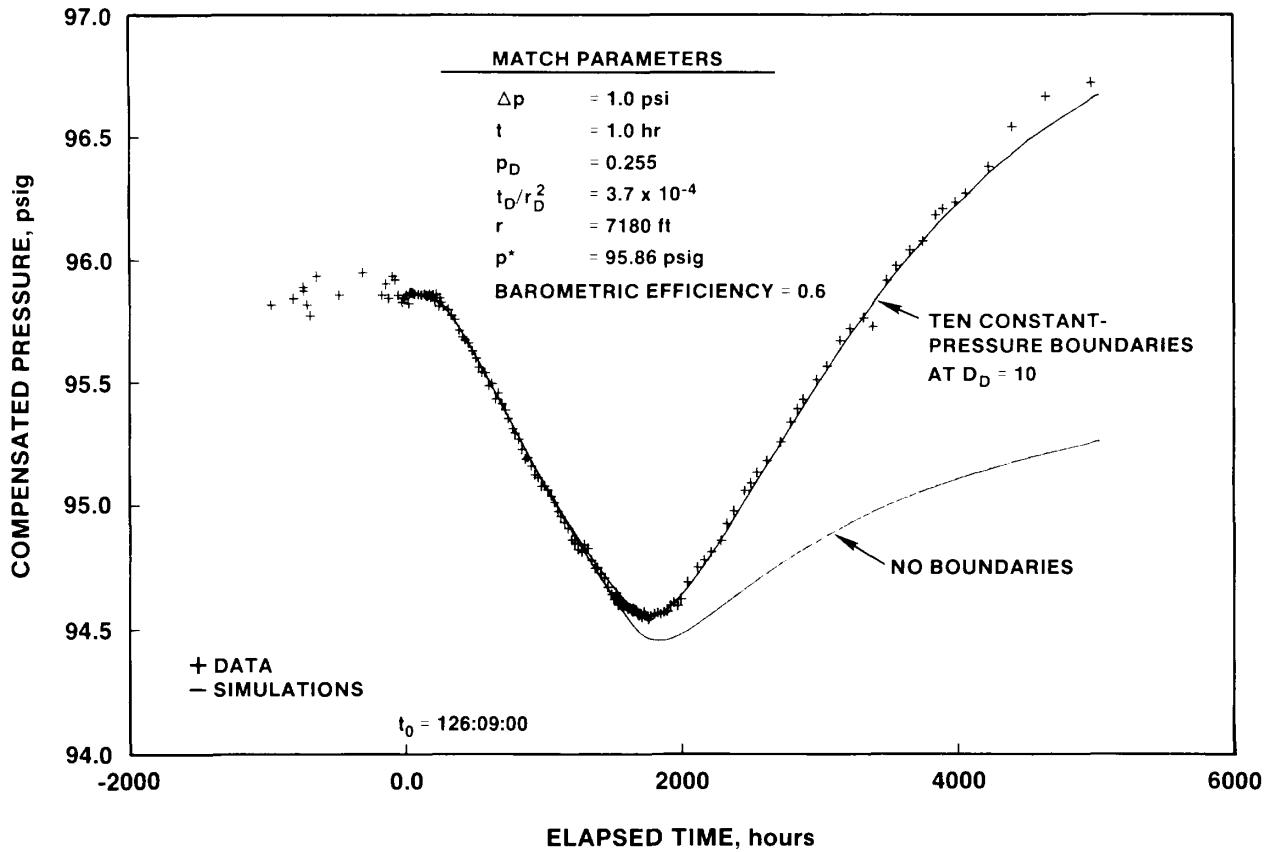
Figure 6-43. Linear-Linear Plot of P-17 Response During the H-11 Multipad Pumping Test.

ten from P-17. This simulation deviates from the other simulation near the end of the pumping period, and provides an improved match to both the transition between drawdown and recovery and the recovery data. The ten constant-pressure boundaries included in this simulation are equivalent to an injection well about 23,000 ft from P-17 injecting water into the Culebra at a rate of about 60 gpm during the exact period when H-11b1 was being pumped.

The two simulations presented in Figure 6-43 appear to show that the drawdown observed at P-17 during the H-11 multipad test pumping period was largely unaffected by other hydraulic stresses. The apparent hydraulic parameters derived from the drawdown analysis should, therefore, be reliable estimates for the region of the Culebra between H-11b1 and P-17. Near the time when the pump was turned off at H-11b1, however, some type of recharge event began affecting water levels at P-17 and continued to do so for the

remainder of the monitoring period (through December 1988). Thus, no independent analysis can be performed of the recovery data.

6.3.13 Cabin Baby-1. The hydraulic behavior observed at well Cabin Baby-1 during the H-11 multipad test was similar to that observed at P-17. Figure 6-44 shows a log-log plot of the drawdown data collected at Cabin Baby-1 during the H-11 multipad test, along with a simulation of the data. The simulation is of a single-porosity medium with an apparent transmissivity of 13 ft^2/day, an apparent storativity of 6.5 × 10^{-5}, and no boundaries (Table 6-1). This apparent transmissivity is intermediate between the transmissivity of 27 ft^2/day determined for H-11b1 (Section 6.3.1) and the transmissivity of 0.28 ft^2/day determined from slug tests performed at Cabin Baby-1 (Beauheim, 1987c). Figure 6-45 shows a dimensionless Horner plot of the Cabin Baby-1
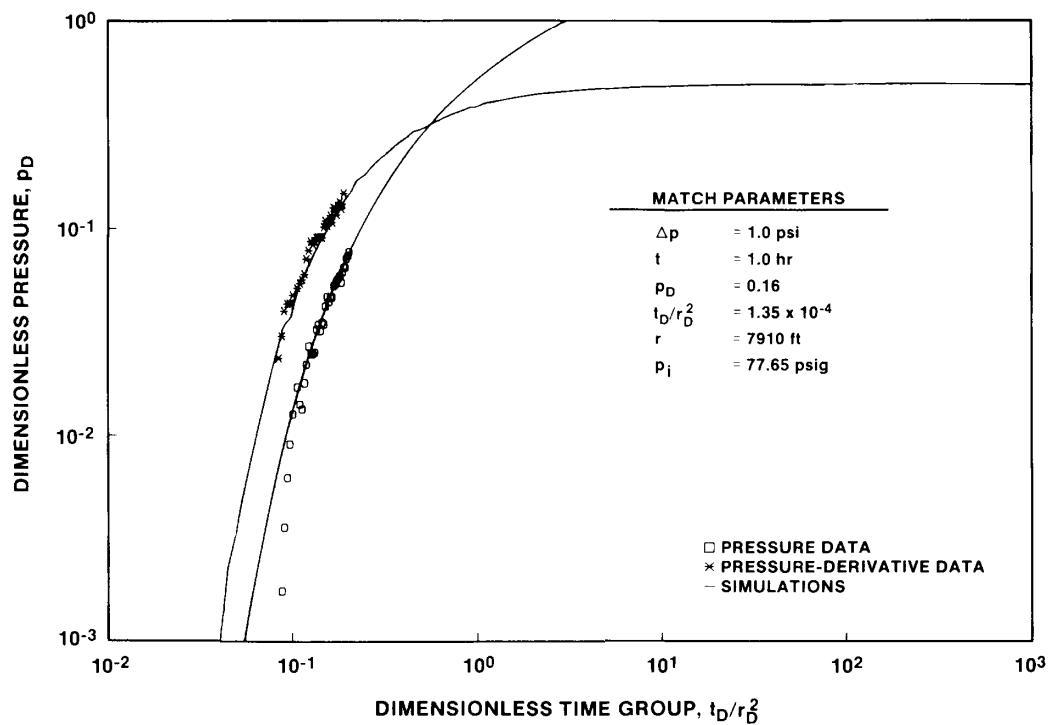
Figure 6-44. Log-Log Plot of Cabin Baby-1 Drawdown During the H-11 Multipad Pumping Test.
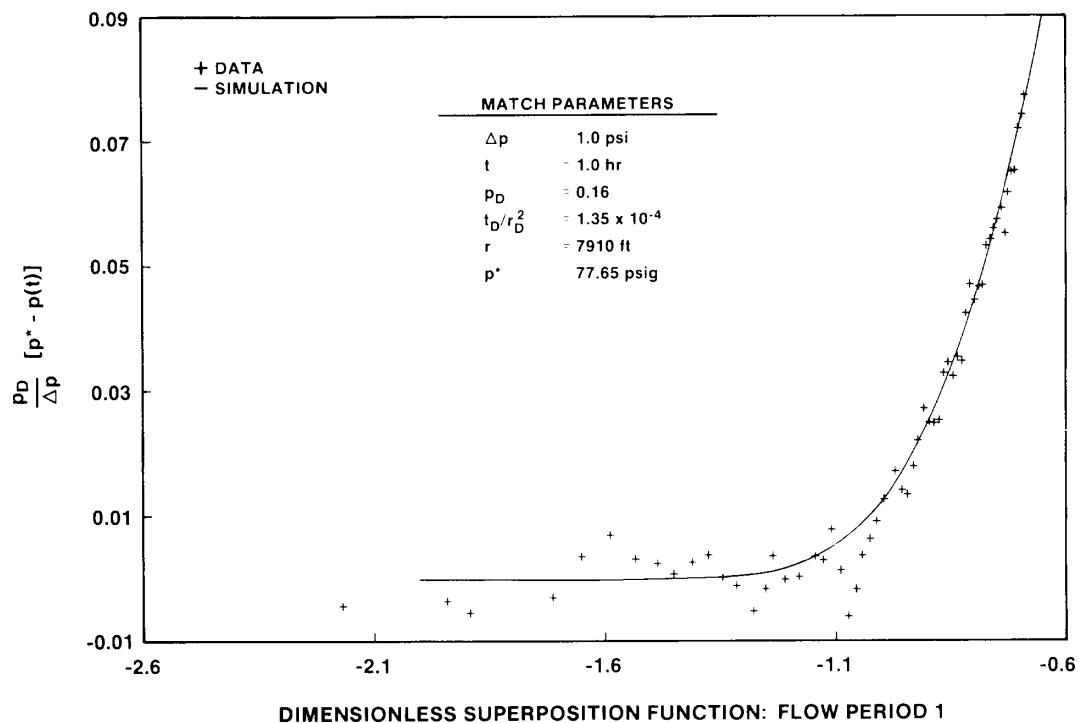
Figure 6-45. Dimensionless Horner Plot of Cabin Baby-1 Drawdown During the H-11 Multipad Pumping Test.

drawdown data with the same simulation. The data and simulation are in good agreement on both plots.

Figure 6-46 shows a linear-linear plot of the drawdown and recovery data from Cabin Baby-1, along with two simulations. The lower of the two simulation curves uses exactly the same model as was derived from the drawdown analysis. This simulation predicts that drawdown would continue longer after the end of the 1512-hr pumping period at H-11b1 than was observed, and that recovery would not be as rapid as was observed. The upper simulation curve uses the same drawdown model with the addition of ten constant-pressure boundaries at a dimensionless distance of 4.5 from Cabin Baby-1. This simulation deviates from the other simulation near the end of the pumping period, and provides an improved match to both the transition between drawdown and recovery and the recovery data, although it overestimates recovery at late time. The ten constant-pressure boundaries

included in this simulation are equivalent to an injection well about 17,000 ft from Cabin Baby-1 injecting water into the Culebra at a rate of about 60 gpm during the exact period when H-11b1 was being pumped.

The two simulations presented in Figure 6-46 appear to show that the drawdown observed at Cabin Baby-1 during the H-11 multipad test pumping period was largely unaffected by other hydraulic stresses. The apparent hydraulic parameters derived from the drawdown analysis should, therefore, be reliable estimates for the region of the Culebra between H-11b1 and Cabin Baby-1. Near the time when the pump was turned off at H-11b1, however, some type of recharge event began affecting water levels at Cabin Baby-1 and continued to do so for the remainder of the monitoring period (through November 1988). Thus, no independent analysis can be performed of the recovery data.
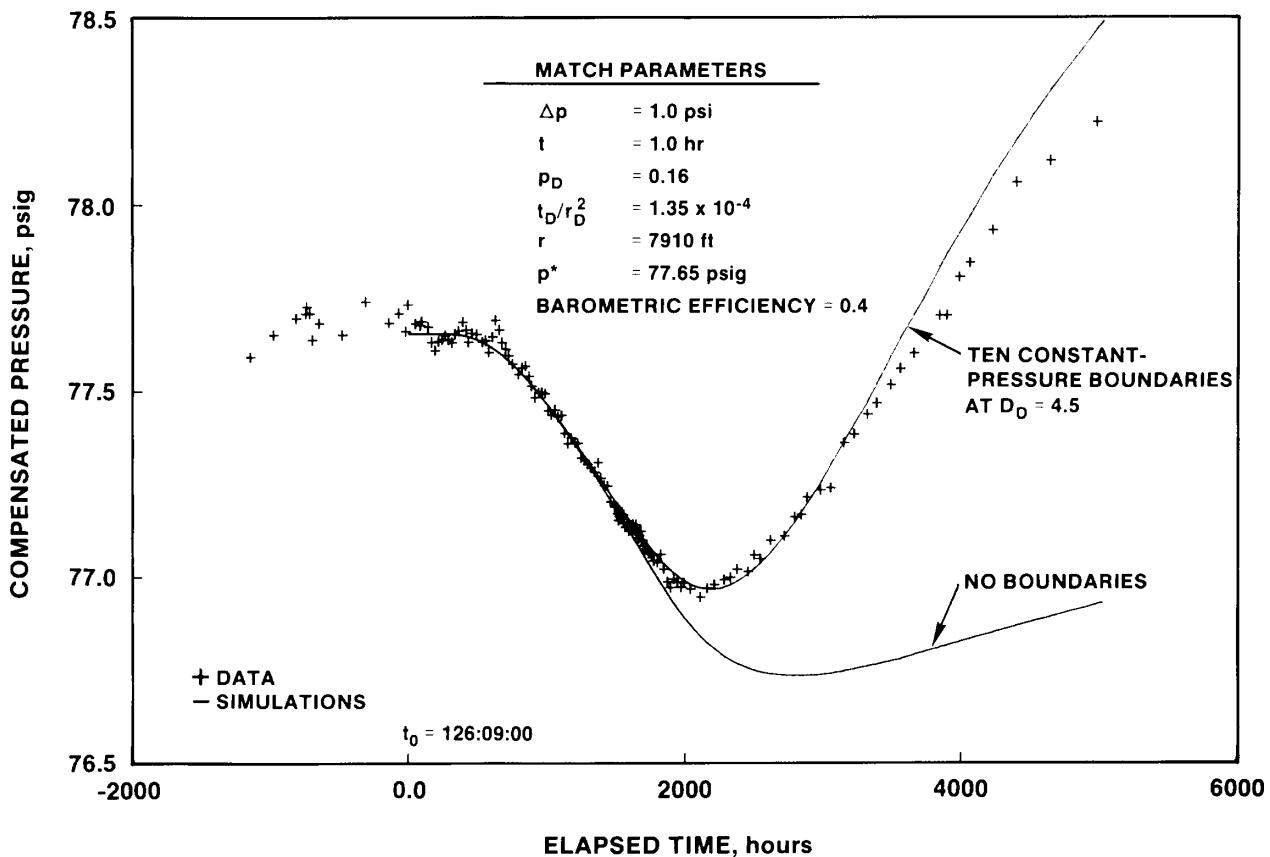
Figure 6-46. Linear-Linear Plot of Cabin Baby-1 Response During the H-11 Multipad Pumping Test.

6.4 Discussion

The individual test responses discussed above are compared and integrated below to provide a broader understanding of the hydraulic behavior of the Culebra dolomite. The hydraulic properties of the Culebra dolomite at the H-11 hydropad are summarized, followed by a discussion of the distribution of hydraulic properties indicated by the responses of the distant observation wells. Finally, different hypotheses to explain the anomalous water-level rises observed are discussed.

6.4.1 Culebra Hydraulic Properties at the H-11

Hydropad. Interpretation of the slug tests performed in H-11b4 indicated that the Culebra probably behaved hydraulically as a double-porosity medium with a transmissivity of 40 to 43 ft²/day at that location. The interpretation of the results of the H-11b4 pumping test confirmed these conclusions. The models found to best simulate the responses observed at H-11b4 and H-11b1 during the H-11b4 pumping test indicate that the Culebra behaves hydraulically as a double-porosity medium with spherical (as opposed to slab-shaped) matrix blocks and unrestricted interporosity flow. The transmissivity appears to be 41 to 42 ft²/day, in close agreement with the slug-test interpretations. The total-system storativity is 3.4×10^{-5}, and the storativity ratio appears to be in a range from 0.025 to 0.08 (Table 6-1). The models also required two no-flow boundaries, representing the effects of decreased-transmissivity boundaries, to match the observed data.

The interpretation of the multipad test recovery responses observed at the H-11 hydropad further confirmed these conclusions. The models found to best simulate the responses of H-11b1, H-11b3, and H-11b4 during the multipad test indicate that the Culebra at H-11 behaves hydraulically as a double-porosity medium with spherical matrix blocks and unrestricted interporosity flow. The transmissivity at the H-11 hydropad appears to be 27 to 29 ft²/day (lower than that indicated by the H-11b4 pumping test), the total-system storativity is between 8.2×10^{-5} and 1.5×10^{-4} (higher than that indicated by the H-11b4 pumping test), and the storativity ratio is between 0.015 and 0.028 (Table 6-1). Two no-flow boundaries were required in the simulations to match the observed data.

Saulnier (1987) reported similar results from interpretation of pumping tests performed on the H-11 hydropad in 1984 and 1985. He reported double-porosity behavior, transmissivities averaging 25 ft²/day, total-system storativities (corrected here for an error of a factor of ω) ranging from 1.8×10^{-4} to 2.8×10^{-4}, and storativity ratios ranging from 0.01 to 0.43. Saulnier (1987) also interpreted the presence of two no-flow (decreased-transmissivity) boundaries from the pumping test performed on the H-11 hydropad in 1985.

Thus, all of the testing performed on the H-11 hydropad has produced a consistent conceptualization of the Culebra as a double-porosity medium at that location. The transmissivity of the Culebra appears to vary somewhat over the hydropad, as testing centered at H-11b4 indicates higher transmissivities than testing centered at the other three H-11 wells. An increase in fracturing to the west of H-11b1 toward H-11b4 and beyond could explain the increased transmissivity and decreased storativity seen during the H-11b4 pumping test. The no-flow boundaries indicated by the pumping-test analyses probably reflect the decreases in Culebra transmissivity known to occur to the east toward P-18 and to the south-southeast toward H-17 and H-12 (see Figure 1-3).

6.4.2 Distribution of Culebra Hydraulic Properties Indicated by Responses of Distant Observation Wells. Of the eleven distant observation wells monitored on a regular basis during the H-11 multipad test (Figure 1-3), all but P-18 showed apparent responses to the test. The responses observed at H-4b, H-12, and P-15, however, were too low in magnitude (Table 5-1) and appeared to be too intermingled with responses to an unknown recharge event to allow reliable interpretation. The responses observed at DOE-1, H-3b2, H-15, H-17, P-17, and Cabin Baby-1 also appeared to be affected by some type of recharge event, but enough drawdown data were collected before the effects of the recharge event were evident to allow interpretation of the multipad-test responses. Only H-14 showed no apparent recharge response.

Hydraulic testing on the single-well and single-hydropad scale has indicated that the transmissivity of the Culebra is one to two orders of magnitude higher

at the H-11 hydropad than at any of the distant observation wells that responded to the H-11 multipad test except for DOE-1 (Beauheim, 1987a,c). With the exception of DOE-1, all of the apparent transmissivity values derived from interpretation of the observation-well responses are intermediate between the transmissivities determined at those wells from local-scale testing and the transmissivity determined for the Culebra at the H-11 hydropad. Local-scale transmissivities range from 0.10 ft^2/day at H-15 (Beauheim, 1987c) to 2.9 ft^2/day at H-3 (Beauheim, 1987a). The apparent transmissivity values obtained from the analyses of the responses of the distant observation wells to the H-11 multipad test range from 6.0 ft^2/day for H-14 to 21 ft^2/day for P-17 (Table 6-1), and seem to represent an averaging of the Culebra transmissivity between H-11 and the individual wells.

Modeling studies by Haug et al. (1987) and LaVenue et al. (1988) suggested the existence of a relatively high-transmissivity channel extending through the Culebra south of H-11 between P-17 and H-12. Well H-17 was drilled in an unsuccessful attempt to locate this channel. The highest apparent transmissivity derived from the multipad test responses was 21 ft^2/day for P-17. Given that the local transmissivity at P-17 is only 1.0 ft^2/day (Beauheim, 1987c), the high apparent transmissivity indicated by the multipad test may indicate a relatively high transmissivity for most of the Culebra between H-11 and P-17, as shown in the models of Haug et al. (1987) and LaVenue et al. (1988). The H-11 multipad test provided no indication of the possible southward extent of this hypothesized high-transmissivity channel.

The apparent transmissivity value obtained from the analysis of the response at DOE-1 to the H-11 multipad test, 9.0 ft^2/day, is slightly lower than the 11 ft^2/day reported by Beauheim (1987c) from interpretation of a pumping test at that well. This low apparent transmissivity probably results from the pumping at H-11 drawing more water from the high-transmissivity region around DOE-1 than from lower transmissivity regions to the east or west (see Figure 5-24).

The apparent storativity values determined from the responses of the distant observation wells range from 2.4 × 10^{-6} for DOE-1 to 6.5 × 10^{-5} for Cabin Baby-1 (Table 6-1). All of the values greater than 10^{-5} are from

wells (H-14, H-17, P-17, and Cabin Baby-1) in locations where few or no open fractures have been observed in Culebra core (where available), and where only single-porosity behavior is observed during hydraulic tests. All of the apparent storativity values less than 10^{-5} are from wells north of H-11: DOE-1, H-3b2, and H-15. DOE-1 and H-3b2 are at locations where the Culebra is known to be fractured, and where double-porosity responses have been interpreted from local-scale hydraulic tests. DOE-1 also displayed a double-porosity hydraulic response to the H-11 multipad test (Section 6.3.4). Thus, the low apparent storativities between H-11 and DOE-1 and H-3b2 are probably related to fracture interconnection among these wells. Fracture interconnection also explains why a response was observed within two hr at DOE-1 when multipad-test pumping began, and why drawdown was more pronounced to the north of H-11 than in any other direction (Figure 5-24).

The low apparent storativity, rapid response, and large amount of drawdown observed at H-15 are more difficult to explain. Single-well testing at H-15 has shown it to be in one of the least-transmissive regions of the Culebra at the WIPP site (Beauheim, 1987c), and all fractures found in the Culebra core from H-15 were filled with gypsum (Mercer, in preparation, b). The response to the H-11 multipad test observed at H-15 can be explained, however, by hypothesizing that the fracture network extending from H-11 to DOE-1 also passes close enough to H-15 to allow rapid transmission of hydraulic stresses. A similar response, with a similar explanation, was observed at well WIPP-30 during the WIPP-13 multipad pumping test (Beauheim, 1987b).

6.4.3 Anomalous Water-Level Rises. As discussed above, apparent recharge effects were observed at all of the distant observation wells except for H-14 during the H-11 multipad test. At DOE-1, H-4b, H-12, H-17, P-15, P-17, and Cabin Baby-1, recharge was evidenced by water levels rising higher during the multipad-test recovery period than they were before the multipad test began. At H-3b2 and H-15, water levels did not actually surpass their pretest elevations, but showed clear trends in that direction when recovery monitoring was terminated. The apparent over-recoveries at DOE-1, H-3b2, and H-15 can be explained, at least in part, as continued recovery from

hydraulic stresses that preceded the multipad test. This explanation cannot be applied, however, to the other wells where anomalously high water levels were observed. At these wells, some discrete event appears to have caused water levels to rise.

A significant rise in water levels has also been observed in wells on the H-9 hydropad. The H-9 hydropad lies 6.75 mi south of the H-11 hydropad (Figure 1-3). Water levels in the three H-9 wells completed to the Culebra dolomite began rising in April 1988, shortly before the H-11 multipad test began. By May 1989, water levels in the H-9 wells were nearly 13 ft above their March 1988 levels (Stensrud et al., in preparation). No reason for this rise in water levels is evident. Whether or not the rise observed at the H-9 hydropad is related to the rise observed at the wells to the north is unknown.

Water levels in aquifers can rise for three principal reasons: a decrease in discharge, an increase in recharge, or a change in the mechanical stress field. A decrease in discharge from the Culebra could be related to cessation of pumping or shaft drainage at some location. A sudden increase in recharge to the Culebra would only be likely to occur as some type of injection of fluid through a well. Changes in the recharge rate to the Culebra related to climatic conditions would develop slowly over periods of years or centuries, not over a few months. Changes in the mechanical stress field of a rock mass can cause dilatation of the rock and associated changes in fluid pressures. Changes in the mechanical stress field of the Culebra could be caused by earth tides, fault creep, earthquakes, subsidence, or fracture-aperture changes related to fluid-pressure changes. Earth tides are diurnal events causing regular oscillations in water levels (Bredehoeft, 1967). Creep along fault planes occurs as discrete movements, also stimulating oscillatory water-level changes (Cooper et al., 1965; Johnson et al., 1973). Thus, neither earth tides nor fault creep can explain the long-term rise observed in the Culebra water levels. Earthquakes and subsidence can create long-term changes in mechanical stress fields. Fracture-aperture changes may be either temporary or permanent, depending on the nature of the causal fluid-pressure change.

6.4.3.1 Potential for Decreased Discharge from the Culebra.
Water levels in wells completed to the Culebra could rise if a drain on the system were stopped. A drain could take the form of a pumping well or a draining shaft through the Culebra. The drain would have had to have been constantly active for a number of years because of the length of time that water levels were stable at wells such as H-4b and P-17 before the recent rise. The only wells that could have been pumping relatively constantly from the Culebra for a number of years are stock wells equipped with windmills, but no stock wells completed to the Culebra are present in the region encompassing H-4, H-12, and H-17. Similarly, while potash mine shafts have been draining the Culebra west of the WIPP site in Nash Draw for decades, no shafts have ever been present in the area where water levels are now rising. In addition, water levels in the wells closest to the potash mine shafts, such as H-7 and WIPP-26, are not rising (Stensrud et al., in preparation). Thus, cessation of drainage from the Culebra appears to be an unlikely explanation for the observed rise in water levels.

6.4.3.2 Potential for Injection of Fluid into the Culebra.
Injection of fluid to the Culebra could have occurred as disposal of waste fluids into an injection well, as a loss of drilling fluid in a hole passing through the Culebra, or as an interconnection in a borehole between the Culebra and another water-bearing unit having a higher hydraulic head. Intentional disposal of fluids into the Culebra dolomite is illegal in the State of New Mexico. Furthermore, the New Mexico State Engineer's office has issued no permits for waste injection into any formation in the area south of the WIPP. Therefore, fluid disposal is an unlikely explanation for the rise in water levels.

Some loss of drilling fluid into the Culebra probably occurs in every hole drilled through the Culebra. The only drilling observed in 1988 south of the WIPP site was for a few oil wells targeting the Bell Canyon or deeper formations. As these wells are being drilled, the Rustler Formation is penetrated in at most a few days, and casing is installed and cemented from the upper Salado to the surface before the hole is deepened, in accordance with State regulations.

Thus, the time available for potential drilling fluid loss to the Culebra is limited. For drilling-fluid losses to be responsible for the rise in water levels over the wide area and long period of time observed, the losses would have to have occurred over a prolonged period at a rate easily noticeable to the driller. None of the local drillers or brine haulers contacted have reported any prolonged or unusual losses of drilling fluid.

Injection of fluid into the Culebra could also occur by means of an interconnection through a borehole between the Culebra and another water-bearing unit having a higher hydraulic head. Such an interconnection would be illegal under New Mexico law, but could nevertheless have occurred inadvertently or as a result of deterioration of a well, and would also be likely to have long-term effects once the interconnection was first made. In the area south of the WIPP, units having hydraulic heads higher than that of the Culebra include the Magenta dolomite, the Dewey Lake Red Beds, and the Dockum Group, all overlying the Culebra. Brine reservoirs in the Castile Formation, beneath the Culebra, also have higher heads than that of the Culebra. The transmissivity of the Magenta dolomite is too low over the area affected to provide enough water from a single location to cause the observed rise in Culebra water levels. The Dewey Lake Red Beds and Dockum Group could potentially produce more water than the Magenta, but none of the known wells producing from those formations south of the WIPP penetrate the Rustler Formation (Winstanley and Carrasco, 1986; Lyon, 1989). Hydraulic communication between the Culebra and the Dewey Lake or Dockum could be occurring behind the casing in a throughgoing well, but this would be unlikely to ever be detected. Similarly, hydraulic communication between the Culebra and a Castile brine reservoir could also occur if the cement behind the casing in a throughgoing well had deteriorated. The only reported encounter of Castile brine south of the WIPP is at the Belco well near P-15 and H-4 (Popielak et al., 1983; Figure 1-3).

6.4.3.3 Potential for Changes in Mechanical Stress to Affect Culebra Water Levels. Cooper et al. (1965) reported a water-level fluctuation of 15 ft in a well in Florida following the 1964 Alaskan earthquake. Wood (1985) reported two- to ten-fold increases in spring discharges in Idaho following a magnitude-7.3

earthquake in 1983. He attributed the increases in spring discharge to increases in pore pressure caused by increased contractional strain resulting from the earthquake. However, no unusual seismic activity was observed at the WIPP site in 1988 (Sanford et al., 1988a,b,c; 1989) that might have resulted in an increase in Culebra water levels.

Subsidence can cause increased pore pressures by compressing rock layers. Subsidence in the vicinity of the WIPP could be related to potash or WIPP mining, or to oil withdrawals from the Bell Canyon Formation. Potash mining and oil production have been going on around the WIPP site for decades. If either of these mechanisms was causing subsidence south of the WIPP, similar water-level changes should have been observed during the previous 10 years of water-level monitoring, and not just in 1988. In addition, neither potash mines nor the WIPP underground underlie the region in which water-level rises have been observed, and water levels in wells close to the mines have not changed. Thus, subsidence appears to be an implausible explanation for the rise in Culebra water levels.

A final hypothesis to explain the observed rise in Culebra water levels pertains to the H-11 multipad pumping test itself. As water was pumped from the Culebra during the test, the fluid pressure in interconnected fractures decreased. As the pressure in the fractures decreased, the fracture apertures should have decreased. What effect the changes in fracture apertures would have on the mechanical stress field of the Culebra is uncertain. However, the decrease in fracture permeability that would accompany the aperture reduction should have caused hydraulic heads upgradient to increase through a "damming" effect. The models of Haug et al. (1987) and LaVenue et al. (1988) show flow within the Culebra converging on a high-transmissivity channel near the H-11 hydropad. If the permeability of this channel were reduced, an increase in hydraulic heads upgradient of the channel would occur. All of the wells at which increases in water levels have been observed (except at the H-9 hydropad) are either upgradient of the high-transmissivity channel or within the channel but upgradient of where the maximum permeability reduction should have occurred. This hypothesis explains the coincidence in timing between the H-11 multipad test and the onset of the rise in water levels. This hy-

pothesis would also indicate that the high water levels should be a transient phenomenon, decaying back to near their prepumping levels after the pressure in the fractures recovers and the fractures reopen. Gale (1982), however, indicates that some permanent loss of permeability occurs when fractures undergo depressurization-repressurization cycles. Thus, water levels may restabilize slightly above their pre-multipad-test levels.

6.4.3.4 Summary.
In summary, no clear conclusion as to the cause of the rise in Culebra water levels can be drawn. No evidence has been found of a cessation of drainage from the Culebra, purposeful injection of fluids into the Culebra, or unusual drilling fluid losses. Hydraulic interconnection through a well between the Culebra and a unit having a higher hydraulic head is a theoretical possibility, but difficult to prove or disprove. No major earthquakes occurred during the multipad test pumping period that might have changed the mechanical stress field of the Culebra. No reasons exist for a unique subsidence event to have occurred during the multipad test. Nearly 550,000 gallons of water were pumped from the Culebra during the test. Perhaps this fluid withdrawal reduced fracture permeabilities sufficiently to raise hydraulic heads upgradient. If so, the heads would be expected to decay back to near their pre-multipad-test levels eventually. As of May 1989, however, water levels south of the WIPP site were continuing to rise.

A question remains as to whether or not the rise in water levels observed at the H-9 hydropad is related to the rises observed in the multipad-test observation wells. The rise in water levels in the H-9 wells began before the pump was turned on for the multipad test, indicating no connection between the two events. The closest well to the north of the H-9 hydropad is H-12, about five miles away. Water levels in H-12 were clearly affected by the recharge source/event after the end of the multipad-test pumping period, and may have been affected sometime during the pumping period, but no precise time can be determined because of the concurrent pumping-test drawdown. A similar uncertainty in timing applies to the other multipad-test observation wells at which water-level rises have been observed. Thus, no evaluation of the direction of propagation of the recharge event can be performed to determine if the rise observed at the H-9 hydropad is related to the rises later observed farther north.

7. SUMMARY AND CONCLUSIONS

A large-scale pumping test and convergent-flow tracer test of the Culebra Dolomite Member of the Rustler Formation was performed in 1988 at the WIPP site in southeastern New Mexico. This test, known as the H-11 multipad/tracer test, complemented the H-3 and WIPP-13 multipad tests (Beauheim, 1987a, b) by creating a hydraulic stress that could be measured over the southern portion of the WIPP site. In preparation for this test, well H-11b4 was drilled on the existing H-11 hydropad. DSTs, slug tests, and a 50-hr pumping test were then performed at H-11b4 to evaluate aquifer and well properties at that location to aid in design and interpretation of the planned tracer test. Interpretation of the tracer-test results will be presented in a later report.

The DSTs in H-11b4 were unsuccessful because of too-rapid pressure recovery. The slug tests indicated a Culebra transmissivity between 40 and 43 ft^2/day, and provided a qualitative indication of possible double-porosity hydraulic behavior. In a double-porosity system, fractures provide the bulk of the permeability and matrix pores provide the majority of the storage capacity. The H-11b4 pumping test confirmed the slug-test transmissivity estimates and the double-porosity hydraulic behavior of the Culebra. The test responses at both H-11b4 and H-11b1 were best simulated using a model of a double-porosity medium with spherical matrix blocks, unrestricted interporosity flow, a transmissivity of 41 to 42 ft^2/day, a fracture-to-total-system storativity ratio of 0.025 to 0.08, and a total-system storativity of 3.4×10^{-5}.

The H-11 multipad/tracer test was performed by pumping well H-11b1 at a rate of six gpm for 63 days. This pumping had the dual effect of creating a converging flow field for a test using conservative tracers injected into the other three H-11 wells, and of creating a hydraulic stress that could be measured in wells south of the center of the WIPP site. Fluid-pressure responses were monitored in the pumping well and three other wells on the H-11 hydropad, and water levels were monitored in 11 observation wells at distances ranging from 3970 to 15,530 ft from H-11b1. Responses were observed in 10 of these distant wells.

Individual well tests at various locations around the WIPP site have demonstrated that the Culebra is a heterogeneous water-bearing unit. The responses measured in observation wells to pumping tests in heterogeneous systems cannot be rigorously interpreted using standard analytical (as opposed to numerical) techniques developed for tests in homogeneous porous media. Application of analytical techniques to data from heterogeneous media results in quantitative evaluations of average hydraulic properties between pumping and observation wells that are nonunique in the sense that they are representative only of the responses observed when a hydraulic stress is imposed at a certain location. These "apparent" hydraulic properties do, however, provide a qualitative understanding of the nature and distribution of both hydraulic properties and heterogeneities or boundaries within the tested area.

The analytical interpretations of the multipad-test responses presented in this report had four principal objectives. The first objective was to determine the most appropriate conceptualization of the nature of the Culebra flow system around the H-11 hydropad. Pumping tests performed at the H-11 hydropad in 1984 and 1985 revealed apparent double-porosity hydraulic behavior of the Culebra (Saulnier, 1987), as did the H-11b4 pumping test. Similar hydraulic behavior was observed during the H-11 multipad test, as the responses of the wells on the H-11 hydropad during the test appear to be representative of wells completed in a bounded double-porosity medium with spherical matrix blocks and unrestricted interporosity flow. Low-transmissivity boundaries are evident in the responses of the H-11 wells, reflecting an area of lower Culebra transmissivity lying east and south of the H-11 hydropad.

The second objective was to quantify the hydraulic properties of the Culebra in the vicinity of H-11. The transmissivity of the Culebra at H-11 derived from the multipad-test analyses is about 27 ft^2/day, similar to the values determined by Saulnier (1987). The total-system storativity of the Culebra is 8.2×10^{-5} to 1.5×10^{-4}. The ratio of the fracture storativity to the

total-system (i.e., fractures + matrix) storativity is about 0.025. This latter value indicates the importance of matrix pores as the primary fluid-storage medium.

The third objective was to determine the nature and distribution of heterogeneities within the area of Culebra influenced by the test. Drawdown contours shown in Figure 5-24 indicate that water was derived preferentially from north and south of H-11 during the multipad test. This preference coincides with regions to the north of H-11 where the Culebra is known to be fractured, and with regions south of H-11 where numerical modeling indicates high transmissivities are likely to be present. Apparent recharge effects observed in the over-recovery of observation-well water levels effectively masked other evidence of large-scale heterogeneities within the Culebra.

The fourth objective was to determine the apparent hydraulic properties of the Culebra between H-11 and responding observation wells. The results are listed in Table 6-1 and summarized below. The wells to the south and west of H-11 lie in a region where the Culebra is largely unfractured and has a lower transmissivity than at H-11. The simulations of the responses observed at these wells indicated apparent transmissivities ranging from 6 to 21 ft^2/day, intermediate between that measured on the H-11 hydropad and those measured during local-scale testing at the individual wells, and apparent storativities ranging from 1.8×10^{-5} to 6.5×10^{-5}. DOE-1 and H-3b2 lie to the north and northwest of H-11 in a region of the Culebra characterized by fracturing and double-porosity hydraulic behavior. The simulation of the response observed at DOE-1 indicates that separate fracture and matrix responses to the multipad test are resolvable nearly 4000 ft from H-11, while the H-3b2 simulations indicate only total-system behavior is apparent at a distance of about 8000 ft. H-15 lies 9000 ft north of H-11 where the Culebra has a low transmissivity and where few or no open fractures have been observed in core. Nevertheless, H-15 responded rapidly to the multipad test and showed the second highest amount of drawdown. This rapid and high-magnitude response is interpreted to indicate that the fracture system extending north of H-11 to DOE-1 and H-3b2 also extends close to H-15. Apparent transmissivities interpreted from the responses of DOE-1, H-3b2, and H-15 ranged only from 7.1 to 9.0

ft^2/day, and apparent storativities ranged from 2.4×10^{-6} to 8.4×10^{-6}. These apparent storativity values are nearly an order of magnitude lower than the values interpreted from the responses of the wells in largely unfractured regions of the Culebra south and west of H-11.

The major question arising from the H-11 multipad test has to do with the cause of the anomalous water-level rises observed at most of the observation wells. The two most plausible explanations for the rises involve either injection of fluid to the Culebra, probably through a deteriorated well, or permeability reduction arising from fracture depressurization. Direct proof of either possibility is unlikely to be obtained.

In summary, the analyses of the observed responses to the H-11 multipad pumping test provide a qualitative conceptualization of two distinct domains within a heterogeneous portion of the Culebra dolomite south of the center of the WIPP site. The Culebra is a fractured system around DOE-1, H-3, and H-11. This system appears to extend further to the north toward H-15, although H-15 itself lies in an unfractured, lower transmissivity zone. The fracture system may also extend to the south from H-11, although no wells are currently situated in that area. To the west, southwest, and southeast of H-11, fracturing decreases and the apparent storativity increases. This conceptualization is being refined using numerical-modeling techniques to simulate the H-11 multipad test and other tests at the WIPP site, in an attempt to define a distribution of hydraulic properties that will reproduce the responses observed. The full numerical simulation of Culebra hydrology near the WIPP site is guided by, and must be consistent with, the interpretations presented here.

REFERENCES

Avis, J.D., and Saulnier, G.J., Jr. 1989. *Analysis of the Fluid-Pressure Responses of the Rustler Formation at H-16 to the Construction of the Air-Intake Shaft at the Waste Isolation Pilot Plant (WIPP) Site,* SAND89-7067 (Albuquerque, NM: Sandia National Laboratories).

Barrows, L.J.; Shaffer, S.-E.; Miller, W.B.; and Fett, J.D. 1983. *Waste Isolation Pilot Plant (WIPP) Site Gravity Survey and Interpretation,* SAND82-2922 (Albuquerque, NM: Sandia National Laboratories).

Beauheim, R.L. 1987a. *Analysis of Pumping Tests of the Culebra Dolomite Conducted at the H-3 Hydropad at the Waste Isolation Pilot Plant (WIPP) Site,* SAND86-2311 (Albuquerque, NM: Sandia National Laboratories).

Beauheim, R.L. 1987b. *Interpretation of the WIPP-13 Multipad Pumping Test of the Culebra Dolomite at the Waste Isolation Pilot Plant (WIPP) Site,* SAND87-2456 (Albuquerque, NM: Sandia National Laboratories).

Beauheim, R.L. 1987c. *Interpretations of Single-Well Hydraulic Tests Conducted At and Near the Waste Isolation Pilot Plant (WIPP) Site, 1983-1987,* SAND87-0039 (Albuquerque, NM: Sandia National Laboratories).

Bourdet, D., and Gringarten, A.C. 1980. *Determination of Fissure Volume and Block Size in Fractured Reservoirs by Type-Curve Analysis,* SPE 9293 (Richardson, TX: Soc Pet Eng).

Bourdet, D.; Ayoub, J.A.; and Pirard, Y.M. 1989. "Use of Pressure Derivative in Well-Test Interpretation," SPE Formation Evaluation 4(2):293-302.

Bredehoeft, J.D. 1967. "Response of Well-Aquifer Systems to Earth Tides," *J Geophys Res* 72(12):3075-3087.

Chen, C.C.; Yeh, N.; Raghavan, R.; and Reynolds, A.C. 1984. "Pressure Response at Observation Wells in Fractured Reservoirs," *Soc Pet Eng J* 24(6): 628-638.

Cinco-Ley, H.; Samaniego-V., F.; and Kucuk, F. 1985. *The Pressure Transient Behavior for Naturally Fractured Reservoirs with Multiple Block Size,* SPE 14168 (Richardson, TX: Soc Pet Eng).

Cooper, H.H., Jr.; Bredehoeft, J.D.; Papadopulos, I.S.; and Bennett, R.R. 1965. "The Response of Well-Aquifer Systems to Seismic Waves," *J Geophys Res* 70(16):3915-3926.

Cooper, H.H., Jr.; Bredehoeft, J.D.; and Papadopulos, I.S. 1967. "Response of a Finite-Diameter Well to an Instantaneous Charge of Water," *Water Resources Research* 3(1):263-269.

Crawley, M.E. 1988. *Hydrostatic Pressure and Fluid-Density Distribution of the Culebra Dolomite Member of the Rustler Formation Near the Waste Isolation Pilot Plant, Southeastern New Mexico.* DOE/WIPP 88-030 (Carlsbad, NM: US DOE).

Crawley, M.E. 1988. Personal communications of informal data transmittals to R. Beauheim.

Deruyck, B.G.; Bourdet, D.P.; DaPrat, G.; and Ramey, H.J., Jr. 1982. *Interpretation of Interference Tests in Reservoirs with Double Porosity Behavior--Theory and Field Examples,* SPE 11025 (Richardson, TX: Soc Pet Eng).

de Swaan, A.O. 1976. "Analytical Solutions for Determining Naturally Fractured Reservoir Properties by Well Testing," *Soc Pet Eng J* (June 1976):117-122.

Earlougher, R.C., Jr. 1977. *Advances in Well Test Analysis.* Monograph Volume 5 (Dallas, TX: Soc Pet Eng of AIME), 264 pp.

Ferris, J.G.; Knowles, D.B.; Brown, R.H.; and Stallman, R.W. 1962. *Theory of Aquifer Tests, Ground-Water Hydraulics.* USGS Water-Supply Paper 1536-E (Washington, DC: US GPO), 174 pp.

Freeze, R.A., and Cherry, J.A. 1979. *Groundwater* (Englewood Cliffs, NJ: Prentice-Hall, Inc), 604 pp.

Gale, J.E. 1982. "Assessing the Permeability Characteristics of Fractured Rock," in Recent Trends in Hydrogeology, GSA Special Paper 189 (Boulder, CO: GSA), pp. 163-181.

Grader, A.S., and Ramey, H.J., Jr. 1988. "Slug-Test Analysis in Double-Porosity Reservoirs," SPE Formation Evaluation 3(2):329-339.

Gringarten, A.C. 1984. "Interpretation of Tests in Fissured and Multilayered Reservoirs with Double-Porosity Behavior: Theory and Practice," *J Pet Tech* 36(4):549-564.

Gringarten, A.C. 1986. *Computer-Aided Well Test Analysis,* SPE 14099 (Richardson, TX: Soc Pet Eng).

Gringarten, A.C.; Ramey, H.J., Jr.; and Raghavan, R. 1974. "Unsteady-State Pressure Distributions Created by a Well with a Single Infinite-Conductivity Vertical Fracture," *Soc Pet Eng J* 14(4):347-360.

Gringarten, A.C.; Bourdet, D.P.; Landel, P.A.; and Kniazeff, V.J. 1979. *A Comparison Between Different Skin and Wellbore Storage Type-Curves for Early-Time Transient Analysis,* SPE 8205 (Richardson, TX: Soc Pet Eng).

Haug, A.; Kelley, V.A.; LaVenue, A.M.; and Pickens, J.F. 1987. *Modeling of Ground-Water Flow in the Culebra Dolomite at the Waste Isolation Pilot Plant (WIPP) Site: Interim Report,* SAND86-7167 (Albuquerque, NM: Sandia National Laboratories).

Horner, D.R. 1951. "Pressure Buildup in Wells," *Proc Third World Pet Cong* 2:503-523 (The Hague, Netherlands). Reprinted 1967. Pressure Analysis Methods, AIME Reprint Series 9:45-50 (Richardson, TX: Soc Pet Eng).

HydroGeoChem, Inc. 1985. *WIPP Hydrology Program, Waste Isolation Pilot Plant, SENM, Hydrologic Data Report #1,* SAND85-7206 (Albuquerque, NM: Sandia National Laboratories).

Ibrahim, M.A.; Tek, M.R.; and Katz, D.L. 1971. *Threshold Pressure in Gas Storage.* Project 26-47 Monograph (Arlington, VA: American Gas Association), 309 pp.

INTERA Technologies, Inc. 1986. *WIPP Hydrology Program, Waste Isolation Pilot Plant, Southeastern New Mexico, Hydrologic Data Report #3,* SAND86-7109 (Albuquerque, NM: Sandia National Laboratories).

Jenkins, D.N., and Prentice, J.K. 1982. "Theory for Aquifer Test Analysis in Fractured Rocks Under Linear (Nonradial) Flow Conditions," *Ground Water* 20(1):12-21.

Johnson, A.G.; Kovach, R.L.; Nur, A.; and Booker, J.R. 1973. "Pore Pressure Changes during Creep Events on the San Andreas Fault," *J Geophys Res* 78(5):851-857.

Jones, C.L. 1978. *Test Drilling for Potash Resources: Waste Isolation Pilot Plant Site, Eddy County, New Mexico.* USGS Open-File Rpt 78-592, 2 volumes (Denver, CO).

Kazemi, H. 1969. "Pressure Transient Analysis of Naturally Fractured Reservoirs with Uniform Fracture Distribution," *Soc Pet Eng J* (Dec 1969):451-462.

Kazemi, H.; Seth, M.S.; and Thomas, G.W. 1969. "The Interpretation of Interference Tests in Naturally Fractured Reservoirs with Uniform Fracture Distribution," *Soc Pet Eng J* (Dec 1969):463-472.

Kruseman, G.P., and DeRidder, N.A. 1979. *Analysis and Evaluation of Pumping Test Data.* Bulletin 11 (Wageningen, the Netherlands: International Institute for Land Reclamation and Improvement), 200 pp.

LaVenue, A.M.; Haug, A.; and Kelley, V.A. 1988. *Numerical Simulation of Ground-Water Flow in the Culebra Dolomite at the Waste Isolation Pilot Plant (WIPP) Site: Second Interim Report,* SAND88-7002 (Albuquerque, NM: Sandia National Laboratories).

Lyon, M.L. 1989. *Annual Water Quality Data Report for the Waste Isolation Pilot Plant, April 1989.* DOE/WIPP 89-001 (Carlsbad, NM: US DOE).

Mavor, M.J., and Cinco-Ley, H. 1979. *Transient Pressure Behavior of Naturally Fractured Reservoirs,* SPE 7977 (Richardson, TX: Soc Pet Eng).

Mercer, J.W. in preparation, a. *Basic Data Report for Drillholes at the H-11 Complex (Waste Isolation Pilot Plant - WIPP),* SAND89-0200 (Albuquerque, NM: Sandia National Laboratories).

Mercer, J.W. in preparation, b. *Basic Data Report for Drillholes H-14 and H-15 (Waste Isolation Pilot Plant - WIPP),* SAND89-0202 (Albuquerque, NM: Sandia National Laboratories).

Mercer, J.W. in preparation, c. *Basic Data Report for Drillhole H-12 (Waste Isolation Pilot Plant - WIPP),* SAND89-0201 (Albuquerque, NM: Sandia National Laboratories).

Mercer, J.W. in preparation, d. *Basic Data Report for Drillholes H-17 and H-18 (Waste Isolation Pilot Plant - WIPP),* SAND89-0204 (Albuquerque, NM: Sandia National Laboratories).

Mercer, J.W., and Orr, B.R. 1979. *Interim Data Report on the Geohydrology of the Proposed Waste Isolation Pilot Plant Site, Southeast New Mexico.* USGS Water-Resources Investigations Rpt 79-98 (Albuquerque, NM), 178 pp.

Mercer, J.W.; Davis, P.; Dennehy, K.F.; and Goetz, C.L. 1981. *Results of Hydrologic Tests and Water-Chemistry Analyses, Wells H-4A, H-4B, and H-4C at the Proposed Waste Isolation Pilot Plant Site, Southeastern New Mexico.* USGS Water-Resources Investigations Rpt 81-36 (Albuquerque, NM), 92 pp.

Moench, A.F. 1984. "Double-Porosity Models for a Fissured Groundwater Reservoir with Fracture Skin," *Water Resources Research* 20(7):831-846.

Narasimhan, T.N., and Kanehiro, B.Y. 1980. "A Note on the Meaning of Storage Coefficient," *Water Resources Research* 16(2):423-429.

Nind, T.E.W. 1965. "Definition and Measurement of Losses in Hydraulic Head Around a Well Bore," *Canadian Journal of Earth Sciences* 2:329-350.

Popielak, R.S.; Beauheim, R.L.; Black, S.R.; Coons, W.E.; Ellingson, C.T.; and Olsen, R.L. 1983. *Brine Reservoirs in the Castile Formation, Southeastern New Mexico.* TME 3153 (Albuquerque, NM: US DOE).

Ramey, H.J., Jr.; Agarwal, R.G.; and Martin, I. 1975. "Analysis of 'Slug Test' or DST Flow Period Data," *J Can Pet Tech* 14(3):37-47.

Randall, W.S.; Crawley, M.E.; and Lyon, M.L. 1988. *Annual Water Quality Data Report for the Waste Isolation Pilot Plant, May 1988.* DOE/WIPP 88-006 (Carlsbad, NM: US DOE).

Richey, S.F. 1987. *Water-Level Data from Wells in the Vicinity of the Waste Isolation Pilot Plant, Southeastern New Mexico.* USGS Open-File Rpt 87-120 (Albuquerque, NM), 107 pp.

Sanford, A.; Jarman, C.; and Singer, P. 1988a. *A Report on the Seismicity of the WIPP Site for the Period January 1, 1988 through March 31, 1988.* (Socorro, NM: New Mexico Institute of Mining and Technology), 7 pp.

Sanford, A.; Jarman, C.; and Singer, P. 1988b. *A Report on the Seismicity of the WIPP Site for the Period April 1, 1988 through June 30, 1988.* (Socorro, NM: New Mexico Institute of Mining and Technology), 8 pp.

Sanford, A.; Jarman, C.; and Singer, P. 1988c. *A Report on the Seismicity of the WIPP Site for the Period July 1, 1988 through September 30, 1988.* (Socorro, NM: New Mexico Institute of Mining and Technology), 7 pp.

Sanford, A.; Jarman, C.; and Singer, P. 1989. *A Report on the Seismicity of the WIPP Site for the Period October 1, 1988 through December 31, 1988.* (Socorro, NM: New Mexico Institute of Mining and Technology), 7 pp.

Saulnier, G.J., Jr. 1987. *Analysis of Pumping Tests of the Culebra Dolomite Conducted at the H-11 Hydropad at the Waste Isolation Pilot Plant (WIPP) Site,* SAND87-7124 (Albuquerque, NM: Sandia National Laboratories).

Saulnier, G.J., Jr.; Freeze, G.A.; and Stensrud, W.A. 1987. *WIPP Hydrology Program, Waste Isolation Pilot Plant, Southeastern New Mexico, Hydrologic Data Report #4,* SAND86-7166 (Albuquerque, NM: Sandia National Laboratories).

Stensrud, W.A.; Bame, M.A.; Lantz, K.D.; LaVenue, A.M.; Palmer, J.B.; and Saulnier, G.J., Jr. 1987. *WIPP Hydrology Program, Waste Isolation Pilot Plant, Southeastern New Mexico, Hydrologic Data Report #5,* SAND87-7125 (Albuquerque, NM: Sandia National Laboratories).

Stensrud, W.A.; Bame, M.A.; Lantz, K.D.; Cauffman, T.L.; Palmer, J.B.; and Saulnier, G.J., Jr. 1988a. *WIPP Hydrology Program, Waste Isolation Pilot Plant, Southeastern New Mexico, Hydrologic Data Report #6,* SAND87-7166 (Albuquerque, NM: Sandia National Laboratories).

Stensrud, W.A.; Bame, M.A.; Lantz, K.D.; Palmer, J.B.; and Saulnier, G.J., Jr. 1988b. *WIPP Hydrology Program, Waste Isolation Pilot Plant, Southeastern New Mexico, Hydrologic Data Report #7,* SAND88-7014 (Albuquerque, NM: Sandia National Laboratories).

Stensrud, W.A.; Bame, M.A.; Lantz, K.D.; Palmer, J.B.; and Saulnier, G.J., Jr. in preparation. *WIPP Hydrology Program, Waste Isolation Pilot Plant, Southeastern New Mexico, Hydrologic Data Report #8,* SAND89-7056 (Albuquerque, NM: Sandia National Laboratories).

Stevens, K., and Beyeler, W. 1985. *Determination of Diffusivities in the Rustler Formation from Exploratory-Shaft Construction at the Waste Isolation Pilot Plant in Southeastern New Mexico.* USGS Water-Resources Investigations Rpt 85-4020 (Albuquerque, NM), 32 pp.

Theis, C.V. 1935. "The Relation Between the Lowering of the Piezometric Surface and the Rate and Duration of Discharge of a Well Using Ground-Water Storage," *Trans AGU* 2:519-524.

Warren, J.E., and Root, P.J. 1963. "The Behavior of Naturally Fractured Reservoirs," *Soc Pet Eng J* (Sept 1963):245-255.

Winstanley, D.J., and Carrasco, R.C. 1986. *Annual Hydrogeologic Data Report, 1985/1986.* DOE-WIPP 86-004 (Carlsbad, NM: US DOE).

Wood, S.H. 1985. "Regional Increase in Groundwater Discharge after the 1983 Idaho Earthquake: Coseismic Strain Release, Tectonic and Natural Hydraulic Fracturing," *Proceedings of Workshop XXVIII On the Borah Peak, Idaho, Earthquake, Vol. A,* pp. 573-592 (Menlo Park, CA: USGS).

APPENDIX A

WATER-LEVEL AND FLUID PRESSURE DATA

Table A-1

Pressures at the H-11 Hydropad During the H-11 Multipad Pumping Test

Elapsed Time Since Pump On (hr)	S1 H-11b1 Culebra (psig)	S2 H-11b1 Culebra (psig)	S3 H-11b1 annulus (psig)	S4 H-11b2 Culebra (psig)	S5 H-11b2 annulus (psig)	S6 H-11b3 Culebra (psig)	S7 H-11b3 annulus (psig)	S8 H-11b4 Culebra (psig)	S9 H-11b4 annulus (psig)	S10 barometer (psia)	Comments
-118.666583	125.88	125.97	96.34	127.76	62.23	135.24	127.44	--	98.10	13.02	
-92.299889	125.61	125.57	96.16	127.82	62.15	135.16	127.47	128.83	98.02	12.88	
-71.999778	125.72	125.69	95.48	128.01	62.25	135.35	127.79	129.19	98.14	12.95	
-48.083083	125.74	125.64	95.48	127.86	62.23	135.66	127.93	129.51	98.22	13.07	
-24.999917	125.80	125.74	96.22	127.84	62.31	136.25	128.02	129.45	98.23	13.08	
-22.983111	125.74	125.68	96.18	127.77	62.25	136.22	128.01	129.42	98.20	13.10	
-18.999833	125.76	125.68	96.17	127.77	62.22	136.32	127.94	129.57	98.19	13.06	
-14.999778	125.85	125.79	96.18	127.82	62.22	136.55	127.92	129.78	98.22	13.03	
-12.999972	125.92	125.83	96.22	127.88	62.23	136.67	127.94	129.92	98.26	13.03	
-10.999889	125.92	125.85	96.21	127.88	62.24	136.72	127.97	129.99	98.26	13.04	
-8.999750	125.91	125.84	96.23	127.87	62.26	136.75	128.00	130.07	98.27	13.05	
-6.999917	125.92	125.84	96.23	127.86	62.26	136.79	128.01	130.11	98.27	13.05	
-4.999806	125.93	125.85	96.23	127.87	62.27	136.84	128.01	130.18	98.27	13.04	
-2.999972	125.94	125.87	96.25	127.89	62.28	136.86	128.03	130.27	98.27	13.04	
-0.999833	125.91	125.86	96.22	127.87	62.27	136.84	128.04	130.26	98.25	13.05	
-0.499778	125.90	125.85	96.19	127.84	62.26	136.82	128.04	130.25	98.25	13.06	
-0.001806	125.86	125.81	96.18	127.82	62.24	136.79	128.01	130.26	98.23	13.06	
0.002222	94.64	94.52	96.07	127.65	62.24	136.61	128.02	130.21	98.23	13.06	pump on
0.006417	93.72	93.76	96.09	127.46	62.24	136.42	128.02	130.15	98.23	13.06	
0.010389	93.25	93.27	96.09	127.32	62.24	136.26	128.02	130.09	98.23	13.06	
0.014472	92.90	93.06	96.10	127.22	62.24	136.12	128.02	130.05	98.23	13.06	
0.018444	92.80	92.87	96.11	127.14	62.24	136.00	128.02	130.00	98.23	13.06	
0.022528	92.65	92.76	96.10	127.03	62.24	135.90	128.02	129.96	98.23	13.06	
0.026583	92.56	92.65	96.11	126.97	62.24	135.80	128.02	129.92	98.23	13.06	
0.030556	92.43	92.55	96.11	126.90	62.24	135.72	128.02	129.88	98.23	13.06	
0.034583	92.38	92.52	96.11	126.84	62.24	135.65	128.02	129.85	98.23	13.06	
0.038611	92.42	92.56	96.10	126.79	62.24	135.58	128.01	129.81	98.23	13.06	
0.042556	92.51	92.61	96.12	126.75	62.24	135.51	128.02	129.78	98.23	13.06	
0.046583	92.37	92.51	96.11	126.70	62.24	135.45	128.02	129.76	98.23	13.06	
0.050583	92.40	92.57	96.11	126.66	62.24	135.41	128.01	129.74	98.23	13.06	
0.054583	92.47	92.55	96.11	126.62	62.24	135.35	128.01	129.71	98.23	13.06	
0.058556	92.41	92.50	96.12	126.58	62.24	135.31	128.02	129.68	98.23	13.06	
0.062556	92.49	92.63	96.12	126.55	62.24	135.26	128.02	129.67	98.23	13.06	
0.066528	92.45	92.58	96.12	126.51	62.24	135.23	128.02	129.64	98.23	13.06	
0.070528	92.41	92.47	96.13	126.48	62.24	135.19	128.02	129.62	98.23	13.06	
0.074528	92.36	92.47	96.12	126.46	62.24	135.16	128.02	129.60	98.23	13.06	
0.078472	92.24	92.36	96.13	126.43	62.24	135.13	128.02	129.59	98.23	13.06	
0.082472	92.20	92.32	96.14	126.40	62.24	135.10	128.01	129.56	98.23	13.06	
0.086472	92.20	92.29	96.13	126.37	62.24	135.06	128.01	129.53	98.23	13.06	
0.090444	92.17	92.26	96.14	126.35	62.24	135.04	128.01	129.52	98.23	13.06	
0.094444	92.11	92.19	96.14	126.34	62.24	135.01	128.02	129.51	98.23	13.06	
0.100139	92.06	92.19	96.15	126.29	62.24	134.97	128.01	129.48	98.23	13.06	
0.108500	91.92	92.06	96.15	126.25	62.24	134.92	128.01	129.44	98.23	13.06	
0.116917	91.83	92.03	96.15	126.20	62.24	134.87	128.02	129.41	98.23	13.06	
0.125083	91.80	91.87	96.16	126.16	62.24	134.82	128.01	129.38	98.23	13.06	
0.133444	91.72	91.84	96.15	126.12	62.24	134.79	128.02	129.35	98.23	13.06	
0.141861	91.63	91.77	96.14	126.09	62.24	134.74	128.02	129.33	98.23	13.06	
0.150222	91.53	91.71	96.14	126.05	62.24	134.71	128.02	129.30	98.23	13.06	
0.158361	91.51	91.62	96.15	126.02	62.24	134.68	128.02	129.28	98.23	13.06	
0.166722	91.39	91.53	96.14	125.99	62.24	134.64	128.02	129.25	98.23	13.06	
0.175139	91.36	91.48	96.15	125.96	62.24	134.61	128.02	129.23	98.23	13.06	
0.183556	91.30	91.44	96.15	125.93	62.24	134.59	128.02	129.21	98.23	13.06	
0.191917	91.27	91.39	96.15	125.92	62.24	134.55	128.02	129.17	98.23	13.06	
0.200056	91.24	91.37	96.14	125.87	62.24	134.52	128.02	129.16	98.23	13.06	
0.208472	91.27	91.33	96.16	125.85	62.24	134.50	128.02	129.13	98.22	13.06	
0.216833	91.21	91.37	96.15	125.82	62.24	134.48	128.02	129.11	98.22	13.06	

Table A-1

Pressures at the H-11 Hydropad During the H-11 Multipad Pumping Test (Continued)

Elapsed Time Since Pump On (hr)	S1 H-11b1 Culebra (psig)	S2 H-11b1 Culebra (psig)	S3 H-11b1 annulus (psig)	S4 H-11b2 Culebra (psig)	S5 H-11b2 annulus (psig)	S6 H-11b3 Culebra (psig)	S7 H-11b3 annulus (psig)	S8 H-11b4 Culebra (psig)	S9 H-11b4 annulus (psig)	S10 barometer (psia)	Comments
0.225000	91.14	91.26	96.14	125.80	62.23	134.45	128.02	129.10	98.22	13.06	
0.233361	91.17	91.23	96.13	125.78	62.24	134.42	128.02	129.08	98.23	13.06	
0.241778	91.04	91.19	96.15	125.75	62.24	134.40	128.01	129.05	98.22	13.06	
0.250167	90.97	91.12	96.14	125.73	62.23	134.37	128.02	129.04	98.22	13.06	
0.266861	90.92	91.05	96.14	125.70	62.23	134.33	128.02	128.99	98.22	13.06	
0.283333	91.44	91.54	96.14	125.66	62.23	134.31	128.01	128.97	98.22	13.06	
0.300028	91.33	91.51	96.14	125.62	62.23	134.27	128.01	128.94	98.22	13.06	
0.350222	91.24	91.34	96.13	125.53	62.23	134.17	128.01	128.85	98.22	13.06	
0.400222	91.05	91.22	96.14	125.43	62.23	134.08	128.01	128.77	98.22	13.06	
0.450194	90.91	91.06	96.14	125.36	62.23	134.00	128.01	128.71	98.22	13.06	
0.500111	90.86	91.06	96.14	125.29	62.23	133.93	128.01	128.65	98.22	13.06	
0.600250	90.66	90.77	96.14	125.17	62.23	133.81	128.02	128.53	98.22	13.06	
0.666722	90.53	90.64	96.13	125.09	62.23	133.72	128.01	128.49	98.22	13.06	
0.750083	90.50	90.62	96.15	125.02	62.23	133.64	128.01	128.40	98.22	13.06	
0.833528	90.28	90.40	96.14	124.94	62.23	133.57	128.01	128.34	98.22	13.06	
0.916750	90.21	90.29	96.15	124.87	62.23	133.50	128.00	128.26	98.22	13.06	
1.000222	90.14	90.27	96.15	124.80	62.23	133.43	128.00	128.20	98.22	13.06	
1.166861	89.94	90.09	96.16	124.69	62.23	133.33	128.01	128.09	98.23	13.06	
1.333528	89.80	89.94	96.16	124.59	62.23	133.22	128.01	128.01	98.23	13.06	
1.500056	89.75	89.79	96.17	124.51	62.23	133.13	128.01	127.92	98.23	13.06	
1.666806	89.60	89.62	96.17	124.41	62.23	133.04	128.01	127.85	98.23	13.05	
1.834000	89.48	89.61	96.17	124.33	62.23	132.96	128.01	127.77	98.23	13.05	
2.001361	89.53	89.53	96.17	124.26	62.24	132.89	128.01	127.70	98.24	13.05	
2.166694	89.38	89.49	96.17	124.18	62.22	132.80	128.00	127.64	98.23	13.05	
2.333417	89.29	89.36	96.18	124.11	62.22	132.74	128.00	127.58	98.24	13.05	
2.500111	89.12	89.17	96.18	124.04	62.22	132.67	128.00	127.51	98.24	13.05	
2.666861	89.07	89.14	96.17	123.97	62.22	132.60	127.99	127.45	98.23	13.05	
2.833556	88.99	88.99	96.18	123.91	62.22	132.55	127.99	127.40	98.23	13.05	
3.000028	88.88	88.97	96.17	123.85	62.21	132.47	127.98	127.34	98.22	13.04	
3.166722	88.89	88.95	96.16	123.80	62.22	132.43	127.98	127.29	98.23	13.04	
3.333861	88.72	88.83	96.16	123.74	62.21	132.37	127.97	127.26	98.22	13.04	
3.501111	88.69	88.68	96.17	123.68	62.21	132.31	127.97	127.21	98.22	13.04	
3.666694	88.69	88.66	96.16	123.63	62.21	132.27	127.96	127.19	98.22	13.03	
3.833444	88.66	88.65	96.15	123.58	62.21	132.21	127.96	127.13	98.22	13.03	
4.000167	88.47	88.47	96.16	123.53	62.20	132.16	127.95	127.09	98.21	13.03	
4.333583	88.47	88.47	96.15	123.44	62.20	132.07	127.95	127.01	98.22	13.02	
4.666722	88.36	88.43	96.15	123.35	62.20	131.98	127.94	126.93	98.22	13.02	
5.000528	88.24	88.26	96.15	123.26	62.19	131.91	127.93	126.86	98.22	13.02	
5.333472	88.34	88.28	96.15	123.19	62.19	131.83	127.93	126.79	98.22	13.01	
5.667444	88.09	88.09	96.15	123.11	62.19	131.75	127.92	126.77	98.22	13.01	
6.001222	88.12	88.12	96.14	123.04	62.18	131.70	127.91	126.73	98.21	13.00	
6.501222	88.05	88.00	96.14	122.95	62.18	131.60	127.90	126.70	98.22	12.99	
7.000417	87.97	87.98	96.15	122.86	62.18	131.51	127.89	126.67	98.22	12.99	
7.500194	87.97	87.89	96.15	122.78	62.18	131.43	127.89	126.68	98.23	12.98	
8.001250	87.86	87.75	96.17	122.70	62.19	131.36	127.90	126.71	98.25	12.98	
8.500194	87.71	87.68	96.15	122.63	62.19	131.29	127.90	126.70	98.26	12.97	
9.000250	87.69	87.59	96.16	122.56	62.19	131.21	127.90	126.69	98.26	12.97	
9.500000	87.63	87.57	96.20	122.51	62.20	131.17	127.92	126.68	98.29	12.97	
10.000694	87.64	87.62	96.19	122.43	62.21	131.10	127.93	126.58	98.28	12.97	
11.000139	87.55	87.50	96.19	122.31	62.23	130.97	127.96	126.46	98.30	12.99	
12.000222	87.25	87.17	96.19	122.18	62.23	130.85	127.97	126.35	98.29	12.98	
13.001306	87.15	87.09	96.18	122.07	62.23	130.75	127.98	126.21	98.29	12.99	
15.000056	86.72	86.62	96.19	121.81	62.24	130.51	128.03	125.98	98.30	13.00	
17.000028	86.31	86.27	96.19	121.59	62.25	130.30	128.05	125.76	98.30	13.00	
20.000167	85.84	85.78	96.19	121.30	62.26	130.03	128.05	125.46	98.31	12.99	
25.001306	85.25	85.22	96.13	120.83	62.24	129.57	128.03	124.96	98.27	12.98	
31.001222	84.95	84.89	96.11	120.37	62.20	129.14	127.91	124.51	98.26	12.92	
35.000222	84.75	84.68	96.15	120.18	62.22	128.96	127.95	124.38	98.32	12.91	

106

Pressures at the H-11 Hydropad During the H-11 Multipad Pumping Test (Continued)

Elapsed Time Since Pump On (hr)	S1 H-11b1 Culebra (psig)	S2 H-11b1 Culebra (psig)	S3 H-11b1 annulus (psig)	S4 H-11b2 Culebra (psig)	S5 H-11b2 annulus (psig)	S6 H-11b3 Culebra (psig)	S7 H-11b3 annulus (psig)	S8 H-11b4 Culebra (psig)	S9 H-11b4 annulus (psig)	S10 barometer (psia)	Comments
41.000167	84.28	84.23	96.19	119.81	62.26	128.61	128.05	124.03	98.33	12.94	
45.000250	83.86	83.79	96.19	119.57	62.27	128.40	128.09	123.79	98.34	12.95	
51.000972	83.50	83.44	96.12	119.19	62.21	128.04	128.03	123.37	98.28	12.94	
55.000222	83.28	83.17	96.12	118.98	62.20	127.85	127.97	123.19	98.28	12.90	
61.000056	82.99	82.90	96.16	118.75	62.25	127.65	128.05	123.11	98.34	12.91	
65.000222	82.65	82.56	96.18	118.57	62.27	127.48	128.11	123.03	98.34	12.93	
71.000139	82.21	82.16	96.15	118.20	62.26	127.12	128.18	122.78	98.32	12.99	
75.000028	82.05	81.97	96.14	118.05	62.23	127.00	128.13	122.73	98.30	12.98	
81.000167	81.85	81.74	96.14	117.81	62.22	126.78	128.08	122.67	98.32	12.94	
85.000167	81.54	81.45	96.20	117.67	62.28	126.67	128.18	122.69	98.38	12.98	
91.000194	81.40	81.24	96.22	117.46	62.32	126.49	128.26	122.56	98.37	13.00	
95.000639	81.12	81.00	96.13	117.20	62.26	126.25	128.27	122.35	98.32	13.04	
101.001417	80.92	80.78	96.11	117.01	62.20	126.08	128.16	122.37	98.29	13.02	
111.000111	80.50	80.37	96.17	116.71	62.26	125.85	128.22	122.42	98.35	13.02	
120.000000	80.22	80.10	96.12	116.38	62.27	125.54	128.25	122.31	98.30	13.06	
131.000056	80.20	80.00	96.17	116.12	62.25	125.37	128.11	122.56	98.34	12.99	
141.000194	79.67	79.47	96.19	115.82	62.29	125.11	128.25	122.59	98.34	13.08	
151.000111	79.35	79.15	96.18	115.52	62.46	124.87	128.25	122.62	98.30	13.11	
161.000167	78.98	78.78	96.23	115.28	62.51	124.69	128.34	122.77	98.34	13.12	
171.000167	78.90	78.69	96.16	114.98	62.48	124.46	128.27	122.69	98.28	13.12	
172.750000	116.24	115.90	96.17	117.69	62.47	127.67	128.23	124.66	98.28	13.09	171.817: pump
172.766861	116.26	115.91	96.17	117.71	62.47	127.67	128.23	124.66	98.29	13.09	off
172.816778	116.29	115.97	96.17	117.76	62.48	127.72	128.22	124.69	98.28	13.09	
172.833361	116.30	115.97	96.17	117.77	62.47	127.73	128.23	124.70	98.29	13.09	
172.850250	116.32	115.99	96.17	117.79	62.48	127.73	128.22	124.72	98.28	13.09	
172.866778	116.33	116.00	96.17	117.80	62.48	127.76	128.22	124.73	98.28	13.09	
172.883500	116.34	116.00	96.17	117.82	62.48	127.76	128.22	124.74	98.28	13.09	
172.900222	116.36	116.03	96.17	117.83	62.48	127.78	128.22	124.75	98.28	13.09	
172.916778	116.37	116.05	96.17	117.85	62.48	127.80	128.22	124.75	98.28	13.09	
172.933472	116.38	116.05	96.17	117.86	62.48	127.81	128.22	124.77	98.28	13.09	
172.950250	116.39	116.06	96.17	117.88	62.47	127.81	128.22	124.76	98.28	13.09	
172.965556	116.40	116.08	96.18	117.89	62.48	127.84	128.22	124.79	98.28	13.09	
172.981722	116.41	116.09	96.17	117.90	62.48	127.83	128.22	124.81	98.28	13.09	
172.998000	116.42	116.11	96.17	117.91	62.47	127.85	128.21	124.81	98.28	13.09	
173.014333	116.43	116.10	96.17	117.92	62.47	127.85	128.20	124.82	98.28	13.09	
173.018361	82.68	82.52	96.09	117.82	62.47	127.69	128.21	124.80	98.28	13.09	pump on
173.034500	81.48	81.29	96.11	117.35	62.48	127.15	128.22	124.62	98.28	13.09	
173.050778	81.25	81.09	96.12	117.10	62.48	126.83	128.21	124.49	98.28	13.09	
173.066917	81.28	81.13	96.12	116.93	62.47	126.61	128.21	124.40	98.28	13.09	
173.082778	81.50	81.33	96.13	116.80	62.47	126.46	128.20	124.32	98.28	13.09	
173.102611	81.43	81.24	96.15	116.69	62.47	126.31	128.21	124.24	98.28	13.09	
173.200111	79.83	79.63	96.16	116.32	62.48	125.89	128.21	123.99	98.28	13.09	
173.300000	79.64	79.49	96.16	116.11	62.47	125.67	128.21	123.84	98.29	13.09	
173.400194	79.53	79.39	96.15	115.98	62.47	125.52	128.21	123.72	98.28	13.09	
173.500028	79.51	79.34	96.15	115.87	62.47	125.42	128.21	123.64	98.28	13.09	
173.583417	79.27	79.16	96.16	115.81	62.47	125.36	128.20	123.58	98.28	13.09	
173.666861	79.33	79.13	96.15	115.76	62.47	125.30	128.20	123.52	98.28	13.08	
173.750000	79.29	79.10	96.15	115.71	62.47	125.26	128.20	123.51	98.28	13.08	
173.833528	79.18	79.02	96.15	115.67	62.47	125.22	128.20	123.47	98.28	13.08	
173.916806	79.13	78.96	96.16	115.64	62.48	125.18	128.20	123.43	98.28	13.08	
174.000222	79.10	78.92	96.17	115.61	62.48	125.16	128.20	123.43	98.28	13.08	
175.000028	78.73	78.58	96.17	115.40	62.48	124.96	128.19	123.24	98.27	13.07	
176.000167	78.62	78.43	96.17	115.31	62.48	124.87	128.19	123.22	98.28	13.06	
177.000278	78.39	78.20	96.19	115.24	62.49	124.80	128.19	123.21	98.30	13.06	
178.000111	78.26	78.03	96.18	115.18	62.50	124.74	128.20	123.21	98.32	13.06	
179.000056	78.14	77.90	96.21	115.13	62.51	124.70	128.22	123.21	98.33	13.06	
181.000111	77.88	77.69	96.21	115.04	62.53	124.60	128.26	123.15	98.34	13.07	
183.000194	77.61	77.46	96.20	114.95	62.53	124.52	128.28	123.07	98.33	13.07	

Table A-1

Pressures at the H-11 Hydropad During the H-11 Multipad Pumping Test (Continued)

Elapsed Time Since Pump On (hr)	S1 H-11b1 Culebra (psig)	S2 H-11b1 Culebra (psig)	S3 H-11b1 annulus (psig)	S4 H-11b2 Culebra (psig)	S5 H-11b2 annulus (psig)	S6 H-11b3 Culebra (psig)	S7 H-11b3 annulus (psig)	S8 H-11b4 Culebra (psig)	S9 H-11b4 annulus (psig)	S10 barometer (psia)	Comments
185.000028	77.59	77.42	96.20	114.92	62.53	124.48	128.28	122.99	98.33	13.06	
187.000083	77.44	77.25	96.22	114.88	62.54	124.46	128.28	122.97	98.34	13.06	
189.000222	77.38	77.14	96.23	114.84	62.55	124.42	128.31	122.92	98.34	13.05	
191.000556	77.37	77.17	96.17	114.71	62.53	124.29	128.29	122.76	98.30	13.07	
193.000556	77.30	77.10	96.16	114.64	62.60	124.25	128.28	122.68	98.30	13.07	
195.000083	77.18	77.01	96.15	114.60	62.82	124.21	128.22	122.63	98.28	13.05	
197.000000	77.22	77.00	96.14	114.59	62.81	124.21	128.19	122.66	98.28	13.04	
199.000028	77.30	77.08	96.15	114.59	62.81	124.23	128.15	122.63	98.28	13.01	
201.000139	77.22	77.04	96.17	114.58	62.81	124.24	128.15	122.67	98.30	13.00	
211.000000	76.65	76.36	96.22	114.39	72.02	124.08	128.24	122.55	98.34	13.00	
217.001556	76.43	76.25	96.15	114.19	71.82	123.89	128.23	122.26	98.29	13.02	
217.500250	76.47	76.25	96.16	114.19	69.80	123.89	128.23	122.29	98.30	13.02	
218.000194	78.16	77.91	96.15	114.13	68.51	123.88	128.21	122.27	98.29	13.01	218.001-219.564
218.500167	76.06	75.43	96.13	224.80	70.69	124.23	128.19	122.47	98.28	13.01	tracer injection
219.000250	75.87	75.65	96.14	249.51	68.10	124.26	128.18	122.49	98.27	13.00	in H-11b2
219.500250	74.27	73.99	96.12	215.24	71.37	124.35	128.18	122.58	98.26	13.00	
220.000222	76.23	76.00	96.12	114.34	72.42	124.02	128.16	122.45	98.27	13.00	
220.500000	76.15	75.80	96.13	114.23	76.77	123.98	128.14	122.40	98.26	12.99	220.501-222.084
221.000056	77.12	76.47	96.12	114.71	77.51	125.51	128.08	122.67	98.27	12.98	tracer injection
221.500056	75.75	75.56	96.13	114.81	68.83	124.95	128.04	122.76	98.27	12.98	in H-11b3
222.000194	77.28	77.58	96.12	114.87	68.20	124.91	128.02	122.83	98.27	12.97	
222.533389	77.94	77.70	96.14	114.42	69.23	123.97	128.04	122.57	98.26	12.96	
223.000194	77.06	76.82	96.14	114.35	69.75	123.91	128.06	122.61	98.24	12.96	223.001-224.005
223.500250	76.82	76.57	96.13	114.67	70.95	124.21	128.07	124.86	98.26	12.96	tracer injection
224.000250	75.18	74.78	96.14	114.77	70.69	124.31	128.08	125.96	98.26	12.95	in H-11b4
224.483500	77.91	77.70	96.14	114.47	69.53	124.05	128.08	121.59	98.28	12.95	
227.000028	77.53	77.28	96.17	114.26	76.12	123.88	128.12	121.61	98.35	12.94	
229.000111	77.35	76.91	96.19	114.16	75.21	123.77	128.16	121.62	98.34	12.96	
231.000194	75.85	75.66	96.19	114.07	75.14	123.68	128.16	121.69	98.34	12.96	
241.000083	73.21	72.89	96.14	113.77	74.93	123.43	128.17	121.86	98.31	12.99	
251.000056	76.77	76.48	96.19	113.70	74.62	123.42	128.05	122.09	98.36	12.94	
261.000194	74.77	75.08	96.21	113.47	74.89	123.25	128.03	121.98	98.37	13.00	
271.000083	76.32	76.07	96.15	113.22	66.95	123.09	127.76	121.72	98.31	12.99	
281.000028	75.71	75.47	96.24	113.12	74.99	123.03	127.68	121.73	98.36	12.98	
291.000139	72.45	73.42	96.17	112.92	66.26	122.88	127.50	121.53	98.31	12.98	
301.000167	74.07	73.86	96.21	112.89	75.41	122.91	127.35	121.51	98.35	12.93	
311.000361	74.76	74.56	96.22	112.73	75.31	122.79	127.29	121.28	98.35	12.93	
321.000139	70.73	72.58	96.19	112.59	127.34	122.72	127.09	121.24	98.31	12.86	
331.000028	74.35	74.11	96.25	112.45	127.42	122.63	127.21	121.06	98.37	12.91	
341.000167	74.69	74.43	96.24	112.32	127.38	122.56	127.12	120.99	98.34	12.90	
351.000083	74.39	74.14	96.25	112.26	127.38	122.56	127.16	120.94	98.38	12.92	
365.000000	74.29	74.01	96.24	112.06	127.37	122.46	127.10	120.75	98.37	12.93	
371.000167	74.10	73.85	96.26	112.03	127.40	122.44	127.13	120.75	98.42	12.96	
381.000250	73.12	72.85	96.27	111.89	127.41	122.35	127.25	120.61	98.44	13.02	
391.000083	74.20	74.01	96.23	111.76	127.38	122.26	127.24	120.48	98.35	13.02	
401.000167	73.68	73.43	96.27	111.73	127.42	122.24	129.09	120.43	98.44	13.07	
411.000056	73.72	73.44	96.22	111.64	127.39	122.17	129.10	120.31	98.37	13.05	
414.789056	73.84	73.57	96.23	111.64	127.39	122.18	129.14	120.31	98.33	13.01	
433.000222	74.95	74.70	96.25	111.61	127.40	122.16	129.25	120.18	98.40	13.05	
441.000250	72.55	72.24	96.26	111.50	127.40	122.06	129.02	120.19	98.37	12.99	
451.000083	73.99	73.78	96.30	111.58	127.45	122.17	128.89	120.19	98.44	13.03	
461.000056	74.24	73.95	96.21	111.53	127.40	122.12	128.63	120.07	98.35	13.03	
471.000056	73.78	73.56	96.28	111.49	127.44	122.12	129.29	120.07	98.39	13.04	
481.000361	73.66	73.42	96.23	111.43	127.44	122.02	129.28	119.93	98.38	13.06	
491.000167	73.10	72.95	96.30	111.45	127.46	122.05	129.40	120.02	98.43	13.05	
501.000056	72.96	72.74	96.31	111.43	127.47	122.04	129.37	119.92	98.44	13.06	
521.000083	73.02	72.79	96.30	111.43	127.46	122.07	129.43	119.86	98.39	13.01	
541.000250	73.62	73.29	96.30	111.49	127.45	122.10	129.12	119.86	98.40	12.94	

Table A-1

Pressures at the H-11 Hydropad During the H-11 Multipad Pumping Test (Continued)

Elapsed Time Since Pump On (hr)	S1 H-11b1 Culebra (psig)	S2 H-11b1 Culebra (psig)	S3 H-11b1 annulus (psig)	S4 H-11b2 Culebra (psig)	S5 H-11b2 annulus (psig)	S6 H-11b3 Culebra (psig)	S7 H-11b3 annulus (psig)	S8 H-11b4 Culebra (psig)	S9 H-11b4 annulus (psig)	S10 barometer (psia)	Comments
561.000000	73.08	72.81	96.28	111.47	127.45	122.10	129.13	119.77	98.37	12.91	
581.000028	72.87	72.60	96.27	111.48	127.51	122.05	129.34	119.59	98.32	12.86	
601.000222	72.47	72.22	96.28	111.56	127.55	122.05	129.41	119.49	98.42	12.87	
621.000222	72.21	71.89	96.34	111.55	127.60	122.08	129.27	119.50	98.48	12.93	
641.000083	71.98	71.76	96.35	111.41	127.59	122.03	128.92	119.35	98.44	12.97	
661.000056	71.81	71.49	96.35	111.35	127.60	122.00	129.48	119.28	98.43	12.99	
681.000194	72.89	72.68	96.33	111.32	127.58	122.00	129.41	119.17	98.39	12.98	
701.000194	72.50	72.24	96.33	111.32	127.58	121.88	129.36	118.97	98.44	13.06	
721.000000	72.09	71.84	96.33	111.46	127.60	121.89	128.97	118.87	98.45	13.07	
741.000028	71.50	71.22	96.40	111.48	127.63	121.90	129.47	118.82	98.42	13.02	
761.000111	71.81	71.55	96.39	111.60	127.62	121.80	129.54	118.77	98.49	13.01	
781.000139	72.06	71.78	96.41	111.63	127.63	121.65	129.53	118.77	98.50	13.02	
801.000194	70.90	70.60	96.35	111.70	127.59	121.57	129.40	118.74	98.47	12.95	
821.000083	73.08	72.73	96.32	111.80	127.59	121.50	128.97	118.66	98.44	12.96	
841.000083	72.30	72.05	96.35	111.79	127.63	121.34	129.50	118.54	98.46	13.00	
861.000222	71.49	71.23	96.44	111.78	127.65	121.22	129.62	118.48	98.51	13.11	
881.000250	71.83	71.57	96.41	111.82	127.63	121.26	129.60	118.48	98.50	13.06	
901.000194	71.71	71.45	96.41	111.95	127.65	121.23	129.62	118.52	98.52	13.03	
921.000139	70.98	70.68	96.42	112.07	127.62	121.17	129.58	118.44	98.50	12.96	
941.000139	70.70	70.38	96.38	112.07	127.62	120.96	129.56	118.20	98.45	12.99	
961.000167	70.80	70.52	96.42	112.28	127.65	120.88	129.59	118.04	98.49	13.08	
981.000111	70.05	69.79	96.50	112.44	127.67	120.84	129.63	118.08	98.53	13.13	
1001.000194	69.84	69.54	96.45	112.81	127.65	120.77	129.69	118.03	98.52	13.10	
1021.000167	70.10	69.84	96.45	113.09	127.65	120.78	129.50	118.07	98.53	13.04	
1041.000167	70.40	70.13	96.38	112.73	127.61	120.71	129.49	117.96	98.49	12.97	
1061.000194	70.55	70.28	96.36	112.79	127.54	120.61	129.56	117.84	98.46	13.02	
1081.000139	70.19	69.98	96.39	112.79	127.57	120.56	129.51	117.74	98.48	13.06	
1101.000028	69.86	69.58	96.45	112.77	127.58	120.54	129.64	117.70	98.52	13.06	
1121.000083	69.71	69.44	96.44	112.77	127.57	120.51	129.59	117.74	98.51	13.05	
1141.000111	69.80	69.54	96.43	112.87	127.57	120.50	129.59	117.77	98.52	13.02	
1161.000222	69.76	69.48	96.42	112.95	127.53	120.45	129.53	117.71	98.49	12.98	
1181.000028	69.67	69.43	96.37	113.32	127.53	120.38	129.50	117.57	98.46	13.01	
1201.000083	69.80	69.49	96.38	113.32	127.56	120.33	129.59	117.51	98.47	13.03	
1221.000167	69.29	69.01	96.45	113.31	127.58	120.31	129.69	117.51	98.52	13.04	
1241.000194	69.37	69.11	96.47	113.29	127.56	120.31	129.60	117.54	98.51	13.03	
1261.000083	69.31	69.01	96.46	113.27	127.58	120.31	129.65	117.59	98.52	13.01	
1281.000111	69.27	68.99	96.48	113.23	127.57	120.32	129.58	117.61	98.53	12.99	
1301.000139	69.30	68.98	96.40	113.09	127.53	120.18	129.58	117.38	98.46	12.99	
1321.000250	69.50	69.24	96.45	113.06	127.57	120.20	129.50	117.40	98.49	12.98	
1341.000139	69.23	68.97	96.48	113.05	127.59	120.25	129.62	117.43	98.51	12.94	
1361.000000	68.56	68.32	96.50	112.94	127.62	120.14	129.50	117.35	98.54	12.97	
1381.000028	69.63	69.40	96.47	112.89	127.61	120.13	129.22	117.38	98.54	13.00	
1401.000222	70.13	69.86	96.44	112.84	127.54	120.09	128.86	117.34	98.50	12.96	
1421.000167	69.67	69.44	96.43	112.79	127.54	120.04	129.49	117.27	98.49	12.98	pump off
1441.000250	69.92	69.71	96.43	113.01	127.60	120.20	129.55	117.42	98.49	13.00	1423.850-
1461.000278	69.51	69.30	96.48	112.88	127.62	120.06	129.59	117.29	98.53	13.03	1425.667
1481.000028	70.03	69.79	96.47	112.81	127.61	120.05	129.30	117.28	98.52	13.03	
1501.000028	69.55	69.34	96.49	112.76	127.63	120.02	129.08	117.31	98.54	13.03	
1511.998972	69.31	69.13	96.46	112.75	127.62	119.92	128.96	117.12	98.50	13.04	
1512.003083	106.09	105.83	96.47	112.77	127.62	120.06	128.96	117.12	98.50	13.04	pump off
1512.007222	106.54	106.23	96.46	112.80	127.62	120.23	128.96	117.16	98.50	13.04	
1512.011222	106.79	106.47	96.47	112.84	127.63	120.37	128.96	117.22	98.50	13.04	
1512.015250	106.95	106.63	96.46	112.88	127.62	120.50	128.96	117.25	98.50	13.04	
1512.019250	107.09	106.75	96.47	112.94	127.62	120.61	128.96	117.28	98.50	13.04	
1512.023389	107.18	106.85	96.46	112.99	127.62	120.72	128.96	117.32	98.50	13.04	
1512.027417	107.28	106.94	96.47	113.04	127.62	120.81	128.95	117.34	98.50	13.04	
1512.031528	107.35	107.03	96.47	113.09	127.62	120.89	128.96	117.38	98.50	13.04	
1512.035528	107.43	107.07	96.47	113.14	127.61	120.95	128.96	117.41	98.50	13.04	

Pressures at the H-11 Hydropad During the H-11 Multipad Pumping Test (Continued)

Elapsed Time Since Pump On (hr)	S1 H-11b1 Culebra (psig)	S2 H-11b1 Culebra (psig)	S3 H-11b1 annulus (psig)	S4 H-11b2 Culebra (psig)	S5 H-11b2 annulus (psig)	S6 H-11b3 Culebra (psig)	S7 H-11b3 annulus (psig)	S8 H-11b4 Culebra (psig)	S9 H-11b4 annulus (psig)	S10 barometer (psia)	Comments
1512.039583	107.48	107.15	96.47	113.19	127.62	121.02	128.96	117.43	98.50	13.04	
1512.043583	107.55	107.20	96.47	113.24	127.62	121.07	128.95	117.45	98.50	13.04	
1512.047556	107.59	107.25	96.47	113.28	127.62	121.13	128.96	117.48	98.50	13.04	
1512.051639	107.64	107.30	96.46	113.34	127.61	121.17	128.97	117.50	98.50	13.04	
1512.058417	107.72	107.37	96.47	113.40	127.62	121.26	128.96	117.50	98.50	13.04	
1512.066833	107.79	107.44	96.47	113.50	127.62	121.33	128.96	117.55	98.50	13.04	
1512.075278	107.86	107.51	96.47	113.57	127.62	121.41	128.96	117.57	98.50	13.04	
1512.083417	107.93	107.57	96.47	113.64	127.62	121.46	128.96	117.62	98.50	13.04	
1512.091833	107.99	107.63	96.47	113.71	127.61	121.53	128.96	117.64	98.50	13.04	
1512.100250	108.03	107.70	96.47	113.77	127.62	121.58	128.95	117.66	98.50	13.04	
1512.108389	108.07	107.74	96.47	113.83	127.61	121.63	128.96	117.69	98.50	13.04	
1512.116806	108.12	107.78	96.47	113.88	127.62	121.68	128.96	117.71	98.50	13.04	
1512.125222	108.18	107.82	96.47	113.94	127.62	121.72	128.96	117.73	98.50	13.04	
1512.133333	108.19	107.85	96.47	113.98	127.62	121.76	128.96	117.75	98.50	13.04	
1512.141778	108.24	107.89	96.46	114.03	127.61	121.79	128.96	117.77	98.50	13.04	
1512.150194	108.27	107.93	96.47	114.07	127.62	121.83	128.96	117.80	98.50	13.04	
1512.158583	108.32	107.96	96.47	114.11	127.62	121.86	128.96	117.81	98.50	13.04	
1512.166750	108.33	107.99	96.47	114.13	127.62	121.89	128.96	117.82	98.50	13.04	
1512.175194	108.35	108.01	96.47	114.17	127.62	121.92	128.95	117.84	98.50	13.04	
1512.183333	108.40	108.04	96.46	114.20	127.62	121.94	128.95	117.85	98.50	13.04	
1512.191750	108.41	108.08	96.47	114.23	127.61	121.97	128.95	117.88	98.50	13.04	
1512.200167	108.45	108.09	96.47	114.26	127.61	121.99	128.95	117.88	98.50	13.04	
1512.208583	108.47	108.12	96.47	114.28	127.61	122.03	128.95	117.89	98.50	13.04	
1512.216722	108.49	108.12	96.46	114.31	127.62	122.05	128.95	117.91	98.50	13.04	
1512.225139	108.53	108.16	96.47	114.33	127.61	122.07	128.95	117.91	98.50	13.04	
1512.233417	108.54	108.19	96.47	114.36	127.62	122.08	128.95	117.92	98.50	13.04	
1512.250167	108.58	108.23	96.47	114.41	127.62	122.13	128.95	117.97	98.50	13.04	
1512.300139	108.69	108.35	96.46	114.51	127.61	122.25	128.95	118.03	98.50	13.04	
1512.350111	108.78	108.44	96.46	114.59	127.61	122.34	128.95	118.09	98.50	13.04	
1512.400111	108.89	108.52	96.47	114.67	127.61	122.42	128.95	118.16	98.50	13.04	
1512.450167	108.96	108.61	96.47	114.73	127.60	122.49	128.94	118.22	98.50	13.04	
1512.500194	109.02	108.69	96.47	114.80	127.61	122.57	128.95	118.27	98.50	13.04	
1512.583333	109.13	108.79	96.46	114.88	127.62	122.66	128.94	118.36	98.50	13.04	
1512.666778	109.22	108.88	96.46	114.96	127.61	122.75	128.94	118.43	98.50	13.04	
1512.750194	109.29	108.97	96.47	115.02	127.61	122.82	128.94	118.50	98.50	13.04	
1512.833583	109.38	109.04	96.47	115.09	127.61	122.90	128.93	118.57	98.50	13.04	
1512.916750	109.45	109.10	96.47	115.16	127.61	122.96	128.93	118.61	98.50	13.04	
1513.000167	109.51	109.18	96.47	115.21	127.60	123.02	128.93	118.66	98.50	13.04	
1513.083556	109.57	109.24	96.47	115.27	127.60	123.08	128.93	118.71	98.50	13.04	
1513.166694	109.63	109.28	96.47	115.32	127.60	123.14	128.92	118.78	98.49	13.04	
1513.250111	109.70	109.35	96.47	115.37	127.61	123.19	128.93	118.83	98.50	13.04	
1513.500222	109.81	109.49	96.47	115.51	127.60	123.32	128.92	118.99	98.49	13.04	
1513.666667	109.92	109.59	96.47	115.60	127.60	123.40	128.91	119.06	98.50	13.04	
1513.833361	109.99	109.68	96.47	115.67	127.60	123.48	128.91	119.15	98.49	13.04	
1514.000111	110.07	109.75	96.47	115.75	127.60	123.56	128.90	119.23	98.49	13.04	
1514.166833	110.15	109.83	96.47	115.80	127.59	123.62	128.90	119.31	98.49	13.04	
1514.333583	110.20	109.89	96.47	115.86	127.59	123.69	128.89	119.39	98.49	13.03	
1514.500056	110.27	109.96	96.46	115.93	127.59	123.76	128.88	119.46	98.48	13.03	
1514.666750	110.31	110.03	96.46	116.00	127.59	123.82	128.88	119.51	98.49	13.03	
1514.833500	110.40	110.08	96.46	116.05	127.58	123.87	128.87	119.58	98.48	13.03	
1515.000222	110.43	110.14	96.45	116.11	127.58	123.93	128.86	119.65	98.48	13.03	
1515.500194	110.59	110.31	96.45	116.55	127.57	124.08	128.85	119.83	98.48	13.03	
1516.000167	110.75	110.45	96.46	116.87	127.57	124.23	128.83	120.00	98.48	13.02	
1516.500111	110.87	110.59	96.46	117.05	127.56	124.36	128.86	120.17	98.48	13.01	
1517.000083	111.00	110.72	96.44	117.22	127.56	124.48	128.90	120.27	98.47	13.01	
1517.500639	111.10	110.85	96.44	117.37	127.55	124.60	128.94	120.40	98.47	13.00	
1518.000250	111.22	110.95	96.45	117.50	127.54	124.72	128.99	120.52	98.48	12.99	
1518.500083	111.33	111.05	96.45	117.64	127.55	124.81	129.04	120.63	98.48	13.00	

Pressures at the H-11 Hydropad During the H-11 Multipad Pumping Test (Continued)

Elapsed Time Since Pump On (hr)	S1 H-11b1 Culebra (psig)	S2 H-11b1 Culebra (psig)	S3 H-11b1 annulus (psig)	S4 H-11b2 Culebra (psig)	S5 H-11b2 annulus (psig)	S6 H-11b3 Culebra (psig)	S7 H-11b3 annulus (psig)	S8 H-11b4 Culebra (psig)	S9 H-11b4 annulus (psig)	S10 barometer (psia)	Comments
1519.000111	111.43	111.16	96.46	117.77	127.55	124.92	129.07	120.74	98.48	12.99	
1519.500167	111.52	111.24	96.46	117.89	127.55	125.01	129.10	120.84	98.48	12.99	
1520.000222	111.60	111.34	96.46	117.99	127.55	125.09	129.14	120.98	98.50	12.98	
1520.500056	111.68	111.43	96.46	118.10	127.56	125.18	129.17	121.05	98.50	12.98	
1521.000139	111.77	111.52	96.48	118.21	127.57	125.27	129.22	121.18	98.52	12.98	
1521.500111	111.85	111.59	96.48	118.31	127.58	125.35	129.25	121.26	98.54	12.98	
1522.000056	111.93	111.67	96.48	118.40	127.59	125.41	129.28	121.35	98.53	12.99	
1523.000222	112.05	111.81	96.49	118.58	127.60	125.54	129.36	121.48	98.54	13.00	
1524.000139	112.19	111.94	96.53	118.74	127.65	125.67	129.43	121.64	98.57	13.04	
1525.000028	112.28	112.04	96.55	118.91	127.68	125.78	129.50	121.76	98.58	13.07	
1526.000194	112.38	112.17	96.54	119.05	127.65	125.90	129.52	121.86	98.54	13.05	
1527.000083	112.49	112.28	96.56	119.19	127.65	126.02	129.53	122.01	98.55	13.06	
1528.000167	112.60	112.39	96.55	119.32	127.63	126.13	129.51	122.15	98.53	13.05	
1529.000222	112.70	112.48	96.55	119.45	127.67	126.23	129.57	122.29	98.54	13.06	
1530.000111	112.79	112.57	96.54	119.57	127.64	126.33	129.55	122.40	98.53	13.05	
1531.000194	112.90	112.67	96.55	119.71	127.62	126.44	129.54	122.52	98.53	13.05	
1532.000000	112.98	112.76	96.56	119.83	127.64	126.50	129.56	122.63	98.54	13.05	
1534.000139	113.12	112.91	96.54	120.04	127.63	126.67	129.60	122.75	98.52	13.06	
1536.000389	113.26	113.07	96.52	120.23	127.62	126.81	129.55	122.89	98.51	13.06	
1538.000278	113.43	113.24	96.52	120.42	127.60	126.97	129.53	123.07	98.50	13.06	
1540.000167	113.61	113.38	96.51	120.46	127.59	127.15	129.51	123.28	98.49	13.05	
1542.000056	113.81	113.58	96.55	120.09	127.59	127.34	129.54	123.50	98.54	13.05	
1545.000111	114.02	113.82	96.54	120.26	127.61	127.57	129.57	123.72	98.54	13.03	
1547.000167	114.15	113.94	96.55	120.39	127.63	127.70	129.61	123.86	98.55	13.04	
1551.000028	114.39	114.19	96.55	120.65	127.64	127.96	129.60	124.06	98.54	13.06	
1555.000139	114.65	114.43	96.55	120.90	127.62	128.22	129.58	124.26	98.54	13.03	
1559.000056	114.83	114.62	96.55	121.08	127.64	128.42	129.62	124.44	98.54	13.04	
1563.000222	115.03	114.81	96.53	121.28	127.61	128.61	129.57	124.69	98.52	13.04	
1567.000056	115.32	115.09	96.54	121.55	127.60	128.91	129.56	125.01	98.52	13.01	
1573.000250	115.61	115.40	96.56	121.84	127.63	129.21	129.59	125.31	98.54	13.01	
1577.000139	115.80	115.58	96.55	122.04	127.66	129.40	129.63	125.46	98.54	13.02	
1583.000056	116.01	115.82	96.55	122.26	127.65	129.63	129.64	125.64	98.53	13.02	
1587.000000	116.16	115.96	96.53	122.38	127.62	129.77	129.55	125.84	98.51	13.01	
1593.000250	116.49	116.29	96.56	122.70	127.62	130.11	129.59	126.22	98.53	12.98	
1597.000194	116.61	116.43	96.57	122.85	127.67	130.26	129.67	126.35	98.55	13.02	
1603.000194	116.84	116.66	96.57	123.06	127.66	130.51	129.58	126.49	98.54	13.00	
1607.000028	116.91	116.77	96.54	123.14	127.67	130.61	129.68	126.57	98.53	13.01	
1613.000000	117.13	116.92	96.52	123.33	127.61	130.79	129.54	126.82	98.50	13.00	
1623.000194	117.49	117.32	96.56	123.72	127.68	131.20	129.64	127.21	98.55	13.00	
1633.000056	117.72	117.57	96.51	123.97	127.69	131.43	129.59	127.35	98.51	13.01	
1643.000194	118.12	117.96	96.55	124.34	127.69	131.82	129.59	127.90	98.55	12.97	
1653.000056	118.38	118.20	96.56	124.62	127.70	132.12	129.52	128.02	98.54	12.99	
1663.000111	118.55	118.37	96.51	124.77	127.65	132.29	129.27	128.21	98.51	12.99	
1673.000000	118.81	118.66	96.55	125.03	127.71	132.59	129.28	128.47	98.53	13.00	
1683.000194	118.94	118.81	96.50	125.17	127.68	132.74	129.11	128.59	98.49	13.02	
1693.000056	119.27	119.11	96.58	125.49	127.77	133.07	129.35	128.99	98.56	13.04	
1703.000000	119.40	119.27	96.52	125.67	127.72	133.26	129.48	129.00	98.51	13.03	
1713.000139	119.62	119.47	96.54	125.88	127.69	133.45	129.42	129.28	98.53	13.01	
1723.000083	119.79	119.64	96.58	126.06	127.73	133.64	129.51	129.33	98.53	13.03	
1733.000167	119.87	119.74	96.52	126.15	127.66	133.72	129.39	129.55	98.48	13.03	
1743.000222	120.10	119.97	96.59	126.40	127.74	133.96	129.48	129.81	98.54	13.06	
1753.000111	120.22	120.11	96.54	126.53	127.70	134.09	129.41	129.89	98.49	13.05	
1763.000139	120.44	120.28	96.58	126.76	127.74	134.32	129.33	130.15	98.53	13.02	
1773.000000	120.56	120.40	96.60	126.91	127.73	134.49	129.31	130.22	98.54	13.03	
1783.000000	120.66	120.51	96.53	126.99	127.65	134.58	129.10	130.28	98.48	12.99	
1793.000056	120.84	120.69	96.59	127.20	127.74	134.79	129.17	130.53	98.53	13.01	
1803.000222	120.91	120.78	96.53	127.30	127.70	134.86	129.07	130.56	98.48	13.03	
1813.000139	121.07	120.94	96.60	127.51	127.78	135.05	129.15	130.69	98.54	13.07	

Pressures at the H-11 Hydropad During the H-11 Multipad Pumping Test (Continued)

Elapsed Time Since Pump On (hr)	S1 H-11b1 Culebra (psig)	S2 H-11b1 Culebra (psig)	S3 H-11b1 annulus (psig)	S4 H-11b2 Culebra (psig)	S5 H-11b2 annulus (psig)	S6 H-11b3 Culebra (psig)	S7 H-11b3 annulus (psig)	S8 H-11b4 Culebra (psig)	S9 H-11b4 annulus (psig)	S10 barometer (psia)	Comments
1823.000028	121.12	120.98	96.61	127.58	127.77	135.10	129.20	130.62	98.54	13.14	
1833.000167	121.20	121.06	96.60	127.70	127.72	135.18	129.11	130.84	98.50	13.14	
1843.000083	121.31	121.17	96.62	127.84	127.74	135.26	129.05	130.91	98.52	13.16	
1853.000222	121.40	121.26	96.58	127.96	127.69	135.31	128.84	131.08	98.48	13.15	
1863.000000	121.57	121.45	96.64	128.16	127.75	135.45	128.82	131.21	98.53	13.12	
1873.000222	121.61	121.50	96.58	128.25	127.72	135.48	128.68	131.17	98.50	13.11	
1883.000083	121.80	121.66	96.62	128.46	127.72	135.65	128.53	131.45	98.54	13.04	
1893.000000	121.87	121.74	96.63	128.61	127.75	135.71	128.53	131.40	98.54	13.04	
1903.000139	121.97	121.85	96.57	128.74	127.68	135.79	128.32	131.65	98.49	13.01	
1913.000306	122.06	121.96	96.62	128.91	127.78	135.89	128.41	131.72	98.54	13.05	
1923.000167	122.05	121.95	96.57	128.98	127.72	135.87	128.29	131.70	98.49	13.06	
1933.000167	122.21	122.12	96.62	129.22	127.77	136.03	128.30	131.90	98.55	13.06	
1943.000083	122.21	122.13	96.62	129.36	127.77	136.06	128.30	131.79	98.53	13.08	
1953.000222	122.35	122.28	96.59	129.61	127.71	136.21	128.12	132.00	98.51	13.04	
1963.000139	122.42	122.36	96.63	129.86	127.76	136.31	128.20	132.00	98.53	13.05	
1983.000278	122.53	122.48	96.64	130.35	127.78	136.47	128.11	132.23	98.54	13.06	
1993.000000	122.51	122.48	96.59	130.59	127.78	136.42	128.07	132.14	98.51	13.08	
2003.000250	122.71	122.67	96.63	131.08	127.76	136.59	127.98	132.45	98.55	13.03	
2013.000083	122.77	122.72	96.65	131.54	127.78	136.66	128.04	132.37	98.55	13.06	
2033.000028	122.85	122.81	96.64	132.62	127.78	136.74	127.98	132.51	98.54	13.06	
2065.000083	122.97	122.96	96.61	136.04	127.78	136.87	127.93	132.54	98.51	13.11	
2073.000111	123.06	123.02	96.62	138.21	127.73	136.97	127.82	132.80	98.52	13.04	
2093.000250	123.10	123.09	96.60	227.98	127.71	137.07	127.74	132.83	98.48	13.03	
2113.000111	123.27	123.31	96.61	8235.46	127.77	137.24	127.76	132.84	98.50	13.02	
2133.000083	123.40	123.39	96.66	8236.94	127.80	137.32	127.76	132.87	98.54	13.00	
2153.000000	123.45	123.49	96.70	8236.82	127.83	137.42	127.73	133.20	98.56	13.02	
2173.000222	123.57	123.59	96.68	8235.79	122.44	137.52	127.70	133.32	98.59	13.03	
2193.000167	123.68	123.67	96.65	8235.49	123.21	137.60	127.58	133.24	98.58	12.99	
2213.000083	123.70	123.71	96.61	8235.69	123.63	137.62	127.59	133.30	98.53	13.02	
2233.000028	123.73	123.80	96.63	8235.72	123.82	137.68	127.65	133.19	98.55	13.05	
2253.000250	123.89	123.94	96.67	8237.17	124.03	137.85	127.64	133.52	98.58	13.02	
2273.000167	123.97	124.03	96.66	8237.25	124.45	137.96	127.62	133.44	98.57	13.02	
2293.000194	124.04	124.11	96.68	8236.77	124.49	138.00	127.58	133.66	98.59	13.03	
2313.000222	124.11	124.19	96.65	8236.12	124.48	138.08	127.48	133.82	98.56	12.99	
2333.000167	124.07	124.16	96.61	8236.53	124.34	138.02	127.46	133.78	98.53	13.01	
2352.900028	124.12	124.27	96.71	8236.97	124.59	138.14	127.57	133.76	98.56	--	
2373.000167	124.31	124.42	96.79	8238.84	124.73	138.34	127.59	133.91	98.60	13.01	
2393.000111	124.32	124.45	96.80	8238.36	124.79	138.38	127.60	134.00	98.59	13.01	
2413.000028	124.39	124.54	96.80	8238.60	124.89	138.49	127.63	134.03	98.61	13.03	
2433.000194	124.43	124.58	96.77	8237.39	124.84	138.49	127.54	132.47	98.56	13.02	
2453.000167	124.41	124.55	96.76	8237.22	124.82	138.52	127.54	133.37	98.54	13.04	
2473.000000	124.51	124.66	96.78	8237.41	124.81	138.60	127.56	132.92	98.55	13.05	
2493.000222	124.58	124.75	96.83	8239.25	124.86	138.66	127.67	133.19	98.60	13.04	
2513.000028	124.62	124.79	96.82	8238.79	125.00	138.69	127.66	131.86	98.60	13.03	
2553.000083	124.76	124.92	96.81	8237.61	124.97	138.86	127.55	132.25	98.59	12.96	
2593.000083	124.76	124.97	96.78	8237.37	124.79	138.92	127.58	131.53	98.56	12.98	
2633.000028	124.90	125.11	96.83	8238.22	124.77	139.03	127.68	131.68	98.61	13.02	
2673.000250	124.98	125.18	96.82	8237.38	125.00	139.18	127.61	132.11	98.61	13.04	
2713.000056	124.95	125.10	96.84	8236.94	125.61	139.02	127.58	131.60	98.65	13.04	
2753.000083	125.08	125.26	96.89	8239.17	125.57	139.17	127.67	132.42	98.69	13.04	
2793.000250	125.17	125.38	96.88	8239.05	125.58	139.30	127.63	131.83	98.66	13.07	
2833.000222	125.26	125.51	96.84	8238.09	125.72	139.39	127.46	127.49	97.61	13.00	2811: deflated
2873.000083	125.32	125.57	96.87	8239.43	125.77	139.48	127.54	126.15	97.66	13.03	packer in
2913.000250	125.38	125.68	96.85	8235.15	125.83	139.58	127.49	127.34	97.72	13.05	H-11b4
2953.000028	125.34	125.67	96.83	8234.28	125.89	139.56	127.47	126.77	97.70	13.08	
2993.000194	125.51	125.84	96.88	8235.62	126.03	139.77	127.44	126.21	97.88	13.01	
3033.000194	125.60	125.96	96.82	8233.60	126.05	139.81	127.29	125.65	97.97	12.94	

Table A-1

Pressures at the H-11 Hydropad During the H-11 Multipad Pumping Test (Concluded)

Elapsed Time Since Pump On (hr)	S1 H-11b1 Culebra (psig)	S2 H-11b1 Culebra (psig)	S3 H-11b1 annulus (psig)	S4 H-11b2 Culebra (psig)	S5 H-11b2 annulus (psig)	S6 H-11b3 Culebra (psig)	S7 H-11b3 annulus (psig)	S8 H-11b4 Culebra (psig)	S9 H-11b4 annulus (psig)	S10 barometer (psia)	Comments
3073.000056	125.53	125.91	96.82	8233.67	126.16	139.77	127.45	125.62	97.92	13.03	
3113.000028	125.64	126.02	96.87	8235.16	126.04	139.89	127.44	126.74	98.03	12.98	
3153.000056	125.71	126.06	96.84	8233.80	126.04	139.95	127.41	127.59	98.08	13.00	
3193.000222	125.80	126.11	96.82	8233.09	126.20	140.01	127.41	126.37	98.14	13.02	
3233.000083	125.77	126.12	96.85	8235.04	126.00	140.02	127.52	125.98	98.16	13.03	
3273.000194	125.92	126.26	96.83	8234.03	126.25	140.16	127.34	126.11	98.32	12.90	
3313.000222	125.83	126.21	96.82	8234.42	126.61	140.09	127.50	127.38	98.24	13.02	
3353.000111	125.99	126.31	96.87	8235.52	126.76	140.21	127.55	123.74	98.37	13.03	
3393.000167	126.06	126.40	96.86	8234.75	126.83	140.31	127.48	127.45	98.48	12.99	
3457.000583	126.01	126.45	97.07	8234.24	127.03	140.55	127.59	125.59	98.50	13.09	
3473.000167	126.03	126.38	97.03	8235.21	126.91	140.38	127.55	125.68	98.55	13.03	
3513.000028	126.20	126.54	96.92	8233.98	126.96	140.35	127.44	126.26	98.66	12.95	
3553.000056	126.12	126.54	96.90	8234.66	127.01	140.38	127.61	125.70	98.60	13.08	
3593.000028	126.21	126.57	96.93	8235.77	127.06	140.46	127.64	125.33	98.63	13.10	
3633.000167	126.31	126.63	96.89	8234.65	127.04	140.51	127.51	127.65	98.69	13.08	
3673.000250	126.25	126.62	96.89	8234.84	127.08	140.46	127.54	128.09	98.63	13.12	
3713.000222	126.36	126.71	96.93	8236.04	127.18	140.60	127.51	124.65	98.74	13.10	
3753.000028	126.41	126.70	96.24	8234.50	127.14	136.28	127.24	118.55	98.81	13.04	3749: deflated
3793.000194	126.32	126.64	96.17	8234.49	127.20	136.14	124.79	124.68	98.73	13.16	packers in
3813.000083	126.46	126.73	96.31	8236.55	127.28	136.24	123.58	123.36	98.85	13.10	H-11b1,3
3863.000000	126.47	126.74	96.30	8236.10	127.28	136.23	121.18	126.40	98.87	13.13	
3913.000028	126.51	126.78	96.35	8234.17	127.41	136.28	120.04	127.39	98.93	13.03	
3963.000111	126.54	126.80	96.36	8233.78	127.42	136.33	122.76	125.86	98.98	13.02	
4013.000222	126.64	126.84	96.43	8234.34	127.41	136.40	122.61	124.76	99.04	13.00	
4063.000056	126.68	126.89	97.13	8234.80	127.47	136.95	125.29	128.52	99.30	13.05	4057: inflated
4113.000250	126.81	127.00	97.16	8235.79	127.55	137.23	123.51	131.18	99.32	13.02	packers in
4163.000028	126.89	127.07	97.17	8236.12	127.39	137.32	122.56	128.34	99.32	12.96	H-11b1,3,4
4213.000083	126.91	127.09	97.18	8236.51	127.44	137.37	122.13	124.51	99.33	12.97	
4263.000194	126.88	127.04	97.16	8236.28	127.59	137.32	123.21	123.41	99.30	13.05	
4313.000278	126.88	127.04	97.20	8237.33	127.56	137.33	123.62	122.10	99.32	13.10	end test

113

Table A-2

**Water Levels and Pressures in Observation Well
DOE-1 During the H-11 Multipad Pumping Test**

Elapsed Time Since Pump On (hr)	Depth to Water (ft)	Pressure* (psig)
-1147.0000	497.70	154.48
-980.1667	497.21	154.70
-814.6667	497.38	154.62
-744.3333	497.01	154.79
-737.5833	497.28	154.67
-716.2000	500.23	153.30
-696.0000	502.79	152.12
-672.2500	502.82	152.11
-647.0000	501.64	152.65
-569.0000	499.84	153.49
-480.2500	499.41	153.68
-310.9167	499.84	153.49
-167.0000	501.57	152.69
-137.8000	497.87	154.40
-117.5167	497.93	154.37
-90.8667	497.99	154.34
-69.8667	497.97	154.35
-47.4833	497.90	154.38
-19.5833	497.83	154.41
-2.6667	497.57	154.54
0.0000	497.61	154.52
1.0000	497.61	154.52
2.0000	497.64	154.50
3.0000	497.70	154.48
4.0000	497.80	154.43
5.0000	497.90	154.38
6.0000	498.00	154.34
7.0000	498.10	154.29
8.0000	498.20	154.24
9.0000	498.29	154.20
10.0000	498.39	154.16
11.0000	498.52	154.10
12.0000	498.65	154.04
13.0000	498.79	153.97
14.0000	498.92	153.91
15.0000	499.05	153.85
16.0000	499.21	153.78
17.0000	499.38	153.70
18.0000	499.51	153.64

*Pressure = (831.7 ft - Depth to Water) × 0.4625 psi/ft

114

Table A-2

Water Levels and Pressures in Observation Well
DOE-1 During the H-11 Multipad Pumping Test (Continued)

Elapsed Time Since Pump On (hr)	Depth to Water (ft)	Pressure (psig)
19.0000	499.64	153.58
20.0000	499.77	153.52
21.0000	499.90	153.46
22.0000	500.03	153.40
23.0000	500.16	153.34
24.0000	500.33	153.26
26.0000	500.59	153.14
28.0000	500.85	153.02
30.0000	501.12	152.89
32.0000	501.35	152.79
34.0000	501.57	152.69
36.0000	501.80	152.58
38.0000	502.03	152.47
40.0000	502.26	152.37
42.0000	502.53	152.24
44.0000	502.76	152.13
46.0000	503.02	152.01
48.2500	503.28	151.89
51.6667	503.64	151.73
56.0000	504.10	151.52
60.0000	504.49	151.33
64.0000	504.86	151.16
68.0000	505.35	150.94
72.0000	505.77	150.74
76.0000	506.10	150.59
80.0000	506.50	150.41
85.4167	507.02	150.16
96.0000	507.97	149.73
108.2500	508.92	149.29
120.0000	509.84	148.86
132.1667	510.56	148.53
144.0000	511.52	148.08
156.2500	512.20	147.77
165.0000	512.66	147.56
180.0000	513.22	147.30
193.0000	513.94	146.96
204.4500	514.30	146.80
215.6667	514.90	146.52
228.2500	515.16	146.40
240.0000	515.75	146.13
252.2500	516.11	145.96
263.0000	516.67	145.70
275.0000	517.03	145.53

Table A-2

Water Levels and Pressures in Observation Well
DOE-1 During the H-11 Multipad Pumping Test (Continued)

Elapsed Time Since Pump On (hr)	Depth to Water (ft)	Pressure (psig)
286.0000	517.45	145.34
312.0000	518.24	144.98
335.0000	518.90	144.67
359.0000	519.65	144.32
389.0000	520.57	143.90
413.1667	521.10	143.65
431.0000	521.56	143.44
456.5000	522.08	143.20
486.5000	522.47	143.02
511.3667	522.87	142.83
529.7500	523.29	142.64
552.1667	523.56	142.51
577.3333	523.82	142.39
605.0000	524.15	142.24
626.3333	524.61	142.03
649.9167	524.97	141.86
673.0000	525.16	141.77
697.0000	525.52	141.61
720.5833	525.75	141.50
742.8333	525.98	141.40
775.8333	526.31	141.24
792.6667	526.51	141.15
817.2500	526.71	141.06
842.0000	526.94	140.95
863.6833	527.33	140.77
886.7500	527.43	140.72
912.2500	527.53	140.68
937.5000	527.76	140.57
960.8333	528.05	140.44
985.4167	528.35	140.30
1008.0833	528.41	140.27
1031.7500	528.48	140.24
1056.8333	528.71	140.13
1080.8333	528.90	140.05
1108.0000	529.13	139.94
1127.5000	529.30	139.86
1152.0000	529.40	139.81
1176.9167	529.56	139.74
1201.5000	529.69	139.68
1225.0000	529.92	139.57
1249.1667	530.02	139.53
1273.6667	530.12	139.48
1296.0000	530.18	139.45

Table A-2

**Water Levels and Pressures in Observation Well
DOE-1 During the H-11 Multipad Pumping Test (Continued)**

Elapsed Time Since Pump On (hr)	Depth to Water (ft)	Pressure (psig)
1320.0000	530.18	139.45
1344.9167	530.28	139.41
1368.3333	530.48	139.31
1390.0000	530.54	139.29
1414.0833	530.64	139.24
1440.5000	530.48	139.31
1462.0000	530.71	139.21
1490.5000	530.84	139.15
1511.0000	531.00	139.07
1512.0000	531.00	139.07
1512.5000	531.00	139.07
1513.0000	531.00	139.07
1513.5000	530.97	139.09
1514.0000	530.94	139.10
1514.5000	530.91	139.12
1515.0000	530.87	139.13
1515.5000	530.81	139.16
1516.0000	530.74	139.19
1516.5000	530.68	139.22
1517.0000	530.61	139.25
1517.5000	530.54	139.29
1518.0000	530.45	139.33
1518.5000	530.41	139.35
1519.0000	530.31	139.39
1520.0000	530.22	139.43
1521.0000	530.09	139.49
1522.0000	529.95	139.56
1523.0000	529.86	139.60
1524.0000	529.79	139.63
1525.0000	529.66	139.69
1527.0000	529.36	139.83
1529.0000	529.07	139.97
1531.0000	528.84	140.07
1533.0000	528.61	140.18
1535.0000	528.38	140.29
1543.5833	527.10	140.88
1549.7500	526.41	141.20
1560.0000	525.33	141.70
1567.6667	524.28	142.18
1573.4167	523.72	142.44
1583.2500	522.87	142.83
1591.8333	521.92	143.27
1597.3333	521.49	143.47

Table A-2

Water Levels and Pressures in Observation Well
DOE-1 During the H-11 Multipad Pumping Test (Continued)

Elapsed Time Since Pump On (hr)	Depth to Water (ft)	Pressure (psig)
1607.2500	520.73	143.82
1615.0000	520.05	144.14
1621.2500	519.59	144.35
1633.3833	519.09	144.58
1640.1667	518.21	144.99
1645.3333	517.91	145.13
1656.7667	517.26	145.43
1666.0000	516.60	145.73
1669.4167	516.47	145.79
1680.6667	515.91	146.05
1688.4167	515.45	146.27
1693.1667	515.22	146.37
1704.0000	514.73	146.60
1711.8333	514.37	146.77
1727.4167	513.65	147.10
1735.8333	513.35	147.24
1750.9167	512.73	147.52
1760.0000	512.40	147.68
1775.8833	511.81	147.95
1803.6667	510.89	148.37
1828.5000	510.33	148.63
1848.5833	509.81	148.87
1872.1000	509.15	149.18
1896.2500	508.50	149.48
1920.5833	508.01	149.71
1943.9667	507.58	149.91
1972.5000	506.99	150.18
1992.9167	506.66	150.33
2042.0833	505.87	150.70
2113.7500	504.69	151.24
2160.9167	504.20	151.47
2213.7500	503.54	151.77
2286.4167	502.85	152.09
2328.4167	502.59	152.21
2380.2500	502.13	152.43
2455.4667	501.54	152.70
2501.4167	501.25	152.83
2543.6167	500.98	152.96
2619.7500	500.49	153.18
2713.5333	500.16	153.34
2789.5333	499.87	153.47
2837.2833	499.41	153.68

Table A-2

Water Levels and Pressures in Observation Well
DOE-1 During the H-11 Multipad Pumping Test (Concluded)

Elapsed Time Since Pump On (hr)	Depth to Water (ft)	Pressure (psig)
2879.0833	499.41	153.68
2977.6333	499.05	153.85
3052.1167	498.72	154.00
3144.3333	498.39	154.16
3217.9167	498.13	154.28
3314.5000	497.90	154.38
3384.3833	497.64	154.50
3486.5333	497.28	154.67
3554.2500	497.21	154.70
3651.5000	497.08	154.76
3747.0000	496.88	154.85
3840.5000	496.65	154.96
3892.2500	496.42	155.07
3986.5000	496.39	155.08
4056.9167	496.33	155.11
4225.6667	495.93	155.29
4396.6667	495.47	155.51
4633.5000	495.37	155.55
4971.3333	494.91	155.77

Table A-3

Water Levels and Pressures in Observation Well
H-3b2 During the H-11 Multipad Pumping Test

Elapsed Time Since Pump On (hr)	Depth to Water (ft)	Pressure* (psig)
-1963.8333	410.93	124.69
-1941.7500	411.19	124.57
-1918.5833	411.32	124.51
-1896.8333	411.25	124.54
-1869.0000	411.52	124.42
-1823.0667	411.45	124.45
-1750.9167	411.42	124.47
-1654.8667	411.98	124.22
-1534.6667	411.81	124.29
-1314.5000	411.52	124.42
-1146.8333	411.42	124.47
-979.8333	410.83	124.73
-814.7500	410.53	124.87
-744.2500	410.33	124.96
-737.4167	410.37	124.94
-716.2500	410.53	124.87
-696.0833	410.63	124.82
-672.3333	410.43	124.91
-646.9167	410.30	124.97
-571.0833	410.50	124.88
-480.3333	410.60	124.84
-311.0000	410.43	124.91
-167.0833	410.70	124.79
-138.0000	410.47	124.90
-117.7167	410.66	124.81
-90.9667	410.40	124.93
-69.7333	410.53	124.87
-47.3000	410.66	124.81
-19.5000	410.70	124.79
-2.5667	410.56	124.85
4.1000	410.56	124.85
8.0833	410.50	124.88
12.1333	410.43	124.91
16.1667	410.43	124.91
20.1667	410.43	124.91
24.1667	410.43	124.91
28.1667	410.40	124.93
32.0833	410.40	124.93
36.1333	410.33	124.96

*Pressure = (688.2 ft - Depth to Water) × 0.4497 psi/ft

120

Table A-3

Water Levels and Pressures in Observation Well
H-3b2 During the H-11 Multipad Pumping Test (Continued)

Elapsed Time Since Pump On (hr)	Depth to Water (ft)	Pressure* (psig)
40.1000	410.33	124.96
44.0833	410.37	124.94
48.3333	410.37	124.94
56.0833	410.37	124.94
60.1167	410.33	124.96
66.0000	410.33	124.96
72.0833	410.47	124.90
76.0833	410.43	124.91
80.0833	410.43	124.91
85.5000	410.53	124.87
88.0000	410.47	124.90
96.0833	410.63	124.82
108.0833	410.66	124.81
114.0000	410.60	124.84
120.0833	410.76	124.76
126.0000	410.63	124.82
132.0833	410.73	124.78
137.9167	410.76	124.76
144.0833	410.96	124.67
149.9167	410.93	124.69
156.3333	411.02	124.65
165.0833	411.02	124.65
180.0833	411.06	124.63
193.0833	411.22	124.56
204.5833	411.09	124.62
215.8333	411.25	124.54
228.1667	411.15	124.59
240.0833	411.38	124.49
252.1667	411.35	124.50
263.0833	411.58	124.40
274.8333	411.58	124.40
287.5833	411.75	124.32
312.0833	411.88	124.26
334.6667	412.07	124.18
359.0833	412.34	124.05
388.8333	412.83	123.83
413.2500	413.02	123.75
430.2500	413.25	123.65
456.3333	413.55	123.51
486.4167	413.75	123.42
511.2500	413.98	123.32
529.5833	414.27	123.19
552.0833	414.44	123.11

Table A-3

Water Levels and Pressures in Observation Well
H-3b2 During the H-11 Multipad Pumping Test (Continued)

Elapsed Time Since Pump On (hr)	Depth to Water (ft)	Pressure* (psig)
577.2500	414.53	123.07
604.4167	414.76	122.97
626.2500	415.16	122.79
649.7500	415.45	122.66
672.3333	415.58	122.60
697.0833	415.94	122.44
720.5000	416.14	122.35
742.7500	416.31	122.27
775.7500	416.57	122.15
792.7500	416.77	122.06
817.1667	416.99	121.96
842.1667	417.26	121.84
863.6167	417.65	121.67
886.6667	417.78	121.61
912.0833	417.91	121.55
937.4167	418.11	121.46
960.6667	418.41	121.32
985.2500	418.70	121.19
1008.1667	418.80	121.15
1031.6667	418.86	121.12
1056.9167	419.06	121.03
1080.9167	419.32	120.92
1107.9167	419.55	120.81
1127.5833	419.75	120.72
1151.9167	419.88	120.66
1177.0000	420.08	120.57
1201.4167	420.31	120.47
1225.2500	420.54	120.37
1249.2500	420.70	120.29
1273.5833	420.87	120.22
1294.0833	420.87	120.22
1320.0833	421.03	120.15
1345.0833	421.19	120.07
1368.5333	421.42	119.97
1390.0000	421.56	119.91
1413.9167	421.75	119.82
1440.2500	421.92	119.75
1461.8333	422.15	119.64
1490.3333	422.34	119.56
1510.9167	422.57	119.45
1515.3333	422.51	119.48
1519.3333	422.44	119.51
1522.7500	422.51	119.48

Table A-3

Water Levels and Pressures in Observation Well
H-3b2 During the H-11 Multipad Pumping Test (Continued)

Elapsed Time Since Pump On (hr)	Depth to Water (ft)	Pressure* (psig)
1526.7500	422.61	119.44
1531.1667	422.64	119.42
1535.1667	422.74	119.38
1543.5000	422.64	119.42
1549.5000	422.77	119.36
1559.4167	422.87	119.32
1567.5000	422.74	119.38
1573.2500	422.80	119.35
1583.1667	422.93	119.29
1591.6667	422.83	119.34
1597.1667	422.90	119.31
1607.3333	423.00	119.26
1614.8500	422.93	119.29
1621.1667	422.93	119.29
1633.2000	423.10	119.22
1640.0833	422.93	119.29
1645.1667	423.00	119.26
1656.6333	423.06	119.23
1665.8333	422.97	119.27
1669.3333	423.00	119.26
1680.5000	423.10	119.22
1688.3333	423.00	119.26
1693.0000	423.03	119.25
1703.9000	423.03	119.25
1711.7500	423.03	119.25
1727.6667	423.03	119.25
1735.7500	423.03	119.25
1750.8333	422.97	119.27
1759.9167	422.93	119.29
1775.9500	422.87	119.32
1804.6667	422.77	119.36
1828.3333	422.90	119.31
1848.5000	422.83	119.34
1872.1833	422.67	119.41
1896.1667	422.44	119.51
1920.6667	422.38	119.54
1943.9000	422.31	119.57
1972.5833	422.11	119.66
1993.0000	422.05	119.69
2042.1667	421.75	119.82
2113.5833	421.16	120.09
2160.8333	421.00	120.16

Table A-3

Water Levels and Pressures in Observation Well
H-3b2 During the H-11 Multipad Pumping Test (Concluded)

Elapsed Time Since Pump On (hr)	Depth to Water (ft)	Pressure* (psig)
2213.6667	420.64	120.32
2286.2500	420.28	120.48
2328.9167	420.18	120.53
2380.4167	419.85	120.68
2455.2833	419.46	120.85
2501.5000	419.29	120.93
2543.4167	419.09	121.02
2619.9167	418.73	121.18
2713.4667	418.14	121.45
2789.4500	418.24	121.40
2837.4500	417.81	121.59
2879.0000	417.85	121.58
2977.8333	417.52	121.72
3052.2000	417.22	121.86
3144.5000	416.93	121.99
3217.8333	416.67	122.11
3314.4167	416.47	122.20
3384.4667	416.24	122.30
3486.6667	415.88	122.46
3554.3333	415.78	122.51
3651.5833	415.72	122.53
3747.4167	415.49	122.64
3840.3333	415.32	122.71
3892.3333	415.09	122.82
3986.4167	415.06	122.83
4056.8333	414.99	122.86
4225.5833	414.60	123.04
4396.5833	413.94	123.33
4633.1667	413.65	123.47
4971.2500	413.19	123.67
5237.4167	412.80	123.85
5573.3333	412.01	124.20

Table A-4

Water Levels and Pressures in Observation Well
H-4b During the H-11 Multipad Pumping Test

Elapsed Time Since Pump On (hr)	Depth to Water (ft)	Pressure* (psig)	Compensated Pressure+ (psig)
-980.0000	340.16	72.19	--
-834.0000	339.80	72.35	--
-645.6667	339.90	72.30	--
-479.5833	340.06	72.23	--
-310.6667	339.83	72.33	--
-139.6667	339.96	72.27	--
-70.4833	339.90	72.30	72.23
-3.0000	340.06	72.23	72.22
36.7500	339.90	72.30	72.22
50.6667	339.90	72.30	72.23
85.0000	339.96	72.27	72.23
97.0000	340.03	72.24	72.24
143.5000	340.09	72.22	72.25
192.0000	340.09	72.22	72.22
262.5000	339.96	72.27	72.25
311.4167	339.90	72.30	72.22
358.6667	339.93	72.29	72.22
429.7500	340.16	72.19	72.18
489.7500	340.12	72.20	72.18
530.2500	340.19	72.17	72.15
603.8333	339.99	72.26	72.14
650.7500	340.26	72.14	72.12
671.7500	340.26	72.14	72.11
697.9167	340.39	72.09	72.10
792.4167	340.39	72.09	72.06
817.8333	340.35	72.10	72.06
868.4000	340.62	71.98	72.01
937.8333	340.49	72.04	72.00
985.9167	340.72	71.94	71.99
1031.2500	340.58	72.00	71.99
1108.3333	340.68	71.96	71.96
1150.2500	340.68	71.96	71.94
1201.9167	340.72	71.94	71.92
1274.0000	340.72	71.94	71.92
1318.0833	340.62	71.98	71.93
1370.5000	340.68	71.96	71.93
1439.7500	340.72	71.94	71.90

*Pressure = (503.7 ft - Depth to Water) × 0.4414 psi/ft
+Compensated Pressure = Pressure + 0.6 (Barometric Pressure - 13.06 psia)

Table A-4

Water Levels and Pressures in Observation Well
H-4b During the H-11 Multipad Pumping Test (Continued)

Elapsed Time Since Pump On (hr)	Depth to Water (ft)	Pressure* (psig)	Compensated Pressure+ (psig)
1491.8333	340.85	71.88	71.86
1511.3333	340.88	71.87	71.86
1515.8333	340.85	71.88	71.86
1519.8333	340.81	71.90	71.85
1523.9167	340.81	71.90	71.88
1527.6667	340.85	71.88	71.88
1531.6667	340.88	71.87	71.86
1536.1667	340.88	71.87	71.87
1543.8333	340.88	71.87	71.85
1550.0000	340.88	71.87	71.87
1567.9167	340.85	71.88	71.85
1573.7500	340.81	71.90	71.87
1592.0833	340.81	71.90	71.86
1609.6667	340.81	71.90	71.88
1621.6667	340.75	71.93	71.89
1632.9500	340.78	71.91	71.88
1640.5000	340.78	71.91	71.86
1645.6667	340.75	71.93	71.89
1656.2833	340.75	71.93	71.90
1666.6667	340.75	71.93	71.88
1669.8333	340.75	71.93	71.89
1681.0000	340.78	71.91	71.89
1688.6667	340.78	71.91	71.87
1693.5000	340.78	71.91	71.90
1703.5333	340.81	71.90	71.88
1712.0833	340.81	71.90	71.87
1728.0000	340.81	71.90	71.89
1736.0833	340.81	71.90	71.88
1751.1667	340.85	71.88	71.88
1760.1667	340.81	71.90	71.87
1779.1333	340.78	71.91	71.89
1804.0833	340.75	71.93	71.90
1825.5000	340.91	71.86	71.92
1848.0833	340.94	71.84	71.91
1876.9167	340.78	71.91	71.92
1896.0000	340.72	71.94	71.93
1925.6667	340.65	71.97	71.96
1944.0000	340.72	71.94	71.95
1972.1667	340.65	71.97	71.97
1993.6667	340.62	71.98	72.00
2041.2500	340.55	72.01	72.02
2113.0000	340.52	72.03	72.00

Table A-4

Water Levels and Pressures in Observation Well
H-4b During the H-11 Multipad Pumping Test (Concluded)

Elapsed Time Since Pump On (hr)	Depth to Water (ft)	Pressure* (psig)	Compensated Pressure+ (psig)
2161.5833	340.35	72.10	72.09
2212.8333	340.29	72.13	72.11
2286.9167	340.19	72.17	72.13
2329.5833	340.16	72.19	72.17
2379.6667	340.03	72.24	72.22
2456.4333	339.96	72.27	72.25
2500.8333	339.93	72.29	72.28
2545.1333	339.86	72.32	72.29
2616.8333	339.73	72.38	72.34
2714.4667	339.70	72.39	72.37
2790.9167	339.70	72.39	72.40
2838.5000	339.44	72.50	72.44
2879.5000	339.53	72.46	72.47
2977.4000	339.40	72.52	72.51
3051.7833	339.27	72.58	72.55
3147.0833	339.24	72.59	72.59
3218.1667	339.17	72.62	72.61
3315.7167	339.04	72.68	72.65
3384.1333	338.88	72.75	72.72
3484.5833	338.81	72.78	72.74
3555.2500	338.81	72.78	72.78
3650.7500	338.85	72.76	72.80
3841.1667	338.68	72.84	72.89
3892.0833	338.52	72.91	72.90
3984.8333	338.52	72.91	72.95
4058.8333	338.45	72.94	72.97
4224.8333	338.32	73.00	73.03
4395.6667	337.93	73.17	--
4636.1667	337.89	73.19	--
4970.5000	337.89	73.19	--
5238.4167	337.80	73.23	--

Table A-5

Water Levels and Pressures in Observation Well
H-12 During the H-11 Multipad Pumping Test

Elapsed Time Since Pump On (hr)	Depth to Water (ft)	Pressure* (psig)	Compensated Pressure+ (psig)
-839.9167	464.93	174.72	--
-427.6667	464.99	174.69	--
-136.7500	465.03	174.67	--
-68.2833	464.96	174.70	--
-16.5000	465.12	174.63	174.61
-1.0667	465.16	174.61	174.60
35.5833	465.03	174.67	174.58
83.4167	465.03	174.67	174.61
97.9167	465.06	174.66	174.65
145.5000	465.16	174.61	174.65
193.8333	465.19	174.60	174.60
264.4167	465.06	174.66	174.64
313.4167	464.96	174.70	174.62
360.5000	464.93	174.72	174.65
432.3333	465.12	174.63	174.62
485.1667	465.09	174.64	174.62
528.5000	465.12	174.63	174.60
606.1667	464.86	174.75	174.62
648.6667	465.03	174.67	174.65
678.2500	465.06	174.66	174.61
698.8333	465.12	174.63	174.64
791.8833	465.16	174.61	174.58
815.5000	465.12	174.63	174.59
936.0000	465.19	174.60	174.56
984.1667	465.32	174.53	174.58
1033.5000	465.26	174.56	174.54
1106.5833	465.26	174.56	174.57
1154.5000	465.26	174.56	174.54
1200.0833	465.29	174.55	174.53
1272.2500	465.32	174.53	174.51
1321.3333	465.22	174.58	174.53
1366.0000	465.22	174.58	174.55
1437.5000	465.32	174.53	174.49
1488.5000	465.42	174.49	174.48
1509.9167	465.45	174.47	174.46
1540.6667	465.45	174.47	174.46
1618.4167	465.45	174.47	174.43

*Pressure = (837.7 ft - Depth to Water) × 0.4687 psi/ft
+Compensated Pressure = Pressure + 0.6 (Barometric Pressure - 13.06 psia)

Table A-5

**Water Levels and Pressures in Observation Well
H-12 During the H-11 Multipad Pumping Test (Concluded)**

Elapsed Time Since Pump On (hr)	Depth to Water (ft)	Pressure* (psig)	Compensated Pressure+ (psig)
1664.0000	465.42	174.49	174.44
1706.8333	465.45	174.47	174.46
1802.3333	465.52	174.44	174.42
1826.5000	465.62	174.39	174.45
1874.8333	465.68	174.37	174.38
1944.7500	465.62	174.39	174.41
1991.9167	465.62	174.39	174.40
2040.5000	465.58	174.41	174.42
2118.7000	465.55	174.43	174.37
2160.0833	465.55	174.43	174.42
2212.0000	465.58	174.41	174.40
2284.0000	465.49	174.45	174.43
2330.6667	465.52	174.44	174.43
2378.4167	465.49	174.45	174.44
2457.5833	465.52	174.44	174.41
2499.6667	465.49	174.45	174.45
2544.0833	465.49	174.45	174.43
2618.7500	465.52	174.44	174.40
2716.8333	465.49	174.45	174.42
2788.5000	465.49	174.45	174.47
2880.9167	465.39	174.50	174.51
2976.0833	465.49	174.45	174.45
3047.7500	465.45	174.47	174.45
3145.1667	465.29	174.55	174.55
3316.6333	465.16	174.61	174.57
3383.3833	465.16	174.61	174.58
3485.3333	465.16	174.61	174.57
3653.6667	465.16	174.61	174.63
3842.1667	465.09	174.64	174.69
3983.8333	464.96	174.70	174.73
4224.0000	464.80	174.78	174.81
4466.5000	464.57	174.89	--

Table A-6

**Water Levels and Pressures in Observation Well
H-14 During the H-11 Multipad Pumping Test**

Elapsed Time Since Pump On (hr)	Depth to Water (ft)	Pressure* (psig)
-1198.9167	347.93	91.89
-833.5833	347.38	92.13
-426.8333	347.24	92.19
-139.0833	347.15	92.23
-70.0000	347.05	92.27
-19.7333	347.28	92.17
-2.8333	347.24	92.19
85.2500	347.11	92.24
262.6667	347.08	92.26
311.8333	347.01	92.29
358.8333	347.01	92.29
430.0833	347.18	92.21
529.9167	347.11	92.24
604.2500	346.82	92.37
650.0000	347.05	92.27
672.0833	347.05	92.27
697.5833	347.15	92.23
792.5833	347.11	92.24
817.4167	347.05	92.27
868.7667	347.24	92.19
937.6667	347.11	92.24
985.5833	347.31	92.16
1031.5833	347.21	92.20
1108.0833	347.24	92.19
1150.5833	347.24	92.19
1201.6667	347.21	92.20
1273.7500	347.28	92.17
1318.4167	347.21	92.20
1369.2500	347.24	92.19
1440.5833	347.31	92.16
1492.2500	347.44	92.10
1511.1667	347.47	92.09
1535.9167	347.51	92.07
1621.3333	347.44	92.10
1666.0833	347.47	92.09
1703.7000	347.54	92.06
1803.8333	347.57	92.04
1828.6667	347.80	91.94
1877.0833	347.80	91.94

*Pressure = (559.8 ft - Depth to Water) × 0.4337 psi/ft

Table A-6

Water Levels and Pressures in Observation Well
H-14 During the H-11 Multipad Pumping Test (Concluded)

Elapsed Time Since Pump On (hr)	Depth to Water (ft)	Pressure* (psig)
1945.9167	347.83	91.93
1993.3333	347.83	91.93
2041.6667	347.87	91.91
2113.3333	347.90	91.90
2161.2500	347.97	91.87
2213.2500	348.03	91.84
2286.5833	348.06	91.83
2329.4167	348.13	91.80
2379.8333	348.10	91.81
2455.6000	348.20	91.77
2501.1667	348.26	91.74
2543.5333	348.29	91.73
2619.5833	348.36	91.70
2713.6667	348.33	91.71
2790.7500	348.59	91.60
2837.4167	348.43	91.67
2879.2500	348.56	91.61
2977.5500	348.62	91.59
3052.0333	348.59	91.60
3147.5000	348.69	91.56
3218.0000	348.72	91.55
3314.6667	348.75	91.53
3486.4167	348.75	91.53
3554.1667	348.88	91.48
3651.3333	348.98	91.43
3840.6667	349.02	91.42
3985.2500	348.98	91.43
4225.2500	349.02	91.42
4396.2500	348.79	91.52
4636.5833	348.95	91.45
4970.8333	349.18	91.35
5238.2500	349.21	91.33
5573.7500	348.88	91.48

Table A-7

Water Levels and Pressures in Observation Well
H-15 During the H-11 Multipad Pumping Test

Elapsed Time Since Pump On (hr)	Depth to Water (ft)	Pressure* (psig)
-980.6667	532.38	168.98
-814.5000	533.76	168.29
-743.8333	533.66	168.34
-737.7500	533.66	168.34
-716.0833	533.63	168.36
-695.8333	533.66	168.34
-672.4167	533.69	168.33
-646.8333	533.63	168.36
-569.5000	533.99	168.18
-480.1667	533.96	168.19
-311.4167	533.73	168.31
-167.1667	533.86	168.24
-137.4667	533.83	168.26
-117.3000	533.76	168.29
-91.0833	533.65	168.35
-68.9000	533.60	168.37
-46.5000	533.60	168.37
-18.9167	533.66	168.34
-1.8000	533.63	168.36
12.6333	533.60	168.37
24.3333	533.53	168.41
28.3333	533.53	168.41
32.1667	533.50	168.42
36.2500	533.50	168.42
42.1667	533.46	168.44
48.5000	533.46	168.44
56.0000	533.43	168.46
60.2667	533.43	168.46
72.1667	533.43	168.46
80.1667	533.43	168.46
88.1667	533.50	168.42
96.5000	533.53	168.41
108.0000	533.60	168.37
120.2500	533.69	168.33
132.0000	533.76	168.29
144.2500	533.89	168.23
150.0000	533.96	168.19
156.1667	534.06	168.14
164.8333	534.19	168.08

*Pressure = (873.4 ft - Depth to Water) × 0.4955 psi/ft

Table A-7

Water Levels and Pressures in Observation Well
H-15 During the H-11 Multipad Pumping Test (Continued)

Elapsed Time Since Pump On (hr)	Depth to Water (ft)	Pressure* (psig)
180.1667	534.35	168.00
192.7500	534.48	167.93
204.7167	534.61	167.87
215.6667	534.74	167.81
228.0000	534.88	167.74
240.2500	535.04	167.66
252.0000	535.20	167.58
263.9167	535.37	167.49
275.8333	535.56	167.40
287.8333	535.73	167.32
312.6667	536.09	167.14
334.5833	536.38	166.99
359.9167	536.78	166.80
388.5833	537.37	166.50
413.4167	537.66	166.36
431.7500	537.99	166.20
456.7500	538.35	166.02
485.8333	538.78	165.80
511.1167	539.14	165.63
529.0833	539.40	165.50
551.9167	539.67	165.36
577.0000	539.93	165.23
605.5000	540.22	165.09
626.1667	540.49	164.96
649.2500	540.81	164.80
673.5833	541.14	164.63
697.4167	541.47	164.47
720.7500	541.80	164.31
742.6667	542.13	164.14
776.0833	542.39	164.02
792.9167	542.55	163.94
816.1667	542.78	163.82
841.8333	543.01	163.71
863.8667	543.31	163.56
886.5833	543.57	163.43
912.0000	543.77	163.33
936.5000	543.96	163.24
960.5833	544.19	163.12
984.7500	544.49	162.97
1008.3333	544.72	162.86
1032.3333	544.88	162.78
1056.5833	545.05	162.70
1080.5000	545.28	162.58

Table A-7

Water Levels and Pressures in Observation Well
H-15 During the H-11 Multipad Pumping Test (Continued)

Elapsed Time Since Pump On (hr)	Depth to Water (ft)	Pressure* (psig)
1107.0833	545.51	162.47
1127.6667	545.67	162.39
1152.5000	545.87	162.29
1176.7500	546.03	162.21
1200.7500	546.23	162.11
1225.5833	546.42	162.02
1248.9167	546.59	161.93
1272.8333	546.75	161.86
1294.2500	546.88	161.79
1319.8333	547.05	161.71
1345.2500	547.18	161.64
1368.0000	547.34	161.56
1389.7500	547.51	161.48
1413.6667	547.70	161.38
1440.9167	547.87	161.30
1461.5833	548.03	161.22
1489.9167	548.20	161.14
1510.3333	548.33	161.07
1515.2333	548.36	161.06
1519.2667	548.36	161.06
1522.8333	548.39	161.04
1526.8333	548.39	161.04
1531.4167	548.43	161.02
1535.2500	548.46	161.01
1543.3333	548.52	160.98
1549.2500	548.56	160.96
1562.9167	548.62	160.93
1567.2500	548.65	160.91
1573.0000	548.65	160.91
1583.3333	548.69	160.89
1591.4167	548.72	160.88
1597.0833	548.72	160.88
1607.6667	548.72	160.88
1616.5000	548.75	160.86
1621.0000	548.69	160.89
1633.4833	548.69	160.89
1639.7500	548.62	160.93
1645.0000	548.59	160.94
1656.8500	548.56	160.96
1665.0000	548.49	160.99
1669.1667	548.46	161.01
1680.7500	548.39	161.04
1688.1667	548.33	161.07

Table A-7

Water Levels and Pressures in Observation Well
H-15 During the H-11 Multipad Pumping Test (Continued)

Elapsed Time Since Pump On (hr)	Depth to Water (ft)	Pressure* (psig)
1692.9167	548.29	161.09
1704.0667	548.20	161.14
1711.5833	548.13	161.17
1727.2500	548.00	161.24
1735.6667	547.93	161.27
1750.6667	547.77	161.35
1759.7500	547.64	161.41
1776.5833	547.54	161.46
1803.5000	547.11	161.68
1828.2500	546.88	161.79
1848.7500	546.69	161.88
1872.0000	546.42	162.02
1896.8333	546.03	162.21
1920.1667	545.73	162.36
1943.8167	545.47	162.49
1972.6667	545.14	162.65
1992.5000	544.88	162.78
2042.3333	544.32	163.06
2116.2500	543.57	163.43
2160.5000	543.11	163.66
2211.5833	542.65	163.89
2284.6667	542.03	164.19
2328.0833	541.67	164.37
2378.0000	541.27	164.57
2455.1833	540.75	164.83
2499.3333	540.45	164.98
2543.8333	540.19	165.11
2619.3333	539.67	165.36
2713.3667	539.24	165.58
2789.3667	538.91	165.74
2837.6667	538.58	165.90
2878.2500	538.42	165.98
2978.0000	537.99	166.20
3052.7000	537.63	166.37
3144.8333	537.30	166.54
3219.0000	536.98	166.70
3314.3167	536.68	166.84
3383.6499	536.48	166.94
3486.9167	536.19	167.09
3554.0000	535.99	167.19
3653.0833	535.79	167.29
3747.5833	535.60	167.38

Table A-7

Water Levels and Pressures in Observation Well
H-15 During the H-11 Multipad Pumping Test (Concluded)

Elapsed Time Since Pump On (hr)	Depth to Water (ft)	Pressure* (psig)
3840.2500	535.33	167.51
3891.2500	535.17	167.59
3983.4167	534.91	167.72
4057.0833	534.74	167.81
4133.2500	534.55	167.90

Table A-8

Water Levels and Pressures in Observation Well
H-17 During the H-11 Multipad Pumping Test

Elapsed Time Since Pump On (hr)	Depth to Water (ft)	Pressure* (psig)
-1145.3333	443.60	139.42
-1080.0000	443.37	139.54
-977.0833	443.08	139.68
-813.2500	442.78	139.83
-742.2500	442.75	139.85
-738.0833	442.75	139.85
-715.6667	442.75	139.85
-695.5000	442.81	139.82
-672.5833	442.88	139.78
-646.2500	442.85	139.80
-552.8667	443.18	139.63
-479.8333	443.08	139.68
-310.2500	442.88	139.78
-166.6667	443.01	139.72
-140.5833	442.91	139.77
-118.3167	442.91	139.77
-90.5000	442.81	139.82
-71.2667	442.75	139.85
-20.3833	442.85	139.80
-3.5000	442.85	139.80
6.0833	442.85	139.80
12.0000	442.81	139.82
18.0000	442.78	139.83
27.2500	442.75	139.85
30.3333	442.75	139.85
36.2500	442.72	139.87
42.5333	442.68	139.89
48.7500	442.68	139.89
60.0833	442.68	139.89
72.4167	442.68	139.89
84.3333	442.75	139.85
94.6667	442.81	139.82
108.5000	442.91	139.77
119.6667	443.01	139.72
131.5833	443.08	139.68
143.0000	443.18	139.63
156.8333	443.34	139.55
165.5833	443.44	139.50
180.0833	443.57	139.44

*Pressure = (719.9 ft - Depth to Water) × 0.5046 psi/ft

Table A-8

Water Levels and Pressures in Observation Well
H-17 During the H-11 Multipad Pumping Test (Continued)

Elapsed Time Since Pump On (hr)	Depth to Water (ft)	Pressure* (psig)
190.6667	443.67	139.39
204.0333	443.73	139.36
216.2500	443.86	139.29
228.8333	443.93	139.25
241.4167	444.03	139.20
252.8333	444.13	139.15
261.8333	444.23	139.10
274.1667	444.36	139.04
287.0833	444.49	138.97
297.7500	444.55	138.94
310.9167	444.65	138.89
334.0833	444.82	138.81
358.0000	445.05	138.69
389.7500	445.44	138.49
413.5833	445.70	138.36
429.3333	445.83	138.30
455.7500	446.06	138.18
485.0833	446.33	138.04
510.6667	446.56	137.93
530.8333	446.69	137.86
552.9167	446.78	137.82
576.5000	446.88	137.77
603.0000	446.98	137.72
625.7500	447.15	137.63
651.7500	447.38	137.51
670.5833	447.54	137.43
698.4167	447.74	137.33
720.9167	447.90	137.25
742.4167	448.06	137.17
775.4167	448.20	137.10
790.8333	448.29	137.05
818.3333	448.39	137.00
841.5833	448.49	136.95
886.3333	448.85	136.77
912.9167	448.92	136.74
938.4167	449.02	136.69
961.3333	449.11	136.64
986.5000	449.31	136.54
1007.5000	449.41	136.49
1030.7500	449.48	136.45
1057.7500	449.54	136.42
1079.8333	449.64	136.37
1105.8333	449.74	136.32

Table A-8

**Water Levels and Pressures in Observation Well
H-17 During the H-11 Multipad Pumping Test (Continued)**

Elapsed Time Since Pump On (hr)	Depth to Water (ft)	Pressure* (psig)
1126.0833	449.84	136.27
1149.7500	449.90	136.24
1176.2500	449.97	136.21
1202.4167	450.07	136.16
1224.7500	450.13	136.13
1248.6667	450.23	136.08
1274.6667	450.30	136.04
1293.4167	450.30	136.04
1317.5833	450.36	136.01
1346.0833	450.39	135.99
1371.5000	450.46	135.96
1393.2500	450.56	135.91
1416.5000	450.62	135.88
1438.2500	450.69	135.84
1465.2500	450.79	135.79
1491.1667	450.85	135.76
1509.5000	450.92	135.73
1515.2500	450.92	135.73
1519.2500	450.92	135.73
1523.4167	450.92	135.73
1527.0000	450.95	135.71
1531.0000	450.95	135.71
1539.0000	450.98	135.70
1544.6667	450.98	135.70
1550.8333	450.98	135.70
1558.4167	451.02	135.68
1568.5833	451.02	135.68
1574.5833	450.98	135.70
1582.6667	450.95	135.71
1592.8333	450.95	135.71
1598.6667	450.92	135.73
1606.7500	450.89	135.74
1615.6833	450.85	135.76
1622.6667	450.82	135.78
1632.3333	450.75	135.81
1641.4167	450.72	135.83
1646.1667	450.66	135.86
1655.6500	450.59	135.89
1667.1667	450.52	135.93
1670.3333	450.49	135.94
1681.2500	450.39	135.99
1689.3333	450.36	136.01
1694.3333	450.33	136.03

Table A-8

Water Levels and Pressures in Observation Well
H-17 During the H-11 Multipad Pumping Test (Continued)

Elapsed Time Since Pump On (hr)	Depth to Water (ft)	Pressure* (psig)
1702.7500	450.23	136.08
1712.5667	450.20	136.09
1726.4167	450.07	136.16
1736.5833	450.00	136.19
1751.5833	449.87	136.26
1760.5833	449.77	136.31
1775.3667	449.67	136.36
1801.8333	449.38	136.50
1826.0833	449.25	136.57
1847.5000	449.11	136.64
1871.4667	448.92	136.74
1895.4167	448.62	136.89
1919.7500	448.39	137.00
1943.3333	448.20	137.10
1971.6667	448.00	137.20
1994.1667	447.80	137.30
2015.3333	447.64	137.38
2040.7500	447.44	137.48
2112.4167	446.95	137.73
2212.3333	446.33	138.04
2283.6667	445.90	138.26
2330.2500	445.64	138.39
2378.9167	445.37	138.53
2457.0333	445.08	138.67
2500.3333	444.88	138.78
2544.5000	444.69	138.87
2617.5000	444.36	139.04
2717.1667	444.03	139.20
2790.7500	443.90	139.27
2838.3333	443.64	139.40
2880.6667	443.54	139.45
2976.4167	443.31	139.57
3051.3333	443.01	139.72
3145.9167	442.81	139.82
3219.7500	442.65	139.90
3316.1167	442.42	140.02
3382.8000	442.26	140.10
3485.5833	442.06	140.20
3555.6667	441.99	140.23
3654.2500	441.86	140.30
3749.0833	441.73	140.36
3841.6667	441.57	140.45

Table A-8

Water Levels and Pressures in Observation Well
H-17 During the H-11 Multipad Pumping Test (Concluded)

Elapsed Time Since Pump On (hr)	Depth to Water (ft)	Pressure* (psig)
3891.6667	441.44	140.51
3984.2500	441.24	140.61
4058.3333	441.11	140.68
4224.3333	440.85	140.81
4394.8333	440.49	140.99
4635.5833	440.29	141.09
4970.0000	439.99	141.24

Table A-9

Water Levels and Pressures in Observation Well
P-15 During the H-11 Multipad Pumping Test

Elapsed Time Since Pump On (hr)	Depth to Water (ft)	Pressure* (psig)	Compensated Pressure+ (psig)
-833.7500	304.27	54.28	--
-426.1667	304.43	54.21	--
-139.3667	304.49	54.18	--
-70.2500	304.17	54.33	--
-3.2000	304.66	54.11	54.10
50.5000	304.46	54.20	54.13
97.1667	304.56	54.15	54.15
143.6667	304.69	54.10	54.13
262.3333	304.59	54.14	54.11
311.6667	304.53	54.17	54.09
358.5000	304.49	54.18	54.11
429.9167	304.69	54.10	54.09
604.0000	304.40	54.22	54.10
671.5833	304.66	54.11	54.08
697.7500	304.72	54.08	54.09
792.2500	304.69	54.10	54.07
868.6167	304.82	54.04	54.06
1031.2500	304.79	54.05	54.04
1150.4167	304.79	54.05	54.03
1318.2500	304.69	54.10	54.04
1512.5000	304.82	54.04	54.02
1559.0000	304.89	54.01	53.99
1617.3667	304.79	54.05	54.00
1666.4167	304.72	54.08	54.03
1703.3667	304.82	54.04	54.02
1779.2833	304.86	54.02	54.00
1825.3333	304.99	53.96	54.02
1876.6667	304.95	53.98	53.99
1943.5833	304.92	53.99	54.01
1993.5000	304.92	53.99	54.00
2041.4167	304.92	53.99	54.00
2112.8333	304.92	53.99	53.97
2161.4167	304.92	53.99	53.98
2213.0000	304.92	53.99	53.97
2287.0833	304.92	53.99	53.95
2329.8333	304.92	53.99	53.98
2379.5000	304.86	54.02	54.00

*Pressure = (425.6 ft - Depth to Water) × 0.4474 psi/ft
+Compensated Pressure = Pressure + 0.6 (Barometric Pressure - 13.06 psia)

Table A-9

**Water Levels and Pressures in Observation Well
P-15 During the H-11 Multipad Pumping Test (Concluded)**

Elapsed Time Since Pump On (hr)	Depth to Water (ft)	Pressure* (psig)	Compensated Pressure+ (psig)
2456.6000	304.89	54.01	53.98
2501.0000	304.89	54.01	53.99
2545.0000	304.89	54.01	53.98
2616.7500	304.86	54.02	53.98
2714.6667	304.86	54.02	54.00
2791.0833	304.99	53.96	53.97
2879.6667	304.86	54.02	54.02
2977.2500	304.92	53.99	53.99
3051.6667	304.86	54.02	53.99
3147.2500	304.79	54.05	54.05
3383.9833	304.66	54.11	54.08
3484.7167	304.72	54.08	54.04
3651.0000	304.69	54.10	54.13
3840.8333	304.66	54.11	54.16
3985.0833	304.49	54.18	54.22
4225.0833	304.40	54.22	54.26
4395.8333	304.10	54.36	--
4636.4167	304.13	54.35	--
4970.6667	304.20	54.31	--

Table A-10

Water Levels and Pressures in Observation Well
P-17 During the H-11 Multipad Pumping Test

Elapsed Time Since Pump On (hr)	Depth to Water (ft)	Pressure* (psig)	Compensated Pressure+ (psig)
-977.3333	359.97	95.82	--
-812.7500	359.91	95.84	--
-742.5833	359.81	95.89	--
-738.3333	359.84	95.88	--
-715.3333	359.97	95.82	--
-695.2500	360.07	95.77	--
-646.0000	359.71	95.93	--
-479.4167	359.88	95.86	--
-310.5000	359.68	95.95	--
-166.7500	359.88	95.86	--
-140.0667	359.78	95.90	--
-118.0667	359.91	95.84	--
-90.6500	359.71	95.93	--
-70.7500	359.74	95.92	--
-47.8500	359.88	95.86	--
-20.0000	359.97	95.81	95.83
-4.0000	359.88	95.86	95.85
12.1667	359.78	95.90	95.86
27.6667	359.81	95.89	95.82
36.4167	359.68	95.95	95.87
48.9167	359.71	95.93	95.87
60.2500	359.65	95.96	95.86
72.5833	359.78	95.90	95.86
99.5833	359.84	95.87	95.86
120.5000	359.88	95.86	95.86
143.3333	359.94	95.83	95.86
156.5833	359.97	95.81	95.85
165.2500	359.97	95.81	95.85
179.9167	359.88	95.86	95.86
191.5833	359.91	95.84	95.85
204.2000	359.81	95.89	95.86
216.5000	359.88	95.86	95.83
228.5833	359.74	95.92	95.86
241.8333	359.88	95.86	95.81
252.5833	359.78	95.90	95.84
262.1667	359.88	95.86	95.83
274.3333	359.88	95.86	95.81
311.1667	359.84	95.87	95.80

*Pressure = (572.0 ft - Depth to Water) × 0.4519 psi/ft
+Compensated Pressure = Pressure + 0.6 (Barometric Pressure - 13.06 psia)

144

Table A-10

Water Levels and Pressures in Observation Well
P-17 During the H-11 Multipad Pumping Test (Continued)

Elapsed Time Since Pump On (hr)	Depth to Water (ft)	Pressure* (psig)	Compensated Pressure+ (psig)
334.3333	359.88	95.86	95.77
358.2500	359.94	95.83	95.76
389.2500	360.17	95.73	95.71
413.7500	360.20	95.71	95.69
429.5833	360.27	95.68	95.67
456.0833	360.33	95.65	95.66
485.7500	360.33	95.65	95.63
510.8333	360.40	95.62	95.60
530.4167	360.47	95.59	95.56
552.4167	360.47	95.59	95.54
576.1667	360.37	95.64	95.54
603.5833	360.43	95.61	95.49
625.5833	360.56	95.55	95.50
651.3333	360.76	95.46	95.43
670.7500	360.70	95.49	95.46
698.1667	360.89	95.40	95.41
721.0833	360.93	95.38	95.39
742.1667	360.96	95.37	95.35
775.5833	360.99	95.36	95.31
791.0000	361.06	95.33	95.29
818.0000	361.09	95.31	95.27
841.0833	361.19	95.27	95.23
868.2167	361.42	95.16	95.19
886.0833	361.38	95.18	95.20
912.5000	361.35	95.19	95.16
938.0833	361.42	95.16	95.13
961.0000	361.55	95.10	95.11
986.0833	361.71	95.03	95.08
1007.8333	361.65	95.06	95.08
1031.0833	361.61	95.07	95.06
1057.5000	361.65	95.06	95.04
1079.5000	361.75	95.01	95.01
1105.5000	361.84	94.97	94.98
1126.3333	361.88	94.95	94.96
1150.0000	361.88	94.95	94.93
1175.8333	361.94	94.93	94.91
1202.0833	362.04	94.88	94.86
1224.4167	362.11	94.85	94.85
1248.0000	362.14	94.84	94.82
1274.2500	362.14	94.84	94.81
1293.7500	362.04	94.88	94.84
1317.9167	362.04	94.88	94.83
1345.7500	362.11	94.85	94.78

Table A-10

Water Levels and Pressures in Observation Well
P-17 During the H-11 Multipad Pumping Test (Continued)

Elapsed Time Since Pump On (hr)	Depth to Water (ft)	Pressure* (psig)	Compensated Pressure+ (psig)
1370.7500	362.27	94.78	94.75
1390.3333	362.27	94.78	94.75
1414.3333	362.30	94.76	94.73
1439.5000	362.34	94.75	94.71
1462.2500	362.47	94.69	94.67
1491.5833	362.53	94.66	94.64
1509.1667	362.57	94.64	94.62
1515.5000	362.57	94.64	94.62
1519.5000	362.50	94.67	94.63
1524.1667	362.53	94.66	94.65
1527.4167	362.57	94.64	94.64
1531.4167	362.60	94.63	94.62
1538.8333	362.66	94.60	94.60
1544.2500	362.57	94.64	94.63
1550.3333	362.63	94.61	94.61
1558.6667	362.63	94.61	94.60
1568.2500	362.57	94.64	94.61
1574.0833	362.57	94.64	94.61
1582.9167	362.60	94.63	94.60
1592.3333	362.57	94.64	94.60
1598.2500	362.60	94.63	94.60
1607.0000	362.63	94.61	94.58
1622.0833	362.60	94.63	94.59
1632.7500	362.63	94.61	94.58
1641.0833	362.60	94.63	94.57
1645.8333	362.60	94.63	94.59
1656.1000	362.63	94.61	94.58
1666.8333	362.60	94.63	94.58
1670.0000	362.63	94.61	94.58
1681.5000	362.70	94.58	94.56
1689.0000	362.66	94.60	94.56
1693.9167	362.70	94.58	94.57
1703.1000	362.70	94.58	94.56
1712.2500	362.70	94.58	94.55
1726.0000	362.70	94.58	94.57
1736.2500	362.70	94.58	94.56
1751.2500	362.76	94.55	94.55
1760.3333	362.73	94.57	94.54
1775.6833	362.73	94.57	94.56
1801.5000	362.70	94.58	94.56
1825.7500	362.86	94.51	94.57
1847.7500	362.89	94.50	94.57

Table A-10

Water Levels and Pressures in Observation Well
P-17 During the H-11 Multipad Pumping Test (Concluded)

Elapsed Time Since Pump On (hr)	Depth to Water (ft)	Pressure* (psig)	Compensated Pressure+ (psig)
1870.9333	362.80	94.54	94.57
1895.7500	362.70	94.58	94.58
1918.9167	362.66	94.60	94.60
1942.8333	362.66	94.60	94.61
1972.0000	362.66	94.60	94.60
1993.8333	362.63	94.61	94.63
2041.0833	362.47	94.69	94.69
2112.5833	362.27	94.78	94.75
2161.8333	362.24	94.79	94.78
2212.6667	362.14	94.84	94.81
2283.2500	362.04	94.88	94.86
2330.0000	361.91	94.94	94.93
2379.2500	361.78	95.00	94.98
2456.7500	361.58	95.09	95.06
2500.5833	361.55	95.10	95.09
2544.8000	361.42	95.16	95.14
2617.0833	361.29	95.22	95.18
2717.5000	361.12	95.30	95.26
2790.0833	361.06	95.33	95.34
2838.5000	360.76	95.46	95.39
2880.3333	360.83	95.43	95.43
2976.6667	360.63	95.52	95.51
3051.0833	360.47	95.59	95.57
3146.2500	360.30	95.67	95.67
3219.4167	360.14	95.74	95.72
3315.8667	360.01	95.80	95.76
3382.5000	360.10	95.76	95.73
3485.9167	359.65	95.96	95.92
3555.4167	359.61	95.98	95.98
3654.5833	359.51	96.02	96.04
3748.5833	359.42	96.07	96.07
3841.4167	359.28	96.13	96.18
3891.9167	359.09	96.21	96.21
3984.5833	359.12	96.20	96.23
4058.6667	359.02	96.24	96.27
4224.6667	358.79	96.35	96.38
4395.0833	358.37	96.54	--
4635.9167	358.10	96.66	--
4970.2500	357.97	96.72	--

Table A-11

1988 Water Levels in Observation Well P-18

Day	1988 Hr	Mn	Depth to Water (ft)
2	08	05	587.73
4	13	50	586.65
6	08	45	585.99
8	14	00	585.17
9	11	00	584.88
11	08	15	584.48
12	15	15	584.28
14	11	20	583.20
15	13	45	582.78
18	11	25	581.66
20	08	35	581.14
22	12	45	581.36
26	15	45	581.23
29	13	45	580.77
32	08	30	580.71
36	10	45	579.46
39	13	45	578.93
43	14	25	577.69
46	09	50	576.61
50	10	39	575.46
53	09	25	574.44
57	11	35	573.20
71	15	25	568.54
78	15	15	566.90
85	14	00	564.76
92	10	40	562.99
96	13	10	561.71
99	10	25	560.73
106	09	00	559.19
113	09	25	557.97
120	15	50	556.75
123	12	26	556.82
125	16	10	556.27
126	07	30	556.23
127	20	50	556.36
129	21	05	556.27
130	10	40	556.17
132	10	05	555.61
134	10	30	555.18
137	09	05	554.69
139	10	10	554.23
141	09	20	553.81
144	09	05	553.31
146	14	25	552.95
148	09	40	552.69

Table A-11

1988 Water Levels in Observation Well P-18 (Concluded)

Day	1988 Hr	Mn	Depth to Water (ft)
151	15	00	552.26
153	10	00	552.07
154	15	00	551.87
155	11	40	551.77
158	17	20	551.28
160	08	45	551.25
162	09	00	550.89
165	09	15	550.16
167	09	30	549.67
169	09	40	549.21
172	11	50	548.69
174	09	45	548.23
176	09	30	547.97
179	09	35	548.46
181	09	45	548.65
183	07	21	548.88
186	06	55	548.65
188	09	45	548.56
189	07	10	548.46
190	12	30	548.36
193	19	45	548.43
195	17	15	548.29
197	12	05	548.16
201	12	00	548.26
202	11	50	548.33
204	08	47	547.24
207	08	38	546.23
209	09	20	545.64
214	13	35	544.52
221	13	20	544.23
228	18	58	543.73
235	12	05	542.85
242	15	55	541.96
250	08	50	540.22
257	10	20	538.75
264	13	26	537.63
271	14	05	536.15
278	15	00	534.02
286	10	55	531.92
292	08	35	530.94
302	09	10	529.43
309	10	40	528.67
319	10	55	527.95
333	09	20	525.92
345	10	50	523.88
384	14	40	520.01

Table A-12

Water Levels and Pressures in Observation Well
Cabin Baby-1 During the H-11 Multipad Pumping Test

Elapsed Time Since Pump On (hr)	Depth to Water (ft)	Pressure* (psig)	Compensated Pressure+ (psig)
-1145.0833	343.21	77.59	77.59
-977.1667	343.08	77.65	77.65
-813.0000	342.98	77.69	77.69
-742.5000	342.95	77.71	77.71
-738.2500	342.91	77.72	77.72
-715.5000	342.95	77.71	77.71
-695.4167	343.11	77.63	77.63
-646.0833	343.01	77.68	77.68
-479.2500	343.08	77.65	77.65
-310.4167	342.88	77.74	77.74
-140.3000	343.01	77.68	77.68
-70.9333	342.95	77.71	77.71
-20.1167	343.08	77.65	77.66
-3.7500	342.88	77.74	77.73
50.2167	342.91	77.72	77.68
84.5833	342.95	77.71	77.67
94.8333	342.98	77.69	77.68
143.1667	343.08	77.65	77.67
165.4167	343.18	77.60	77.63
190.8333	343.18	77.60	77.61
216.4167	343.08	77.65	77.63
241.6667	343.04	77.67	77.63
262.0000	343.04	77.67	77.65
287.2500	343.04	77.67	77.63
311.0833	343.01	77.68	77.63
334.2500	342.95	77.71	77.65
358.1667	342.95	77.71	77.66
389.4167	342.98	77.69	77.68
413.9167	343.01	77.68	77.66
429.5000	343.11	77.63	77.63
456.0000	343.08	77.65	77.65
489.4167	343.04	77.67	77.65
530.5833	343.08	77.65	77.63
552.5833	343.04	77.67	77.63
576.0000	343.04	77.67	77.60
603.5000	342.91	77.72	77.64
625.5000	342.91	77.72	77.69

*Pressure = (517.1 ft - Depth to Water) × 0.4462 psi/ft
+Compensated Pressure = Pressure + 0.4 (Barometric Pressure - 13.06 psia)

Table A-12

Water Levels and Pressures in Observation Well
Cabin Baby-1 During the H-11 Multipad Pumping Test (Continued)

Elapsed Time Since Pump On (hr)	Depth to Water (ft)	Pressure* (psig)	Compensated Pressure+ (psig)
651.5000	343.01	77.68	77.66
671.3333	343.08	77.65	77.63
698.2500	343.18	77.60	77.61
721.1667	343.21	77.59	77.59
748.3333	343.21	77.59	77.57
791.1333	343.27	77.56	77.54
818.1667	343.21	77.59	77.56
841.3333	343.21	77.59	77.57
868.1500	343.37	77.52	77.54
886.0000	343.41	77.50	77.51
912.5833	343.41	77.50	77.48
938.1667	343.37	77.52	77.49
961.1667	343.44	77.49	77.50
986.2500	343.50	77.46	77.49
1007.6667	343.57	77.43	77.45
1030.9167	343.54	77.44	77.43
1057.5833	343.50	77.46	77.45
1079.6667	343.57	77.43	77.43
1105.6667	343.57	77.43	77.43
1126.2500	343.67	77.38	77.39
1149.9167	343.70	77.37	77.36
1176.0000	343.67	77.38	77.37
1202.2500	343.70	77.37	77.36
1224.5833	343.73	77.36	77.36
1248.1667	343.80	77.33	77.32
1274.4167	343.80	77.33	77.31
1293.6667	343.80	77.33	77.30
1317.7500	343.80	77.33	77.29
1345.9167	343.80	77.33	77.28
1371.2500	343.80	77.33	77.31
1390.5000	343.90	77.28	77.26
1414.5000	343.93	77.27	77.24
1438.4167	343.93	77.27	77.24
1462.4167	344.06	77.21	77.20
1491.4167	344.09	77.20	77.19
1509.3333	344.13	77.18	77.17
1515.4167	344.09	77.20	77.19
1519.4167	344.13	77.18	77.15
1523.5833	344.13	77.18	77.16
1527.2500	344.13	77.18	77.18
1531.2500	344.16	77.17	77.16
1541.0000	344.16	77.17	77.16
1544.4167	344.16	77.17	77.15

Table A-12

Water Levels and Pressures in Observation Well
Cabin Baby-1 During the H-11 Multipad Pumping Test (Continued)

Elapsed Time Since Pump On (hr)	Depth to Water (ft)	Pressure* (psig)	Compensated Pressure+ (psig)
1550.5000	344.16	77.17	77.17
1558.5833	344.19	77.15	77.14
1568.3333	344.19	77.15	77.13
1574.3333	344.19	77.15	77.13
1582.8333	344.19	77.15	77.14
1592.5833	344.19	77.15	77.12
1615.5000	344.16	77.17	77.14
1622.3333	344.16	77.17	77.14
1632.5000	344.19	77.15	77.13
1641.2167	344.16	77.17	77.13
1646.0000	344.16	77.17	77.14
1655.8833	344.23	77.13	77.11
1667.0000	344.23	77.13	77.10
1670.1667	344.23	77.13	77.11
1680.8333	344.23	77.13	77.12
1689.1667	344.26	77.12	77.09
1694.0833	344.29	77.11	77.10
1702.9667	344.32	77.09	77.08
1712.4167	344.32	77.09	77.07
1726.1667	344.36	77.08	77.07
1736.4167	344.36	77.08	77.06
1751.4167	344.39	77.06	77.06
1760.4167	344.36	77.08	77.06
1775.5667	344.42	77.05	77.04
1801.6667	344.42	77.05	77.04
1825.9167	344.49	77.02	77.06
1847.6667	344.59	76.97	77.02
1875.1667	344.59	76.97	76.99
1895.6667	344.59	76.97	76.97
1919.5000	344.55	76.99	76.99
1944.2500	344.59	76.97	76.98
1971.9167	344.59	76.97	76.97
1994.0000	344.59	76.97	76.98
2040.9167	344.62	76.96	76.97
2112.5000	344.62	76.96	76.94
2161.9167	344.59	76.97	76.97
2212.5833	344.55	76.99	76.98
2283.4167	344.52	77.01	76.99
2330.1667	344.52	77.01	77.00
2379.0833	344.46	77.03	77.02
2456.9167	344.46	77.03	77.01
2500.5000	344.39	77.06	77.06

Table A-12

Water Levels and Pressures in Observation Well
Cabin Baby-1 During the H-11 Multipad Pumping Test (Concluded)

Elapsed Time Since Pump On (hr)	Depth to Water (ft)	Pressure* (psig)	Compensated Pressure+ (psig)
2544.7000	344.39	77.06	77.05
2617.2500	344.26	77.12	77.10
2717.4167	344.23	77.13	77.11
2791.3333	344.19	77.15	77.16
2838.2500	344.06	77.21	77.17
2880.5000	344.06	77.21	77.21
2976.5833	344.00	77.24	77.23
3051.1667	343.96	77.26	77.24
3146.0833	343.73	77.36	77.36
3219.5833	343.64	77.40	77.38
3316.0000	343.50	77.46	77.44
3382.6667	343.44	77.49	77.47
3485.7500	343.31	77.55	77.52
3555.5833	343.27	77.56	77.56
3654.4167	343.21	77.59	77.60
3841.5000	343.04	77.67	77.70
3891.8333	342.95	77.71	77.70
3984.5000	342.78	77.78	77.80
4058.5000	342.68	77.83	77.84
4224.5000	342.49	77.91	77.93
4395.0000	342.16	78.06	78.06
4635.7500	342.03	78.12	78.12
4970.1665	341.80	78.22	78.22

Table A-13

1988 Magenta Water Levels in Observation Well H-3b1

Day	1988 Hr	Mn	Depth to Water (ft)
15	10	05	251.25
33	14	20	251.02
48	11	55	250.66
62	10	40	250.39
92	10	10	250.07
123	15	25	249.80
137	11	30	249.84
154	09	25	249.67
191	08	40	249.67
214	10	40	249.54
221	15	20	249.48
228	16	23	249.40
235	13	00	249.34
242	15	35	249.48
250	10	45	249.41
257	09	35	249.38
265	10	40	249.34
271	15	38	249.31
278	12	40	249.44
286	09	25	249.54
292	11	20	249.54
302	10	30	249.67
309	12	30	249.67
319	09	25	249.97
333	11	10	250.33
344	13	55	250.72
383	14	15	251.25

Table A-14

1988 Magenta Water Levels in Observation Well H-4c

Day	1988 Hr	Mn	Depth to Water (ft)
33	12	50	193.24
62	9	45	192.75
91	15	05	192.49
123	13	43	192.39
137	10	30	192.45
154	8	55	192.39
194	8	30	192.35
223	10	40	198.92
253	12	52	194.98
292	9	55	193.90
319	12	15	193.57
344	14	30	193.50
383	15	10	193.21

APPENDIX B

TECHNIQUES FOR ANALYZING HYDRAULIC-TEST DATA

TECHNIQUES FOR ANALYZING HYDRAULIC-TEST DATA

Different analytical techniques are used to interpret data from slug tests and from pumping tests. The analysis of data from pumping tests may be further divided into analysis of the pumping-well data and analysis of the observation-well data. The different techniques used for the analyses presented in this report are discussed below. The well-test interpretation code INTERPRET is also described.

B.1 SLUG-TEST DATA ANALYSIS

Slug-test data were analyzed using a method first presented by Cooper et al. (1967), and later discussed by Ramey et al. (1975). The method is used for calculating the transmissivity of a homogeneous, isotropic, confined porous medium of uniform thickness which is fully penetrated by a well. To initiate a slug test with a packer on tubing in a well, a pressure differential is established between the wellbore and the surrounding formation by shutting in the test interval, swabbing the fluid from the tubing (in the case of a rising-head or slug-withdrawal test) or adding fluid to the tubing (in the case of a falling-head or slug-injection test), and then opening the test interval to the tubing. The resulting transient flow of groundwater is described mathematically in radial geometry by the diffusivity equation:

$$\frac{\partial^2 h}{\partial r^2} + \frac{1}{r}\frac{\partial h}{\partial r} = \frac{S}{T}\frac{\partial h}{\partial t} \tag{B-1}$$

where in consistent units:

h = hydraulic head differential (at radius r and time t), L
r = radius from well center, L
t = elapsed time, T
S = formation storativity
T = formation transmissivity, L^2/T.

The solution to this equation utilized for analysis of slug-test data is presented in the form of curves of $[H/H_o]$ (Figure B-1) and $[(H_o-H)/H_o]$ (Figure B-2) versus the dimensionless time parameter β for each of several values of α, where in consistent units:

$$\beta = Tt/r_c^2 \tag{B-2}$$

$$\alpha = r_s^2 S/r_c^2 \tag{B-3}$$

and: H_o = initial (maximum) head differential, L
H = head differential at time t, L
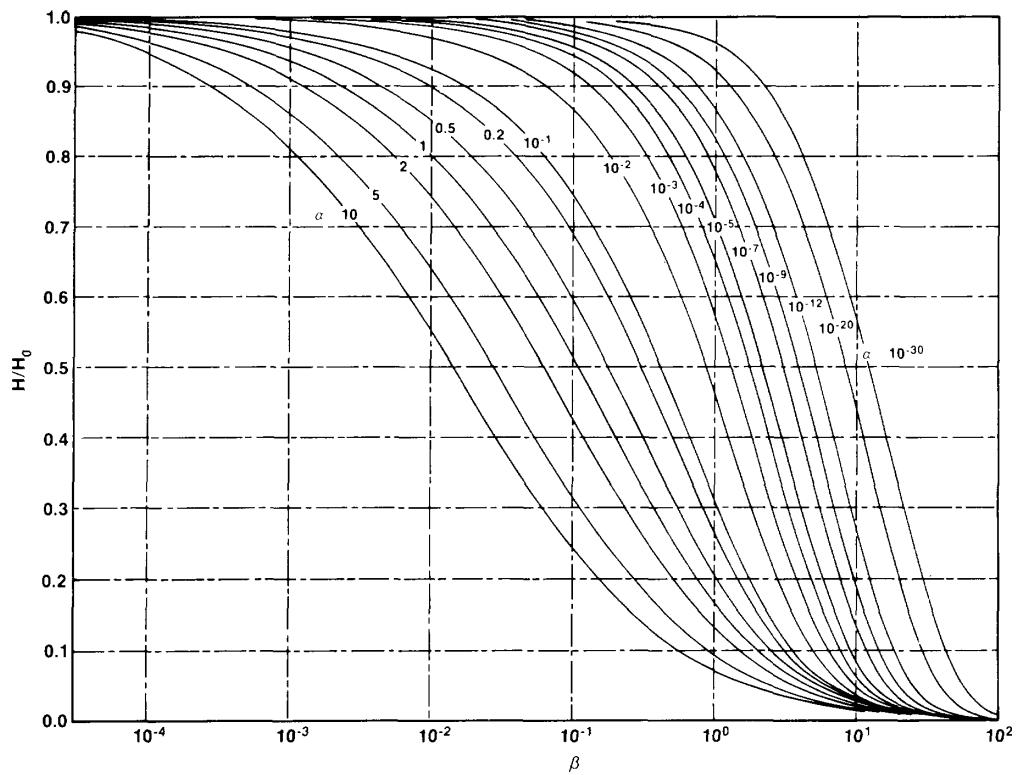
Figure B-1. Semilog Slug-Test Type Curves
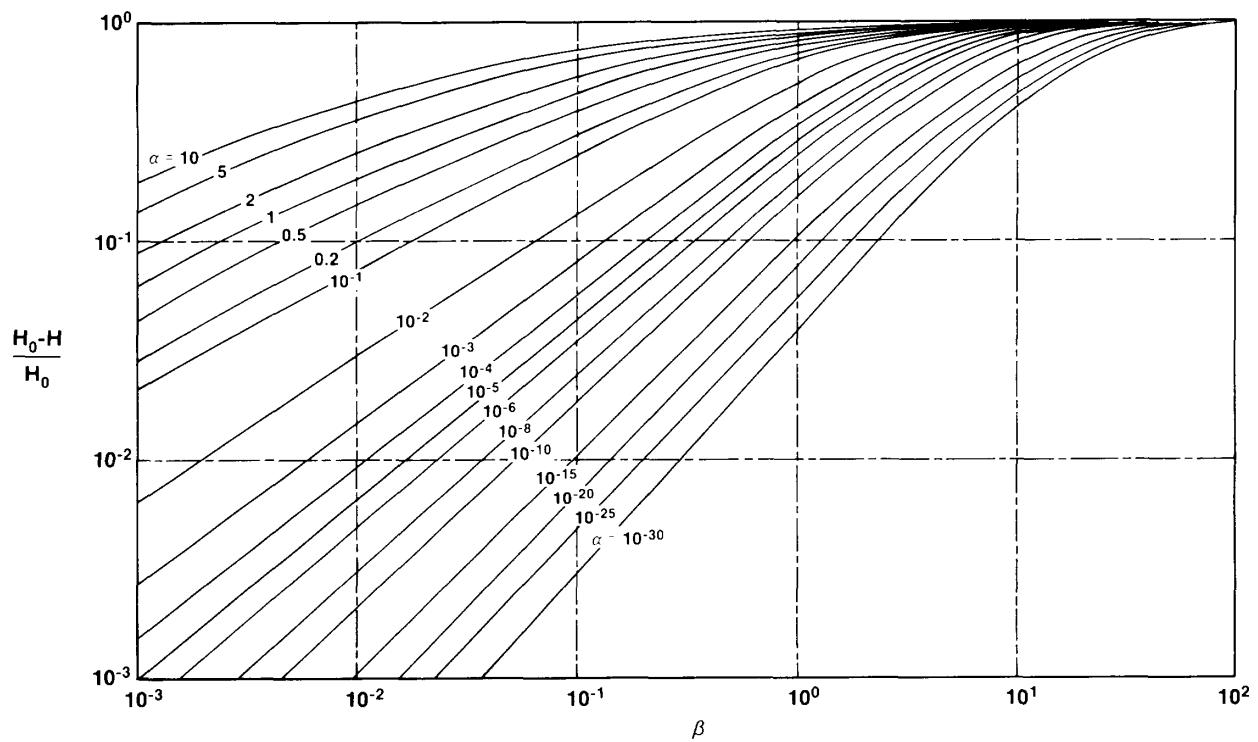
Figure B-2. Early-Time Log-Log Slug-Test Type Curves

t = time elapsed since test began, T

r_s = radius of borehole, L

r_c = inside radius of tubing string, L.

Plots of the quantities [H/H_o] and [(H_o-H)/H_o] versus t are made on semilog and log-log paper, respectively, of the same scale as the type curves. Semilog plotting and type curves are best used when a minimum of about seventy percent recovery has occurred. For lesser degrees of recovery, log-log plotting techniques provide a more definitive type-curve match (Ramey et al., 1975). The type curves are placed over the test-data plots and translated horizontally with the horizontal axes coincident until the best possible match between the data and one of the type curves is achieved. In this position an arbitrary match point is chosen, and the corresponding values of α and β are read from the type curve, and t is read from the data plot. The transmissivity (T) is then calculated from the following rearrangement of Eq (B-2), using the coordinates of the match point:

$$T = r_c^2 \, \beta/t \qquad \qquad \text{(B-4)}$$

B.2 PUMPING-TEST DATA ANALYSIS

Slightly different techniques are used for pumping-test data analysis, depending on whether the data are from the pumping well or from an observation well. Specifically, the pumping-well data analysis must include consideration of wellbore storage and skin, whereas observation-well data analysis may use simpler line-source solutions. Pumping-test data from either type of well may be analyzed with either single-porosity or double-porosity interpretation techniques, and with log-log and semilog plotting techniques. These techniques are described below. Ideally, drawdown and recovery data should be analyzed separately. Consistency of results between the drawdown and recovery analyses validates the conceptual model used.

B.2.1 Pumping-Well Data Analysis

Log-log and semilog techniques for analyzing pumping-well data from single- and double-porosity systems are discussed below.

B.2.1.1 Single-Porosity Log-Log Analysis. Single-porosity log-log analysis of drawdown and recovery data from a pumping well may be performed using a method presented by Gringarten et al. (1979) and modified to include the pressure-derivative technique of Bourdet et al. (1984). This method applies to both the drawdown and recovery during or after a constant-rate flow period of a well that fully penetrates a homogeneous, isotropic, horizontal, confined porous medium. When used to interpret a test performed in a heterogeneous, anisotropic aquifer, the method provides volumetrically averaged results.

Gringarten et al. (1979) constructed a family of log-log type curves of dimensionless pressure, p_D, versus a dimensionless time group defined as dimensionless time, t_D, divided by dimensionless wellbore storage, C_D, where:

$$p_D = \frac{kh}{141.2qB\mu} \, \Delta p \qquad \qquad \text{(B-5)}$$

$$t_D = \frac{0.000264 \, kt}{\phi \mu c_t r_w^2} \qquad \qquad \text{(B-6)}$$

$$C_D = \frac{0.8936\, C}{\phi c_t h r_w^2}$$

(B-7)

$$\frac{t_D}{C_D} = \frac{0.000295\, kht}{\mu C}$$

(B-8)

and:

k = permeability, millidarcies (md)
h = test interval thickness, ft
Δp = change in pressure, psi
q = flow rate, barrels/day (BPD)
B = formation volume factor (B = 1.0 in single-phase water reservoir)
μ = fluid viscosity, centipoises (cp)
t = elapsed time, hours
ϕ = porosity
c_t = total-system compressibility, 1/psi
r_w = wellbore radius, ft
C = wellbore storage coefficient, barrels/psi.

Each type curve in the family of curves (Figure B-3) is characterized by a distinct value of the parameter $C_D e^{2s}$, where:

s = skin factor.

A positive value of s indicates wellbore damage, or a wellbore with a lower permeability than the formation as a whole as a result of drilling effects such as drilling-mud invasion of the formation. A negative value of s indicates a wellbore with enhanced permeability, usually caused by one or more fractures intersecting the wellbore. High-permeability fractures in direct communication with a wellbore may act as additional production surfaces to the well in addition to the wellbore itself. Jenkins and Prentice (1982) term this type of wellbore-fracture system an "extended" well.

Earlougher (1977) relates skin factor to an "effective" wellbore radius (r_e) quantitatively by the following equation:

$$r_e = r_w e^{-s}$$

(B-9)

Eq (B-9) indicates that a well with a positive skin factor behaves hydraulically like a well with a smaller radius. Conversely, a well with a negative skin factor should behave like a well with a larger radius.

The type curves in Figure B-3 begin with an initial segment having a unit slope corresponding to early-time wellbore storage and skin effects. The duration of this unit slope segment is proportional to the amount of wellbore storage and skin that are present. At late time, the curves flatten as infinite-acting radial-flow effects dominate.

Bourdet et al. (1984) added the pressure derivative to the analytical procedure by constructing a family of type curves of the semilog slope of the dimensionless pressure response versus the same dimensionless time group, t_D/C_D. The semilog slope of the dimensionless pressure response is defined as:
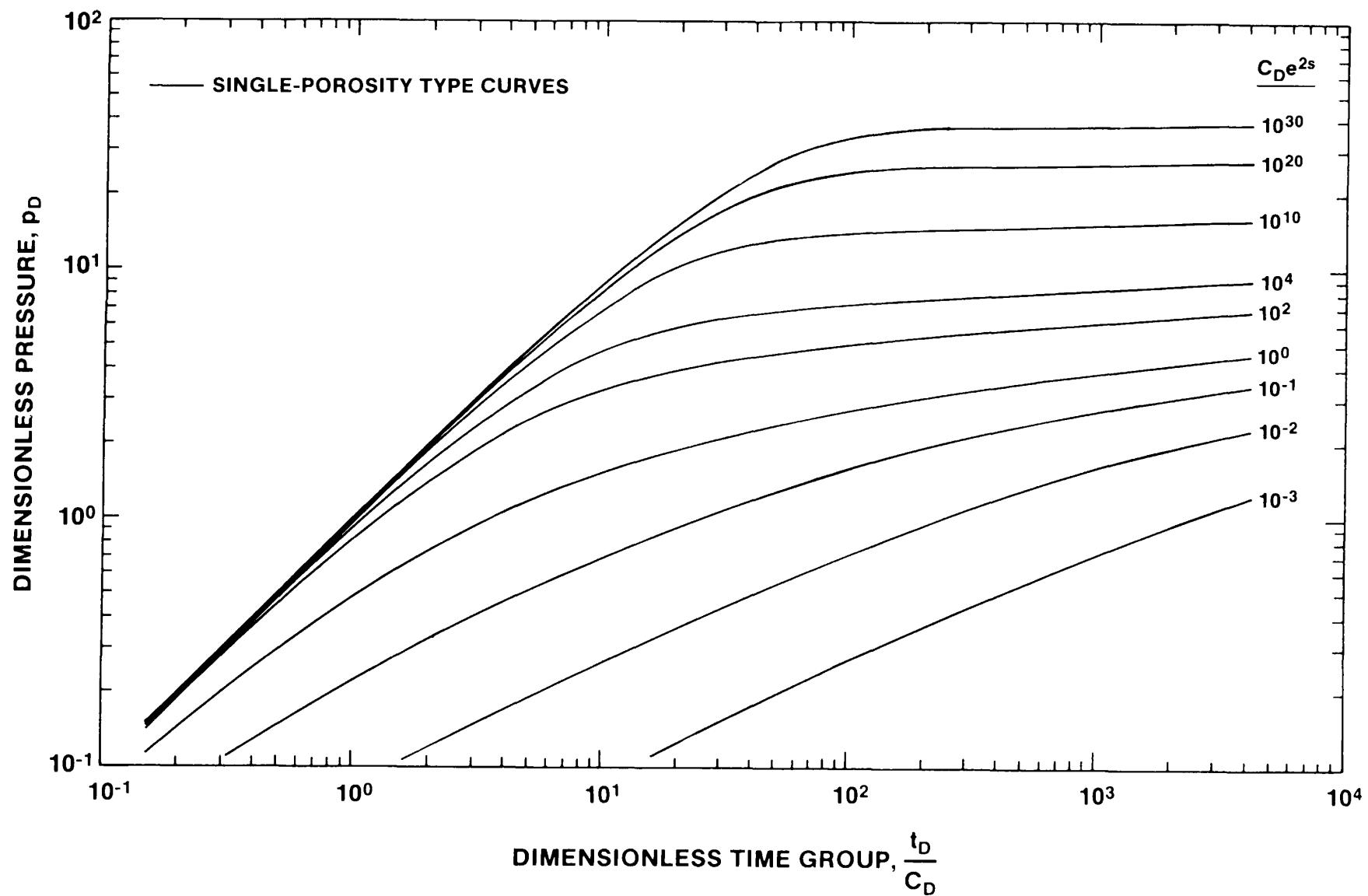
Figure B-3. Single-Porosity Type Curves for Wells with Wellbore Storage and Skin.

$$\frac{dp_D}{d\ln(t_D/C_D)} = \frac{t_D}{C_D}\frac{dp_D}{d(t_D/C_D)} = \frac{t_D}{C_D}\ p'_D \tag{B-10}$$

where: p'_D = dimensionless pressure derivative.

These curves are plotted on the same log-log graphs as the type curves of Gringarten et al. (1979), with the vertical axis now also labeled $(t_D/C_D)p'_D$ (Figure B-4). Again, each individual type curve is characterized by a distinct value of $C_D e^{2s}$. Pressure-derivative type curves begin with an initial segment with unit slope corresponding to early-time wellbore storage and skin effects. This segment reaches a maximum that is proportional to the amount of wellbore storage and skin, and then the curve declines and stabilizes at a dimensionless pressure/semilog slope value of 0.5 corresponding to late-time, infinite-acting, radial-flow effects.

Pressure-derivative data in combination with pressure data are much more sensitive indicators of double-porosity effects, boundary effects, nonstatic antecedent test conditions, and other phenomena than are pressure data alone. For this reason, pressure-derivative data are useful in choosing between conflicting phenomenological models that often cannot be differentiated on the basis of pressure data alone. Pressure-derivative data are also useful in determining when infinite-acting, radial-flow conditions occur during a test, because these conditions cause the pressure derivative to stabilize at a constant value.

For any given point, the pressure derivative is calculated as the linear-regression slope of a semilog line fit through that point and any chosen number of neighboring points on either side. The equation for the derivative follows:

$$p' = \frac{n\sum_{i=1}^{n}x_iy_i - \sum_{i=1}^{n}x_i\sum_{i=1}^{n}y_i}{n\sum_{i=1}^{n}x_i^2 - \sum_{i=1}^{n}x_i^2} \tag{B-11}$$

where, for a single constant-rate flow period:

n = number of points to be fitted
x_i = $\ln \Delta t_i$
y_i = Δp_i
Δt_i = elapsed test time at point i, hr
Δp_i = pressure change at Δt_i, psi.

For a multi-rate flow period or a recovery period, the time parameter is a superposition function calculated as:

$$x_i = \left\{ \sum_{i=1}^{n-1}(q_i - q_{i-1})\ \log\ \left[\left(\sum_{j=1}^{n-1}\Delta t_j\right) + \Delta t\right]\right\} + (q_n - q_{n-1})\ \log\ \Delta t \tag{B-12}$$
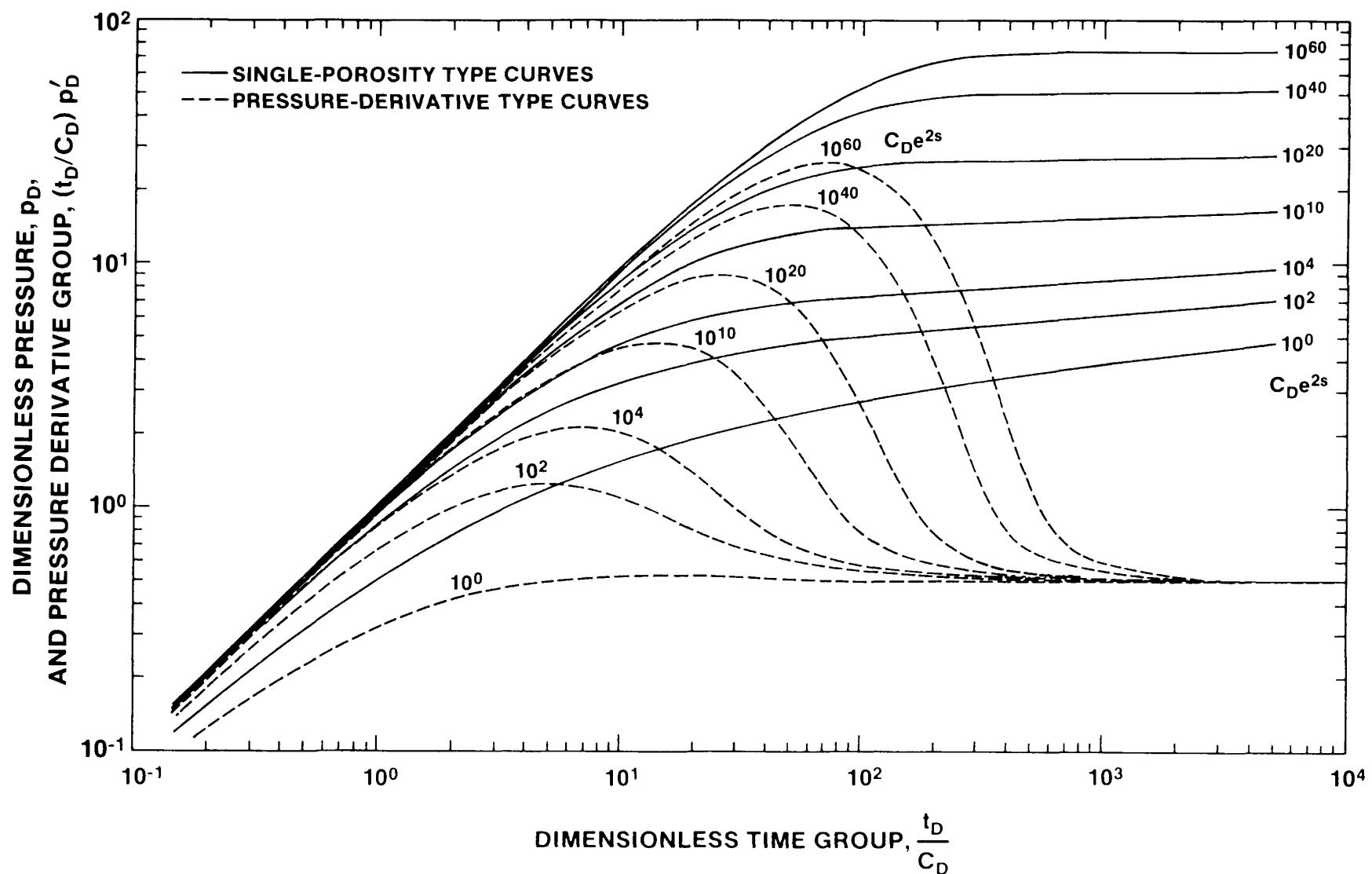
Figure B-4. Single-Porosity Type Curves and Pressure-Derivative Type Curves for Wells with Wellbore Storage and Skin.

where: q   = flowrate, BPD
         Δt = elapsed time during a flow period, hr

with subscripts:

         i   = individual flow period
         j   = individual flow period
         n   = number of flow periods considered.

In general, the fewer the number of points used in calculating the derivative, the more accurate it will be. Three-point derivatives, calculated using only the nearest neighbor on either side of a point, usually provide enough resolution to distinguish most important features. However, excessive noise in the data sometimes makes it necessary to use five- or seven-point derivatives, or various "windowing" procedures, to obtain a smooth curve. Unfortunately, this may also smooth out some of the features sought.

The type curves published by both Gringarten et al. (1979) and Bourdet et al. (1984) were derived for drawdown (flow-period) analysis. In general, the curves can also be used for recovery (buildup-period) analysis, so long as it is recognized that, at late time, recovery data will fall below the drawdown type curves because of superposition effects.

If the test analysis is to be done manually, the recovery data are plotted as *pressure change* since recovery began (Δp) versus *elapsed time* since recovery began (t) on log-log paper of the same scale as the type curves. The derivative of the pressure change is also plotted using the same vertical axis as the Δp data. The data plot is then laid over the type curves and moved both laterally and vertically, so long as the axes remain parallel, until a fit is achieved between the data and pressure and pressure-derivative curves with the same $C_D e^{2s}$ value. When the data fit the curves, an arbitrary match point is selected, and the coordinates of that point on both the data plot, t and Δp, and on the type-curve plot, p_D and t_D/C_D, are noted. The permeability-thickness product is then calculated from a rearrangement of Eq (B-5):

$$kh = 141.2qB\mu \, (p_D / \Delta p) \tag{B-13}$$

The groundwater-hydrology parameter transmissivity, T, is related to the permeability-thickness product by the following relationship, modified from Freeze and Cherry (1979):

$$T = kh\rho g/\mu \tag{B-14}$$

where: ρ = fluid density, M/L^3
         g   = gravitational acceleration, L/T^2
         μ = fluid viscosity, M/LT.

When T is given in ft^2/day, kh is given in millidarcy-feet, ρ is given in g/cm^3, g is set equal to 979.17 cm/s^2 (Barrows et al., 1983), and μ is given in centipoises, Eq (B-13) becomes:

$$T = 2.7393 \times 10^{-3} \, kh\rho/\mu \tag{B-15}$$

166

The wellbore storage coefficient is calculated from a rearrangement of Eq (B-8):

$$C = \frac{0.000295\,kht}{\mu t_D / C_D} \qquad \text{(B-16)}$$

Finally, if estimates of porosity and total-system compressibility are available, the skin factor can be calculated from the value of the $C_D e^{2s}$ curve selected and Eq (B-7):

$$s = 0.5 \ln \left[\frac{C_D e^{2s}}{0.8936 C / \phi c_t h r_w{}^2} \right] \qquad \text{(B-17)}$$

B.2.1.2 Double-Porosity Log-Log Analysis. Double-porosity media have two porosity sets that differ in terms of storage volume and permeability. Typically, the two porosity sets are (1) a fracture network with higher permeability and lower storage, and (2) the primary porosity of the rock matrix with lower permeability and higher storage. During a hydraulic test, these two porosity sets respond differently. With high-quality test data, the hydraulic parameters of both porosity sets can be quantified.

During a hydraulic test in a double-porosity medium, the fracture system responds first. Initially, most of the water pumped comes from the fractures, and the pressure in the fractures drops accordingly. With time, the matrix begins to supply water to the fractures, causing the fracture pressure to stabilize and the matrix pressure to drop. As the pressures in the fractures and matrix equalize, both systems produce water to the well. The total-system response is then observed for the balance of the test.

The initial fracture response and the final total-system response both follow the single-porosity type curves described above. By simultaneously fitting the fracture response and the total-system response to two different $C_D e^{2s}$ curves, fracture-system and total-system properties can be derived. Information on the matrix, and additional information on the fracture system, can be obtained by interpretation of the data from the transition period when the matrix begins to produce to the fractures. Two different sets of type curves can be used to try to fit the transition-period data.

Transition-period data are affected by the nature, or degree, of interconnection between the matrix and the fractures. Warren and Root (1963) published the first line-source solution for well tests in double-porosity systems. They assumed that flow from the matrix to the fractures (interporosity flow) occurred under *pseudosteady-state* conditions; that is, that the flow between the matrix and the fractures was directly proportional to the average head difference between those two systems. Other authors, such as Kazemi (1969) and de Swaan (1976), derived solutions using the diffusivity equation to govern interporosity flow. These are known as *transient* interporosity flow solutions. Mavor and Cinco-Ley (1979) added wellbore storage and skin to the double-porosity solution, but still used pseudosteady-state interporosity flow. Bourdet and Gringarten (1980) modified Mavor and Cinco-Ley's (1979) theory to include transient interporosity flow, and generated type curves for double-porosity systems with both pseudosteady-state and transient interporosity flow.

Pseudosteady-state and transient interporosity flow represent two extremes; all intermediate behaviors are also possible. Gringarten (1984), however, indicates that the majority of tests he has seen exhibit pseudosteady-state interporosity flow behavior.

In recent years, Gringarten (1984, 1986) has suggested that the terms "restricted" and "unrestricted" interporosity flow replace the terms "pseudosteady-state" and "transient" interporosity flow. He believes that all interporosity flow is transient in the sense that it is governed by the diffusivity equation. But in the case where the fractures possess a positive skin similar to a wellbore skin (caused, for example, by secondary mineralization on the fracture surfaces) that restricts the flow from the matrix to the fractures, the observed behavior is similar to that described by the pseudosteady-state formulation (Moench, 1984; Cinco-Ley et al., 1985). "Transient" interporosity flow is observed when there are no such restrictions. Hence, the terms "restricted" and "unrestricted" more accurately describe conditions than do the terms "pseudosteady-state" and "transient." The recent terminology of Gringarten is followed in this report.

Restricted Interporosity Flow

Warren and Root (1963) defined two parameters to aid in characterizing double-porosity behavior. These are the storativity ratio, ω, and the interporosity flow coefficient, λ. The storativity ratio is defined as:

$$\omega = \frac{(\phi V c_t)_f}{(\phi V c_t)_{f+m}}$$

(B-18)

where: ϕ = ratio of the pore volume in the system to the total-system volume
         V = the ratio of the total volume of one system to the bulk volume
         c_t = total compressibility of the system

with subscripts:

         f   = fracture system
         m   = matrix.

The interporosity flow coefficient is defined as:

$$\lambda = \alpha r_w^2 (k_m/k_f)$$

(B-19)

where α is a shape factor characteristic of the geometry of the system and other terms are as defined above.

The shape factor, α, is defined as:

$$\alpha = \frac{4n (n + 2)}{\ell^2}$$

(B-20)

where: n = number of normal sets of planes limiting the matrix
         ℓ = characteristic dimension of a matrix block (ft).

168

Bourdet and Gringarten (1980) constructed a family of transition type curves for restricted interporosity flow on the same axes as the C_De^{2s} curves of Gringarten et al. (1979), with each transition curve characterized by a distinct value of the parameter λe^{-2s}. Together, the single-porosity type curves and the transition type curves make up the double-porosity type curves (Figure B-5).

In manual double-porosity type-curve matching, a log-log plot of the data is prepared as in single-porosity type-curve matching. The data plot is then laid over the double-porosity type curves and moved both laterally and vertically, so long as the axes remain parallel, until (1) the early-time (fracture flow only) data fall on one C_De^{2s} curve, (2) the middle portion of the transition data falls on a λe^{-2s} curve, and (3) the late-time (total-system) data fall on a lower C_De^{2s} curve. In computer-aided analysis, pressure-derivative curves for double-porosity systems may also be prepared (Gringarten, 1986). The number of possible curve combinations, however, precludes preparation of generic pressure-derivative curves for manual double-porosity curve fitting.

When a fit of the data plot to the type curves is achieved, an arbitrary match point is selected, and the coordinates of that point on both the data plot, t and Δp, and the type-curve plot, t_D/C_D and p_D, are noted. The values of C_De^{2s} and λe^{-2s} of the matched curves are also noted. The permeability-thickness product of the fracture system (and also of the total system because fracture permeability dominates) and the wellbore storage coefficient are calculated from Eqs (B-13) and (B-16). The storativity ratio, ω, is calculated from:

$$\omega = \frac{(C_De^{2s})_{f+m}}{(C_De^{2s})_f}$$

(B-21)

The dimensionless wellbore storage coefficient for the matrix is calculated as:

$$(C_D)_m = \frac{0.8936\ C}{(V\phi c_t)_m hr_w^2}$$

(B-22)

This leads to the dimensionless wellbore storage coefficient for the total system:

$$(C_D)_{f+m} = (C_D)_m \times (1 - \omega)$$

(B-23)

Then the skin factor is calculated as:

$$s = 0.5\ \ln\left[\frac{(C_De^{2s})_{f+m}}{(C_D)_{f+m}}\right]$$

(B-24)

The interporosity flow coefficient is calculated from:

$$\lambda = (\lambda e^{-2s})/(e^{-2s})$$

(B-25)
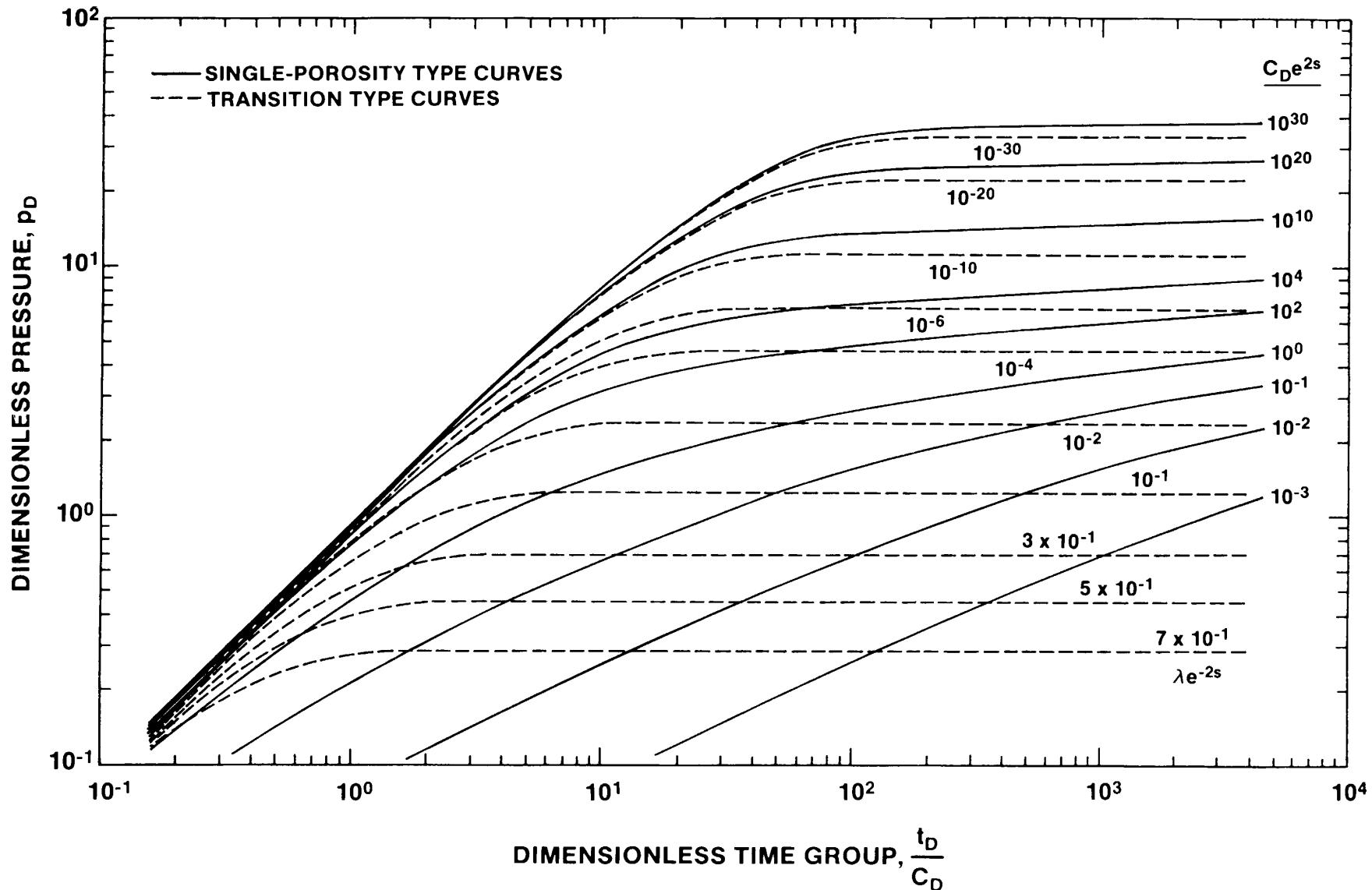
Figure B-5. Double-Porosity Type Curves for Wells with Wellbore Storage, Skin, and Restricted Interporosity Flow.

If matrix permeability and geometry are known independently, Eqs (B-19) and (B-20) can be used to determine the effective dimensions of the matrix blocks.

Unrestricted Interporosity Flow

Matrix geometry is more important for unrestricted interporosity flow than for restricted interporosity flow, because the former is governed by the diffusivity equation. A different set of type curves is used, therefore, to match transition-period data when unrestricted interporosity flow conditions exist (Figure B-6). Bourdet and Gringarten (1980) characterize each curve with a different value of the parameter β, the exact definition of which is a function of the matrix geometry. For example, for slab-shaped matrix blocks, they give:

$$\beta = \frac{6}{\gamma^2} \; \frac{(C_D e^{2s})_{f+m}}{\lambda e^{-2s}} \tag{B-26}$$

and for spherical blocks they give:

$$\beta = \frac{10}{3\gamma^2} \; \frac{(C_D e^{2s})_{f+m}}{\lambda e^{-2s}} \tag{B-27}$$

where: γ = exponential of Euler's constant (= 1.781).

Moench (1984) provides an extensive discussion on the effects of matrix geometry on unrestricted interporosity flow.

Manual double-porosity type-curve matching with unrestricted-interporosity-flow transition curves is performed in exactly the same manner as with restricted-interporosity-flow transition curves, described above. The same equations are used to derive the fracture and matrix parameters, except that the matrix geometry must now be known or assumed to obtain the interporosity flow coefficient, λ, from rearrangement of Eq (B-26) or (B-27).

B.2.1.3 Semilog Analysis.
Two semilog plotting techniques are commonly employed in the interpretation of hydraulic-test data. These produce a Horner plot and a dimensionless Horner plot.

Horner Plot

Horner (1951) provided a method of obtaining permeability and static formation pressure values independent of log-log type-curve matching, although the two methods are best used in conjunction. Horner's method applies to the recovery of the pressure after a constant-rate flow period in a well that fully penetrates a homogeneous, isotropic, horizontal, infinite, confined, single-porosity or double-porosity reservoir. For a recovery after a single flow period, Horner's solution is:

$$p(t) = p^* - \frac{162.6qB\mu}{kh} \; \log \left[\frac{t_p + dt}{dt} \right] \tag{B-28}$$

where: $p(t)$ = pressure at time t, psi
    p^* = static formation pressure, psi
    t_p = duration of previous flow period, hr
 dt = time elapsed since end of flow period, hr
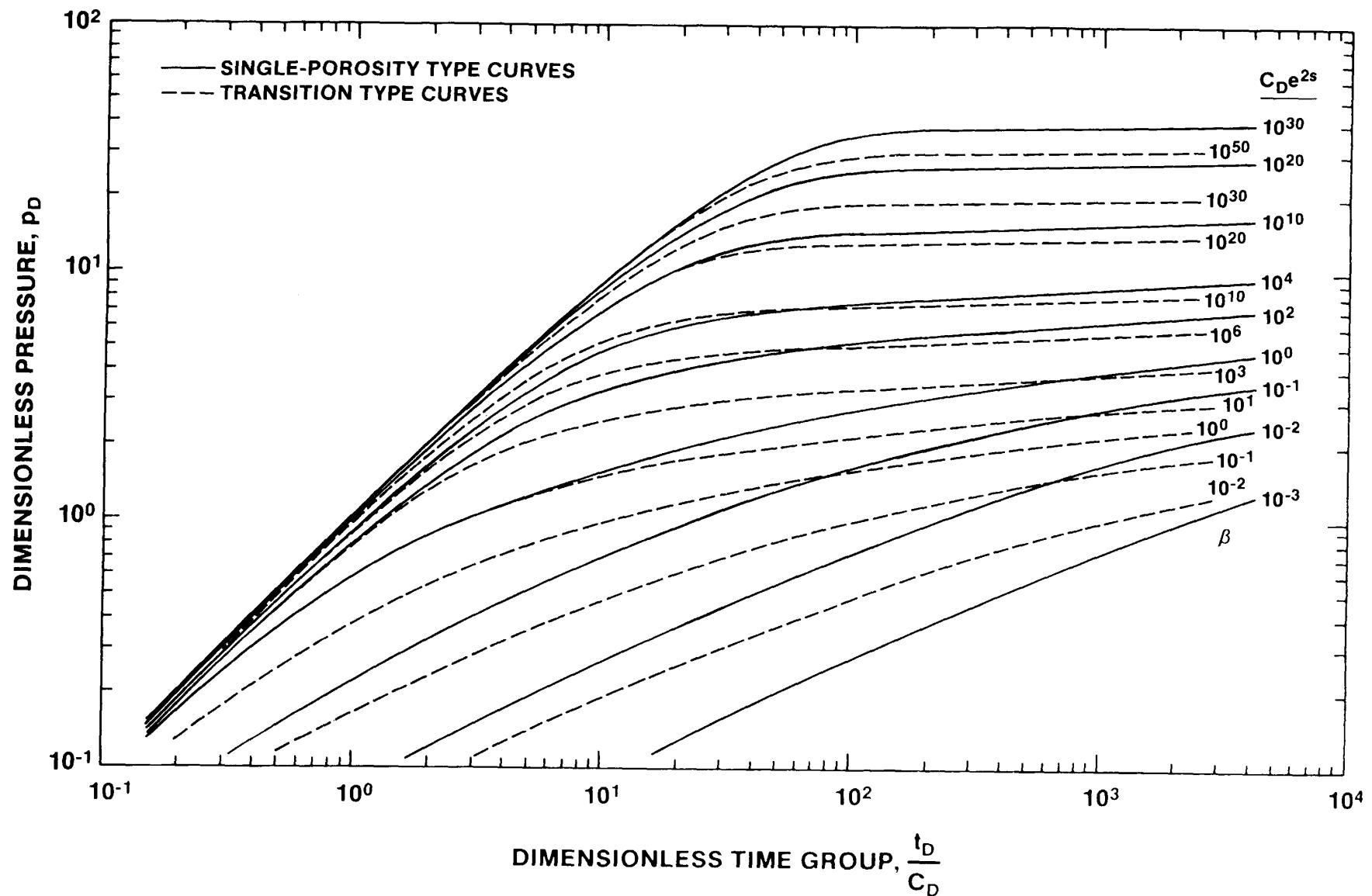
Figure B-6. Double-Porosity Type Curves for Wells with Wellbore Storage, Skin, and Unrestricted Interporosity Flow.

and other terms are as defined above under Eq (B-8). For a recovery after multiple flow periods, the time group in Eq (B-28) is replaced by the superposition function given in the right-hand side of Eq (B-12).

The permeability-thickness product (kh) is obtained by (1) plotting p(t) versus log $[(t_p + dt)/dt]$ (or the superposition function), (2) drawing a straight line through the data determined from the log-log pressure-derivative plot to be representative of infinite-acting radial flow, and (3) measuring the change in p(t) on this line over one log cycle of time (m). Equation (B-28) can then be rearranged and reduced to:

$$kh = 162.6 \, qB\mu/m \tag{B-29}$$

Static formation pressure is estimated by extrapolating the radial-flow straight line to the pressure axis where log $[(t_p + dt)/dt] = 1$, representing infinite recovery time. In the absence of reservoir boundaries, the pressure intercept at that time should equal the static formation pressure.

Dimensionless Horner Plot
The dimensionless Horner plot represents a second useful semilog approach to hydraulic-test interpretation. Once type-curve and match-point selections have been made through log-log analysis, this technique allows the single- or double-porosity $C_D e^{2s}$ type curves to be superimposed on a normalized semilog plot of the data. Logarithmic dimensionless times for the data are calculated using:

$$\frac{q_{n-1} - q_n}{|q_{n-1} - q_n|} \left[\sum_{i=1}^{n-1} \frac{q_i - q_{i-1}}{q_{n-1} - q_n} \log \left(\sum_{j=i}^{n-1} \Delta t_j + \Delta t \right) - \log \Delta t \right] \tag{B-30}$$

where all parameters are as defined above. The dimensionless times calculated using Eq (B-30) are plotted on a linear scale. Dimensionless pressures for the data are calculated using:

$$\frac{p_D}{\Delta p} \, [p^* - p(t)] \tag{B-31}$$

where p_D and Δp are the log-log match-point coordinates, and the other parameters are as defined above. Dimensionless pressures are also plotted on a linear scale.

The type curves are plotted on the same axes with dimensionless time defined as:

$$\frac{q_{n-1} - q_n}{|q_{n-1} - q_n|} \left[\sum_{i=1}^{n-1} \frac{q_1 - q_{i-1}}{q_n - q_{n-1}} \, p_D \left(\sum_{j=1}^{n-1} \Delta t_j + \Delta t \right) - \log \Delta t \right] \tag{B-32}$$

and dimensionless pressure defined as:

173

$$\frac{q_{n-1} - q_n}{|q_{n-1} - q_n|} \left[\sum_{i=1}^{n-1} \frac{q_i - q_{i-1}}{q_n - q_{n-1}} \log \left(\sum_{j=1}^{n-1} \Delta t_j + \Delta t \right)_D - p_D (\Delta t)_D \right]$$ (B-33)

The dimensionless Horner plot is a very sensitive indicator of inaccuracies in type-curve, match-point, and static-formation-pressure selections (Gringarten, 1986). By iterating between dimensionless Horner and log-log plots, very accurate hydraulic parameters can be obtained.

B.2.2 Observation-Well Data Analysis

Both log-log and semilog techniques can be used to analyze observation-well pumping-test data from single- and double-porosity systems. Log-log techniques are discussed below. The semilog techniques discussed in Section B.2.1.3 for pumping-well data can also be applied to observation-well data.

B.2.2.1 Single-Porosity Log-Log Analysis.
For observation wells monitored during pumping tests in single-porosity media, the drawdown and recovery data can be analyzed using a method first described by Theis (1935). Theis (1935) created a log-log drawdown type curve of p_D versus t_D/r_D^2 (Figure B-7) using an exponential integral (Ei) solution for drawdown caused by a line-source well in a porous medium:

$$p_D = -0.5 \, \text{Ei} \, (-r_D^2/4t_D)$$ (B-34)

where:
$$\frac{t_D}{r_D^2} = \frac{0.000264 \, kht}{\phi \mu c_t h r^2}$$ (B-35)

$$r_D = r/r_w$$ (B-36)

r = radial distance to pumping well, ft

The terms p_D and t_D are defined by Eqs (B-5) and (B-6), respectively; other terms are as defined above in Section B.2.1.1. This type curve applies to the analysis of drawdown at both pumping wells (assuming no wellbore storage) and observation wells.

Elapsed pumping time (t) and drawdown (Δp) are plotted on log-log paper of the same scale as the type curve. The observed data are matched to the line-source type curve, thus defining a match point. The two sets of coordinates of that point, t and Δp, and t_D/r_D^2 and p_D, are used with Eq (B-13) and the following rearrangement of Eq (B-35) to calculate the permeability-thickness product and the porosity-compressibility-thickness product, respectively:

$$\phi c_t h = \frac{0.000264 \, kht}{\mu r^2} \frac{r_D^2}{t_D}$$ (B-37)

174
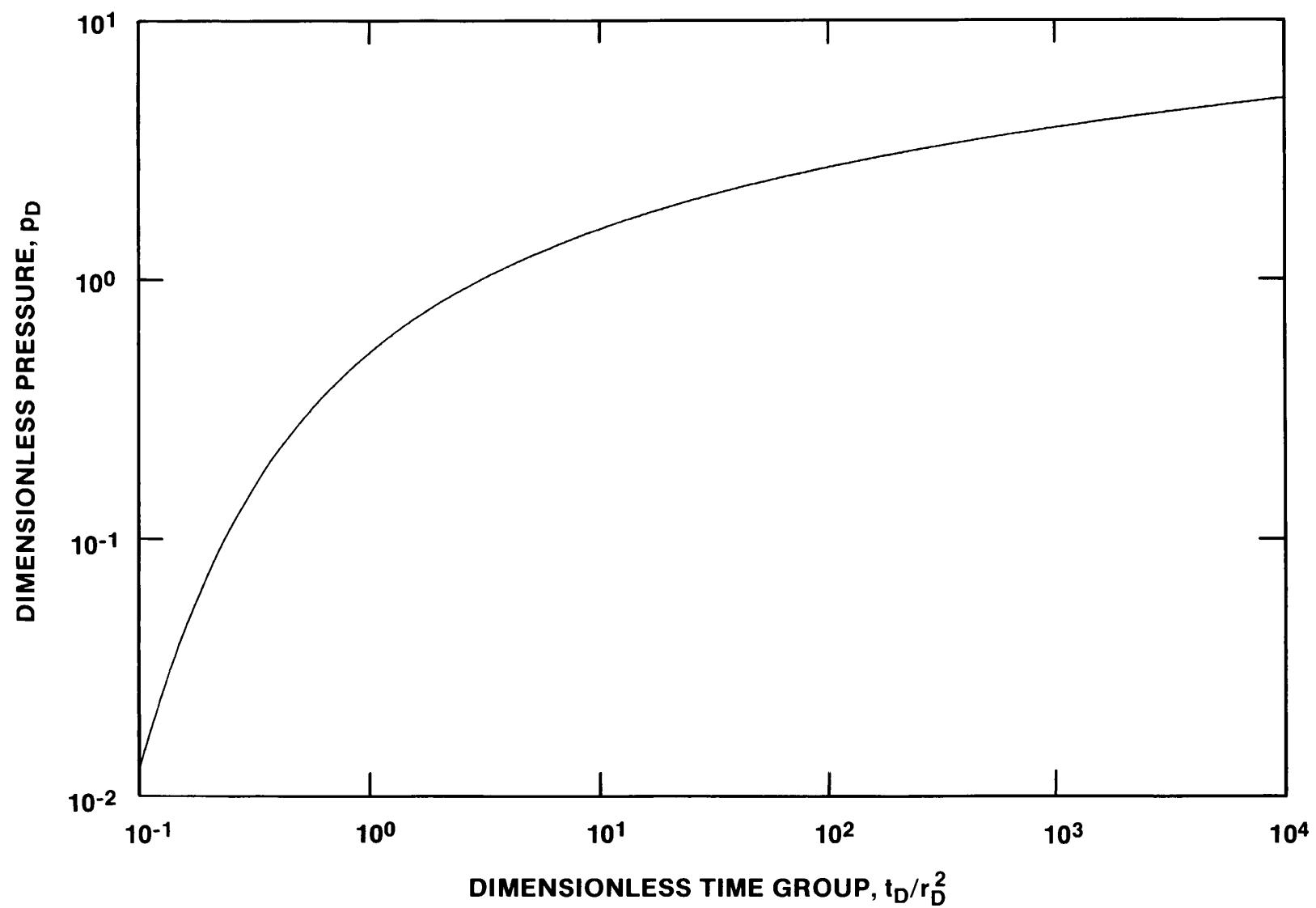
Figure B-7. Theis Line-Source-Solution Type Curve.

The permeability-thickness product is related to transmissivity through Eqs (B-14) and (B-15). Narasimhan and Kanehiro (1980) give the relationship between the porosity-compressibility-thickness product and the groundwater-hydrology parameter storativity, S, in consistent units as:

$$S = \phi c_t h \rho g \qquad\qquad (B\text{-}38)$$

When total compressibility, c_t, is in units of 1/psi, thickness, h, is in units of ft, fluid density, ρ, is in units of g/cm^3, and gravitational acceleration, g, is set equal to 979.17 cm/s^2 (Barrows et al., 1983), Eq (B-38) becomes:

$$S = 0.4329\ \phi c_t h \rho \qquad\qquad (B\text{-}39)$$

B.2.2.2 Double-Porosity Log-Log Analysis. Deruyck et al. (1982) extended the use of Theis' (1935) line-source solution to observation wells in double-porosity systems. In a double-porosity system, both the initial fracture response to a pumping test and the final total-system response should follow Theis curves. Deruyck et al. (1982) created a family of Theis curves of p_D versus t_D/r_D^2 separated along the time axis by different values of the storativity ratio, ω (Figures B-8 and B-9). Values of p_D on the pressure axis are as defined by Eq (B-34). Values of the dimensionless time group, t_D/r_D^2, can be cast in terms of either the fracture system or the total system using:

$$\left[\frac{t_D}{r_D^2}\right]_{for\ f+m} = \frac{0.000264\ kht}{\mu hr^2\ (\phi V c_t)_{for\ f+m}} \qquad\qquad (B\text{-}40)$$

If the time axis is defined in terms of the fracture system, as shown in Figures B-8 and B-9, the left-most Theis curve occupies the same position as the single-porosity Theis curve in Figure B-7. This curve represents the fracture system while one of the Theis curves propagating to the right will represent the total system, depending on the value of the storativity ratio in any particular instance. If the time axis is defined in terms of the total system, as implemented in INTERPRET, the right-most Theis curve will occupy the same position as the single-porosity Theis curve in Figure B-7. In this case, this curve will represent the total system, while the fracture system will be represented by one of a family of curves propagating to the left.

By simultaneously fitting the fracture response and the total-system response to two different Theis curves, the transmissivity of the total system and the storativities of both the fractures and total system can be derived. The permeability-thickness product can be determined using the match-point coordinates and Eq (B-13). The porosity-compressibility-thickness product is determined using Eq (B-37) for whichever system the dimensionless time group is defined. The porosity-compressibility-thickness product of the other system is determined by multiplying (to obtain $[\phi c_t h]_f$) or dividing (to obtain $[\phi c_t h]_{f+m}$) by the storativity ratio.

Information on the matrix can be obtained by interpretation of the data from the transition period when the matrix begins to produce to the fractures. Type curves for both restricted and unrestricted interporosity flow can be used to try to fit the transition-period data. For restricted interporosity flow, Deruyck et al. (1982) defined a family of transition curves characterized by distinct values of the parameter λr_D^2. These transition curves are shown in Figure B-8. For unrestricted interporosity flow, the transition curves are characterized by values of the parameter
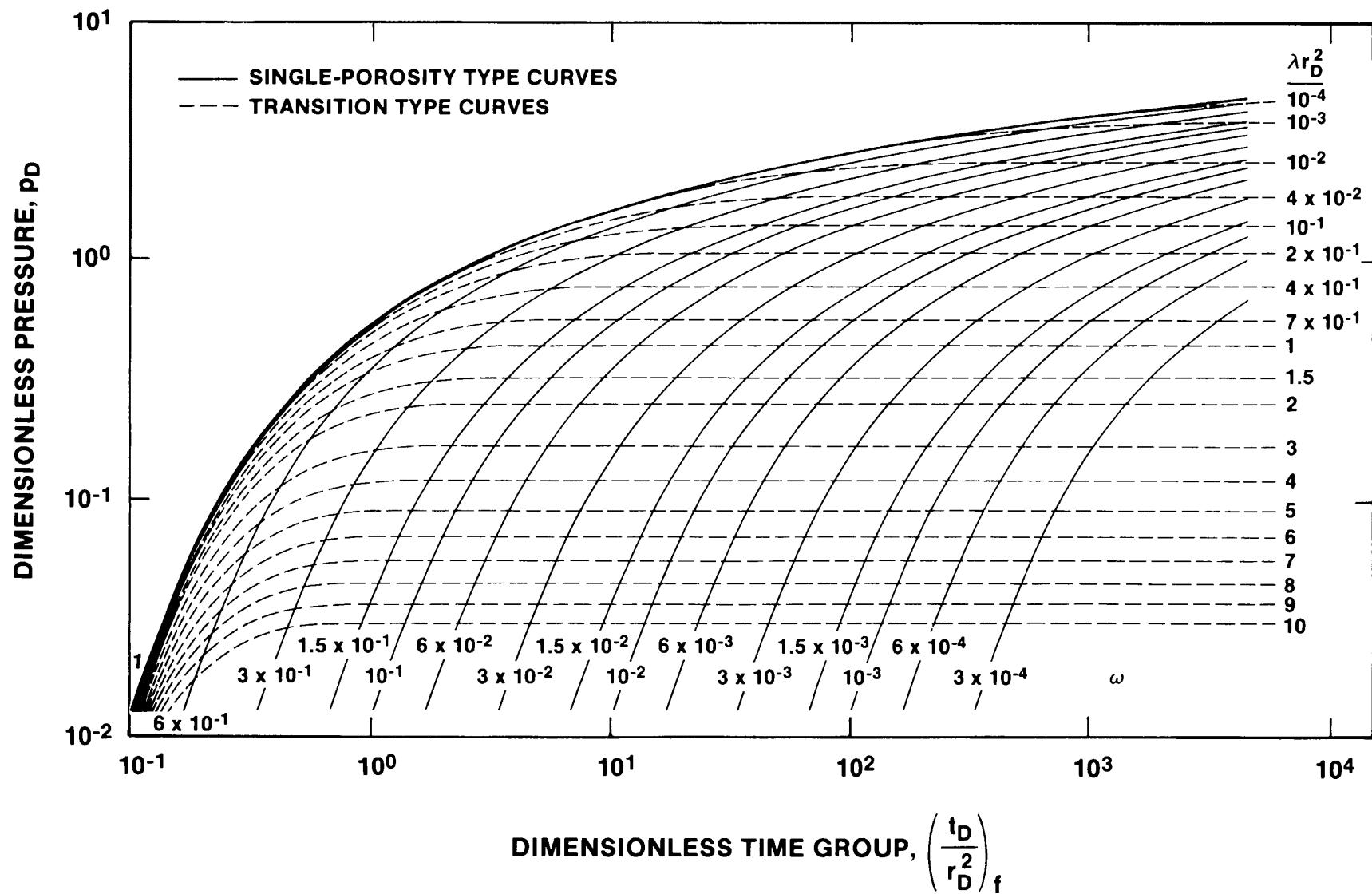
Figure B-8. Double-Porosity Line-Source-Solution Type Curves for Aquifers with Restricted Interporosity Flow.
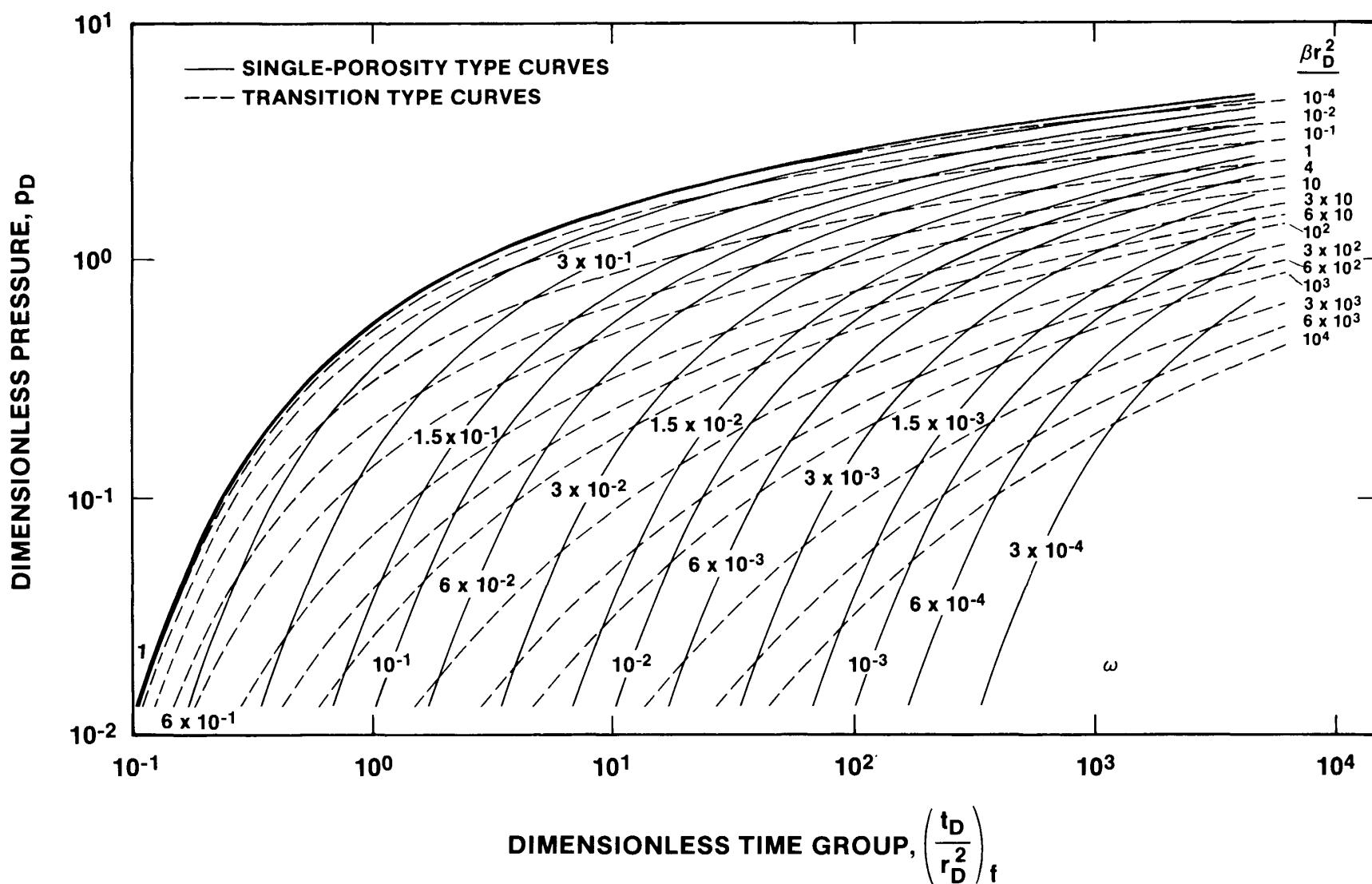
Figure B-9. Double-Porosity Line-Source-Solution Type Curves for Aquifers with Unrestricted Interporosity Flow.

$\beta r_D{}^2$, whose definition depends on matrix geometry. For a double-porosity medium with slab-shaped matrix blocks, Deruyck et al. (1982) give:

$$\beta r_D{}^2 = \frac{1}{3} \frac{\lambda}{\omega} \left[\frac{r}{r_\omega} \right]^2 \qquad \text{(B-41)}$$

and for spherical blocks they give:

$$\beta r_D{}^2 = \frac{3}{5} \frac{\lambda}{\omega} \left[\frac{r}{r_\omega} \right]^2 \qquad \text{(B-42)}$$

Transition curves for unrestricted interporosity flow are shown in Figure B-9. Once a match between data and the Theis and transition curves has been made, the interporosity flow coefficient, λ, can be determined. If matrix permeability and geometry are known independently, Eqs (B-19) and (B-20) can be used to determine the effective dimensions of the matrix blocks.

Transition from fracture-only to total-system behavior occurs at an earlier stage of the total-system response as the value of either $\lambda r_D{}^2$ or $\beta r_D{}^2$ increases. Thus, because of the inclusion within these parameters of a distance term, fracture and transition responses become less evident with increasing distance from the pumping well. When an observation well is sufficiently far from the pumping well that only total-system behavior can be resolved, use of the single-porosity interpretation techniques discussed in Section B.2.2.1 is justified. Generally, observable double-porosity responses are limited to a maximum distance of hundreds to perhaps a few thousands of feet from the pumping well.

B.3 INTERPRET WELL-TEST INTERPRETATION CODE

Manual type-curve fitting is a time-consuming process limited by the published type curves available, and by the degree of resolution/differentiation obtainable in manual curve fitting. The analyses presented in this report were not performed manually but by using the well-test analysis code INTERPRET developed by A.C. Gringarten and Scientific Software-Intercomp (SSI). INTERPRET is a proprietary code that uses analytical solutions. It can be leased from SSI.

INTERPRET can analyze drawdown (flow) and recovery (buildup) tests in single-porosity, double-porosity, and fractured media. For pumping-test data analysis, it incorporates the analytical techniques discussed above, and additional techniques discussed in Gringarten et al. (1974), Bourdet and Gringarten (1980), and Gringarten (1984). Rather than relying on a finite number of drawdown type curves, INTERPRET calculates the precise drawdown or recovery type curve corresponding to the match point and data point selected by the user. For interpretation of observation-well data, the INTERPRET code uses the line-source solution of Theis (1935) for single-porosity analyses, and the technique of Deruyck et al. (1982) for double-porosity analyses.

After type-curve selection, INTERPRET simulates the test with the chosen parameters so that the user can see how good the match truly is. Through an iterative parameter-adjustment process, the user fine-tunes the simulation until satisfied with the results. Log-log, semilog (Horner and dimensionless Horner), and linear-linear plotting techniques are all employed to ensure consistency of the final model with the data in every respect. Once the final model is selected, INTERPRET carries out all necessary calculations and provides final parameter values. Analyses obtained using INTERPRET have been verified by manual checks.

In addition to standard type-curve analysis, INTERPRET allows the incorporation of constant-pressure and no-flow boundaries in analysis, using the theory of superposition and image wells discussed by Ferris et al. (1972) and others. A constant-pressure boundary can be simulated by adding a recharge (image) well to the model. A no-flow boundary can be simulated by adding a discharge (image) well to the model. Drawdowns/rises from multiple discharge/recharge wells are additive. In INTERPRET, an image well (either discharge or recharge) is included by specifying a dimensionless distance for the image well from the pumping or observation well, and by using the line-source solution of Theis (1935; see Section B.2.2.1) to calculate the drawdown or recovery caused by that well at the well under consideration. In the case of a pumping well, the dimensionless distance to the image well is related to the "actual" distance to the image well, r_i, by the following:

$$r_i = r_w \sqrt{C_D D_D} \tag{B-43}$$

where: D_D = dimensionless distance

and other terms are as defined above. The actual hydraulic boundary is then half of the distance to the image well from the pumping well.

Defining distances to hydraulic boundaries from observation-well data is more complex. The dimensionless distance to the image well is related to the "actual" distance to the image well, r_i, by the following:

$$r_i = r \sqrt{D_D} \tag{B-44}$$

The hydraulic boundary is then tangential to a circle having radius r_i centered midway between the pumping well and the observation well. Data from three or more observation wells are required to define the location and orientation of this boundary precisely.

180

APPENDIX C

DOUBLE-POROSITY INTERPRETATION OF THE DOE-1 RESPONSE TO THE H-3 MULTIPAD PUMPING TEST

DOUBLE-POROSITY INTERPRETATION OF THE DOE-1 RESPONSE TO THE H-3 MULTIPAD PUMPING TEST

The DOE-1 response to the H-3 multipad pumping test was originally interpreted by Beauheim (1987a). After correcting the data for a 0.27 psi/15 days pre-existing rising trend, he fit a single-porosity simulation to the data that matched the total amount of drawdown and the time at which recovery began (Figure C-1). The simulation predicted recovery would be more rapid than was observed. Beauheim (1987a) attributed this discrepancy to his having used a linear compensation for the pretest trend which, if the trend decayed with time, would give the appearance of less recovery than actually occurred at late time. Beauheim (1987a) interpreted an apparent transmissivity of 5.5 ft^2/day and an apparent storativity of 1.0 x 10^{-5} from his analysis.

After the interpretation of the DOE-1 response to the H-11 multipad pumping test showed apparent double-porosity behavior (Section 6.3.4), the DOE-1 data from the H-3 multipad test were re-examined. This re-examination showed that a double-porosity model with a no-flow boundary could produce a better fit to the data than the single-porosity model presented by Beauheim (1987a). Figure C-2 shows a log-log plot of the DOE-1 drawdown data with a bounded double-porosity simulation. The simulation uses spherical matrix blocks, unrestricted interporosity flow, an apparent transmissivity of 5.8 ft^2/day, an apparent total-system storativity of 1.1 x 10^{-5}, a storativity ratio of 0.05, and a no-flow boundary at a dimensionless distance of eight. The no-flow boundary corresponds to an image discharge well about 15,000 ft from DOE-1.

Figure C-3 shows a dimensionless Horner plot of the DOE-1 drawdown data with a simulation derived from the model discussed above. The data and simulation are in excellent agreement throughout the drawdown period. Figure C-4 shows a linear-linear plot of the DOE-1 drawdown and recovery data and simulation. This simulation fits the entire data record, particularly during recovery, much better than does the single-porosity simulation shown in Figure C-1. (Note that the last eight data points on Figures C-1 and C-4 reflect a malfunction in the DAS, not the real pressure response.) Figure C-5 shows a dimensionless Horner plot of the DOE-1 recovery data and simulation. Again, the agreement between the data and the simulation is excellent.

The no-flow boundary included in the double-porosity model may be partially an artifact of the pretest-trend compensation. The boundary tends to slow recovery, just as an overcompensation for the pretest trend would do. If less of a compensation for the trend were made, the optimal distance for the boundary from DOE-1 would increase. In any case, the boundary as modelled was not felt until late in the drawdown period, by which time the match between the data and simulation was already well established. Thus, regardless of the "best" location for the boundary, the values derived for apparent transmissivity and storativity are reliable.

In summary, the response of DOE-1 to the H-3 multipad test can be better simulated using a bounded double-porosity model than by the unbounded single-porosity model presented by Beauheim (1987a). The interpreted hydraulic parameters differ by only five to ten percent between the two models. Use of the double-porosity model is consistent with interpretations of a pumping test at DOE-1 (Beauheim, 1987c) and of the response of DOE-1 to the H-11 multipad test (Section 6.3.4).
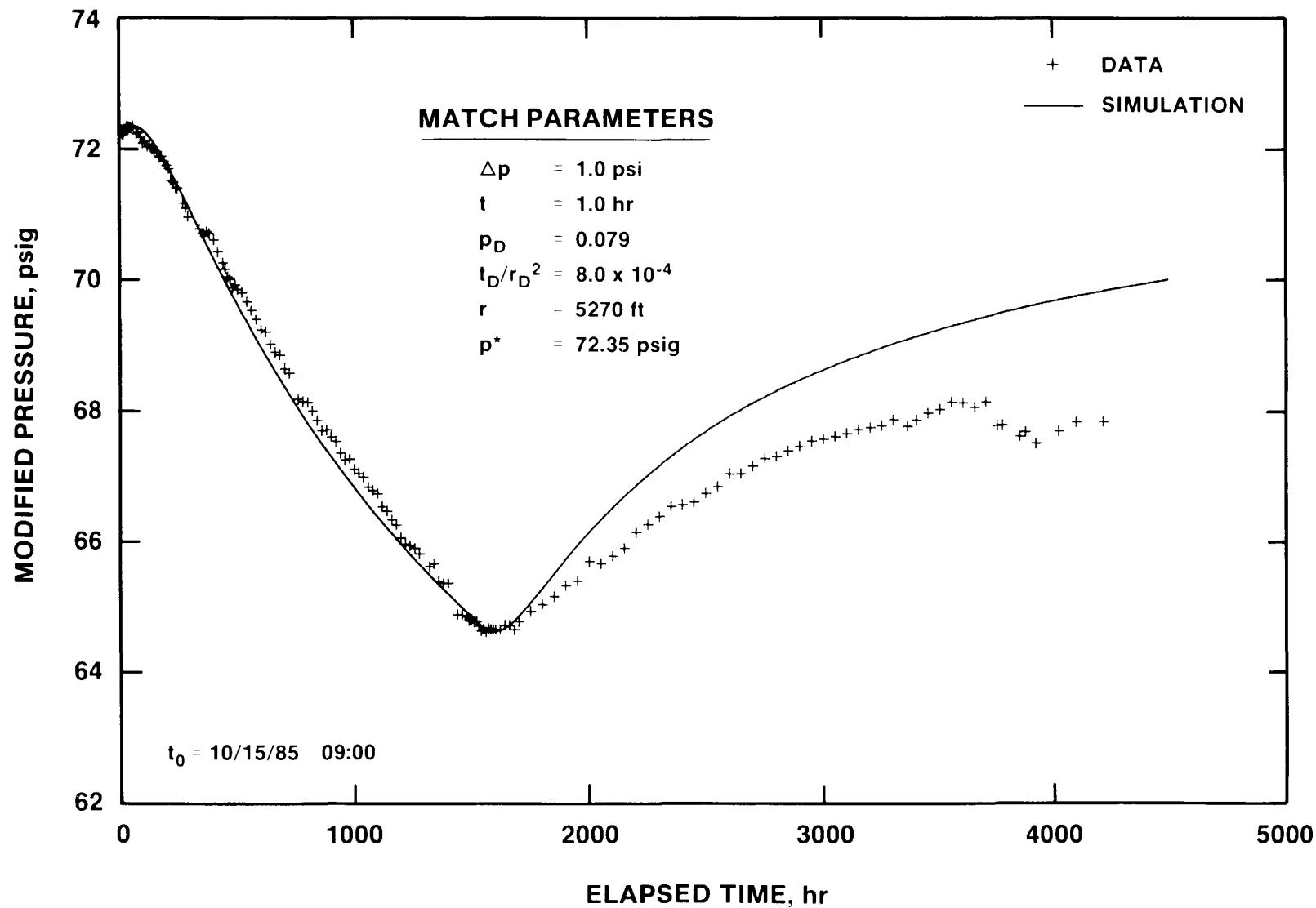
Figure C-1.   Linear-Linear Plot of DOE-1 Response During the H-3 Multipad Pumping Test with an Unbounded Single-Porosity Simulation.
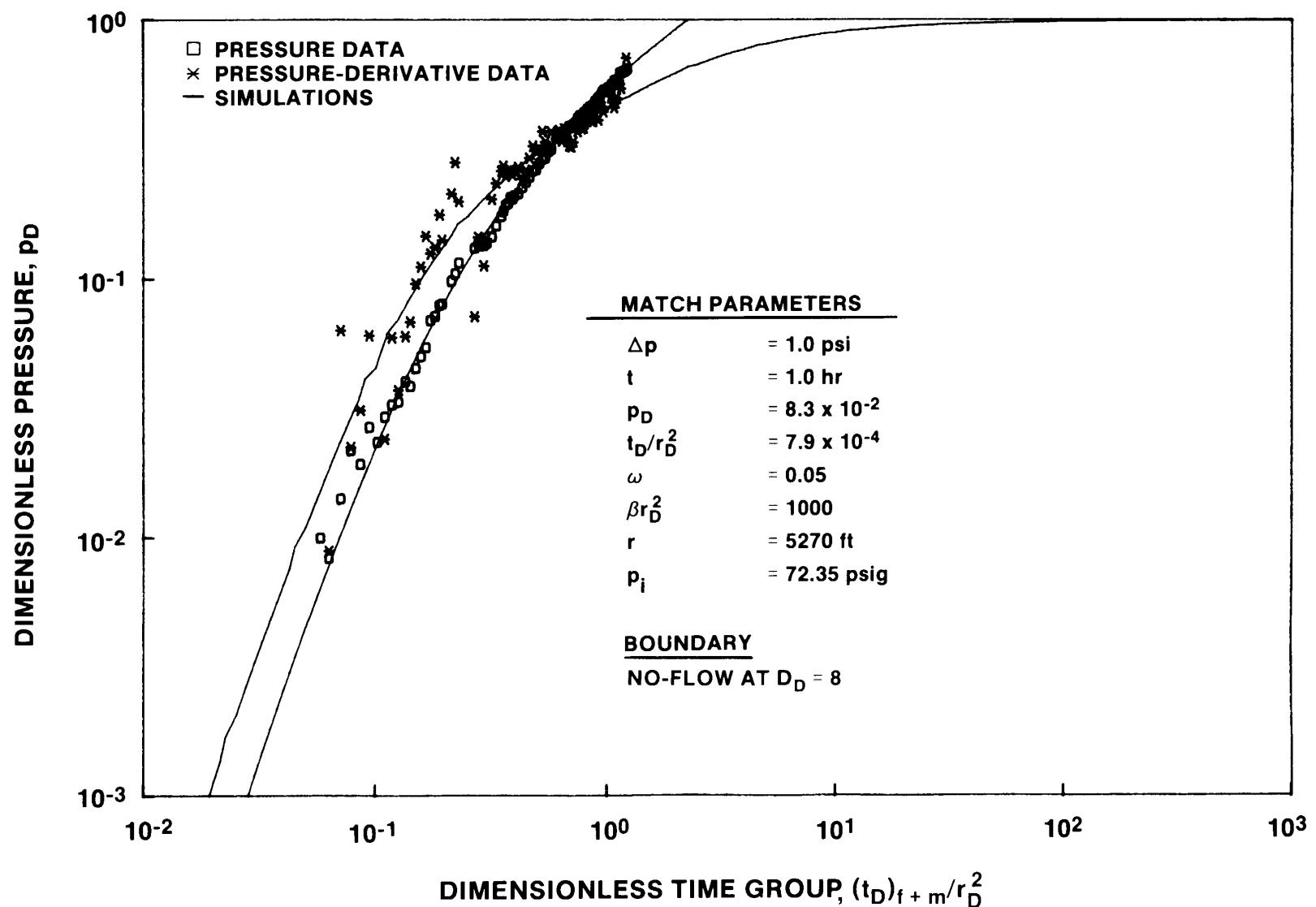
Figure C-2. Log-Log Plot of DOE-1 Drawdown During the H-3 Multipad Pumping Test with a Bounded Double-Porosity Simulation.

MATCH PARAMETERS

Δp	= 1.0 psi
t	= 1.0 hr
p_D	= 8.3 x 10^{-2}
t_D/r_D^2	= 7.9 x 10^{-4}
ω	= 0.05
βr_D^2	= 1000
r	= 5270 ft
p^*	= 72.35 psig

BOUNDARY
NO-FLOW AT D_D = 8

+ DATA
— SIMULATION

y-axis: $\dfrac{p_D}{\Delta p}$ [p^* - p(t)]

DIMENSIONLESS SUPERPOSITION FUNCTION: FLOW PERIOD 1
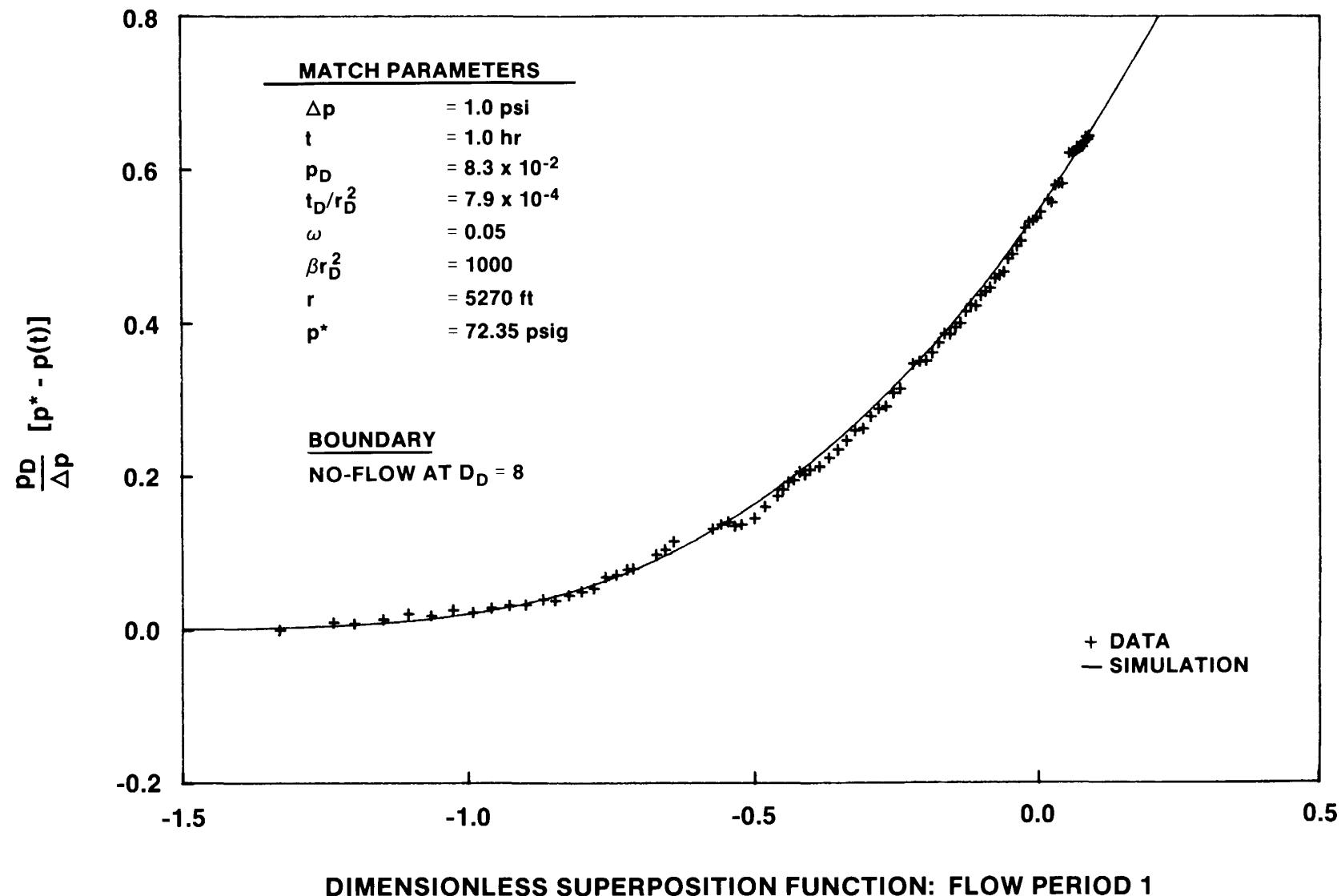
Figure C-3. Dimensionless Horner Plot of DOE-1 Drawdown During the H-3 Multipad Pumping Test with a Bounded Double-Porosity Simulation.

MATCH PARAMETERS

Δp	= 1.0 psi
t	= 1.0 hr
p_D	= 8.3 x 10^{-2}
t_D/r_D^2	= 7.9 x 10^{-4}
ω	= 0.05
βr_D^2	= 1000
r	= 5270 ft
p*	= 72.35 psig

BOUNDARY

NO-FLOW AT D_D = 8

+ DATA
— SIMULATION

t_0 = 10/15/85   09:00
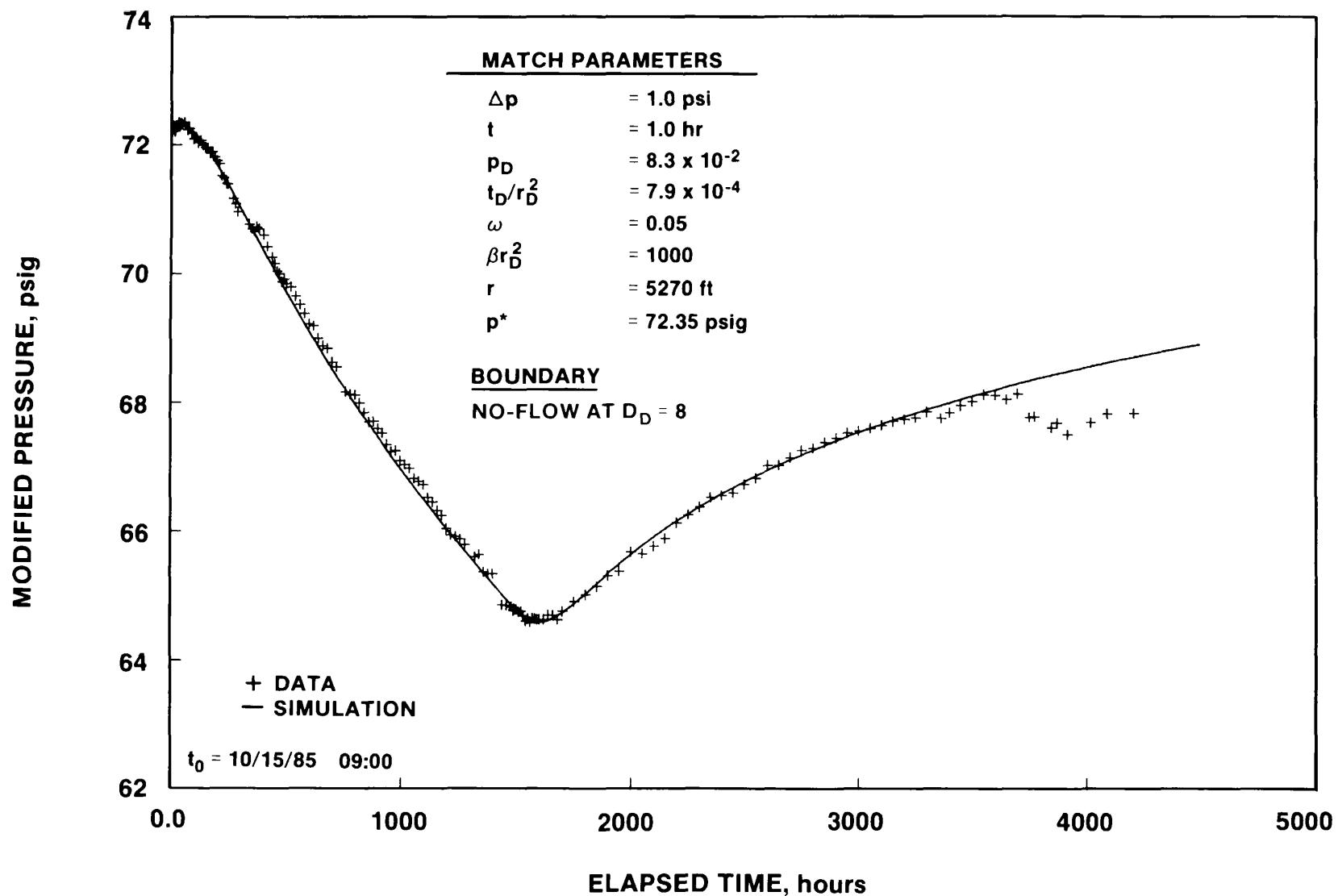
Figure C-4.   Linear-Linear Plot of DOE-1 Response During the H-3 Multipad Pumping Test with a Bounded Double-Porosity Simulation.
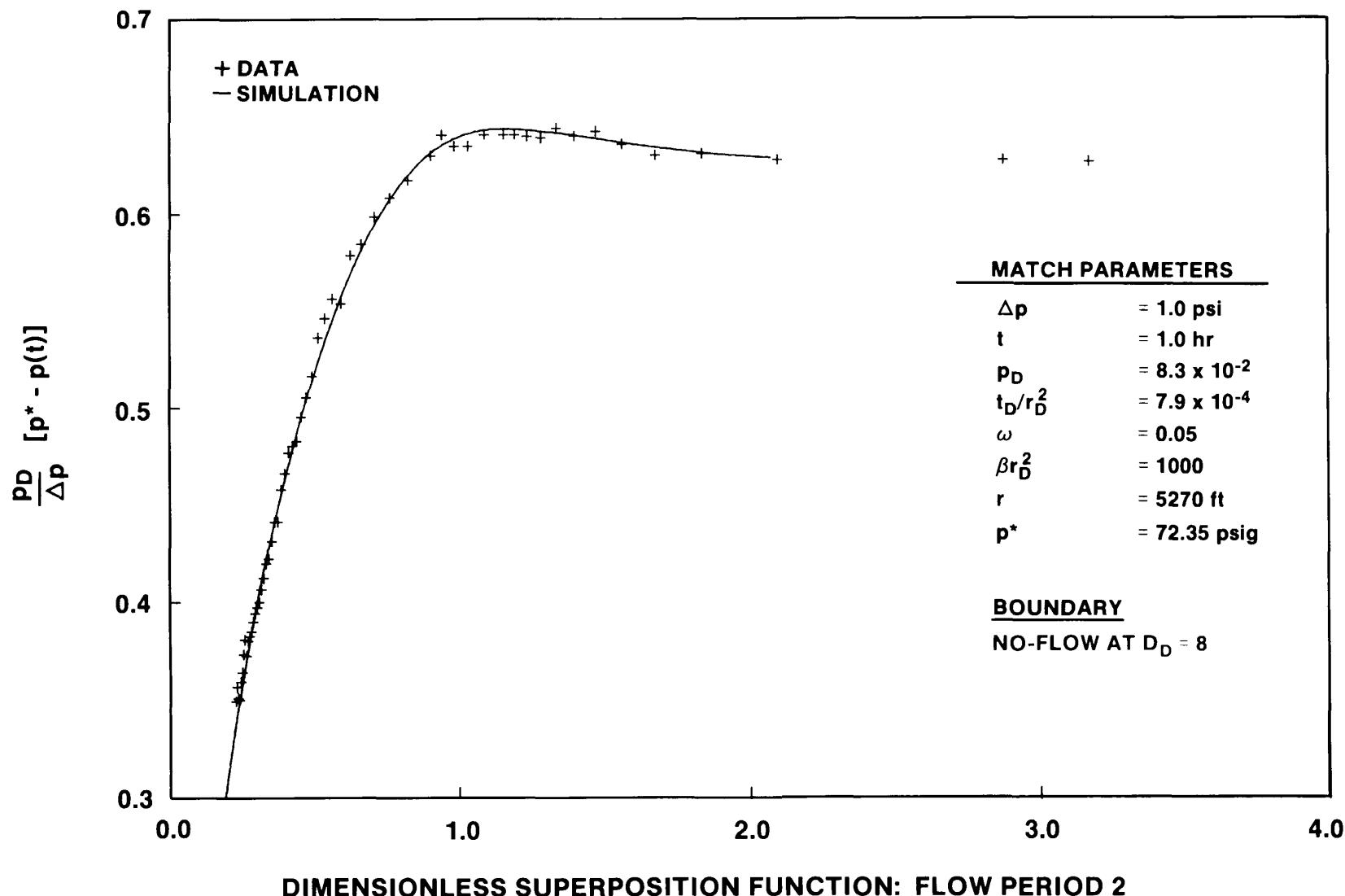
Figure C-5. Dimensionless Horner Plot of DOE-1 Recovery During the H-3 Multipad Pumping Test with a Bounded Double-Porosity Simulation.

DISTRIBUTION:

U. S. Department of Energy (5)
Office of Civilian Radioactive Waste
   Management
Office of Geological Repositories
Forrestal Building
Washington, DC   20585
   Deputy Director, RW-2
   Associate Director, RW-10
      Office of Program Administration
         and Resources Management
   Associate Director, RW-20
      Office of Facilities Siting and
         Development
   Associate Director, RW-30
      Office of Systems Integration
         and Regulations
   Associate Director, RW-40
      Office of External Relations and
         Policy

U. S. Department of Energy (3)
Albuquerque Operations Office
P.O. Box 5400
Albuquerque, NM   87185
   B. G. Twining
   J. E. Bickel
   R. Marquez, Director
      Public Affairs Division

U. S. Department of Energy/AL
Attn: National Atomic Museum Librarian
P.O. Box 5400
Albuquerque, NM   87185

U. S. Department of Energy (9)
WIPP Project Office (Carlsbad)
P.O. Box 3090
Carlsbad, NM   88221
   J. Tillman (4)
   A. Hunt
   T. Lukow (2)
   B. Young
   V. Daub

U. S. Department of Energy
Research & Waste Management Division
P.O. Box E
Oak Ridge, TN   37831
   W. R. Bibb, Director

U. S. Department of Energy, SRPO (4)
Salt Repository Project Office
P.O. Box 9334
Amarillo, TX   79105
   J. O. Neff
   R. Wunderlich
   G. Appel
   R. Wu

U. S. Department of Energy
Richland Operations Office
Nuclear Fuel Cycle & Production
   Division
P.O. Box 500
Richland, WA   99352
   R. E. Gerton

U. S. Department of Energy (5)
Office of Defense Waste and
   Transportation Management
Washington, DC   20545
   T. B. Hindman ---- DP-12
   C. H. George ----- DP-124
   M. Duff ---------- DP-123
   A. Follett ------- DP-122
   J. Mather -------- DP-123

U. S. Department of Energy (2)
Idaho Operations Office
Fuel Processing and Waste
   Management Division
785 DOE Place
Idaho Falls, ID   83402

U. S. Department of Energy (4)
Savannah River Operations Office
Waste Management Project Office
P.O. Box A
Aiken, SC   29802
   S. Cowan
   W. J. Brumley
   J. R. Covell
   D. Fulmer

U. S. Environmental Protection Agency
Office of Radiation Programs (ANR460)
Washington, DC   20460
   D. J. Egan, Jr.
   M. Cotton

U. S. Nuclear Regulatory Commission (4)
Division of Waste Management
Mail Stop 623SS
Washington, DC   20555
   M. Bell
   H. Miller
   J. Philip
   NRC Library

U. S. Geological Survey
Branch of Regional Geology
MS913, Box 25046
Denver Federal Center
Denver, CO   80225
   R. Snyder

U. S. Geological Survey (2)
Water Resources Division
Suite 200
4501 Indian School, NE
Albuquerque, NM   87110
   C. Peters

New Mexico Institute of Mining and
   Technology (3)
Environmental Evaluation Group
7007 Wyoming Blvd., NE, Suite F-2
Albuquerque, NM   87109
   R. H. Neill, Director

NM Department of Energy & Minerals
P.O. Box 2770
Santa Fe, NM   87501
   K. LaPlante, Librarian

New Mexico State Engineers Office
District II, 909 E. Second
P.O. Box 1717
Roswell, NM   88201
   A. Mason

U. S. Geological Survey
Conservation Division
P.O. Box 1857
Roswell, NM   88201
   W. Melton

New Mexico Bureau of Mines
   and Mineral Resources (2)
Socorro, NM   87801
   F. E. Kottolowski, Director
   J. Hawley

Battelle Pacific Northwest
   Laboratories (6)
Battelle Boulevard
Richland, WA   99352
   D. J. Bradley
   J. Relyea
   R. E. Westerman
   S. Bates
   H. C. Burkholder
   L. Pederson

Battelle Memorial Institute (12)
Project Management Division
P.O. Box 9334
Amarillo, TX   79105
   ONWI Library
   W. Carbiener, General Manager (3)
   V. Adams
   S. Gupta
   J. Kirchner
   A. LaSala
   T. Naymik
   W. Newcomb
   A. Razem
   J. Treadwell

Bechtel Inc. (2)
P.O. Box 3965
45-11-B34
San Francisco, CA 94119
    E. Weber
    H. Taylor

Westinghouse Electric Corporation (8)
P.O. Box 2078
Carlsbad, NM 88221
    Library
    W. C. Moffitt
    W. P. Poirer
    W. R. Chiquelin
    V. F. Likar
    R. F. Kehrman
    K. Broberg
    D. J. Moak

Oak Ridge National Laboratory (4)
Box Y
Oak Ridge, TN 37830
    R. E. Blanko
    E. Bondietti
    C. Claiborne
    G. H. Jenks

INTERA Technologies, Inc. (9)
6580 Austin Center Blvd., #300
Austin, TX 78731
    G. E. Grisak
    J. F. Pickens
    G. J. Saulnier
    V. A. Kelley
    A. Haug
    A. M. LaVenue
    M. Reeves
    T. L. Cauffman
    Library

INTERA Technologies, Inc.
P.O. Box 2123
Carlsbad, NM 88221
    W. Stensrud

IT Corporation (2)
P.O. Box 2078
Carlsbad, NM 88221
    D. Deal

IT Corporation (4)
5301 Central Ave., NE
Suite 700
Albuquerque, NM 87108
    R. F. McKinney
    M. E. Crawley
    R. M. Holt
    J. Myers

RE/SPEC, Inc. (5)
P.O. Box 725
Rapid City, SD 57709
    L. L. Van Sambeek
    T. Pfeifle
    G. Callahan
    J. L. Ratigan
    J. D. Osnes

RE/SPEC, Inc. (2)
P.O. Box 14984
Albuquerque, NM 87191
    W. E. Coons
    P. F. Gnirk

S-Cubed (2)
P.O. Box 1620
La Jolla, CA 92038
    E. Peterson
    P. Lagus

University of Arizona
Department of Nuclear Engineering
Tucson, AZ 85721
    J. G. McCray

University of Wisconsin-Madison
Department of Geology and Geophysics
1215 W. Dayton St.
Madison, WI 53706
    M. P. Anderson

The Pennsylvania State University
Materials Research Laboratory
University Park, PA 16802
    D. Roy

Texas A&M University
Center of Tectonophysics
College Station, TX   77840
    J. Handin

University of Texas at El Paso
Department of Geological Sciences
El Paso, TX   79968
    D. W. Powers

University of New Mexico (2)
Geology Department
Albuquerque, NM   87131
    D. G. Brookins
    Library

New Mexico Tech (3)
Department of Geoscience
Socorro, NM   87801
    J. Wilson
    F. Phillips
    C. S. Chen

Argonne National Laboratory
9700 South Cass Avenue
Argonne, IL   60439
    D. Hambeley

Los Alamos National Laboratory
Los Alamos, NM   87545
    B. Erdal, CNC-11

Brookhaven National Laboratory
Associated Universities, Inc.
Upton, NY   11973
    P. W. Levy, Senior Scientist

National Academy of Sciences,
    WIPP Panel:

    Dr. Charles Fairhurst, Chairman
    Department of Civil and
    Mineral Engineering
    University of Minnesota
    500 Pillsbury Dr., SE
    Minneapolis, MN   55455

Dr. Frank L. Parker
Department of Environmental and
    Water Resources Engineering
Vanderbilt University
Nashville, TN   37235

Dr. John O. Blomeke
Route 3
Sandy Shore Drive
Lenoir City, TN   37771

Dr. John D. Bredehoeft
Western Region Hydrologist
Water Resources Division
U. S. Geological Survey
345 Middlefield Road
Menlo Park, CA   94025

Dr. Karl P. Cohen
928 N. California Avenue
Palo Alto, CA   94303

Dr. Fred M. Ernsberger
250 Old Mill Road
Pittsburgh, PA   15238

Dr. Rodney C. Ewing
Department of Geology
University of New Mexico
200 Yale, NE
Albuquerque, NM   87131

Dr. George M. Hornberger
Department of Environmental Sciences
Clark Hall
University of Virginia
Charlottesville, VA   22903

Dr. D'Arcy A. Shock
233 Virginia
Ponca City, OK   74601

Dr. Christopher G. Whipple
Electric Power Research Institute
3412 Hillview Avenue
Palo Alto, CA   94303

Dr. Peter B. Meyers, Staff Director
National Academy of Sciences
Committee on Radioactive Waste
  Management
2101 Constitution Avenue
Washington, DC   20418

Ina Alterman
National Academy of Sciences
Board on Radioactive Waste
  Management
GF462
2101 Constitution Avenue
Washington, DC   20418

Hobbs Public Library
509 N. Ship Street
Hobbs, NM   88248
  M. Lewis, Librarian

New Mexico Tech
Martin Speere Memorial Library
Campus Street
Socorro, NM   87810

New Mexico State Library
P.O. Box 1629
Santa Fe, NM   87503
  I. Vollenhofer

Zimmerman Library
University of New Mexico
Albuquerque, NM   87131
  Z. Vivian

WIPP Public Reading Room
Atomic Museum
Kirtland East AFB
Albuquerque, NM   87185
  G. Schreiner

WIPP Public Reading Room
Carlsbad Municipal Library
101 S. Halagueno St.
Carlsbad, NM   88220
  L. Hubbard, Head Librarian

British Nuclear Fuels, PLC
Risley, Warrington, Cheshire
WA3 6AS 1002607 GREAT BRITAIN
  D. R. Knowles

Institut für Tieflagerung (4)
Theodor-Heuss Strasse 4
D-3300 Braunschweig
FEDERAL REPUBLIC OF GERMANY
  K. Kuhn

Bundesanstalt für
  Geowissenschaften
  und Rohstoffe (2)
Postfach 510 153
D-3000 Hannover 51
FEDERAL REPUBLIC OF GERMANY
  M. Langer
  P. Vogel

Hahn-Meitner Institut für
  Kernforschung
Glienicker Strasse 100
100 Berlin 39
FEDERAL REPUBLIC OF GERMANY
  W. Lutze

Bundesministerium für Forschung
  und Technologie
Postfach 200 706
D-5300 Bonn 2
FEDERAL REPUBLIC OF GERMANY
  Rolf-Peter Randl

Physikalisch-Technische
  Bundesanstalt
Postfach 33 45
D-3300 Braunschweig
FEDERAL REPUBLIC OF GERMANY
  P. Brenneke

Kernforschung Karlsruhe
Postfach 3640
D-7500 Karlsruhe
FEDERAL REPUBLIC OF GERMANY
  K. D. Closs

Japan Atomic Energy Research Institute
Tokai-Muri, Naka-Gun
Ibaraki-Ken 319-11, JAPAN
    Shingo Tashiro

Svensk Kärnbränsleforsorjning AB
Project KBS
Karnbranslesakerhet
Box 5864
S-102 48 Stockholm, SWEDEN
    F. Karlsson

Svensk Kärnbränslehantering AB (2)
Box 5864
S-102 48 Stockholm, SWEDEN
    A. Ström
    K.-E. Almén

Atomic Energy of Canada, Ltd. (4)
Whiteshell Nuclear Research
    Establishment
Pinewa, Manitoba, CANADA
ROE 1L0
    P. Haywood
    J. Tait
    C. C. Davison
    D. Stevenson

Studiecentrum Voor Kernenergie
Centre D'Energie Nucleaire
SCK/CEN
Boeratang 200
B-2400 Mol, BELGIUM
    A. Bonne

Ontario Hydro Research Lab (2)
800 Kipling Avenue
Toronto, Ontario, CANADA
M8Z 5S4
    D. K. Mukerjee
    A. T. Jakubick

Centre D'Etudes Nucleaires
    De La Vallee Rhone
CEN//VALRHO
S.D.H.A. BP 171
30205 Bagnols-Sur-Ceze, FRANCE
    C. Sombret

OECD Nuclear Energy Agency
Division of Radiation Protection
    and Waste Management
38, Boulevard Suchet
75016 Paris, FRANCE
    J-P Olivier

Netherlands Energy Research
    Foundation ECN (2)
3 Westerduinweg
P.O. Box 1
1755 ZG Petten, THE NETHERLANDS
    T. Deboer, Mgr.
    L. H. Vons

Nationale Genossenschaft für die
    Lagerung Radioaktiver Abfälle (3)
Parkstrasse 23
CH-5401 Baden, SWITZERLAND
    P. Hufschmied
    C. McCombie
    M. Thury

Sveriges Geologiska AB
Pusterviksgatan 2
S-413 01 Goteborg, SWEDEN
    A. Winberg

Environment Canada
National Water Research Institute
Canada Centre for Inland Lakes
867 Lakeshore Road
P.O. Box 5050
Burlington, Ontario
L7R 4A6 CANADA
    K. S. Novakowski

Energy, Mines and Resources Canada
Geological Survey of Canada
601 Booth St.
Ottawa, Ontario
K1A 0E8 CANADA
    D. Boyle

Technical Research Center of Finland
Nuclear Engineering Laboratory
P.O. Box 169
SF-00181 Helsinki, FINLAND
V. Taivassalo

Gartner-Lee Limited
140 Renfrew Drive
Markham, Ontario
L3R 6B3 CANADA
K. G. Kennedy

University of British Columbia
Department of Geological Sciences
Vancouver, British Columbia
V6T 1W5 CANADA
R. A. Freeze

ANDRA
31 Rue de la Federation
75015 Paris, FRANCE
D. Alexandre, Deputy Director

Oak Ridge National Laboratory
Building 2001
Ecological Sciences Information
  Center
P.O. Box X
Oak Ridge, TN 37830
C. S. Fore

Princeton University
Department of Civil Engineering
Princeton, NJ 08504
G. Pinder

Rockwell International
Rocky Flats Plant
Golden, CO 80401
C. E. Wickland

Rockwell International (3)
Atomics International Division
Rockwell Hanford Operations
P.O. Box 800
Richland, WA 99352
J. Nelson (HWVP)
P. Salter
W. W. Schultz

National Ground Water
  Information Center
6375 Riverside Drive
Dublin, OH 43017
J. Bix

University of California (3)
Lawrence W. Berkeley Laboratory
Berkeley, CA 94720
P. A. Witherspoon
J. C. S. Long
S. M. Benson

Kansas Geological Survey
University of Kansas
1930 Constant Avenue, Campus West
Lawrence, KS 66046
J. Butler

Roswell Public Library
301 N. Pennsylvania Avenue
Roswell, NM 88201
N. Langston

U. S. Geological Survey
Water Resources Division
521 W. Seneca St.
Ithaca, NY 14850
R. M. Yager

U. S. Geological Survey (2)
Water Resources Division
345 Middlefield Rd.
Menlo Park, CA 94025
P. Hsieh
A. F. Moench

Texas A&M University
Department of Geology
College Station, TX 77843
P. A. Domenico

Pannell Library
New Mexico Junior College
Lovington Highway
Hobbs, NM 88240
R. Hill

Government Publications Dept.
General Library
University of New Mexico
Albuquerque, NM 87131

Savannah River Laboratory (6)
Aiken, SC 29801
N. Bibler
E. L. Albenisius
M. J. Plodinec
G. G. Wicks
C. Jantzen
J. A. Stone

Savannah River Plant
Building 704-S
Aiken, SC 29808
R. G. Baxter

Arthur D. Little, Inc.
Acorn Park
Cambridge, MA 01240-2390
C. R. Hadlock

University of Arizona
Department of Hydrology
Tucson, AZ 85721
S. P. Neuman

S. S. Papadopulos and Assoc., Inc.
12596 W. Bayaud Ave., Suite 290
Lakewood, CO 80228
J. W. Anthony

Golder Associates
4104 148th Avenue NE
Redmond, WA 98052
T. W. Doe

Scientific Software-Intercomp
1801 California, 2nd Floor
Denver, CO 80202
J. M. Sofia

SAIC
10260 Campus Point Drive
San Diego, CA 92121
H. R. Pratt

SAIC
Suite 1250
160 Spear St.
San Francisco, CA 94105
M. B. Gross

SAIC
101 Convention Center Dr.
Las Vegas, NV 89109
G. Dymmel

Thomas Brannigan Library
106 W. Hadley St.
Las Cruces, NM 88001
D. Dresp, Head Librarian

Emcon Associates
1921 Ringwood Avenue
San Jose, CA 95131
F. W. Fenzel

Tech. Reps., Inc. (2)
5000 Marble NE
Suite 222
Albuquerque, NM 87110
J. Stikar

Sandia Internal:

1510	J. W. Nunziato	6342	M. G. Marietta
1520	C. W. Peterson	6342	R. P. Rechard
1521	R. D. Krieg	6343	T. M. Schultheis
1521	H. S. Morgan	6344	E. Gorham
3141	S. A. Landenberger (5)	6344	R. L. Beauheim (10)
3151	W. I. Klein (3)	6344	P. B. Davis
3154-1	C. L. Ward, for DOE/OSTI (8)	6344	S. J. Finley
6000	D. L. Hartley	6344	A. L. Jensen
6230	W. C. Luth	6344	R. Z. Lawson
6232	W. R. Wawersik	6344	R. Z. Lawson
6233	T. M. Gerlach	6344	M. D. Siegel
6253	D. A. Northrup	6345	A. R. Lappin
6253	N. R. Warpinski	6345	L. Brush
6300	R. W. Lynch	6345	K. L. Robinson
6310	T. O. Hunter	6346	J. R. Tillerson
6311	A. L. Stevens	6346	D. J. Borns
6312	F. W. Bingham	6346	S. J. Lambert
6313	T. E. Blejwas	6416	E. J. Bonano
6315	L. E. Shephard	7100	C. D. Broyles
6316	R. P. Sandoval	7110	J. D. Plimpton
6317	S. Sinnock	7120	M. J. Navratil
6340	W. D. Weart	7125	R. L. Rutter
6340	S. Y. Pickering	7125	J. T. McIlmoyle
6341	R. C. Lincoln	7130	J. O. Kennedy
6341	R. L. Hunter	7133	O. Burchett
6341	Sandia WIPP Central Files (5)	7133	J. W. Mercer
	(700HIND)	7135	P. D. Seward
6342	D. R. Anderson	8524	J. A. Wackerly (SNLL Library)
6342	K. Brinster		